

MECHANOBIOLOGY OF COMPLEX LOADING IN FUNCTIONAL SPINAL UNITS

by

Robert Allen Hartman

Bachelor of Science, University of Pittsburgh, 2008

Master of Science, University of Pittsburgh, 2010

Submitted to the Graduate Faculty of
The Swanson School of Engineering in partial fulfillment
of the requirements for the degree of
Doctor of Philosophy

University of Pittsburgh

2014

UNIVERSITY OF PITTSBURGH
SWANSON SCHOOL OF ENGINEERING

This dissertation was presented

by

Robert Allen Hartman

It was defended on

July 21, 2014

and approved by

James D. Kang, MD, Department of Orthopaedic Surgery

Richard E. Debski, PhD, Department of Bioengineering

Bryan N. Brown, PhD, Department of Bioengineering

Dissertation Director: Gwendolyn A. Sowa, MD, PhD, Department of Physical Medicine &
Rehabilitation, Department of Bioengineering, and Department of Orthopaedic Surgery

Copyright © by Robert Hartman

2014

MECHANOBIOLOGY OF COMPLEX LOADING IN FUNCTIONAL SPINAL UNITS

Robert Allen Hartman, Ph.D.

University of Pittsburgh, 2014

A majority of back pain, a costly condition and leading cause of disability, is mechanical in origin involving the intervertebral disc, facet joints, or ligamentum flavum. Mechanical loading may be beneficial or detrimental to spinal tissues depending on loading mode, magnitude, frequency, and duration. *Ex vivo* mechanobiology systems have been used to explore how axial loading parameters influence intervertebral disc biology, but flexion/extension (F/E) and combined rotations, loading modes relevant to back pain, have not been investigated. Moreover, biological responses in facet cartilage (FC) and ligamentum flavum (LF) have not been studied. A novel experimental platform was developed to assess simultaneous biological responses to six degrees-of-freedom (DOF) loading of intact functional spinal units (FSUs) in annulus fibrosus (AF), nucleus pulposus (NP), FC and LF. A bioreactor previously validated for assessment of axially compressed FSUs was attached to a robotic testing system and validated for rigid fixation and unrestricted movement in F/E and axial torsion (AT). At first, neutral F/E of varying range-of-motion and cycle number was applied. F/E loading elicited a predominantly catabolic response from spinal tissues with significant up-regulation of catabolic gene expression in AF and FC. Range-of-motion modulated aggrecan fragmentation in AF. AT was then added to F/E in small and large magnitudes to simulate mild and severe axial asymmetries treated clinically. F/E with coupled AT was pro-inflammatory in all spinal tissues and was pro-catabolic in AF and LF. In FC, which is gapped by torsion on one side and compressed on the other, pro-inflammatory changes were higher in gapped joints, and catabolic loss of matrix was higher in compressed joints. These findings point to a role for altered segmental mechanics in driving pro-inflammatory,

catabolic processes in spinal tissues that may play a role in spinal disorders involved in back pain. Finally, multiple regression analysis was performed to assess how well mechanical responses predicted changes in gene expression. Mechanical predictors accounted for more variation in gene expression in FC and LF than AF and NP. The development of this system provides spine and orthopaedic research with a novel experimental platform that can evaluate complex loading and simulated *in vivo* motions.

TABLE OF CONTENTS

PREFACE	XVII
INTRODUCTION	1
1.0 BACKGROUND	4
1.1 BACK PAIN	4
1.2 SPINAL FUNCTION	6
1.2.1 Mechanotransduction	10
1.3 DEGENERATION: MECHANICAL CONSEQUENCES	13
1.3.1 Compositional & Mechanical Changes	14
1.3.2 Cellular Changes and Mechanotransduction	17
1.4 MECHANICS IN TREATMENT	18
1.5 MECHANOBIOLOGY RESEARCH	21
1.5.1 <i>In vitro</i> Studies	22
1.5.2 <i>In vivo</i> Studies	24
1.5.3 <i>Ex vivo</i> Systems	28
2.0 GOAL AND SPECIFIC AIMS	33
2.1 SYSTEM DEVELOPMENT	33
2.2 SPECIFIC AIM 1 – FLEXION/EXTENSION	35
2.3 SPECIFIC AIM 2 – COMPLEX LOADING	36
2.4 REGRESSION MODELING	37
3.0 SYSTEM DEVELOPMENT	38
3.1 SYSTEM REQUIREMENTS	38

3.2	KINEMATIC AND KINETIC PRECISION OF THE TESTING SYSTEM..	40
	
3.2.1	Introduction	40
3.2.2	Methods	41
	3.2.2.1 Robot Testing System	41
3.2.3	Results.....	46
	3.2.3.1 Robot Testing System	46
3.2.4	Conclusions.....	50
3.2.5	Acknowledgements	52
3.3	RIGIDITY OF THE FIXATION SYSTEM.....	53
3.3.1	Introduction	53
3.3.2	Methods	53
	3.3.2.1 Statistics	58
3.3.3	Results.....	59
	3.3.3.1 Interface Motion.....	59
	3.3.3.2 Stiffness	62
3.3.4	Conclusions.....	63
3.3.5	Acknowledgements	65
3.4	ATTACHMENT TO ROBOT TESTING SYSTEM.....	66
3.4.1	Repeatable attachment.....	67
3.4.2	COR position.....	69
3.4.3	Orientation about COR.....	71
3.4.4	Conclusion	72
3.5	MEMBRANE EFFECTS	73

4.0	MECHANICAL LOADING PROTOCOL DEVELOPMENT	77
4.1	INTRODUCTION	77
4.2	PARAMETER DETERMINATION	80
4.2.1	Loading duration	80
4.2.2	Flexion/extension moment magnitudes.....	81
4.2.3	Axial torsion moment magnitudes	86
4.2.4	Loading rate	87
5.0	FLEXION/EXTENSION: RANGE-OF-MOTION & CYCLES	89
5.1	INTRODUCTION	89
5.2	METHODS.....	91
5.2.1	Specimen Preparation	91
5.2.2	<i>Ex vivo</i> Flexion/Extension	91
5.2.3	Biological Assessments	95
5.2.4	Statistical Analysis.....	97
5.3	RESULTS	98
5.3.1	<i>Ex vivo</i> Flexion/Extension- Mechanical Characterization	98
5.3.2	Biological Assessment of Flexion/Extension: Range-of-Motion	99
5.3.3	Biological Assessment of Flexion/Extension: Cycles and Duration	102
5.4	DISCUSSION.....	104
6.0	COMPLEX LOADING: FLEXION/EXTENSION AND AXIAL TORSION.....	110
6.1	INTRODUCTION	110
6.2	METHODS.....	112
6.2.1	Specimen Preparation	112
6.2.2	<i>Ex vivo</i> Combined Loading: Axial Torsion + Flexion/Extension	113

6.2.2.1	Mechanical Assessments	113
6.2.2.2	Biological Assessments	114
6.2.3	Statistical Analysis	116
6.3	RESULTS	117
6.3.1	Mechanical Response: Axial Torsion + Flexion/Extension	117
6.3.2	Biological Response: Relative Gene Expression	120
6.3.3	Biological Response: Western Blotting	123
6.4	DISCUSSION	126
7.0	MECHANICAL CONTRIBUTION OF FSU COMPONENTS	132
7.1	INTRODUCTION	132
7.2	METHODS	133
7.3	RESULTS	135
7.4	DISCUSSION	142
7.4.1	Neutral F/E	142
7.4.2	Combined loading: AT+F/E	144
7.4.3	Limitations	146
7.4.4	Conclusions	147
7.4.5	Acknowledgements	148
8.0	REGRESSION ANALYSIS: CORRELATING MECHANICAL AND BIOLOGICAL RESPONSES	149
8.1	INTRODUCTION	149
8.2	METHODS	152
8.2.1	Mechanical Factor Reduction	155
8.2.2	Principal Component Analysis	155
8.2.3	Multiple Regression-Part I: Hierarchical Entry Rationale	156

8.2.4	Multiple Regression-Part II: Final Regression	159
8.3	RESULTS	161
8.3.1	Data Reduction: Autocorrelation.....	161
8.3.2	Principal Component Analysis.....	163
8.3.3	Multiple Regression—Part I: Important Predictors Identified	164
8.3.4	Multiple Regression—Part II: Summary in All Tissues	165
8.3.5	Tissue-Specific Regression Analysis.....	168
8.3.6	Annulus Fibrosus (AF).....	168
8.3.6.1	MMP-1	170
8.3.6.2	MMP-3	171
8.3.6.3	ADAMTS-5	172
8.3.6.4	ACAN.....	173
8.3.7	Facet Cartilage (FC).....	175
8.3.7.1	ADAMTS-5	176
8.3.7.2	COX-2	177
8.3.7.3	ACAN	179
8.3.8	Nucleus Pulposus (NP)	180
8.3.8.1	ACAN	181
8.3.9	Ligamentum Flavum (LF)	183
8.3.9.1	MMP-1	184
8.3.9.2	ADAMTS-5	185
8.3.9.3	COX-2	187
8.3.10	Comparisons Across Tissues	188
8.4	DISCUSSION.....	189

8.4.1	Conclusions.....	195
9.0	DISCUSSION	197
9.1	SUMMARY	197
9.2	LIMITATIONS.....	202
9.3	BROADER IMPACTS & FUTURE DIRECTIONS.....	206
	APPENDIX A: UNLOADED CULTURE VS. BASELINE.....	211
	APPENDIX B: EFFECT OF AGE ON BIOLOGICAL OUTCOMES	218
	APPENDIX C: LINEAR MULTIPLE REGRESSION.....	224
	APPENDIX D: MATLAB CODE - MECHANICS	273
	APPENDIX E: AGGRECAN FRAGMENT WESTERN BLOT PROTOCOL	333
	GLOSSARY OF TERMS.....	338
	BIBLIOGRAPHY	340

LIST OF TABLES

Table 1. <i>In vivo</i> mechanobiology of rotational loading	27
Table 2. <i>Ex vivo</i> mechanobiology of rotational and complex loading.....	30
Table 3. Mean translational and rotational precision for AP, AT, and F/E in ‘Replay’ and ‘Pathseek’	50
Table 4. Mean (SD) ratios of FSU-to-fixture interface stiffness for both fixation methods in F/E, AT,and AP	63
Table 5. <i>In vivo</i> and <i>in vitro</i> human lumbar spine flexion/extension range-of-motion	81
Table 6. Ratio of <i>in vitro</i> to <i>in vivo</i> flexion/extension range-of-motion	82
Table 7. Human L4-5 F/E ROM in activities	85
Table 8. Rabbit flexion/extension moment-rotation properties: Determining moment targets ...	85
Table 9. F/E moment targets	85
Table 10. AT torsion moment targets	87
Table 11. List of quantitative real-time reverse transcription-polymerase chain reaction primer sequences	96
Table 12. Energetics: Mean (SD) work and hysteresis measures per group	99
Table 13. Kinetics: Mean (SD) moment-rotation properties and neutral zone stiffness for each group	99
Table 14. Moment-rotation and stiffness properties for F/E.....	117
Table 15. AT properties at extremes and middle of F/E.....	118
Table 16. Work and hysteresis properties for flexion/extension per and across cycles	119
Table 17. Percent contribution to F/E moments by resected structures in Neutral F/E and AT+F/E	137
Table 18. List of predictors and outcomes for multiple regression	154

Table 19. Tissue-specific order of predictor groups	156
Table 20. Mechanical factors not correlated or redundant to other factors	162
Table 21. Uncorrelated ($R < 0.6$) mechanical factors correlated with PCs ($R > 0.6$) with highest R values	164
Table 22. Predictors identified in preliminary regression ($\beta > 0.3, p < 0.2$) with p-values	165
Table 23. R -values and significance of final regression models.....	166
Table 24. Summary of significant predictors and their standardized coefficients (β).....	167
Table 25. Description of regression models for AF.....	169
Table 26. Description of model predictors for AF.....	169
Table 27. Description of regression models for FC.....	176
Table 28. Description of model predictors for FC.....	176
Table 29. Description of regression models for NP.....	181
Table 30. Description of model predictors for NP.....	181
Table 31. Description of regression models for LF	183
Table 32. Description of model predictors for LF	184
Table 33. Simple correlation (Pearson's R) of age with relative gene expression for the effect of loading.....	219
Table 34. Correlations of age with protein outcomes (1) raw densitometry of unloaded (only) and (2) load response (normalized to unloaded).....	221
Table 35. Principal Component Analysis: Eigenvalues and variance explained.....	226
Table 36. Simple correlation of original predictors with principal components	226
Table 37. Sample calculations for protein extraction process	335

LIST OF FIGURES

Figure 1. Anatomy of a functional spinal unit (FSU)	8
Figure 2. FSU within robot testing system and instrumented with reflective markers.....	42
Figure 3. VICON Marker System and Global Reference Frame.....	43
Figure 4. Fixture and FSU reference frame and anatomical motions and directions	44
Figure 5. Representative ‘Pathseek’ F/E (Mx) plot of minimized off-axis forces (top) and moments (bottom).....	47
Figure 6. Force and moment precision measurements in F/E.....	48
Figure 7. Robot testing system kinematic precision depicted for translational and rotational DOF	49
Figure 8. Global and local coordinate systems defined by reflective markers	55
Figure 9. Specimen-fixture interface motions in 6 DOF for FSU movements in F/E, AT,and AP.	61
Figure 10. Superior (SV-EE) and inferior (IV-B) fixture-specimen interface stiffness in F/E, AT,and AP	62
Figure 11. Axial view of FSU aligned in inferior fixture with COR estimates for F/E and AT .	68
Figure 12. COR measurements from robot to bioreactor	69
Figure 13. Effects of COR placement in z-direction on F/E moment-rotation curves	70
Figure 14. Effects of COR placement in z-direction ($< \pm 3$ mm) on F/E moment-rotation curves	71
Figure 15. Intentional variation in axial plane orientation: effects on F/E moment-rotation curves	72
Figure 16. Flexed FSU in bioreactor with inner dialysis and outer rubber membranes with tension illustrated.....	74
Figure 17. Effect of dialysis membrane with and without folds on F/E moment-rotation curves	75

Figure 18. Effect of folded, outer rubber membranes on F/E moment-rotation curves.....	76
Figure 19. Representative load-to-failure moment-rotation profile for axial torsion	87
Figure 20. Bioreactor attached to robot testing system circulating media with enclosed, flexed FSU	92
Figure 21. Representative F/E moment-rotations to small (x) and large (o) ROM (curve-fit)....	94
Figure 22. Mean fold (\pm SEM) change in relative gene expression of NP,FC, AF, and LF with loading.....	100
Figure 23. (A) Representative immunoblots against G1 for NP, FC, and AF. (B) Mean (\pm SEM) normalized densitometry for MMP- and ADAMTS-cleaved G1 fragments.	102
Figure 24. Mean fold change (\pm SEM) in relative gene expression NP, FC, AF, and LF with loading.....	104
Figure 25. Mean (\pm SEM) mechanical responses in AT+F/E: (A) Relaxation of F/E moments, (B) Relaxation of F/E NZk, EZk flexion, and EZk extension, (C) Cumulative work and hysteresis, and (D) Relaxation of work and hysteresis.	120
Figure 26. Mean fold change (\pm SEM) in relative gene expression NP, FC, AF, and LF with loading.....	122
Figure 27. Mean (\pm SEM) fold change in relative gene expression of left and right FC with loading	123
Figure 28. (A) Representative immunoblots against G1 fragments and CHAD for NP, FC, and AF. (B) Mean (\pm SEM) normalized densitometry for each protein per tissue.	125
Figure 29. (A) Representative immunoblots against G1 fragments and CHAD are shown for left (L) and right (R) facet cartilage (FC) with loading. (B) Mean (\pm SEM) normalized densitometry for each protein per side of FC per group across samples.	126
Figure 30. Representative F/E moment-rotation curve with serial resection of FSU components	136
Figure 31. Percent flexion (left) and extension (right) moment resistance per structure in Neutral and AT+F/E	137
Figure 32. Distribution of FSU component loading (percent contribution) in flexion in different species	138
Figure 33. Changes in resultant force magnitudes in neutral F/E and AT+F/E with serial resection	139

Figure 34. Change in component forces with serial resection of FSU structures in Neutral F/E	141
Figure 35. Change in component forces with serial resection of FSU structures in Large AT+F/E	141
Figure 36. Overview of data reduction and sequential multiple regression	162
Figure 37. Principal component eigenvalues and percent variance explained per principal component.....	164
Figure 38. Relative gene expression in NP, FC, and AF of MMP-3 and COX-2 normalized to t_0	213
Figure 39. MMP-cleaved (left, ~54kDa) and ADAMTS-cleaved (right, ~67kDa) aggrecan fragments in cultured tissues normalized to baseline.	214
Figure 40. CHAD expression (~36kDa) in spinal tissues in normalized to t_0	215
Figure 41. Age vs. Relative Gene Expression: The two strongest correlations between age and load responsive changes in gene expression.....	220
Figure 42. Correlation of age with MMP-cleaved aggrecan raw densitometry values in NP ...	221
Figure 43. Correlation of age with ADAMTS-cleaved aggrecan raw densitometry values in NP	222
Figure 44. Correlation of age with CHAD raw densitometry values in NP	222
Figure 45. Overview of Matlab Code	273

PREFACE

The completion of a doctoral dissertation is by definition individualistic in nature, but the *de facto* reality, at least so far as this work is concerned, could hardly be more different. I owe a great debt of gratitude to a number of persons who have helped to guide, assist, and support me in this effort. My first thanks belong to my committee. Dr. Gwendolyn Sowa deserves my first thanks; she has encouraged intellectual curiosity, broad interests, and critical thinking, challenged and refined every idea and finding from this work, tirelessly read through countless and verbose drafts of this document and many others, and demonstrated a consistent, genuine care and concern for me as a person and professional. I want to thank Dr. James Kang for his gracious leadership and for opening the door of spine research to me as an undergraduate engineer. He has maintained wide-open doors of opportunity within the Ferguson Laboratory for critical, independent thinking and investigation within the context of an unwavering pursuit of clinically relevant research that influences an international research community. Dr. Richard Debski, who advised and taught me as undergraduate engineer and encouraged my interests in orthopaedic biomechanics, deserves my gratitude. I want to thank Dr. Bryan Brown as well, for stepping aboard my dissertation committee mid-stream and serving amiably as an involved adviser with consistent, constructive criticism and an eye for weaving the various elements of this research together. While not formally a member of my committee, Dr. Nam Vo consistently provided valuable feedback, important criticism, and endless enthusiasm for my work. Dr. Michael Schneider, who served as a mentor on my NIH/NCCAM F31 predoctoral fellowship, consistently made time to discuss my research, provide clinical insight from a manual therapist's point of view, and instruct me in the art of grant writing.

A number of other people were critical to the success of this work and to my professional development during the process of dissertation research. Dr. Takashi Yurube spent nearly three years in the Ferguson Laboratory, during which time he worked alongside me on this project and others and taught me how to be a scientist in relentless pursuit of the truth while maintaining a wonderful sense of humor, patience, and compassion that lifts others up. Dr. Kevin Bell has been my longest-standing mentor in research, and his stabilizing influence, his friendship, and his contribution to developing the mechanical systems used in this work are deeply appreciated. Paulo Coelho and Kevin Ngo were selfless and patient in helping me to run countless plates of RT-PCR.

Personally, I would like to thank my wife, Meaghan Hartman, for her loving, patient support of me during this long process of training and discovery. I want to dedicate this work to her. My family—parents, siblings, nieces and nephews—friends, and church family are too numerous to thank individually, but their encouragement (and ailments!) have motivated my work in rehabilitation and orthopaedic research. Finally, I want to thank and esteem my Lord and Savior, whose marvelous handiwork I have the privilege of peering in to and whose redeeming love is the source and direction of all I do and all that I am.

INTRODUCTION

Back pain is the most common cause of pain and disability in the United States [1, 2] with greater than a quarter of Americans experiencing back pain annually [3] and approximately 80% of the population experiencing back pain over their lifetimes [4]. Not only do individual patients experience dramatic reduction in quality of life, but direct and indirect costs amount to an annual national economic burden of nearly \$100B [5]. Consensus for diagnosis, prevention, and treatment of back pain remains elusive as evidenced by rising costs of care that outpace increases in prevalence [6, 7] without associated improvements in disability.

Identification and implementation of cost-effective prevention and treatment strategies is required. For years, immobilization and bed rest have been known to be ineffective and potentially deleterious [8], pointing to the importance of motion preservation in treatment. Conversely, overloading can exacerbate symptoms and worsen underlying causes [9]. It seems clear then that thresholds of loading exist, beyond which loading can be beneficial or detrimental to the health of spinal tissues. Motion-based therapies and preventative strategies are among the leading candidate approaches for low-cost, effective solutions. Such methods include manual therapy provided by physical therapists, chiropractors, and osteopathic physicians, as well as active exercise programs and integrative medicine training routines like yoga. While these approaches demonstrate moderate effectiveness [10-13], the mechanisms by which they provide benefit are poorly understood [14-16]. Evidence suggests that different types of back pain patients respond

differently to various motion-based therapies [17, 18]. Also, certain types of mechanical loading appear to benefit some sub-groups of patients but not others [18, 19]. However, a lack of clinical evidence for tailoring motion-based therapies to appropriate sub-groups of patients and an incomplete understanding of the mechanisms by which motion-based therapies act limits their effectiveness, adoption, and integration with other treatments [20, 21]. Scientific research needs to elucidate the effects of different types of mechanical loading relevant to motion-based therapies on tissue involved in degeneration and back pain.

Basic science studies have begun exploring regulation of cell viability, cell phenotype, inflammation, and matrix homeostasis in response to mechanical loading. Primarily, researchers have focused on the biological response of the intervertebral disc to varying magnitudes, frequencies, and modes of loading [22]. Disc degeneration warrants investigation as a leading cause of back pain [3, 23], but degenerative changes involved in back pain commonly occur in other spinal tissues concomitantly or independently [24-26], and these changes are also mediated by mechanical factors [27-29]. Further, previous mechanobiology studies have focused almost exclusively on axial compression [22, 30] despite the importance of other degrees-of-freedom in spinal function and spinal disorders [18, 31, 32]. Translation of mechanobiology requires assessment of all relevant spinal tissues and additional physiologic modes of loading.

Among the experimental platforms used for investigating loading effects on cell and tissue biology, *ex vivo* organ culture models are important because they maintain *in-situ* mechanical transduction and permit fine control of environmental conditions and mechanical loading. A range of biological outcomes that measure matrix composition, matrix catabolism, matrix synthesis, inflammation, cell viability, and cell metabolism have been used to evaluate the effect of loading on cells and tissue. Recent advances in *ex vivo* organ culture include validation of a human disc

model [33], development of high-throughput systems [34, 35], and applied loading in torsional and asymmetric compression [36, 37]. Despite this progress, systems are still limited by exclusion of posterior structures, perturbed load transmission [38-40], and lack of physiological rotational loading. By improving the capability of applied loading in *ex vivo* systems to include rotational loading (flexion/extension most notably) and expanding the array of target tissues (i.e. facets and spinal ligaments), *ex vivo* mechanobiological studies will facilitate improved and expanded understanding of the role of mechanics and other environmental variables in regulating the health of spinal tissues involved in back pain and will help to improve prescription of motion-based therapy.

1.0 BACKGROUND

1.1 BACK PAIN

Low back pain is a common, complex, and often debilitating disorder that erodes the quality of life for those who suffer from it [2]. Back pain poses an enormous socioeconomic burden on the global population [41]. In the US, it has a prevalence of nearly 25% [3] and amounts to an annual cost, including direct and indirect measures, approaching \$100B [5]. Identifying the primary cause of back pain is often difficult. While genetic heritability accounts for a majority of the variation back pain [42], a number of environmental factors, principally mechanical loading, account for much of the remaining variability. Risk factors include degeneration [23, 43, 44], smoking [45], obesity [46, 47], psychological conditions [48, 49], occupational heaving loading [50], and sedentary lifestyle [23].

Low back pain comprises numerous classifications or subgroups. Initial or recurring episodes of back pain are characterized as acute if symptoms persist less than twelve weeks [51]. Historical guidelines suggested that a large majority of acute back pain resolves spontaneously, but a recent series of studies with one-year follow-up show that the majority of patients do not recover [52-54] but persist in mild (18-36%) to severe (8-21%) chronic pain or transition to recurring or episodic pain (13-35%) [53]. Chronic back pain poses a disproportionate financial burden on the health system, accounting for over three-quarters of overall costs associated with back pain [48, 55, 56]. Those with persistent or frequently recurring back pain may also be categorized by their avoidance or persistence in physical activity; evidence suggests different pain mechanisms may underlie symptoms in “avoiders” vs. “endurers.” [57, 58]. Similarly, back pain

patients may be grouped by directional movement-associated provocation of pain [18, 19]. For example, some patients experience pain in flexion but not extension, while others have the opposite directional preference [18, 19]. Clearly, treating back pain as a monolithic entity is inappropriate in terms of elucidating underlying mechanisms of pain and degeneration. Consideration of numerous factors, including chronicity of pain, engagement in activity, and movement-associated pain provocation, is critical to tailoring treatment strategies to patient sub-groups.

While the risk factors for development of back pain are numerous and specific diagnosis for most patients remains inconclusive, a majority of back pain is mechanical in origin [3, 50, 59]. Symptoms arise from various spinal structures including intervertebral discs and facet joints [3, 60]. Degeneration of these tissues, marked by matrix catabolism, inflammation, and maladaptive remodeling [61], is associated with various spinal disorders that can lead to back pain. Imaging studies of these spinal structures in back pain patients show associations of degeneration with back pain [23, 43, 44], although high rates of asymptomatic degeneration are also evident [62, 63]. These structures, which provide passive mechanical support to spinal segments, are variably loaded in different physiologic motions. Movement-associated provocation of pain [19] and altered directional kinematics in lumbar motions with back pain [64, 65] imply that injury or mechanical loading in these spinal structures can contribute to underlying damage, inflammation and degenerative changes.

Mechanical loading plays a salient role in back pain. Overloading or mechanical failure of discs, endplates, facets, and spinal ligaments can lead to the development of pain and degeneration [26, 28, 66, 67]. Occupational activities including repeated combined loading—torsion and flexion/extension—are associated with development of back pain [68, 69]. Sporting activities with high levels of combined loading have been associated with high rates of back pain [70, 71].

Chronic, aberrant loading is suspected of accelerating degenerative changes or provoking overuse injuries in spinal tissues [72]. Asymmetric or complex spinal loading increases the likelihood of structural failure [73] and is thought to promote inflammatory, degenerative changes in spinal tissues [74-78]. However, it is equally clear that physiologic loading is important to spinal tissue health from research that shows that the absence of compressive loading or induced hypomobility can also lead to degenerative changes in spinal tissues [9, 79]. Therefore, identifying thresholds of non-physiologic loading that exacerbate painful symptoms and determining thresholds of physiologic loading that are protective or beneficial is important to preventing and managing back pain [9].

1.2 SPINAL FUNCTION

A primary role of the spinal column is support of axial compression from the head and torso as well as facilitation of multi-directional movement of the head and trunk. As elsewhere in the musculoskeletal system, anatomical form and tissue composition reflect physiologic function; the unique structure and makeup of tissues of the spinal column enable their specific functions. The spinal column comprises twenty-six motion segments that are grouped in to four regions: the cervical (C0-7), thoracic (T1-12), lumbar (L1-5), and sacral (S1-3) spine. Each level is composed of longitudinal ligaments, which run anterior and posterior to the vertebral column. Situated between vertebral bodies lies an intervertebral disc made up of a central, gelatinous nucleus pulposus (NP) surrounded by a ringed annulus fibrosus (AF) composed of fibrous collagen lamella that, along with cartilage endplates (CEPs) on the bony surfaces of adjacent vertebral bodies (VB), encapsulate the highly hydrated NP. Immediately posterior to the vertebral bodies runs the spinal

cord or cauda equina, which is surrounded by bony lamina and transverse and spinous processes that protect the neural tissue. A thick, elastic ligament, the ligamentum flavum (LF) spans the gap between bony lamina. Lateral to the lamina on either side of the spine are diarthrodial joints called facets. Facet joints comprise two articulating surfaces of hyaline cartilage (facet cartilage, FC) enclosed by a joint capsule, lined with synovium, and filled with synovial fluid. Additional ligaments, interspinous and supraspinous ligaments (ISL and SSL), run posteriorly between the spinous processes. The passive, osteoligamentous components of each level of the spine, composed of vertebrae, a disc, facet joints and spinal ligaments (Figure 1), are termed a functional spinal unit (FSU).

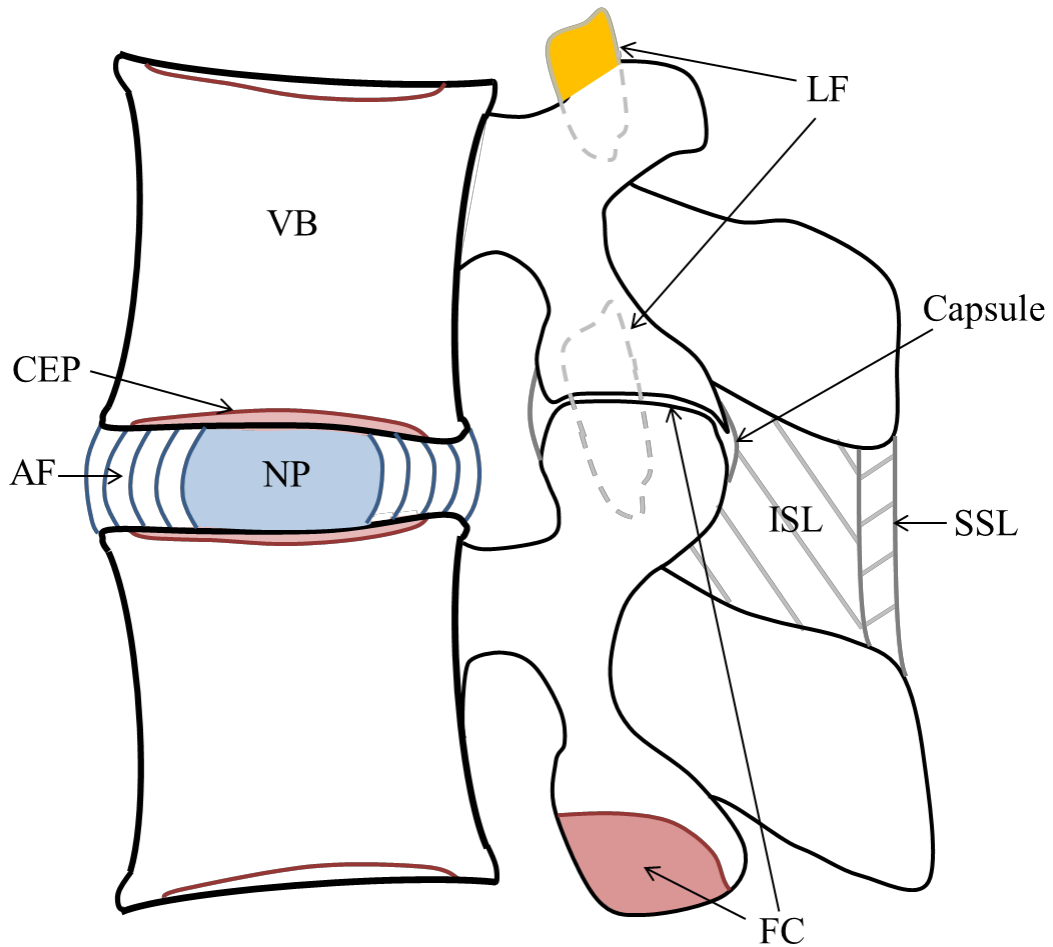


Figure 1. Anatomy of a functional spinal unit (FSU)

The NP and AF mechanically interact to support compressive loading and resist motion in all degrees-of-freedom (DOF). In axial compression, swelling pressure in the highly hydrated, proteoglycan-rich NP absorbs and dissipates compressive loading. Swelling pressure is constrained by the bulging AF and cartilage end plate (CEP). In distraction, the fibers of the AF, which insert in the bone and CEP of adjacent vertebral bodies, restrict axial translation. In bending modes, the NP translates within the AF to accommodate rotation but continues to contribute to load resistance via swelling pressure opposing compression in the disc [80]. The AF supports compression in the disc region in the direction of bending and provides tensile resistance on the

contralateral side [80]. The AF also provides the predominant amount of resistance to axial torsion [81] through circumferential tensile resistance of collagen and elastin fibers [82]. Additionally, swelling pressures in the NP transiently decrease with torsion [83], offset by increased compressive stress in the AF [84]. Thus, the disc is a primary contributor to spinal function in all loading modes.

Facet joint articulation contributes to load resistance and guides motion in axial compression, extension, axial rotation, and anterior shear. Facet cartilage is engaged primarily in compression in each of these motions, though the magnitude and location of compression across the cartilage surface varies with loading mode [85]. Changes in cartilage mechanics, including the involvement of shear loading, with physiologic loading remain unstudied [67]. The orientation of facet joint faces, which varies markedly along the spinal column, dictates their ability to restrict motion in each physiologic plane. In the lumbar spine, facets' vertical orientation relative to the transverse plane limits their contribution to axial compression and extension, though studies show 3-25% of axial compression [27, 39] and 16-40% of extension is borne by lumbar facets joints [86-88]. More importantly, the alignment of facet joints relative to the sagittal plane leads to a prominent role of facets in axial torsion resistance and high torsional stiffness in the lumbar spine [89-91]. Finally, facet joints resist up to 87% of anterior shear of lumbar FSUs [92]. Facet articulation strongly influences physiologic load distribution within FSUs [85, 92].

Spinal ligaments of the posterior complex, predominantly the ligamentum flavum, are important in flexion, lateral bending, and axial rotation of FSUs. Their primary role is restriction of flexion moments [86, 87], but they play a secondary or tertiary role in resisting lateral bending and axial rotation as well [93, 94]. As in other joints of the body, spinal ligaments exhibit non-linear stiffness that depends strongly on the direction of joint rotation. In directions of loading

where ligaments are recruited in tension, collagen fibers are initially lax due to fiber crimp, giving rise to low stiffness movements. As joints continue to rotate, collagen fibers are stretched and engaged in tension, leading to high stiffness and greater restriction of motion [95]. This non-linear response in spinal ligaments contributes to the non-linear moment-rotation response of FSUs in flexion and bending [87, 94]. The LF in particular contains a large fraction of elastin in addition to collagen fibers [96]. Elastin fibers are present in tissues that undergo repeated cyclic loading. The presence of elastin in tissue matrix provides elastic recoil, enabling the restoration of shape and storage of mechanical energy [97]. Its unique composition renders the LF an important stabilizer of rotational movements, particularly flexion, throughout the non-linear motion path of spinal segments [87].

1.2.1 Mechanotransduction

Applied mechanical loading to spinal segments is distributed among spinal tissues and transduced within each tissue to the cellular microenvironment. Transduction of applied mechanical loads to cellular mechanical stimuli varies with magnitude, frequency, duration, and mode of loading [22, 30]. In general, applied loading induces changes in stresses and strains within the solid matrix, hydrostatic pressure of the fluid phase, osmotic pressure, interstitial fluid-flow, and streaming potentials [98]. In a process that is mediated by interactions of the cell membrane, pericellular matrix (PCM), and extracellular matrix (ECM), cells can experience shape change, volumetric and deviatoric deformation of membranes and/or nuclei, stretch of certain membrane receptors and channels, altered ionic gradients, and electrokinetic effects [98]. While the way in which cellular mechanics effect changes in cellular signaling and processes remains understudied, it is known that cytoskeletal remodeling [99], focal adhesion signaling [100], and Ca^{2+} ion signals [101] can

be activated by altered mechanics in disc and chondrocyte cells. Indirect effects may include generation of matrix fragments, conformational changes of the ECM, and release of embedded factors that may also influence cellular signaling [102-104]. The type of stimuli experienced by cells varies based on cellular origin, resident tissue, tissue region, age and degeneration-related changes to tissues and cells [30].

In healthy, functional tissues, mechanical stimulus transduction is strongly tissue-specific. NP cells (NPCs), which comprise cells derived from notochordal cells and chondrocyte-like cells that have differentiated from notochordal cell progenitors or migrated in to the NP from the inner AF or adjacent CEP [105-107], are spheroidal in shape and reside at very low densities embedded in the highly hydrated matrix with low concentrations of un-aligned type-2 collagen [30]. NPCs are predicted to experience hydrostatic pressurization, modest volumetric strains with small tensile circumferential and compressive axial strains, and fluid shear stress [108, 109]. They express chondrocytic markers like aggrecan, type-2 collagen, and Sox-9 but have much higher aggrecan-to-type-2 collagen expression ratios than chondrocytes [110]. Accordingly, they synthesize large amounts of proteoglycan [106]. Conversely, AF cells (AFCs) are mesenchymal cells that express a composite fibroblastic and chondrocytic phenotype. They are primarily ellipsoidal, becoming more elongated in the outer AF and more spheroidal in the inner AF. AFCs are aligned with collagen fibers in the direction of tensile loading [30, 106] or exist between lamella as a distinct subpopulation of cells [111]. In contrast to NPCs, they experience large amounts of volumetric and deviatoric strain, which match ECM strain in elongation and actually amplify radial strain, and lower magnitudes of transient fluid pressurization and fluid flow [112]. AFCs also express chondrocytic markers, but they additionally express type-1

collagen in higher ratios relative to type-2 collagen; ratios decrease inwardly in the radial direction [110], reflecting the shift in mechanical environment from tension in bulging in the outer AF to support of compression in the inner AF [30].

Facet cartilage mechanics vary significantly by tissue region. Normal facet cartilage, like hyaline cartilage layers in other diarthrodial joints, is composed of (1) a tangential zone with collagen fibers oriented parallel to the surface, (2) a transition zone in which the fibers bend toward the subchondral bone, (3) a deep zone composed of fibers oriented perpendicular to the surface and rich in proteoglycans, and (4) calcified cartilage that transitions between articular cartilage and subchondral bone. Articular chondrocytes experience volumetric change, shape change, fluid pressurization, and fluid flows that vary with tissue depth and radial position [113]. Cells in the surface zone assume an ellipsoidal shape aligned with collagen fibers and undergo higher deformations with greater volume change compared to cells in deeper zones that, though aligned with matrix fibers, are largely spheroidal and primarily subjected to greater hydrostatic pressurization, small volumetric deformation, and greater electrokinetic effects [114]. Chondrocytes differ from intervertebral disc cells in terms of basic phenotypic markers, the local microenvironment, and mechanical loading experienced [106, 108, 112, 115]. They express expected phenotypic markers—type-2 collagen, aggrecan, Sox-9—but native gene expression and mechano-responsive synthetic activity varies with zone of origin [116, 117]. The nature of macroscopic loading and cellular response varies not only with tissue depth but also across the lateral profile of the tissue [118]. In facet cartilage, where the center of pressure (a surrogate for regional loading) varies significantly with loading mode, compression, and degeneration [85, 92], the lateral variation of loading is significant.

LF fibroblasts exist at low densities as elongated cells, oriented within the dense elastin-collagen matrix [119]. A small fibrocartilaginous cell population exists near the lamina [96]. In physiologic rotations, LF is subject to large strains [120], particularly in the posterior portion [121], and interstitial fluid flows [122]. LF fibroblasts express TGF- β [121, 123] and other fibroblastic markers like type-1 collagen, which are reinforced by mechanical stretch [124]. In summary, cellular mechanics are influenced by cell type, matrix and cell mechanical properties, matrix-cell coupling, and regional variation within and between tissues.

1.3 DEGENERATION: MECHANICAL CONSEQUENCES

Degeneration of spinal tissues, which results from a combination of genetic, age-related, and environmental factors, is a leading cause of back pain [23, 26, 125]. Degeneration is marked by elevated catabolic degradation of phenotypic matrix components and by fibrotic or maladaptive remodeling. Early stages of degeneration are marked by altered cellular activity, elevation of local inflammation, and matrix remodeling [126-128]. Later stages of degeneration are characterized by loss or repopulation of cells in a structurally inferior matrix [67, 129]. Normal composition and function of intervertebral disc, facet cartilage, and spinal ligaments are compromised by degradation, inflammation, and maladaptive remodeling of spinal tissues in degenerative disorders.

1.3.1 Compositional & Mechanical Changes

Intervertebral disc degeneration is widely studied because of its role in numerous spinal disorders. In the disc, the earliest signs of degeneration typically occur in the NP, where proteoglycan breakdown and loss of hydration lead to reduced swelling pressure and decoupling of normal NP-AF-CEP interaction. Degradation of aggrecan, the predominant proteoglycan of disc and cartilage [130, 131], occurs via the catabolic action of specific enzymes that cleave the protein core and remove glycosaminoglycan (GAG) side-chains from the aggrecan aggregate [132-135]. Reduced quantity and quality of aggrecan may also be associated with changes in biosynthesis of aggrecan components, the foremost of which being GAGs [133, 136-138]. The resultant lowered fixed charge density reduces the capacity of the NP to imbibe water. As a putative response to decreased fluid content, increased loading of the solid matrix, and altered cellular micromechanics, fibrotic remodeling occurs [139, 140]. Loss of viscoelasticity is reflected in large increases in the shear modulus in the NP with degeneration [141, 142]. These dramatic changes significantly compromise the ability of the NP to dissipate loading, and they alter load distributions within spinal segments, shifting loading to other structures.

This shift in load changes tissue mechanics in spinal tissues. Reduced swelling pressure in the NP increases compressive loading in the AF, manifested by an increased compressive modulus in the AF with degeneration [143]. Altered loading increases tissue strains and can damage the AF [144]. The inner AF, which bears more compression, becomes more cartilaginous with fewer elastic fibers and elevated proteoglycan composition [143, 145]. Degeneration may also arise from annular or endplate injury [81, 146, 147], both of which result in depressurization and fibrotic remodeling that can accelerate degenerative processes. Altered loading causes disorganization and delamination of collagen sheets, altering mechanical interactions between sheets, decreasing radial

permeability and increasing axial permeability. These changes result in an overall reduced structural integrity [144] and increased loss of proteoglycan matrix fragments previously trapped in the dense, impermeable matrix [148]. Degradation of matrix components, including proteoglycans, and fibrotic remodeling are also evident in AF [149]. Degeneration de-couples AF-NP interactions, leading to general dysfunctional support of loading in all modes of segmental mechanics.

Osteoarthritis of facet joints frequently occurs as a coupled process with disc degeneration [150], but has also been observed as an independent degenerative process [25, 125]. Excessive or abnormal (e.g. asymmetric) loading of the facets, resulting from degenerative collapse of the disc, appears to initiate and accelerate degenerative changes [25, 27, 75, 150, 151]. Similar to osteoarthritis in major musculoskeletal joints, facet cartilage is damaged through elevated inflammation, matrix degradation, loss of proteoglycan and altered hydration, surface damage, collagen matrix disorganization, and eventual erosion of cartilage [152]. The progressive destruction of cartilage and loss of compressive support prompts dramatic remodeling in subchondral bone that can include bony tropism and bone spur formation [153]. These changes can lead to segmental instability, altered capsular mechanics, inflammatory paracrine effects on neighboring tissue (e.g. facet capsules), and compression of nerve roots leading to possible pain generation [25].

The LF also commonly undergoes degeneration with consequences including spinal stenosis [26] that can lead to neurogenic claudication and radiculopathy [154]. Degenerative changes in the LF manifest in elastin depletion, collagen fiber disorganization, and reduced cellularity [155, 156]. The hallmark of LF pathology is a thickening of the ligament within the spinal canal, which is mediated by elevated inflammation, increased hypertrophic processes,

fibrotic remodeling, altered proteoglycan content and metabolism [96, 121, 128, 155-157]. Thickening of the LF is also associated with disc degeneration [158] and facet joint osteoarthritis [75]. It is postulated that LF thickening is a response to altered loading [159] and that LF mechanical properties change significantly as a result. Particularly, increased fibrosis, depletion of elastin fibers, and altered proteoglycan metabolism lead to morphologic changes that can impact neural structures and to increased tensile and compressive stiffness [155, 156] that can alter segmental mechanics.

Degenerative changes in individual tissues do not occur in isolation; degeneration in a particular spinal structure may have direct or indirect detrimental effects on other spinal tissues. As evidence of this, facet joint osteoarthritis is highly associated with disc degeneration [150]. Loss of disc height and segmental hypermobility appear to alter facet loading and lead to degenerative changes of the facet joints [160]. In lower lumbar levels where facet forces are higher, facet osteoarthritis can precede disc degeneration through putative overloading of facet joints and possibly lead to onset of disc degeneration through altered segmental mechanics [25, 125]. Thickening of the ligamentum flavum (LF) is also associated with disc degeneration [158] and facet joint osteoarthritis [75]. Altered loading associated with loss of disc height or facet joint degradation may induce buckling or overloading of the LF, which leads to inflammation and hypertrophy [124, 161]. Thus, an inclusive analysis of mechanical loading must encompass all the relevant tissues of the FSU. Research that characterizes interactions of component tissues within FSUs subjected to degenerative stimuli or mechanical loading is needed to support this broader understanding.

1.3.2 Cellular Changes and Mechanotransduction

Beyond changes in load distribution within the FSU and changes in mechanical properties of individual spinal tissues, changes in the cellular microenvironment occur as well. Current views hold that degeneration is a cell-mediated process of matrix degradation and tissue remodeling [162]. The type of loading and signal transduction experienced by cells changes dramatically with degeneration [30]. Alterations in cell population and cell phenotype coupled with derangement of normal mechanotransduction help to drive the degenerative cascade in these tissues.

Cellular changes in the disc begin early in life. The loss of notochordal cells, mediated at least in part by reduced nutrition and increased loading [163-165], can be viewed as the earliest sign of aging or degeneration [166]. In more advanced degeneration, mature chondrocyte-like NPCs live in an environment with a reduced fluid fraction, subjecting cells to reduced fluid pressurization, fluid shear stress, and higher strains [30, 109]. The consequences include cell death, senescence, and increased type-1 collagen synthesis with reduced or defective proteoglycan synthesis [30]. Cellular changes in the AF are less dramatic than in the NP but have similarly altered activity. With degeneration, altered mechanical properties and tissue permeability result in macroscopic radial, circumferential, and axial strains that lead to altered cellular deformations, which vary between inner and outer AF, increased fluid flows, and altered electrokinetic effects [148, 167]. Changes in the local cellular environment result in increased cell death, senescence, and fibrotic expression [168].

Cellular changes in facet osteoarthritis vary with location in the tissue and stage of degeneration. Little is known about the cellular changes in facet joint osteoarthritis, but it is suspected that disruption and disorganization of the collagen matrix exposes surface chondrocytes to higher strains [169] resulting in inflammatory signaling or cell death [67]. Cells in the deeper

zones experience reduced, more transient fluid pressurization and likely experience greater deformations and fluid flows [115]. Cells in the subchondral bone appear to experience higher loading with evident bone deposition in response to increased stresses [170].

The LF comprises predominantly fibroblasts, but, due to its vascularity and innervation, it also contains vascular, neural, and immune cells. Fibroblasts are known to be involved in inflammation, which stimulates degenerative changes in the LF, and macrophages and resident vascular endothelial cells have predominantly been associated with hypertrophic remodeling [155]. Regions of elevated inflammation are marked by reduced elastin content and matrix organization as well as expression of inflammatory markers, MMPs, and transforming growth factors [155, 156]. Cells in these fibrotic, inflammatory regions likely serve as centers of hypertrophy and, possibly, eventual ossification [128, 157]. Contextual evidence suggests the altered micro environment, including local mechanics, drives pathologic changes in the LF [158].

1.4 MECHANICS IN TREATMENT

Treatment of back pain and spinal disorders is highly varied. As described previously, the number and nature of subgroups within back pain patients warrant tailored approaches [18, 58]. In clinical settings, classification of patients in subgroups by identification of the underlying mechanisms of back pain—including identification of the tissues and structures involved and the origin of pain or dysfunction—remains elusive [3, 7]. Despite a vast amount of research in studying the etiologies of back pain and spinal disorders, the complexity of and variability within the disorders have to date prevented a unified, standardized approach to patient care. As a result, an abundant diversity of treatment options exists, reflecting a range of philosophies and approaches to correct or

ameliorate symptoms. Treatments span a broad spectrum, including prescription of cognitive behavioral therapy [171], pharmacologic [172, 173], herbal therapies [174], steroid injections [175], acupuncture [176], spinal manipulations [177], exercise and motion-based therapies [178-180], and surgery [181]. Some treatments seek simply to mitigate pain, but others seek to also strengthen, repair, or protect damaged or degenerating tissues. Directly or indirectly, these latter approaches modify mechanical loading in spinal segments as a part of treatment.

While mechanical loading can lead to detrimental effects through overuse, asymmetry, or hypomobility, it can also play a protective or potentially therapeutic role. Motion-based treatment paradigms that have shown efficacy in treating back pain, including physical therapy, chiropractic medicine, osteopathic medicine, exercise, and yoga [10, 12, 13, 180, 182], influence spinal loading in back pain patients. Though strategies differ, they share the aim of restoring healthy mechanical loading in spinal segments through enabling or training potentially protective, symmetric, coordinated spinal movement patterns [15, 183-186]. Different theoretical models and practical approaches are employed, but a common variable in all of these therapies is application of loading, be it passive or active, to spinal tissues with the goal of improved spinal mechanics in functional movements.

Despite the popularity and modest efficacy of these approaches, the mechanism by which these interventions exert an effect remains inconclusive [14-16]. Motion-based therapies like rehabilitative exercise regimens, general exercise, and yoga typically target trunk movement coordination, core strength, and core flexibility [185, 187-189]. They presume that aberrant movement patterns associated with back pain place damaged or degenerating spinal tissues at risk for recurring injury or exacerbation of symptoms [15]. Developing protective movement patterns through neuromuscular training, increasing core bracing in potentially irritating movements, and

improving mobility in hypomobile patients are common therapeutic goals. Non-specific effects of motion-based therapy include reduced systemic inflammation [190] and enhanced metabolic exchange [191] in spinal tissues that could promote repair or improve the local tissue milieu [192]. Whatever the systemic or neuromuscular effects, mechanical loading applied to spinal structures impacts mechanotransduction and resulting biological responses within each spinal tissue.

Similarly, multiple models have been proposed to explain the mechanisms of action in spinal manipulation. Early mechanical theories explained that entrapped synovial folds or meniscoids, hypertonic muscles, segmental dislocation, or articular or periarticular adhesions caused segmental asymmetries or articular dysfunction leading to (i) activation of nociceptive signaling in nerves of the facet capsules and posterior annulus or (ii) compression of nerve roots [193]. Manipulation was thought to release articular entrapments, relax muscle tonicity, disrupt adhesions, and unbuckle spinal segments [193]. These theories are difficult to substantiate given the challenges in diagnosis and specifically treating putative mechanical causes of segmental dysfunction [14]. Neurophysiologic effects of manipulation, which may occur in the presence or absence of mechanical effects, are now thought to account for much of the efficacy of manipulation [14, 194]. These models suggest that changes in motor neuron activity, afferent discharge, pain sensitivity and muscle activity observed following manipulation may result from gating of nociception at the spinal cord via mechanoreceptors, direct stimulation of spinal reflexes, direct stimulation of central pain centers, or other modulatory effects of sensorimotor control [14, 194, 195]. In all models, regardless of their accuracy, the physical effects of spinal dysfunction on spinal tissues in segmental motions may promote degenerative changes. The applied mechanical loading of manipulation and the intended consequence of restored symmetric mechanics point to possible roles for mechanical signaling to mediate detrimental responses.

Spinal motions in manipulation, rehabilitation exercises, yoga, and activities of daily living (ADL) are complex, involving varying modes and amplitudes of motion. Spinal manipulations, which include torsion and anterior-posterior translations with or without coupled flexion/extension [186, 196, 197] cause mechanical changes in all spinal structures [198]. Exercise, yoga, and ADLs, while more heterogeneous, involve pure and complex rotations in all physiologic planes in a wide range of ranges-of-motion (ROM) [199-201]. Empiric studies suggest large amplitudes in certain loading modes may be harmful [32, 202, 203], and basic science studies support the notion that large ROM is catabolic while small to moderate ROM is anti-catabolic [36, 204-206]. But, the effect of mode and amplitude of loading, particularly in rotational and complex loading, on biological processes within relevant spinal tissues remains largely unknown and unstudied.

Motion-based treatments have shown modest clinical efficacy [207], but their general enhancement, customization to individual patients or conditions, and integration with medical care require a mechanistic knowledge of these interventions. Basic science studies are needed to achieve this advancement. If a clear understanding of how a motion-based therapy influences specific biological processes (e.g. inflammatory signaling) were known, therapy could be rationally prescribed for specific conditions and integrated with other therapies. Model systems are needed to facilitate the study of how loading parameters in motion-based therapies influence relevant biological processes such as inflammation, catabolism, and anabolism.

1.5 MECHANOBIOLOGY RESEARCH

Mechanical loading plays an important role in initiating and mediating degenerative processes in spinal tissues. Teasing thresholds of detrimental and beneficial loading in conjunction with

different inflammatory and therapeutic interventions has been the domain of disc mechanobiology for nearly a decade. However, the influence of mechanical loading has been restricted primarily to axial mechanics in disc studies [22]. Only a few studies have looked at bending or complex loads [36, 37, 208, 209], and flexion/extension and combined rotational loading remain entirely uninvestigated, despite their importance in spinal movements *in vivo* [210-212]. Moreover, little is known about mechanobiology outside of disc tissue in general; no research has explored biological responses to varying doses of mechanical parameters—magnitude, frequency, and duration—in FC or LF [67, 124]. Summarizing the history and findings of mechanobiology in disc tissue provides a basis for relating biological effects of axial loading to those in complex loading. A review of extensive findings in disc and limited findings in other tissues also provides a framework for evaluating FC and LF mechanobiology [67]. In general, mechanobiology investigations occur at different levels—in cell culture *in vitro*, in animal models *in vivo*, and in tissue explants *ex vivo*.

1.5.1 *In vitro* Studies

In vitro studies have identified threshold effects of mechanical parameters— magnitude, frequency, rate, and duration—on cellular behavior. Loading applied to cell cultures is intended to approximate tissue mechanics *in vivo*. NPCs, for example, are seeded in three-dimensional alginate or agarose constructs that are subjected to hydrostatic or axial compressive loading [30]. Chondrocytes have not been isolated from facet cartilage for mechanobiology studies [67]; however, chondrocytes from other sources of articular cartilage have been studied frequently by similarly seeding them in hydrogels and subjecting them to hydrostatic pressure, axial compression, and shear flow [213, 214]. In contrast, AFCs, which exist within or between collagen

sheets and undergo predominantly tensile stretch as the disc bulges in all loading modes, are typically seeded in monolayer and subjected to tensile stretch [30]. LF fibroblast mechanobiology has not been extensively investigated; fibroblasts in monolayer have been subjected to tensile stretch [124, 215] and centrifugal force [161], but loading parameters were not varied experimentally.

In vitro studies permit probing in to the effects of applied loading by identifying thresholds of well-controlled loading parameters and elucidating cellular mechanisms involved in biological responses. Studies of NPCs confirm sensitivity to magnitudes, durations, and frequencies of loading [22, 205, 216]. Researchers have shown the involvement of integrin $\alpha_5\beta_1$ and cytoskeletal filaments in transducing mechanical signaling to cells [99, 217]. In chondrocytes from major diarthrodial joints, researchers have shown biological sensitivity to magnitude, duration, and frequency of loading [218]. Chondrocytes subjected to physiologic magnitudes and frequencies of loading exhibited protective effects against inflammatory and catabolic stimuli signaling through p38 MAPK, JNK, and NF κ B pathways [219, 220]. However, the absence of compression, high magnitudes of compression, and high amounts of fluid shear cause chondrocytes to undergo cell death and respond with pro-inflammatory, pro-catabolic behavior [221-227]. Responses have been shown to occur through ion channels, β_1 integrins, and kinase cascades (associated with focal adhesions) [228]. The biological effects of stretch magnitude, frequency and duration in AFCs were thoroughly investigated [204]. They examined gene expression of catabolic, anti-catabolic, and inflammatory markers and production of prostaglandin E2 (PGE₂) and identified beneficial levels of loading. Moderate strains at low frequencies (6% strain, 0.1 Hz) were most protective. Responses to applied stretch have involved integrins, cytoskeletal remodeling, F-actin dependent Ca²⁺ transients, and interleukin receptors [99-101, 229]. Finally, magnitude of stretch elongation

has been titrated in LF fibroblast culture examining hypertrophic and ossification markers. Mechanically induced elevation of transforming growth factor- β (TGF- β) was found to depend on Angptl-2 mediation of TFG- β /Smad signaling [215], and mechanical stretch was found to modulate β -catenin in LF fibroblasts in the elevation of ossification markers [230]. A growing body of work *in vitro* is exploring the effects of mechanical loading and activated signaling pathways in all FSU cell types.

In vitro systems permit probing of cellular responses to specific modes of mechanical transduction with coupled stimulators and inhibitors. Cellular responses are helpful in framing how well characterized loading patterns and tissue properties may influence cell behavior; *in vitro* systems are not well suited for characterizing the effects of complex loading where tissue-and cell-scale mechanics remain unstudied. Recent multi-scale models have demonstrated a dependency of mechanical changes on cell and PCM geometry, relative positioning, material properties, and spatial distribution. Approximating *in-situ* cell-PCM-ECM interconnections, simulating appropriate ECM and PCM composition and properties, and producing appropriate ionic and osmotic environments remains difficult. Thus, translating cell-culture outcomes directly to *in vivo* scenarios is not tenable.

1.5.2 *In vivo* Studies

In vivo studies in animal models demonstrate the role of altered segmental mechanics in initiating and mediating disc degeneration and facet osteoarthritis. For decades, researchers have altered segmental mechanics through imposed bipedalism [231], static compression [232], dynamic compression [233, 234], instability [235, 236], endplate perforation [237], and annular puncture [238, 239]. Subsequent biological responses were used to simulate degenerative cascades [231]

and to establish models of degeneration in which therapeutic candidates could be tested [240, 241]. To explore the effect of mechanical parameters on biological responses in discs, transcutaneous load applicators have been attached to rodent tails and rabbit lumbar spines to induce static bending [208], static compression [242], dynamic compression [233], and torsion [206]. A set of studies has also been conducted to study biological effects of mechanical parameters on supraspinous ligaments in feline spines [243], but ligamentum flavum mechanobiology remains unstudied *in vivo*. Effects of traumatic, excessive and asymmetric loading of facet joints have also been explored in a few rodent studies [79, 244, 245], and animal models have also been used in a small number of studies to examine the interaction of degenerative processes in facet and disc tissue [79, 246, 247], but none of these studies involving facets examined the effects of mechanical parameters.

Researchers have identified different responses in disc tissue to parameters of mechanical loading: mode, magnitude, frequency, and duration. Sustained compressive loading or immobilization leads to cell death and increased catabolic, pro-inflammatory, and anti-anabolic markers in AF, NP, and FC [165, 244, 248-250]. Higher levels of static compression down-regulate structural protein expression, up-regulate catabolic protein expression [233, 248, 250], and increase cell death [234, 250]. Dynamic loading has proved, in general, to be healthier for the disc than static loading [9]. The NP appears to be more biologically responsive to frequency than the AF, with low to moderate frequencies (0.01-0.2 Hz) promoting structural gene expression and down-regulating catabolic gene expression [233]. The AF at all frequencies and the NP at the high frequency (1.0 Hz) exhibited reduced structural and increased catabolic expression. Finally,

studies illustrate the importance of duration on biologic outcomes [251, 252]; generally, increased duration without rest or recovery leads to decreased structural expression and maintained or increased catabolic expression [251].

Rotational loading, such as torsion or bending, have been explored *in vivo*, albeit to a much lesser extent (Table 1). Static bending in murine tails has been shown to be detrimental to cell viability, anabolic matrix expression, and matrix integrity, especially in the convex side of the AF [208]. Dynamic torsion in rat tails has been shown to up-regulate elastin in AF and to be catabolic and pro-inflammatory in AF at high magnitudes [206]. The NP was not as responsive to varying magnitudes of applied torsion [206]. No disc studies have explored flexion/extension or complex loading in which loading is applied in multiple DOF.

Table 1. *In vivo* mechanobiology of rotational loading

Objective	Mode	Loading Parameters	Levels	Species	Major Findings
To compare tensile and compressive strains[208]	Bending	Magnitude: 42° (large) and 18° (slight) Frequency: Static, Duration: 1 wk	c9-10	Mice	Concave: ↑cell death, ↓ <i>ACAN</i> , ↓matrix organization, Both sides: ↓ <i>Col-2</i>
To assess recovery duration after damaging bending[253]	Bending	Magnitude: 42° Frequency: Static Duration: 1 wk + 3 wk (short), 1 wk + 3 mo (long)	c9-10	Mice	Short recovery: high amounts of apoptosis
To investigate magnitudes of torsion and compare torsion to compression [206]	Axial Torsion	Magnitude: ±5°, 15°, 30° Frequency: 1 Hz Duration: 90 min	c8-9	Rat	All Magnitudes: ↑ <i>Elastin</i> (AF), ↓ <i>IL-1β</i> (NP) High Magnitude: ↑ <i>ADAMTS-4</i> , <i>IL-1β</i> , <i>TNF-α</i> (AF), ↑ <i>ACAN</i> , <i>TIMP-3</i> (NP) 30° AT vs 1MPa AC: ↑AF all genes, ↑NP catabolic genes
Limitations: (1) Only small animal caudal discs have been used (no posterior elements). (2) No investigation of flexion/extension or complex loading.					
Legend: NP-nucleus pulposus, AF-annulus fibrosus, mRNA expression: <i>ACAN</i> -aggrecan, <i>MMP</i> -matrix metalloprotease, <i>ADAMTS</i> -a disintegrin and metalloprotease with thrombospondin motif, <i>Col</i> -collagen, <i>IL</i> -interleukin, <i>TNF</i> -tumor necrosis factor					

The benefit of stable physiologic conditions with preserved systemic responses makes *in vivo* systems ideal for long-term studies assessing chronic conditions, remodeling processes, effects of inflammation and host cells, and candidate therapeutic agents. However, the costs and challenges of long-term animal research make it impractical for assessment of short-term biological responses, which are clinically relevant for examining loading parameters in motion-based therapies. Difficulties in translating popular caudal disc models, which lack posterior structures and have different anatomy and matrix composition than lumbar discs [254], limit their applicability. It is difficult to assess the effect of isolated environmental conditions like nutrition, local inflammation, or pH *in vivo*. Measuring the load-responsive release of local

breakdown fragments, matrix components, and inflammatory mediators is elusive in the absence of local sampling and immediate access to tissue. Finally, it is more challenging to control loading modes accurately and precisely *in vivo*.

1.5.3 *Ex vivo* Systems

Ex vivo organ culture is an intermediate level of mechanobiological analysis that preserves *in-situ* load transmission and the native cell microenvironment but permits greater mechanical and environmental control than *in vivo* research [255]. Typical *ex vivo* systems apply uniaxial loading at varying magnitudes, frequencies, and durations to disc explants within an incubator [256-259] with the goal of (1) elucidating biological thresholds of loading as a function of loading variables and (2) providing an experimental platform with which to investigate the effect of regenerative therapies [260-262].

Organ culture systems are relatively recent experimental tools in disc research. Early systems were developed nearly a decade ago; those systems employed simple static loading [258] or no mechanical loading whatsoever [255, 263, 264]. Initial loading methods applied diurnal static compression to disc explants with modified endplates to promote cell viability [256-258]. Wang et al. and Ganetenbeim et al. introduced dynamic compression to simulate physiologic loading conditions more accurately and explore non-physiologic or injurious effects [256, 259, 265]. Recent studies using these types of *ex vivo* systems have added scale and sophisticated diurnal loading approximation to explore dynamic compression in great scope and detail [34, 266].

New trends in organ culture are expanding beyond compression applied to animal disc explants. Notably, researchers have established methods to preserve loaded human discs for more than four months in culture [33]. While the advances are in the model system and not the applied

mechanics, the human disc organ culture system minimizes the translational gap between scientific *ex vivo* and clinical *in vivo* investigations and permits long-term investigations of biological and mechanical interventions. Further, human disc culture can confirm findings from animal studies, where differences in cell populations and tissue composition may influence mechanotransduction [267, 268]. However, human disc studies are limited by the short supply and high variance between samples.

Other researchers have developed systems that apply complex axial loads to large animal discs (Table 2) [37, 209]. Walter et al. used wedge loading to apply asymmetric compression, and Chan et al. combined torsion with compression by affixing tooth-textured platens to treated endplates [37, 209]. Asymmetric compression was detrimental to annular cell viability and aggrecan content on the concave side and to annular catabolic and inflammatory gene expression on the convex side [37]. In combined compression and torsion, Chan et al. observed few changes in gene expression in NP, but decreased cellular activity with increasing torsion. In AF, trends of increasing aggrecan and MMP-13 were evident with increasing torsion [209]. Both systems represent advances in the field of disc mechanobiology, but like other organ culture systems, removal of vertebrae and posterior structures along with modification of the cartilaginous endplate perturbs *in-situ* load transmission, alters endplate biochemistry and biology—which may influence disc biology—and prevents assessment of resected tissues.

Table 2. Ex vivo mechanobiology of rotational and complex loading

Objective	Mode	Loading Parameters	Levels	Species	Major Findings
To compare wedged vs. pure compression	Asymmetric AC	Magnitude: 0°, 15° wedge + 0.2 MPa AC Frequency: Static Duration: 1 wk	c2-3, c3-4, c4-5	Bovine	Concave: ↑cell death, ↑apoptosis, ↓aggrecan Convex: ↑ <i>MMP-1</i> , <i>ADAMTS-4</i> , <i>IL-1β</i> , <i>IL-6</i> ; ↓aggregate modulus
To investigate magnitudes of torsion with constant compression	AT (dynamic) + AC (static)	Magnitude: ±2°, 5°, 10° + 0.2 MPa AC Frequency: 0.1 Hz Duration: 1h/d, 4 d	caudal levels	Bovine	Increasing torsion: ↓ metabolic activity (NP), ↑ <i>ACAN</i> , <i>MMP-13</i> (AF)
To investigate combined loading of cyclic & dynamic torsion & compression	AT + AC: CC: dynamic AC (no AT) CT: dynamic AT + static AC CCT: dynamic AT+AC	Magnitude: ±2° (AT) 0.6 ±0.2 MPa (AC) Frequency: Static or 0.2 Hz Duration: 8h/d, 15 d	caudal levels	Bovine	CCT: ↓Cell Viability (NP), ↑ <i>Col-1</i> , <i>Col-2</i> , <i>MMP-13</i> (AF); generally higher AF gene expression vs. CC and CT AT vs AC: ↑Cell Activity (NP), ↑ <i>ADAMTS-4</i> (NP)
Limitations: (1) Only caudal discs have been used (no posterior elements). (2) No investigation of bending (esp. flexion/extension) or complex rotations to date.					
Legend: AT-axial torsion, AC-axial compression, NP-nucleus pulposus, AF-annulus fibrosus, mRNA expression: <i>ACAN</i> -aggrecan, <i>MMP</i> -matrix metalloprotease, <i>ADAMTS</i> -a disintegrin and metalloprotease with thrombospondin motif, <i>Col</i> -collagen, <i>IL</i> -interleukin, <i>TNF</i> -tumor necrosis factor					

All previous organ culture systems have contributed to elucidation of loading thresholds and have begun to be used to assess regenerative therapies, but load application has been limited primarily to axial compression [22], evaluation has been limited to disc tissue, and modification of endplates and removal of vertebrae has altered *in-situ* load transmission [38]. To investigate complex motions and *in-situ* load transmission in all relevant tissues, intact functional spinal units (FSUs) must be preserved in mechanically loaded organ culture. Further, intact FSUs are necessary to study coupled biological responses to applied mechanics in multiple spinal tissues. A recently developed system, the subject of this dissertation, expands the scope of organ culture

beyond the disc to include the whole spine by culturing and loading intact FSUs. This system was validated for maintaining stable environmental conditions and adequate cell viability in axial compression for 24 hours [269]. It was designed, however, to investigate physiologic rotational loading—flexion/extension, lateral bending, and axial rotation. Retention of spinal ligaments, facet joints, and intact endplates enables *in-situ* loading; it provides physiologic transmission of applied loading throughout joint structures. Further, preservation of intact FSUs enables unique questions to be posed and answered regarding the simultaneous response to loading (or other environmental experimental condition) of different spinal tissues. The primary drawback of this approach is the short window of stable cell viability, a result of reduced metabolic exchange in disc tissues due to diffusion barriers in intact endplates and vertebral bodies. Nevertheless, a timeframe of 24 hours is compatible with the immediate goal of this system: investigation of simulated spinal motions during recreational, occupational, or therapeutic activities.

The development of a system which preserves intact FSUs and subjects them to complex, 6 DOF loading opens multiple frontiers of important research in spinal mechanobiology. The ultimate goal of the robotic, FSU culture system is to help to bridge the gap between *in vivo* loading and *in vitro* mechano-responses. Successful completion of this project will expand scientific knowledge by mechanistically elucidating the effects of amplitude in relevant motions on outcomes related to disc degeneration—matrix catabolism and local inflammation. Based on this knowledge, clinical studies could be rationally designed and therapy could be prescribed for patient subgroups most likely to benefit from a particular motion-based regimen. Ultimately, in a translated clinical example, if a patient has an acute flare with inflammation exacerbated in extension, a loading strategy that reduces inflammatory mediators in appropriate tissue targets like facet cartilage would be prescribed. Alternatively, if a patient is undergoing disc collapse through

an imbalance in matrix homeostasis, a loading regimen that inhibits catabolism or promotes anabolism would be assigned. Without mechanistic studies in relevant spinal tissues, direct effects of loading remain inferred from empiric data. With mechanistic understanding of these effects, clinicians could coordinate motion-based therapies with other approaches to optimize treatment of individual patients.

2.0 GOAL AND SPECIFIC AIMS

The goal of this project was to complete development of a novel *ex vivo* functional spinal unit mechanobiological system. The system had to be capable of physiologic rotational loading—including bending and torsion—and assessment of cellular and matrix responses in multiple spinal tissues—AF, NP, FC, and LF. In order to accomplish this goal, a system capable of 6 DOF loading of intact FSUs with biological assessment of spinal tissues had to be validated. Retained FSU structures are essential to *in-situ* loading and evaluation of tissues involved in multiple spinal disorders. Biological assessments must be sensitive and relevant to previous or parallel studies. Stable biologic activity of cultured FSUs is essential. The utility of the system had to be demonstrated in rotational and complex loading of FSUs. Relating mechanical responses from novel loading modes to biological responses was to permit insight into how mechanical parameters account for changes in biology.

2.1 SYSTEM DEVELOPMENT

Previous development and validation of the bioreactor established well-characterized mechanical inputs, controlled environmental parameters, and the capability of supporting an array of biological outcome measures that demonstrate baseline stability and responsiveness to mechanical loading [269]. Adapting the bioreactor from the axial testing machine (ATM) to the robot testing system required validation of additional factors related to rotational loading modes. In scaling up from

axial compression to 6 DOF robotic testing, a number of design requirements needed to be added and validated. Briefly, in bending and torsional DOF, the system had to:

- (1) integrate precisely with the robot testing system,
- (2) exhibit sufficient precision and resolution of movement,
- (3) rigidly attach FSUs, and
- (4) permit full, unrestricted FSU range-of-motion.

Development of the bioreactor system showed successful assessment of (a) disc cell viability/metabolic activity, (b) disc gene expression of catabolic (e.g. MMP-1, MMP-3), inflammatory (e.g. COX-2), and structural (e.g. aggrecan) genes, (c) matrix fragment (CTX-II, CS-846) detection from conditioned media, and (d) enzymatic activity of catabolic enzymes from conditioned media. Tissue-based outcomes were exclusive to disc tissue and surrounding conditioned media in the initial iteration of the system. To build on previous work, the requirements for assessment of FSUs subjected to 6 DOF loading representative of *in vivo* motions included (1) gene expression of previous markers in NP, FC, AF, and LF, (2) left and right side-specific gene expression of previous markers in FC, (3) sensitive assessment of aggrecan fragments and matrix components by Western blot in NP, FC and AF. While conditioned media analyses were not used for this dissertation, preserving the capability for passive concentration of released proteins in dialysis membranes encapsulating FSUs was an important system requirement. A system attaining these design constraints represents a significant advancement in *ex vivo* experimental platforms for investigations of simulated *in vivo* movements (e.g. rehabilitation exercises, occupational tasks) on inflammation and matrix homeostasis in relevant spinal tissues.

2.2 SPECIFIC AIM 1 – FLEXION/EXTENSION

The goal of the first experimental aim, as initial proof of system utility, was to test the biological effects of range-of-motion in flexion/extension (F/E) of FSUs. Spine-intensive occupational, recreational, and rehabilitation tasks involve large F/E ROM [69, 70, 178, 203, 211, 270, 271] that place lumbar spinal segments in the linear, high-stiffness region of moment-rotation curves. By contrast, activities of daily living and mild exercise typically involve in F/E angles of smaller ROM [200, 210, 272] that occur within the low-stiffness, neutral zone of spinal segments. FSUs were assigned to small and large ROM groups defined by 0.17/0.05 and 0.5/0.15 Nm moment targets in F/E. Moment targets were experimentally determined so that specimens assigned to small ROM remained within the low stiffness region and specimens assigned to large ROM entered the high stiffness portion of moment-rotation curves. Kinematics were replayed for one hour. Mechanical outcomes including ROM, moment relaxation, hysteresis, work, and neutral zone stiffness were calculated. After loading, relative gene expression of pro-inflammatory, catabolic, and anabolic markers and aggrecan breakdown fragments in NP, AF, FC, and LF were assessed relative to tissues from unloaded control FSUs. It is hypothesized that larger motions would increase catabolic and inflammatory gene expression and increase aggrecan fragmentation in all tissues, and smaller motions would reduce catabolic and inflammatory gene expression and not impact aggrecan fragments in all tissues relative to unloaded controls.

Because time and loading rate were fixed rather than cycle number, which would differ between large and small ROM, a separate set of experiments was performed to examine the effect of cycle number. FSUs were subjected to large ROM load targets for one hour (1h Cycle), two hours (2h Cycle), or one hour of cycling followed by one hour of static culture (1h Cycle_1h Static). Comparing 1h Cycle to 1h Cycle_1h Static demonstrates the effect of doubling culture

duration, and comparing 1h Cycle_1h Static to 2h Cycle isolates the effect of doubling cycles. The same set of mechanical outcomes and identical relative gene expression was measured and calculated. It was hypothesized that increasing the number of cycles would elevate catabolic, inflammatory, and structural gene expression.

2.3 SPECIFIC AIM 2 – COMPLEX LOADING

Complex, asymmetrical loading, including combined torsion and bending, is associated with elevated risk of injury and back pain [32, 68]. Further, various treatment paradigms diagnose and seek to correct segmental dysfunction frequently marked by unilateral rotation within a spinal segment [76, 77, 79, 196]. The objective of this aim is to elucidate the inflammatory, catabolic, and anabolic responses to AT combined with F/E *ex vivo* in viable functional spinal units (FSUs). FSUs were grouped by amount of applied AT—0, 0.4 or 0.8Nm—which reflect neutral, mild (~20% of failure), and severe (~40% of failure) rotations. These moment targets are comparable to those used in human lumbar testing representing mid and end ROM in AT [31, 273]. FSUs were preconditioned with three cycles of left-sided AT followed by three cycles of F/E to 0.5/0.15Nm at the final rotated position. Combined kinematics (AT+F/E) were repeated for 1 h. Identical mechanical and biological outcomes to Specific Aim 1 were calculated, with additional immunoblotting for chondroadherin, a matrix component depleted by catabolic stimuli and elevated compression in scoliotic discs. It was hypothesized that increasing magnitudes of AT and F/E would increase catabolic and inflammatory markers in all tissues compared to neutral F/E. We further hypothesized that FC contralateral to the rotation (right) would increase catabolic and inflammatory markers relative to gapped, ipsilateral FC (left).

2.4 REGRESSION MODELING

In an effort to integrate the previous aims and examine how well mechanical parameters account for measured changes in biological responses, multiple regression analysis was used to model biological responses in terms of mechanical responses to applied loading. The purpose of this analysis was (1) to identify the most important mechanical predictors (i.e. those most correlated with principal components of the predictor data set), (2) to quantify the amount of variation in biological responses that can be attributed to mechanical predictors of F/E loading and (3) to determine how the predictive capacity varied with gene, tissue, and mechanical predictors. The total set of candidate predictors was reduced by autocorrelation analysis. Principal component analysis (PCA) was then applied to the reduced set of mechanical predictors to identify those that accounted for the most variation in mechanical data. Important predictors were identified per tissue and gene using hierarchical multiple regression analysis applied to all mechanical predictors identified by PCA. Final regression models were formed per tissue and gene using only the important predictors identified in the preliminary regression analysis. Significant models, amount of variation accounted for in models, generalizability of findings, and size and significance of model coefficients were reported. Assumptions of multiple regression were analyzed and reported per model. The objective of the study was to identify whether (1) there were differences between tissues in how well mechanical predictors accounted for more biological variation, (2) there were differences between genes in how well mechanical predictors accounted for more biological variation, (3) there were certain mechanical predictors that factored more heavily in regression models across genes and tissues, and (4) energetic or relaxation parameters, in particular, explained variation in biological responses.

3.0 SYSTEM DEVELOPMENT

3.1 SYSTEM REQUIREMENTS

System development began with design requirements for performance that reflect the goal of multi-DOF rotational movement of rabbit FSUs within a bioreactor that simulates physiologic conditions and enables biological assessment of tissue and media. Previously, the following aspects of the bioreactor system were validated: rigidity in axial compression, temperature control of media to 37° C ($\pm 0.5^\circ$ C), dissolved oxygen concentration of media to 5% ($\pm 1\%$), and force transmission via intradiscal pressure readings. Cell viability was also confirmed using a metabolic activity assay, MTT (3-(4,5-dimethylthiazol-2-yl)-2,5-diphenyltetrazolium bromide), up to 24 hours in culture [274]. Biological outcomes—relative gene expression of *MMP-1*, *-3*, *COX-2*, *ACAN* within disc tissue and matrix fragment (CTX-II, CS-846) detection and quantification of enzymatic activity (MMP-1, MMP-3) of conditioned media—were measured following four hours of constant compression to demonstrate system utility for evaluating disc mechanobiology [274]. The system, however, was designed to enable 6 DOF motions and analyze other spinal tissues, and these capabilities were not previously validated. In order to do so, the following design requirements had to be met. The system had to:

1. Exhibit sufficient precision and resolution of movement

- a. The accuracy and precision of the robotic system in active path determination needs to be less than 10% of the moment/force targets and subsequent rotations/translations selected for non-destructive mechanical testing in that DOF. The 10% criterion is based on the standard of error in a system being less than an order of magnitude below the measured quantity [275].
 1. Force/moment accuracy
 - a. Primary moment target accuracy: error <10% of moment magnitude (<0.03 Nm)
 - b. Off-axis force minimization accuracy:
 - i. <2 N in magnitude [276, 277]
 - ii. >0.3 Nm/N ratio of primary moment relative to RMSE (Fx,Fy,Fz) [87, 276, 277]
 - c. Off-axis moments: error <0.02 Nm [277, 278]
 2. Force/moment precision: error <10% maximum force/moments (2 N/0.03 Nm) [87, 276, 277]
- b. The accuracy and precision of the robotic system in replay of stored joint angles ('Replay') needs to be less than 10% of the rotations/translations selected for non-destructive mechanical testing in that DOF [276]
- c. The resolution of robotic movements: <10% of the maximum amplitude per DOF [279]

2. Integrate precisely with the robot testing system

- a. Method for fixture alignment to robot testing system and center-of-rotation estimation had to be made

3. Rigidity in rotational motions

- a. Primary rigidity (direction of movement and stiffness):
 - i. Interface motions <10% of ROM in F/E, AT, and AP (1.5°, 0.3°, 0.1 mm)
 1. Fixation error ought to be at least an order of magnitude less than the measured motions so that specimen movements represent FSU motion with error < 10% [269].
 - ii. Interface stiffness <10% of FSU stiffness in that DOF
 1. Based on a model of two springs in series, fixture stiffness should be ten times higher than joint stiffness so that fixture laxity contributes less than 10% error to recorded displacements [269].

- b. Compare to gold standard attachment methods
 - i. Relative primary motions
 - ii. Off-axis motions
 - iii. Stiffness

4. Permit full, unrestricted FSU ROM.

- a. Fluid flow through the bioreactor must occur at 1.10 mL/min, representative of interstitial fluid flows [257], and not be inhibited by robotic motion
- b. Dialysis membrane (inner collection membrane), latex membrane (fluid containment), and nitrile membrane (gas permeability barrier) must not contribute to moments or forces sensed by the robot testing system's universal force sensor (UFS).

3.2 KINEMATIC AND KINETIC PRECISION OF THE TESTING SYSTEM

3.2.1 Introduction

Integrating the novel bioreactor system with an existing robotic testing system to explore 6 DOF motion mandated characterization of the system used to apply mechanical loading in the context of requirements for rabbit FSU testing. The rotational DOF most relevant to this dissertation are F/E and AT, thus system control and precision were assessed in these motions. Also, initial testing plans for Specific Aim 2 involved AP translation to simulate mobilization, so this translational DOF was assessed as well. Robot testing occurred in two steps. First, a pure-moment path of spinal segments was determined by quasi-statically rotating segments to moment targets with an updating center-of-rotation and minimizing off-axis forces throughout the motion path. Second, the stored path was replayed at a faster rate for a specified number of cycles. In path determination, attaining target moments and minimizing forces are critical; kinematics are expected to vary. In replayed motions, high kinematic precision is essential. Therefore, the first objective was to

quantify and assess error in controlling FSU kinetics during active path determination ('Pathseek') measured by (a) accuracy in reaching the primary moment, (b) accuracy in off-axis force and moment minimization, and (c) precision of forces and moments in repeated 'Pathseek' motion paths. The second objective was to describe the kinematic precision in repeated motion paths ('Replay'). To perform the Objective 1a and 1b, the accuracy of the system in reaching moment/force targets under adaptive-displacement control was compared with a specimen (i.e. "loaded") to scenarios without a specimen (i.e. "unloaded"). To evaluate the kinetic performance of serial linkage robots in general, applied loads and system stiffness must be considered. Thus, to perform the Objective 1c and 2, the robot force/moment (N/Nm) and translation/rotation (mm/°) precision were assessed "loaded" and "unloaded" to add relevant stiffness to the robot based system.

3.2.2 Methods

3.2.2.1 Robot Testing System

The robot-based spine testing system consisted of a serial-linkage robot (Staubli RX90, Staubli Inc., Duncan, SC), an on-board universal force sensor (0-90N /0-11 Nm detection range with 0.27N /0.0023 Nm resolution, UFS Model 90M38A-150, JR3 Inc., Woodland, CA) and custom fixtures (Figure 2 – end-effector fixture coordinate system (EEFCS) and base fixture coordinate system (BFCS)). The robot was controlled via a program written in MATLAB (Mathworks Inc., Natick, MA) and operated under (i) adaptive displacement control ('Pathseek') in a quasi-static manner as described previously [278] and (ii) under kinematic replay where stored joint angles were replayed. The manufacturer lists kinematic precision at ± 0.02 mm for this robot without any payload [280]. The robot testing system precision was assessed with and without rabbit lumbar

FSUs (\pm FSU) to compare kinematic performance with and without added relevant stiffness and to assess load control accuracy and precision with relevant forces/moments. Rabbit L4-5 FSUs ($N=3$) were subjected to flexion/extension (1.0° step size) and axial rotation (0.5° step size) using a 0.3 Nm target and to anterior translation (0.125 mm step size) to a 20 N target. For tests without FSUs ($n=3$), the robot was rotated or translated to paths of the same movement with the same robotic step size. Ten cycles of active path determination ('Pathseek') were performed (after three cycles of preconditioning), and then the final cycle's kinematics were replayed ten times ('Replay').

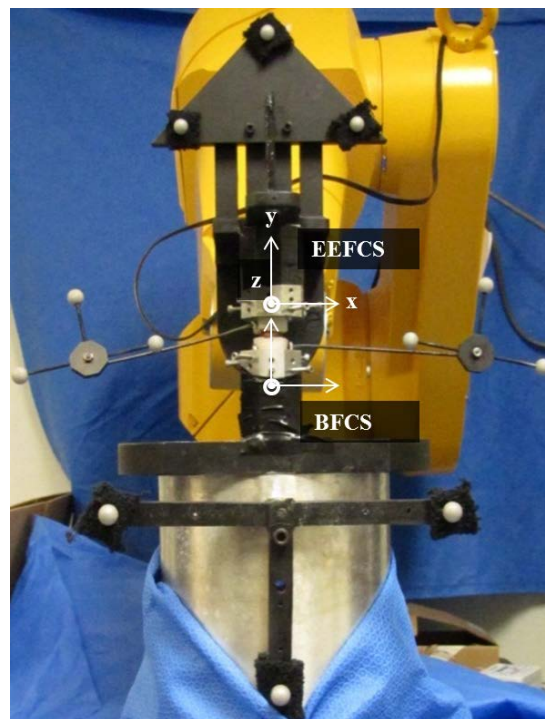


Figure 2. FSU within robot testing system and instrumented with reflective markers.

Motion collection: Kinematics of the robot testing system were measured using a five-camera passive-reflector marker system (VICON 460, Vicon, Centennial, CO) that measures rigid body motion (Figure 3).

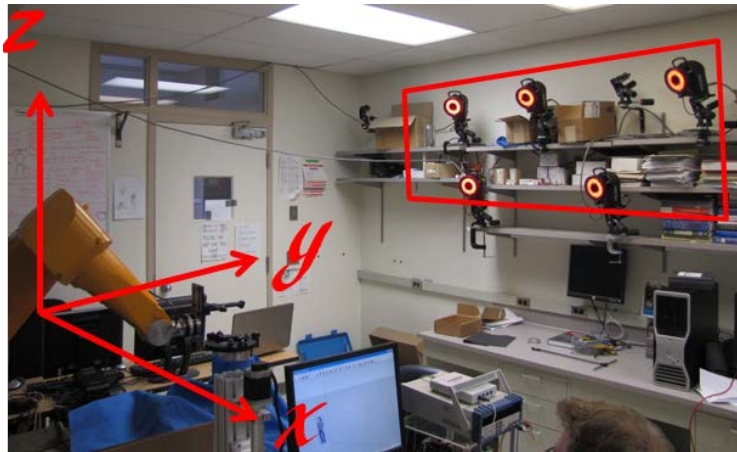


Figure 3. VICON Marker System and Global Reference Frame

Reflective passive markers with 9.65 mm \varnothing (VICON) were used throughout testing. Mean accuracy and precision were 155 μm , and 33 μm . Three reflective markers were attached to the end-effector and base (Figure 2). Fixtures were attached to the robot with or without the FSU. Prior to motion (i.e. at static positions), using a stylus with four reflective markers, a local coordinate system was created using three points on each fixture (Figure 2) to define the orientation of a “fixture” coordinate systems (end-effector fixture coordinate system (EEFCS) and base fixture coordinate system (BFCS), i.e. the local reference frame of the fixtures about which the robot rotates) (Appendix D.2.1). The infrared camera collection sampling was set to 10 Hz, and stylus positions were collected for three seconds each. During dynamic trials of robot motion, a two-second pause was inserted at each step of movement to collect 20 frames of position data for each marker. Mean marker position data at each step in each movement was used to construct a

measured local coordinate system (LCS) in the global reference for the end-effector and the base, $T_{G,M_{ee}}$ and T_{G,M_b} . Post-hoc processing was used to transform measured LCSs in to fixture LCSs, $T_{M,F_{ee}}$ and T_{M,F_b} , using fixture-to-global transformations defined with the stylus prior to testing ($EEFCS = T_{G,F_{ee}}$, $BFCS = T_{G,F_b}$),

$$T_{M,F_{ee}} = (T_{G,M_{ee}})^{-1} (T_{G,F_{ee}}) \text{ and}$$

$$T_{M,F_b} = (T_{G,M_b})^{-1} (T_{G,F_b})$$

From the fixture reference frames, movements of the end-effector relative to the base were calculated at each step,

$$T_{F_b,F_{ee}} = (T_{M,F_b})^{-1} T_{M,F_{ee}}$$

and Euler angles (R_x , R_y , R_z) and displacements (D_x , D_y , D_z) were extracted from $T_{F_b,F_{ee}}$ assuming an order of rotations, $(R_x)(R_y)(R_z)$ (Appendix D.2.2). This fixture reference frame is visualized in a rabbit FSU. The fixture coordinate system was aligned closely with the anatomical reference frame of FSUs, as shown in Figure 4.

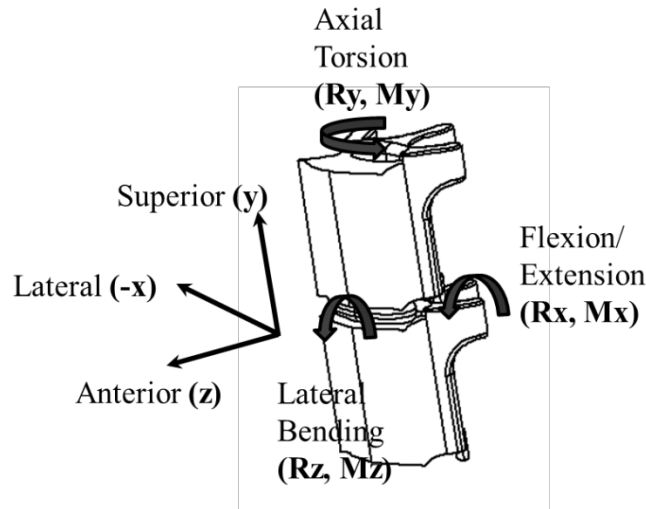


Figure 4. Fixture and FSU reference frame and anatomical motions and directions

‘Pathseek’ control: Accuracy of robot control of forces/moments was evaluated in F/E. It was quantified by calculating (1) error in force minimization—root mean square error (RMSE) of forces in each translational DOF of the universal force sensor (UFS) (F_x , F_y , F_z) across trials per cycle—and (2) error in moment target achievement—average difference from 0.3 Nm at maximal rotation across cycles. Simply evaluating the magnitudes of error rather than using a ratio, acceptable control of off-axis force/moments for rabbit FSUs was average RMSE of forces < 2.0 N [276]. Error in moment target achievement should be $< 10\%$ of the moment target (< 0.03 Nm for F/E). These thresholds of acceptability were used to evaluate robotic force/moment accuracy in path determination. Alternatively, force/moment target achievement was compared to ratios of moment target to off-axis force RMSE (Nm/N); these ratios range from 0.318 for rabbits [276] to 0.60 for pigs [87] to 1.0 for humans [277].

Force/moment precision was also measured by averaging across trials the RMSE of all forces and moments during each step of ‘Pathseek’ motion paths. Precision of the UFS was assessed with and without FSUs (\pm FSUs). Acceptable precision of off-axis force/moments for rabbit FSUs was RMSE of forces < 2.0 N and moments < 0.02 Nm [276]. Force/moment changes in ‘Replay’ are a measure of load relaxation, so its precision is not relevant to system performance. Force/moment thresholds of acceptability were established using the criterion that $\text{RMSE} < 10\%$ of applied moments (i.e. $\text{RMSE} < 0.03\text{Nm}$).

System kinematic precision: The robot testing system kinematic precision was assessed over ten cycles of F/E, AT, and AP in ‘Replay’ and ‘Pathseek’. Kinematic precision of robotic movements aligned with an anatomical reference frame (based on fixture orientation and positioning) was quantified using the VICON 460 in F/E, AT, and AP. The RMSE of rotation angles and displacements were calculated per step across ten trials in ‘Pathseek’ and ‘Replay’ to

quantify system precision error under both control schemes (Appendix D.2.3). Translation/rotation thresholds of acceptability were established using the criterion that error < 10% of measured motions. Applying this criterion to research studies of rabbit lumbar segments yields precision error thresholds in F/E <1°, AT <0.3°, and AP <0.1 mm [276, 281, 282].

Kinematic precision is not essential to ‘Pathseek’ motions, but it was measured and calculated (as described below) (i) to quantify the amount of variation between loading paths in ‘Pathseek’ and (ii) to compare ‘Pathseek’ to ‘Replay’ to illuminate differences in the control methods. It was reported alongside kinematic precision in ‘Replay’.

3.2.3 Results

3.2.3.1 Robot Testing System

‘Pathseek’ Control: Robot control in ‘Pathseek’ was assessed in F/E; a representative 6 DOF loading of flexion is displayed in Figure 5. The mean primary moment target achievement error was 0.022 (\pm 0.015) Nm, an error 7.2% of the moment target. The mean off-axis force RMSE in Fx, Fy, Fz was 0.081 (\pm 0.007), 0.510 (\pm 0.196), 0.148 (\pm 0.150) N, respectively.

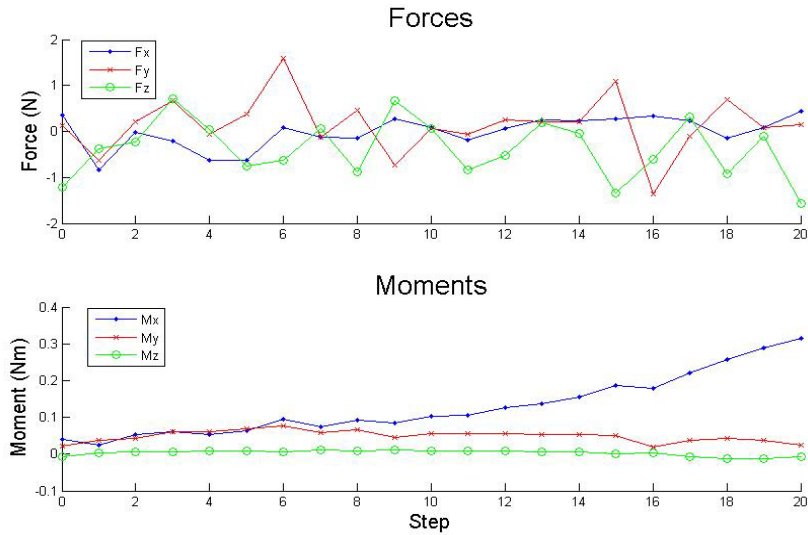


Figure 5. Representative 'Pathseek' F/E (Mx) plot of minimized off-axis forces (top) and moments (bottom)

Precision of force/moment detection and robotic system positioning are depicted in Figure 6. The primary moment (Mx) precision error was 0.0109 Nm, a value well below ($\sim 1/3$) the threshold value, 0.03 Nm. Mean force (mean of Fx, Fy, & Fz) and moment (mean of Mx, My, & Mz) precision were 0.246 ± 0.076 N and 0.009 ± 0.002 Nm, respectively. These mean values (individual DOF values shown in Figure 6) are below thresholds of 2 N and 0.03 Nm, respectively. Primary moment precision error was less than 3% of moment targets.

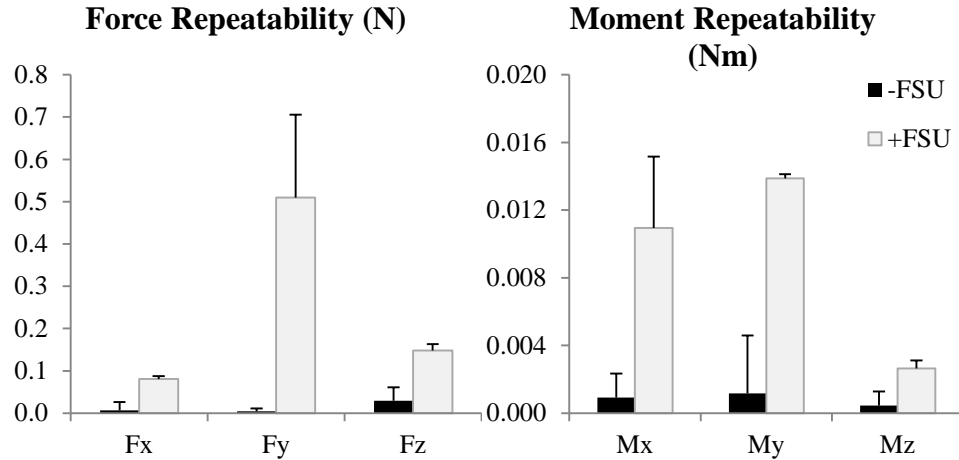


Figure 6. Force and moment precision measurements in F/E

System kinematic precision: Figure 7 summarizes the kinematic precision of the robot testing system in all DOF with and without attached FSUs under both robotic control schemes. Mean kinematic translational (mean Dx, Dy, & Dz) and rotational (mean Rx, Ry, & Rz) precision for F/E, AT, and AP are depicted in Table 3. Robot precision for both control schemes with and without FSUs in primary DOF of all motions were below established targets: for Rx in F/E, $.023-.074^\circ < 1^\circ$; for Ry in AT, $0.01 - 0.101^\circ < 0.3^\circ$; and, for Dz in AP, $0.025-0.082 \text{ mm} < 0.1 \text{ mm}$. Mean translational precision error (across off-axis translational DOF) for F/E, AT and AP in ‘Replay’ was $<.044 \text{ mm}$, and mean rotational precision error (across 3 rotational DOF) was $<.0173^\circ$. The presence of added stiffness with FSUs did not affect ‘Replay’ precision.

Precision in ‘Pathseek’ was higher and more variable than that of ‘Replay’ for all DOF in each movement. Attachment of the FSU did not reduce kinematic precision in ‘Pathseek’; in fact, improved mean translation precision is evident. ‘Pathseek’ mean rotational precision is below thresholds ($<.114^\circ$) for rotational motions (F/E and AT) with or without FSU attachment, but is above thresholds in AP translation (.194-.346 mm) with or without FSU attachment (Table 3).

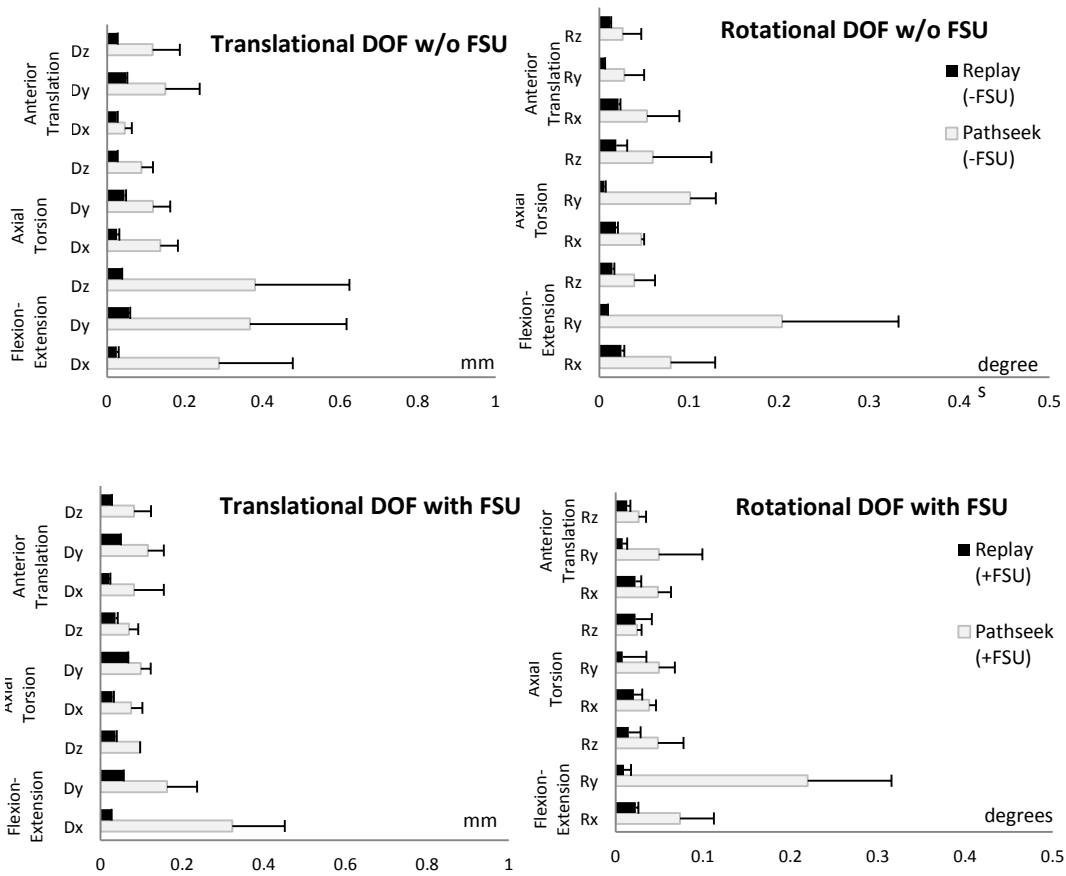


Figure 7. Robot testing system kinematic precision depicted for translational and rotational DOF

Table 3. Mean translational and rotational precision for AP, AT, and F/E in ‘Replay’ and ‘Pathseek’

		Replay				Pathseek			
Motion DOF	Mean DOF	-FSU		+FSU		-FSU		+FSU	
Anterior Translation	<i>translation (mm)</i>	0.04	(0.001)	0.04	(0.007)	0.35	(0.21)	0.19	(0.063)
	<i>rotation (°)</i>	0.02	(0.002)	0.02	(0.001)	0.11	(0.04)	0.11	(0.039)
Axial Torsion	<i>translation (mm)</i>	0.03	(0.002)	0.04	(0.018)	0.11	(0.03)	0.08	(0.023)
	<i>rotation (°)</i>	0.01	(0.005)	0.02	(0.002)	0.07	(0.03)	0.04	(0.007)
Flexion-Extension	<i>translation (mm)</i>	0.03	(0.003)	0.03	(0.005)	0.10	(0.05)	0.09	(0.051)
	<i>rotation (°)</i>	0.01	(0.001)	0.01	(0.001)	0.04	(0.02)	0.04	(0.024)

3.2.4 Conclusions

The robot testing system was capable of performing ‘Pathseek’ with acceptable load-control error using rabbit FSUs. The error in reaching the primary moment target (7.2%) was below the 10% moment magnitude error threshold for acceptance [275]. Resolution at prescribed moment/force targets was below 10% thresholds for F/E and AT but not AP (System Requirement 1.c). Forces were minimized during pure moment testing; RMSE of off-forces during ‘Pathseek’ was <0.165 N (Fz). This is well below the 2 N threshold from comparable systems used to test rabbit spinal segments [276]. Researchers that have used robot spine testing systems have established ratios for acceptable moment target to off-axis force RMSE (Nm/N); these ratios range from 0.318 for rabbits [276] to 0.60 for pigs [87] to 1.0 for humans [277]. The ratio for the present study is 0.588, suggesting the error in robotic control for rabbit FSUs in this system, evaluated by variance in off-axis forces, is acceptable. Also, mean off-axis moment RMSE values were <.015 Nm, which is ~5% of moment targets and meets criteria (<0.02 Nm) established by other researchers [276, 277]. This result of adequate control and precision is

likely a result of the low payload and would need to be reassessed at much higher payloads. Thus, kinetic control and precision of the robot testing system meet standards for adequate control (System Requirement 1.a).

Kinematic precision of the robot testing system was acceptable in 'Replay' and 'Pathseek' for rotational motions (System Requirement 1.b). Positional precision error was worse than that specified by the robot manufacturer, but that is expected. Positional measurements were near to the precision of the VICON measuring system. However, using the principle that the error of measurement in systems must be an order of magnitude lower than the quantities they measure, the robot precision error could not be fairly judged because it was closer than this disparity. Therefore, this study is not a definitive assessment of robot manipulator precision but does provide evidence that precision was below thresholds for primary rotational DOF in rabbit FSU. The apparently high precision of the robot testing system reflects, at least in part, the low payload and small working volume needed to control rabbit FSUs. This finding is most relevant to mechanobiology testing as the majority of testing involves cycling in repeated motion paths using 'Replay.'

Kinematic precision results were mixed for 'Pathseek.' Rotational precision was acceptable for F/E and AT regardless of FSU attachment in 'Pathseek', but translational precision worsened beyond acceptable thresholds without FSUs. Lack of FSU attachment likely causes more variable positioning because force/moment inputs are largely noise. Precision for AP was generally unacceptable in 'Pathseek'. Because 'Pathseek' control involves integrating force feedback in position attainment and 'Replay' involves simply moving robot joints to stored positions, it is expected that 'Replay' would have lower error in precision than 'Pathseek.'

Further, the application of the robot testing system in rabbit FSU mechanobiology spends most of its time in ‘Replay’, not ‘Pathseek’, which does not rely on kinematic precision, so these results have little impact on narrowing this system’s application.

Kinematic precision was evaluated in the context of precision needed for amplitudes of motion in rabbit rotations—F/E and AR—and translation—AP. As such, precision of calculated angles and displacements similar to those used in experimental testing, which depend on spatial transformations and an assumed rotation sequence (Appendix D), was used rather than precision of raw position measurements. Kinematic analysis likely increased the error of measurements, but these measurements were more applicable to study outcomes.

In conclusion, F/E and AT kinematic precision are acceptable, using the most rigorous assessment, in ‘Replay’ and ‘Pathseek’ with an FSU attached. AP translation in ‘Replay’ and ‘Pathseek’ is acceptable based on primary DOF evaluation, but consideration of precision in all DOF presents modest caution, especially in ‘Pathseek.’ **The kinematic precision of the robot system is adequate to fulfill the aims of this dissertation research.**

3.2.5 Acknowledgements

Technical expertise was provided by Kevin Bell and Yiguo Yan, and execution of experiments on VICON system accuracy and precision was driven by Yiguo Yan.

3.3 RIGIDITY OF THE FIXATION SYSTEM

3.3.1 Introduction

The rigidity of this system has been measured in axial compression [269]; however, its rigidity in rotational DOF has not been quantified. The rigidity of the fixture-specimen interface must be tested to demonstrate (1) that displacements and rotations of the specimen relative to the fixtures are small relative to measured joint motion, and (2) similarly, as a corollary, that the fixture-specimen interface has a stiffness of an order of magnitude greater than that of the joint. The performance of the fixtures depends on the loading mode, so relevant motions to Specific Aims 1 and 2 (AP was a preliminary DOF to be used in Chapter 6.0) were assessed: flexion/extension (F/E), axial torsion (AT), and anterior/posterior translation (AP). The critical assessment of rigidity was performed in the primary DOF, that is, the motions and stiffness of the interface were compared to primary motions and stiffness values of the FSU in that DOF. For example, in F/E, the R_x (see Figure 4) of the interface was compared to R_x of the specimen, and K_{rx} of the interface was compared to K_{rx} of the FSU. To ensure that mechanical results from this system are comparable to traditional biomechanical orthopaedic testing and to provide a standard for evaluating off-axis laxity, the novel fixation system was compared to the standard bone fixation technique of screw attachment to bones potted in epoxy resin.

3.3.2 Methods

Rationale: The novel fixation method used in the bioreactor (Screw Only fixation) was compared to the existing standard in conventional orthopaedic biomechanical testing—potting of bone in

epoxy resin with subsequent screw attachment to cylindrical fixtures. In the absence of clear standards for rigidity and few papers published reporting bone-fixture rigidity, epoxy resin potting was compared directly to the novel Screw Only fixation.

Specimen Preparation: Rabbit L4-5 FSUs were attached to fixtures by (1) epoxy resin potting methods or (2) novel Screw Only attachment (n=5 for each group). Sets of three 9.65 mm Ø reflective markers (VICON) were attached to the vertebral bodies (Figure 4) by drilling tunnels through the vertebral body, placing PMMA into the tunnels, and threading 4-40 rods through the vertebra with adjoining washers to lock the rod position. Following marker attachment, potted FSUs (“Epoxy” Group) were embedded in epoxy resin (Bondo Body Filler, 3M, Inc., Atlanta, GA), aligned within fixtures, and attached to fixtures using sixteen 6-32 screws that penetrated the cylindrical, hard epoxy. “Screw Only” FSUs were placed directly in fixtures, similarly aligned, and attached to fixtures using sixteen rubber-capped 6-32 screws tightened iteratively against the irregular vertebral bone. Attached FSUs for both groups were aligned and mounted to the robot end-effector and base with dual ¼-20” screw attachment for both superior and inferior fixtures.

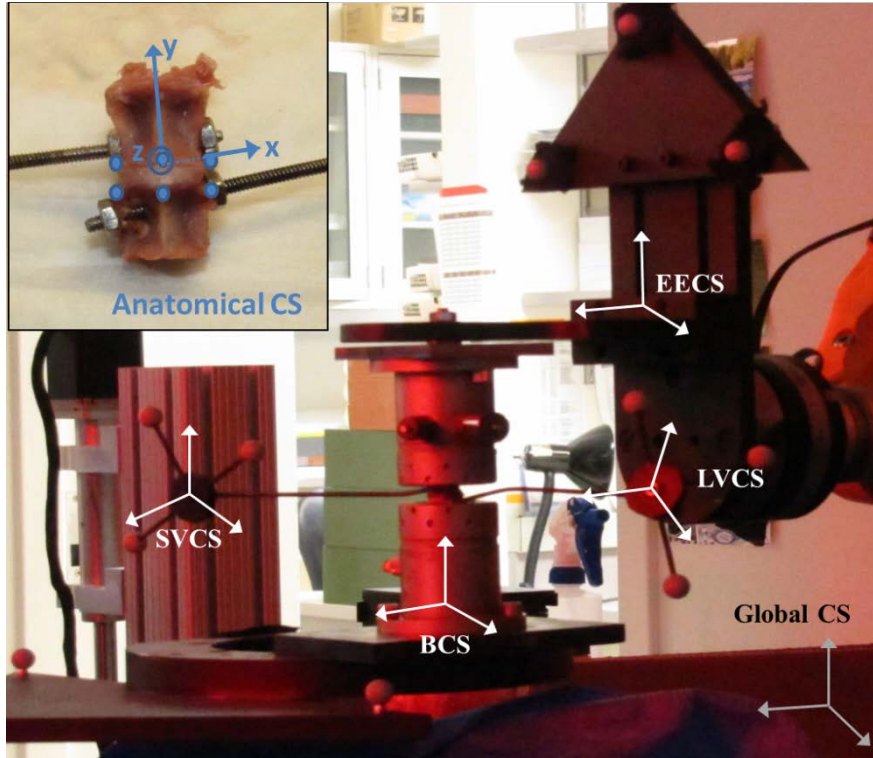


Figure 8. Global and local coordinate systems defined by reflective markers

Motion Capture: Rigidity of the fixture systems for rabbit FSU attachment was assessed using the passive-marker five-camera VICON 460 motion collection system (VICON) in conjunction with the robot testing system similar to Methods described in Section 4.2.2. The serial-linkage robot (Staubli RX90) and on-board UFS (JR3) were controlled via a program written in MATLAB (Mathworks) to operate under (i) adaptive displacement control ('Pathseek') in a quasi-static manner as described previously [278] and (ii) kinematic replay ('Replay') where stored joint angles are replayed. In addition to markers attached to FSUs, three reflective markers were attached to the end-effector and base (Figure 8) to form end-effector and base coordinate systems (EECS and BCS). During a static trial prior to motion, a stylus with four reflective markers was used to create an anatomical reference frame for superior and inferior vertebrae (SVCS and IVCS, respectively), $T_{G,A_{SV}}$ and $T_{G,A_{IV}}$, using standard anatomical landmarks for

vertebrae [283]. Also, as in Section 3.2.2.1, fixture “anatomic” reference frames, $T_{G,A_{ee}}$ and T_{G,A_b} , were created using marks on the fixtures to better align measured robotic movements with specimen anatomy (Appendix D.2.1). The infrared camera collection sampling was set to 10 Hz, and stylus positions were collected for three seconds each. During dynamic trials of robot motion, a two-second pause was inserted at each step of movement to collect 20 frames of position data for each marker. Mean marker position data at each step in each movement was used to construct an orthonormal, measured local coordinate system (CS) in the global reference frame for the superior fixture, inferior fixture, superior vertebra, and inferior vertebra, $T_{G,M_{ee}}$, T_{G,M_b} , $T_{G,M_{SV}}$, $T_{G,M_{IV}}$, respectively. Post-hoc processing transformed measured LCSs in to orthonormal anatomical LCSs, $T_{M,A_{ee}}$, T_{M,A_b} , $T_{M,A_{SV}}$, $T_{M,A_{IV}}$, using anatomic-to-global transformations defined prior to testing,

$$T_{M,A_{ee}} = (T_{G,M_{ee}})^{-1} (T_{G,A_{ee}}),$$

$$T_{M,A_b} = (T_{G,M_b})^{-1} (T_{G,A_b}),$$

$$T_{M,A_{SV}} = (T_{G,M_{SV}})^{-1} (T_{G,A_{SV}}), \text{ and}$$

$$T_{M,A_{IV}} = (T_{G,M_{IV}})^{-1} (T_{G,A_{IV}}),$$

From the anatomical reference frames, movements of (1) the superior vertebra relative to end-effector (superior fixture laxity), (2) the base relative to the inferior vertebra (inferior fixture laxity), and (3) the superior vertebra relative to the inferior vertebra (FSU movement) were calculated at each step,

$$(1) T_{A_{ee},A_{SV}} = (T_{M,A_{ee}})^{-1} T_{M,A_{SV}}$$

$$(2) T_{A_b,A_{IV}} = (T_{M,A_b})^{-1} T_{M,A_{IV}}$$

$$(3) T_{A_{IV},A_{SV}} = (T_{M,A_{IV}})^{-1} T_{M,A_{SV}}$$

Euler angles (R_x , R_y , R_z) and displacements (D_x , D_y , D_z) were extracted from each transformation matrix assuming an order of rotations, $(R_x)(R_y)(R_z)$ equivalent to $(F/E)(AT)(LB)$ (Appendix D.2.1). Rotations and translations were calculated by subtracting angles and displacements at the starting position from extremes of motion (Appendix D.3.1). These angles and displacements constitute the rotations and displacements at the (1) superior specimen-fixture interface, (2) inferior specimen-fixture interface, and (3) FSU joint.

Rigidity Assessment: Rigidity was assessed for both groups in ‘Replay’ control for three DOF movements: F/E, AT, and AP. Following ten cycles of ‘Pathseek’ to 15° , 3° , and 1 mm—representative rotation angles and translational displacements resulting from load-control with 0.3 Nm (F/E, AR) and 20 N (AP) used previously—the final path kinematics were replayed ten times. Forces and moments were recorded for each DOF (F_x , F_y , F_z , M_x , M_y , M_z) at each step of movement per motion path. Rigidity was assessed in two ways: (1) specimen-fixture interface motion and (2) relative stiffness of interfaces compared to FSUs. First, 6 DOF motions at the specimen-fixture interfaces—differences in angles and displacements between starting and final positions from $T_{A_{ee},A_{SV}}$ and $T_{A_{b},A_{IV}}$ —quantify how much the vertebra rotated and translated with respect to the fixture (Appendix D.3.1). To evaluate the novel Screw Only fixation method, motion in the primary DOF was compared to a threshold of 10% of overall motion (1.5° , 0.3° and 0.1 mm in F/E, AT, and AP) as well to the standard set by the Epoxy fixation method. Primary motions were Euler angle R_x in F/E, R_y in AT, and D_z in AP. To evaluate off-axis motions, Screw Only motions were compared to Epoxy motions with the goal of showing non-inferiority. Off-axis motions constitute all other translations and rotations per movement.

Second, stiffness in the primary DOF was calculated for and compared between the FSU and the fixture interface. Differences in stiffness should be an order of magnitude apart for minimal contribution (~10%) of fixation laxity to mechanical outcomes. As above, primary motions were differences between initial and final positions in Euler angle R_x in F/E, R_y in AT, and D_z in AP from $T_{A_b,A_{IV}}$ for superior interface motions, $T_{A_{ee},A_{SV}}$ for inferior interface motions, and $T_{A_{IV},A_{SV}}$ for FSUs. Corresponding primary forces/moments measured by the UFS at the final position of the motion path were then used to calculate stiffness. The measured force/moment in the primary DOF, i , (F/M_i) was divided by this translation/rotation in the same DOF, T/R_i , to evaluate fixture-vertebra interface stiffness.

Equation 1. Fixture-specimen interface stiffness

$$K_{\text{interface}} = \frac{F/M_i}{T/R_i}$$

Specimen stiffness is simply F/M_i divided by primary motion T/R_i of the FSU given by relative anatomical motions.

Equation 2. FSU stiffness

$$K_{\text{specimen}} = \frac{F/M_i}{T/R_i}$$

Based on the criterion stated above, a rigid system should adhere to the following criterion:

$$\frac{K_{\text{specimen}}}{K_{\text{interface}}} < 0.10$$

3.3.2.1 Statistics

All results are presented as mean \pm standard deviation. The Mann-Whitney U test was used (i) to determine if interface motions for each DOF were different from 0° or mm (i.e. no motions) for both fixation groups and (ii) to compare 6 DOF translations and rotations between fixation

methods. The Mann-Whitney U test was also employed to compare fixation system stiffness measures between conventional and novel fixation groups in the primary DOF. A significance level of $p < .05$ was chosen. Matlab was used to perform statistical analysis.

3.3.3 Results

3.3.3.1 Interface Motion

The relative motions for each DOF (translations (D_x , D_y , D_z) and rotations (R_x , R_y , R_z) in x, y, and z) at the interface between the specimen and fixture are depicted in Figure 9 for (A) F/E, (B) AT, and (C) AP. Primary DOF are marked by arrows, and dashed lines represent thresholds of acceptable movement restriction in the primary DOF. As the chief measure of interface rigidity, mean primary motions at superior and inferior fixture interfaces for Screw Only fixation were $R_x = 0.333 \pm 0.196^\circ$ and $0.059 \pm 0.050^\circ$ in F/E, $R_y = 0.018 \pm 0.052^\circ$ and $0.021 \pm 0.030^\circ$ in AT, and $D_z = 0.037 \pm 0.066\text{mm}$ and $0.002 \pm 0.070\text{mm}$ in AP across trials; these values are well below thresholds for acceptable interface laxity for primary motions (dashed lines in Figure 9). In F/E, Screw Only fixation is significantly increased compared to 0° in R_x , but this motion is less than 40% of the error threshold, and the difference relative to Epoxy fixation was not significant ($p = .0952$). Primary DOF interface movements in AT and AP were not significantly different from “no motion” for either group.

Secondarily, the motions at the interface in all DOF were examined. Rotational off-axis motions were below primary DOF thresholds in F/E and AT, and, likewise, translational off-axis motions were below the primary DOF threshold in AP. Considering translations in F/E, D_x interface motion was significantly increased for both fixation methods; however, the increase in the Screw Only group ($-0.151 \pm 0.105\text{ mm}$) tended to be smaller than the epoxy method ($-0.406 \pm$

0.499 mm). In AT, no interface motions for the Screw Only group were significantly increased, and mean values were similar to or less than primary DOF error thresholds. For the Epoxy group, however, Dy and Rz motions were significantly larger than no motion. Interestingly, in AP, while translational motion errors were small (<.084 mm), Rx motion was elevated in both groups for the superior fixture ($p=.0079$ for both groups) and in the Screw Only group for the inferior fixture ($p=.0079$). This demonstrates a significant coupled sagittal rotation with AP translation. Further, this coupling was larger in Screw Only fixation group than the Epoxy group ($p=.0159$).

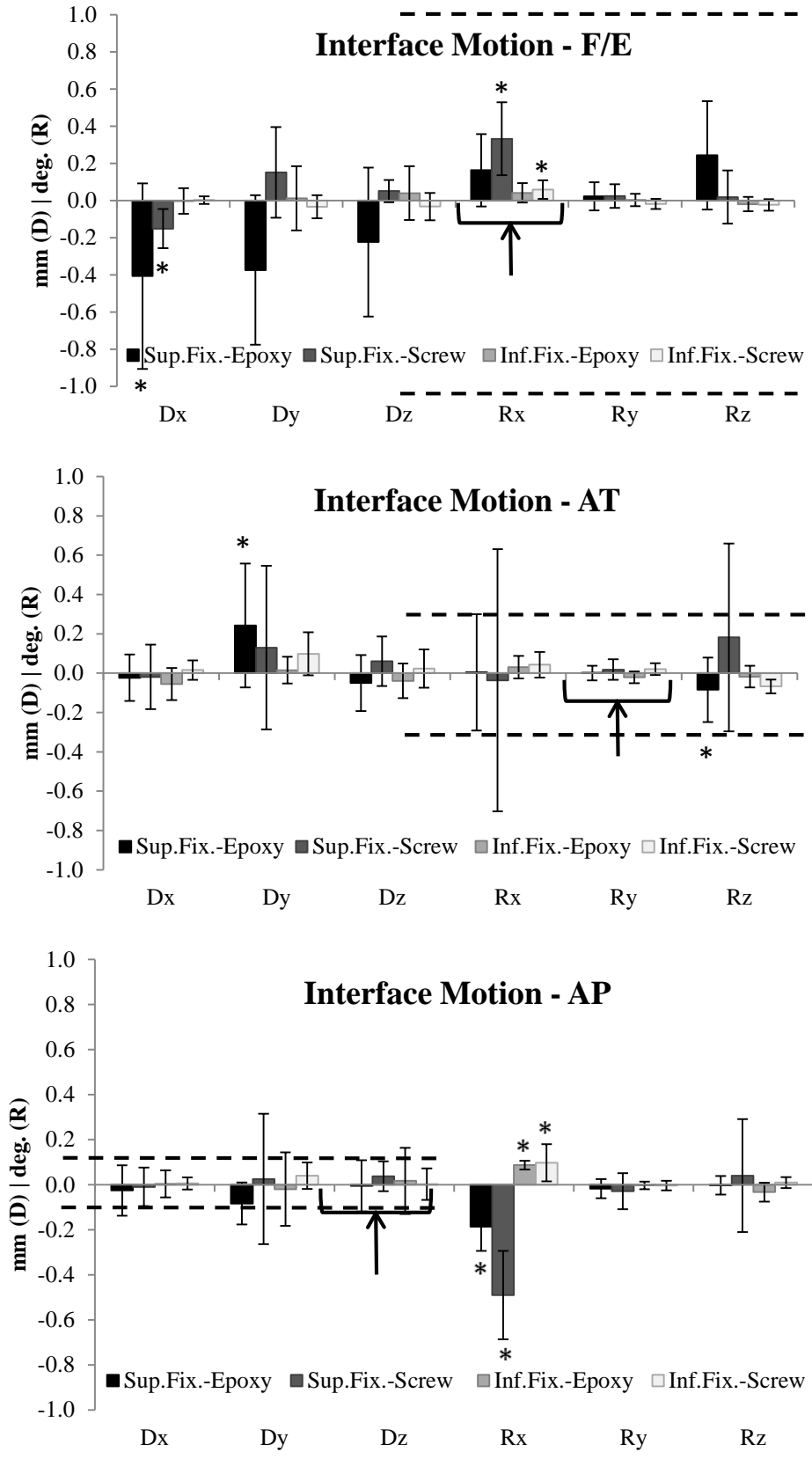


Figure 9. Specimen-fixture interface motions in 6 DOF for FSU movements in F/E, AT, and AP.

3.3.3.2 Stiffness

Fixture stiffness in the DOF of motion was calculated for F/E, AT, and AP for both fixation methods (Figure 10). Figure 10 shows mean stiffness values compared to ten times the FSU stiffness (10x FSU_k) values—the minimum threshold for acceptable rigidity. Stiffness values are shown for the superior vertebra-end effector (SV-EE) fixture and inferior vertebra-base (IV-B) fixture interfaces. Across all motions, interface stiffnesses for the two fixation methods were not significantly different. However, in F/E, Screw Only fixation trended toward lower fixation stiffness than Epoxy fixation at the superior and inferior interfaces ($p=.0952$ and $p=.0555$, respectively). Nonetheless, the Screw Only interface stiffness in F/E exceeds FSU stiffness by 22.8x and 80.7x at superior and inferior fixtures, respectively, clearly passing the minimum standard of 10x FSU stiffness (~2 and 4x the threshold). The interface stiffness in AT exceeds FSU stiffness by 37.5x and 139.0x at the superior and inferior interfaces, respectively. Thus, the Screw Only fixture system is more rigid in AT than F/E, though both are adequately rigid. In AP, the Screw Only superior fixture stiffness (40.84 N/mm) clearly does not meet the standard of 10x FSU AP stiffness (288.3 N/mm), although Screw Only fixation is not statistically different from epoxy fixation ($p=0.222$).

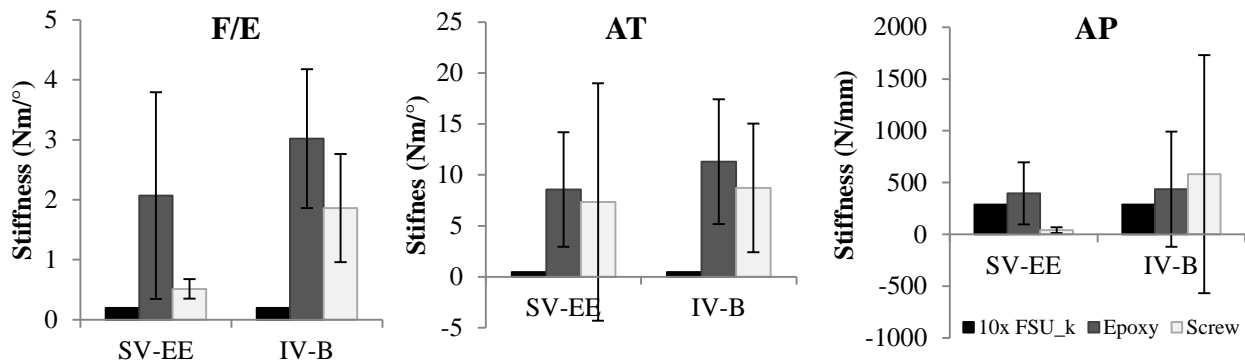


Figure 10. Superior (SV-EE) and inferior (IV-B) fixture-specimen interface stiffness in F/E, AT, and AP

The same data is presented as a ratio of FSU stiffness to fixture stiffness to place the fixtures stiffness magnitude in the context of FSU stiffness (Table 4). F/E and AT stiffness for both fixation techniques are well below the critical ratio of 0.1. AP stiffness exceeds 0.1, albeit slightly, for both fixtures in epoxy fixation, and screw only fixation exceeds 0.1 by nine-fold at the superior interface but met expectations at the inferior interface.

Table 4. Mean (SD) ratios of FSU-to-fixture interface stiffness for both fixation methods in F/E, AT, and AP

DOF	Fixture	Epoxy Fixation		Screw Only Fixation	
F/E	Superior	0.022	(0.025)	0.044	(0.022)
	Inferior	0.008	(0.004)	0.012	(0.006)
AR	Superior	0.006	(0.003)	0.027	(0.022)
	Inferior	0.005	(0.003)	0.007	(0.006)
AP	Superior	0.146	(0.133)	0.916	(0.410)
	Inferior	0.141	(0.095)	0.044	(0.068)

3.3.4 Conclusions

Rigidity of the novel Screw Only fixation technique in F/E and AT was sufficient compared to conventional epoxy potting with screw attachment (i.e. the “gold standard”) and to FSU stiffness. In primary DOF of relevant loading modes—F/E, AT, and AP—the Screw Only fixation was below laxity thresholds for interface motion (System Requirement 3.a.i). The stiffness of fixtures in F/E and AT exceeded the stiffness of FSUs by more than 20x (twice the minimum threshold of 10x), indicating a sufficient difference between stiffness of the fixation interface and specimen to allow mechanical testing (System Requirement 3.a.ii). Considering off-axis motions (non-primary DOF) at the interface, the Screw Only fixation technique was similar or equivalent to the gold standard in F/E and AT but not AP.

Interface stiffness was sufficiently stiff in F/E. The novel fixation method permitted significant rotation in F/E in the primary DOF (Rx), which tended to be larger than the epoxy method. This rotation (0.332°) is well below the 1.0° threshold, representing only 1.7–3.3% of maximum flexion angles. Moreover, the superior and inferior interface stiffnesses in the Screw Only technique in F/E were 22.8x and 80.7x the FSU stiffness, more than doubling and quadrupling the minimum stiffness threshold, respectively. While coupled translations were evident in Dx for the novel fixtures, these translations were smaller than those present in the “gold standard” Epoxy group. Thus, the novel fixation method is sufficiently stiff for rabbit FSU F/E mechanics (System Requirement 3.b).

Screw Only fixation in AT was very rigid. Interface rotations were generally smaller ($0.079 \pm 0.399^\circ$) than the minimum threshold of 0.3° and were not significant. Off-axis rotations were smaller than epoxy potted specimens, so Screw Only fixation outperformed the gold standard. Coupled translations in the Screw Only group were not larger than 0.1 mm and were not significant. Again, Screw Only fixation outperformed Epoxy fixation in that the latter had significant Dy translation greater than 0.1 mm. In terms of stiffness, Screw Only fixation (0.027 and 0.007 for superior and inferior interfaces) was well below the 0.1 FSU-to-interface ratio. Mean interface stiffness relative to FSU stiffness was highest in AT. Taken together, these findings indicate that the novel fixtures had the least error in AT (System Requirement 3.b).

AP translation presented challenges to rigid fixation for both groups, and violations of rigid fixation were worse for the Screw Only method. While interface motions in translational DOF were insignificant and smaller than the 0.1 mm threshold, both groups had significant coupled Rx rotations at the superior fixture, and the Screw Only group demonstrated significant Rx rotations at the inferior fixture as well. Rx rotations were significantly larger in the Screw Only group at

the superior fixture, suggesting unacceptable, repeatable coupling. Further, interface stiffness in the Screw Only group at the superior fixture was over nine times greater than the acceptable limit and nearly nine times greater than the Epoxy group. More fundamentally, the precision of the robot testing system in AP motions could not be tested because of their small size relative to VICON precision, so movement repeatability itself is in doubt in this DOF. Thus, use of the Screw Only fixation technique in AP translation of rabbit FSU is not advisable (System Requirement 3.b). However, this has minimal impact on the dissertation because AP was not chosen as a motion to simulate.

These data contribute important information to orthopaedic biomechanical testing in general (i) by providing a new technique for spinal segment fixation and (ii) by quantifying rigidity of conventional epoxy potting methods. While the generalizability of these findings are limited by the relatively small applied force/moment magnitudes ($<0.3 \text{ Nm}/20 \text{ N}$), they do suggest that (1) small but significant coupled translations can occur in bending and torsion ($<0.4 \text{ mm}$ at 15°) and (2) coupled rotations can occur in translations (0.2° at 1 mm). **Most importantly, these results support the use of the novel Screw Only fixation method for rotational loading modes—F/E and AT—in rabbit FSUs.**

3.3.5 Acknowledgements

Thanks to Kevin Bell and Yiguo Yan for helping with VICON data collection (calibration, anatomical reference frame collection).

3.4 ATTACHMENT TO ROBOT TESTING SYSTEM

Adaptive displacement control, the algorithm employed by the robot testing system in active path determination ('Pathseek') requires an initial estimate of the joint's center of rotation (COR) to begin testing. Forces and moments sensed by the UFS are transformed to the local anatomical coordinate system defined by the axes of the COR [284]. Initial force/moment readings and displacements are made about the estimated COR. At each step of rotation, the COR is updated based on a repositioning algorithm that minimizes all forces acting on the FSU [285]. As FSUs rotate or translate from their starting position, the COR becomes more accurate with each step. Nonetheless, initial estimation of rabbit FSUs needs to be accurate due to the small size of rabbit FSUs, which are inherently less tolerant of measurement errors than larger human FSUs.

Estimates of rabbit COR in F/E were based on existing data in human lumbar segments. Human lumbar segmental overall CORs in F/E are located in the posterior third of the disc, near to the disc superior/inferior midline in disc cross-section in the mid-sagittal plane [286, 287]. COR location is also clearly dynamic, translating posteriorly in extension and anteriorly in flexion [85]. Rabbit segmental anatomy is fairly similar to human. Rabbit disc geometric properties (disc height, disc width, NP dimensions and placement), when normalized by disc width and area, are <26% different from human disc properties [254]. Like human lumbar facets, rabbit facets have a predominantly vertical alignment with comparable sagittal alignment to human facets (unpublished observations from our laboratory). Nevertheless, practical COR estimation in rabbits had to be confirmed experimentally. Further, because rubber membrane walls of the bioreactor obscure visual measurement of FSU anatomy on the robot, a protocol for repeatable attachment and orientation of FSUs relative to the robot end-effector were established (System Requirement 2).

3.4.1 Repeatable attachment

Before COR measurement can be determined, FSUs must be attached within the bioreactor in a repeatable manner so that measurements of external aspects of the fixtures precisely relate to rabbit FSU anatomy. FSUs were visually centered and aligned at neutral angles in the sagittal, coronal, and axial planes within fixtures by tightening rubber-capped, 6-32 screws to variable depths against the irregular vertebrae. Screws were tightened to a manually-determined similar torque magnitude. The distance between the posterior of the fixtures and the estimated F/E COR (COR_{est}), z_{dist} in Figure 11, can be measured prior to encapsulating fixtures with opaque rubber membranes. This distance is added to the distance between the posterior of the fixtures and the robot to ascertain the position of the COR in the anterior-posterior (z) direction relative to the UFS. Based on existing data in human lumbar spines and preliminary *in vitro* mechanical studies in rabbit FSUs [282], COR_{est} was placed at the posterior third of the disc in the anterior-posterior (z) direction and at the disc mid-height in the superior-inferior (y) direction [85, 286]. Similarly, the axial torsion COR_{est} (AT COR_{est} in Figure 11) was oriented vertically, placed in the sagittal midline in the medial-lateral (x) direction [287].

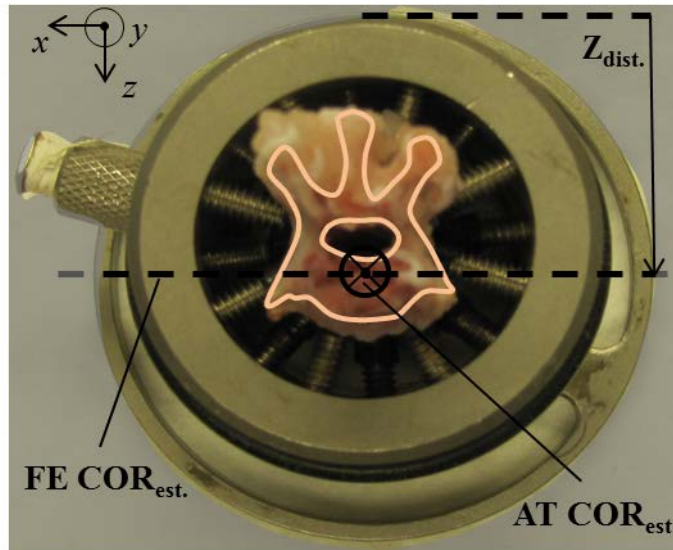


Figure 11. Axial view of FSU aligned in inferior fixture with COR estimates for F/E and AT

Following encapsulation, bioreactor fixtures were mounted to a base plate and the end-effector of the robot spine testing system. The placement of the bioreactor in the anterior-posterior (z) direction was precisely performed using markings on both the base plate and end-effector (z_{COR} in Figure 12). Measurements were made relative to the center of the face of the load cell block immediately proximal to the end-effector. Placement of the bioreactor in the medial-lateral (x) direction is precisely performed by screw holes in the base plate and end-effector (out-of-plane movement in Figure 12). Fixtures were aligned with the UFS in the left-right center by the position of screw holes in the base plate, thus ensuring repeatable, central positioning of the AT COR in the medial-lateral (x) direction. Vertical placement of the COR (y_{COR}) is set by constant inter-fixture spacers. Orientation of the bioreactor in the axial plane was similarly performed using markings on the base plate and end-effector (not pictured). Orientation in the sagittal and coronal planes was vertical and neutral. This protocol for alignment of the FSU within the

fixtures (Figure 11) and the fixtures relative to the robot testing system (Figure 12) enabled close alignment of the FSU relative to a local coordinate system about which initial robot rotations occurred.

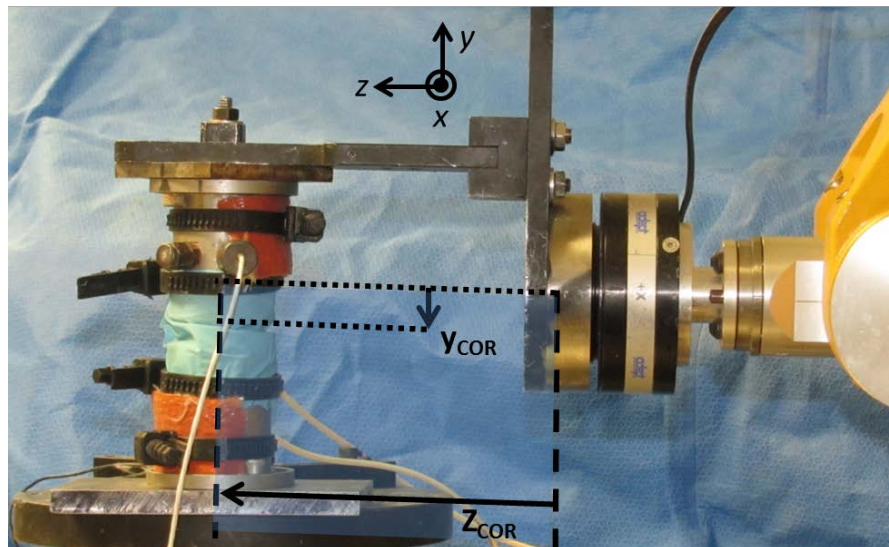


Figure 12. COR measurements from robot to bioreactor

3.4.2 COR position

This process of positioning and measuring COR distances from the robot was confirmed by varying z_{COR} . The goal of varying these distances was (1) to confirm the location of these axes in rabbit FSUs used in previous *in vitro* testing [282] and (2) to quantify the sensitivity of positioning error in these measurements. In Figure 13, F/E curves are shown for an FSU in which the prescribed z_{COR} (posterior third of the disc) was 160mm. Specimen loading started at the edge of the NZ near extension and rotated in to flexion with loading. Error in the F/E moment-rotation curves is evident in the first 8-10° by deviant moments with a $z_{COR} = 145\text{mm}$ (A), 147mm (B), and 151mm (C). The effect is diminished dramatically (2° only) when z_{COR} is brought to within 5 mm

(D) of the prescribed z_{COR} (E). Error in the moment-rotation curve is also evident with overestimates of z_{COR} (F); in fact, error of comparable magnitude is worse with overestimating than underestimating (D vs. F).

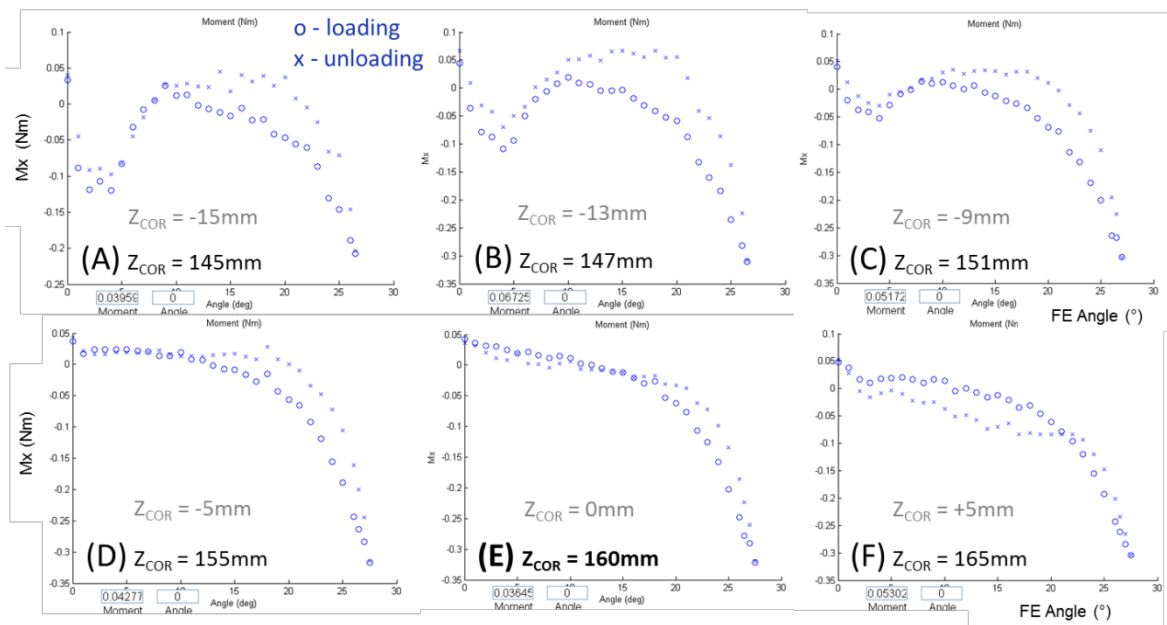


Figure 13. Effects of COR placement in z-direction on F/E moment-rotation curves

Variation of $\pm 3\text{mm}$ (i.e. 157 and 163 cm) had similar, small effects on the moment-rotation curves in (A) and (B) in Figure 14. These effects were smaller than those seen at $\pm 5\text{mm}$. Variation of $\pm 1\text{mm}$ had no discernible effect on the initial steps of the moment-rotation curves.

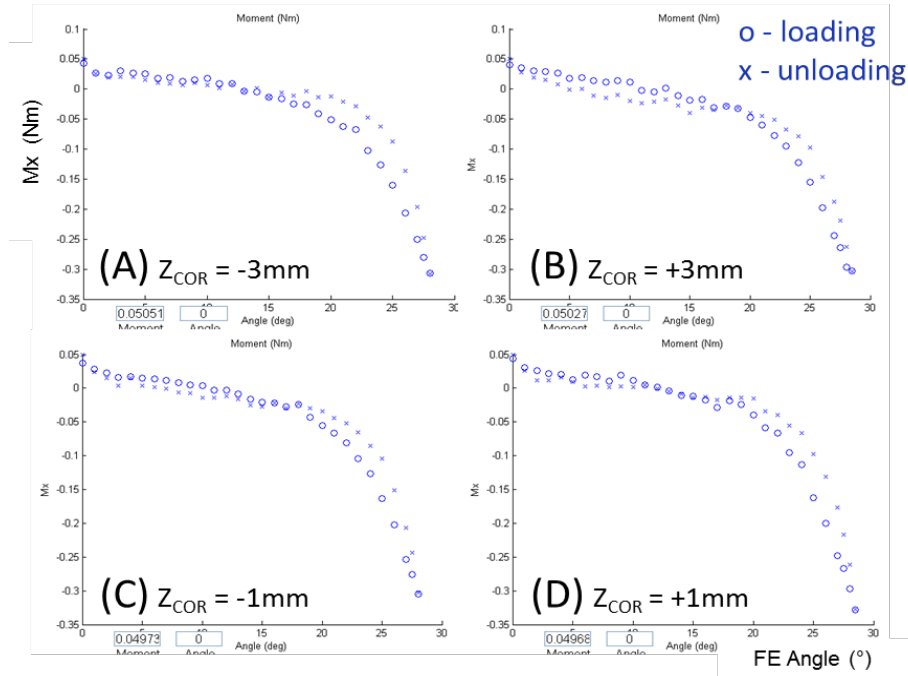


Figure 14. Effects of COR placement in z-direction (± 3 mm) on F/E moment-rotation curves

3.4.3 Orientation about COR

Similarly, the axial orientation of the bioreactor relative to the robot was varied to assess the ability of the robot testing system to adapt to mal-alignment. It was hypothesized that deviations of $<5^\circ$ from proper alignment would not introduce error in the moment-rotation curve. Thus, the orientation of the bioreactor was rotated by small and large angles ($\theta=7.5^\circ$ and $\theta=15^\circ$) from neutral sagittal alignment (Figure 15), and FSUs were subjected to flexion (moving from extension, as in Figure 13 and Figure 14). Deviations in the F/E moment-rotation curve from neutral alignment ($\theta < 2^\circ$) curves were noted. Visible rotation of the robot end-effector was confirmed as it minimized forces and determined the sagittal rotation plane of the FSU. The results, displayed in Figure 15, show that adaptive displacement control quickly adjusts for deviations in axial plane orientation.

The initial two-to-three steps of F/E show deviation from neutral F/E moment-rotation curves, but deviations are small and normal stiffness readings are recovered for both angle values by the fourth step. These deviations are generally smaller than those observed in varying COR.

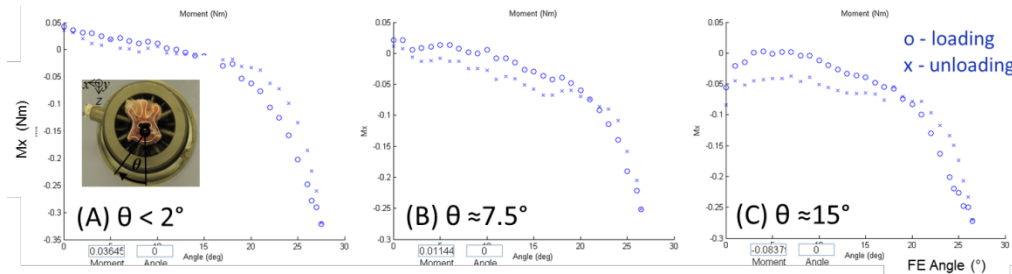


Figure 15. Intentional variation in axial plane orientation: effects on F/E moment-rotation curves

3.4.4 Conclusion

COR placement was confirmed as feasible with achievable precision in attachment and alignment. This protocol for alignment of the FSU within the fixtures and the fixtures relative to the robot testing system enabled repeatable alignment of the FSU relative to the testing system's local coordinate system. Based on perturbing COR positions in the z-direction, placement of the F/E COR at the posterior third of the disc produced optimal moment-rotation curves devoid of evident miss-steps. Secondly, error in the first few steps of F/E was present with overestimation and underestimation $\geq 5\text{mm}$. Error became very small at $\pm 3\text{mm}$ and was negligible at $\pm 1\text{mm}$. Thus, measurement and positioning error $\leq 3\text{mm}$ has little effect on F/E moment-rotation curves. Given the protocol for specimen and bioreactor alignment and positioning, this tolerance is tenable. Large errors are corrected by the adaptive displacement, albeit after many steps, as

evidenced by comparable curves beyond 8-10°. Errors in attachment and measurement should be below the 3mm threshold, with any violations ≤ 5 mm pose little risk to the specimen or inject undue variation between tests.

Errors in orientation of the chamber were even more tolerant. Deviations of 7.5° had only small effects in the first 2-3° of the neutral zone in F/E. Larger deviations (15°) affected early steps dramatically, but adaptive displacement control was able to recover normal moment-rotation curves within 3-4° of F/E as well. Thus, for error magnitudes most likely to occur in FSU attachment and bioreactor assembly and positioning within the robot testing system, mechanical consequences are mild or negligible. For rare events where positioning and orientation are dramatically erroneous, only initial steps made by the robot testing system were sensitive as adaptive displacement control quickly adjusts. Thus, methods for COR estimation and bioreactor placement and orientation are established.

3.5 MEMBRANE EFFECTS

The bioreactor walls are composed of inner latex and outer nitrile membranes to facilitate unrestricted movement in 6 DOF. Interior to the latex membrane, a layer of dialysis tubing surrounds the FSU beneath rubber-capped screws (Figure 6). In compression, the only loading mode explored previously [269], resistance of membranes is not involved (no tension). In bending, however, membranes have the potential to undergo tension on the convex side and thereby influence forces/moments sensed by the universal force sensor (UFS) in the robot testing system.

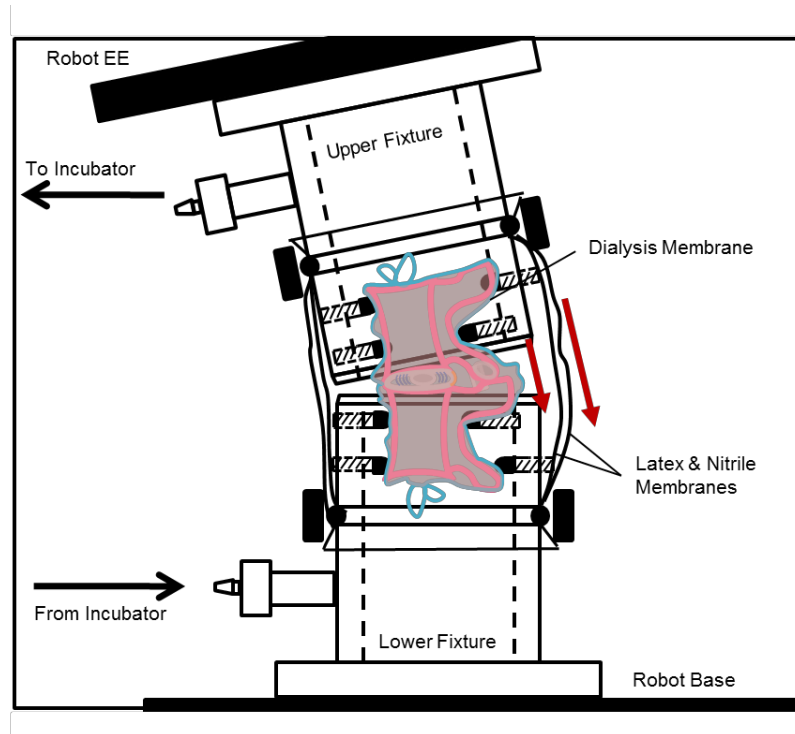


Figure 16. Flexed FSU in bioreactor with inner dialysis and outer rubber membranes with tension illustrated

The effect of membrane tension on F/E moment-rotation curves was identified and corrected by adding folds (additional material) in membranes. First, the bioreactor and sample were prepared as described previously [269]. As Figure 17 shows, without creating slack in the dialysis membrane (unfolded membrane), it increased moments, contributing to the measured moments and obscuring the FSU non-linear moment-rotation profile. Adding redundant material to the region of the dialysis membrane between the fixtures enabled normal non-linear stiffness to be evident (System Requirement 4.b). This was done routinely thereafter to ensure unshielded loading of FSUs; redundant material contributed to modest increases (2-3 ml) in conditioned media in the inner volume.

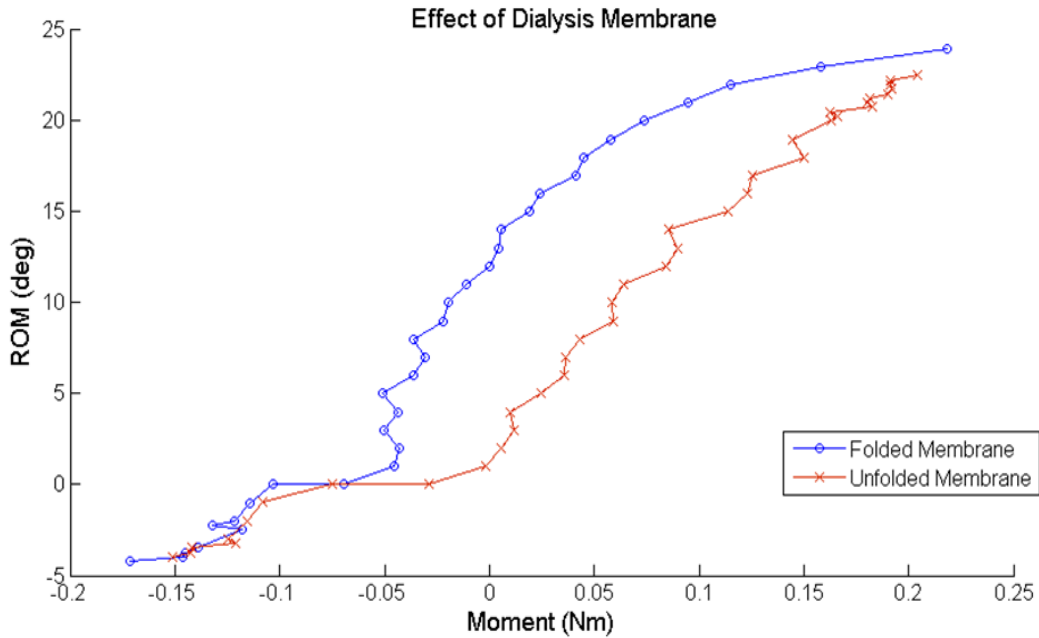


Figure 17. Effect of dialysis membrane with and without folds on F/E moment-rotation curves

Secondly, the effect of the outer rubber membranes was assessed, and membranes were modified to facilitate unrestricted rotational movements. Learning from the effects of an unfolded dialysis membrane on moment magnitudes and stiffness profiles, folds were added to the latex and nitrile membranes between the fixtures (Figure 18). Fluid filled the bioreactor and was pumped through at 1.1 mL/min. This preparation method enabled normal stiffness and moment-rotation profiles to develop; neither membrane tension nor fluid effects altered moment-rotation properties. Membrane attachment and media flow-through was done routinely thereafter without moment distortion, swelling membranes or pooling media (System Requirements 4.a and 4.b).

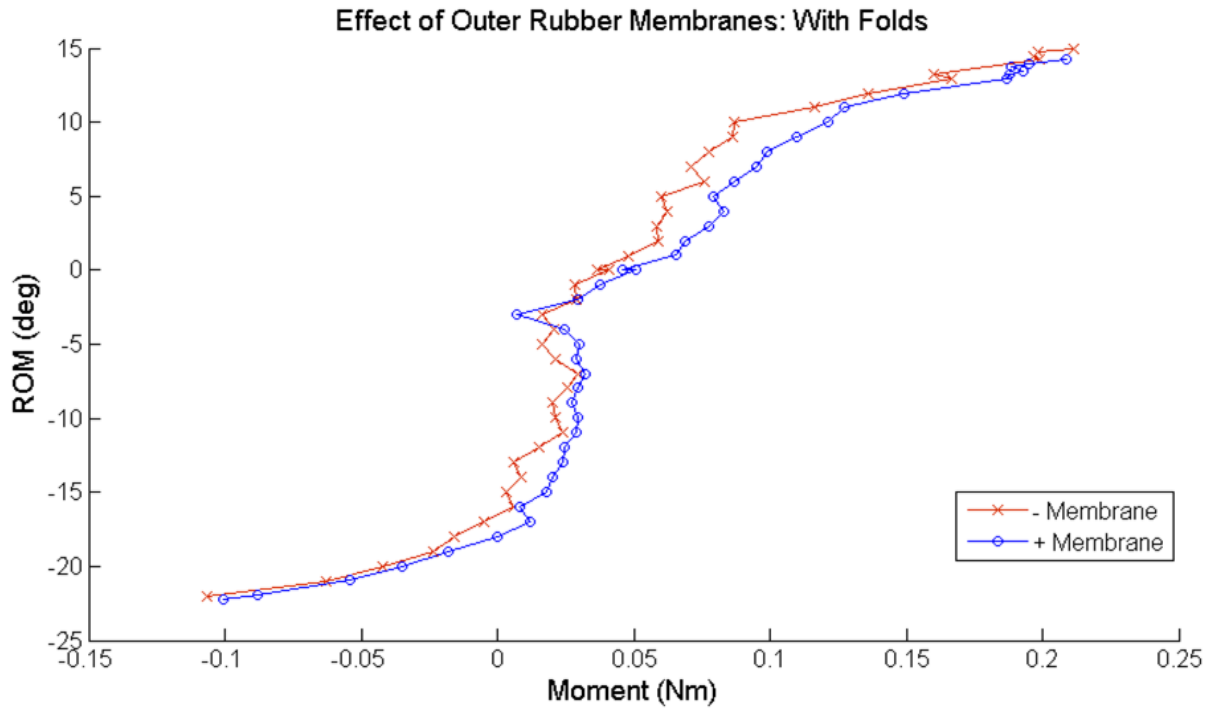


Figure 18. Effect of folded, outer rubber membranes on F/E moment-rotation curves

4.0 MECHANICAL LOADING PROTOCOL DEVELOPMENT

4.1 INTRODUCTION

Mechanobiology depends on the transduction of mechanical forces to intracellular centers that integrate changes in the local environment that result from loading and modulate cellular activity [104]. Establishing mechanical and biological testing conditions that reflect *in-situ* loading and maintain physiologic conditions is paramount to achieving accurate mechanotransduction *ex vivo*. While physiologic conditions can be simulated by controlling *ex vivo* boundary conditions—temperature, oxygen tension, media osmolarity, and nutrition concentrations—selecting mechanical testing parameters that replicate *in vivo* loading is more difficult. The selection of load targets, loading rates, and methods for controlling load application that recapitulate *in vivo* kinematics remains an area of active research [288-290]. Not only is matching *in vitro* loading with *in vivo* kinematics not trivial within a species, but attempts to simulate activities relevant to humans in animal models adds another layer of difficulty in approximation. Matching biological responses to loading between species is inherently uncertain because of the differences in cells, matrix, environmental factors, etc., but matching applied mechanics between species is an essential goal for translatable research.

In disc explant mechanobiology, magnitudes of compressive loading in animal discs are related to human loading based on intradiscal pressure [268]. Beckstein et al. performed constant compression of frequently used animal models and human lumbar discs and showed that, for equal pressure loading, inter-species variation in time-dependent mechanical properties diminished by normalizing responses to compression by disc height and cross-sectional area. The creep

properties of numerous animal model discs, including New Zealand White (NZW) rabbits, were comparable to humans [268]. Similarly, Showalter et al. compared torsional properties between human lumbar discs and numerous animal species and found that, by normalizing by disc height and polar moment of inertia, most animals, including NZW rabbits, had torsional properties and collagen content similar to humans [291]. Thus, in axial compression and torsional loading modes, rabbits have mechanical properties similar to those of humans.

In physiologic rotations of spinal segments involving flexion/extension (F/E), axial torsion (AT), or lateral bending (LB), structural properties of animal spinal segments must first be evaluated as to how well they approximate human segmental properties. The properties that commonly serve as a basis for comparison are range-of-motion (ROM), neutral zone (NZ) width ($^{\circ}$) and stiffness ($\text{Nm}/^{\circ}$), and elastic zone stiffness ($\text{Nm}/^{\circ}$). These properties describe how the structures of spinal segments interact to restrict and facilitate motion for a given DOF. In rabbits, Grauer et al. examined the kinetic response of NZW rabbit lumbar spinal segments in comparison to human lumbar segments in F/E, AT, and LB [281]. Their findings show that rabbit lumbar segments adequately approximate human lumbar ROM and stiffness in F/E and AT, although NZ width in rabbit spines was significantly larger than humans. In general, the authors noted that rabbit lumbar segments had greater laxity [281].

Thus, there are apparent differences in segmental loading between rabbits and humans. The loading of different structures within an FSU is a function of overall kinematics, spinal anatomy, component interactions, and tissue composition. Rabbit lumbar anatomy is close to human lumbar anatomy. Compared to other large animal models often used to evaluate rotational motions, rabbit facet size and orientation in the lumbar spine is similar to humans [292]. Further, previous studies using rabbit facets argue for their similarity to human facets [293]. FSU extension

and AT properties, which are governed to a large extent by facet properties, are similar to humans [281, 291]. Additionally, resection of facets in rabbit lumbar FSUs in Chapter 7.0 demonstrates comparable contribution of facets to extension moments and similar facet joint forces when normalized to bodyweight (Section 7.4.2). Anatomically, the size and shape of the rabbit disc and the NP within the AF is similar (<26% different across listed dimensions) to human discs [254]. The location and composition of posterior ligaments is also comparable to primates [294]. In particular, the salient role of the ligamentum flavum in flexion is shared in both human [278] and rabbit spinal segments (Table 17). Mechanical testing in Chapter 7.0 (Figure 31) and preliminary studies in human spines in our lab show that the ligamentum flavum plays a role in axial torsion in both human and rabbit as well [278]. Understanding differences in moment-rotation curves and anatomy is essential to evaluating the biological response of different tissues from spinal segments belonging to different species. Without a basis for anticipating similarities and differences in the mechanics of different tissues and structures, it would be difficult to conclude how biological changes in rabbit segments related to human responses to comparable mechanical loading.

After establishing the suitability of an animal model (e.g. rabbit lumbar spine) in a particular loading mode (F/E and AT), the magnitudes, rates, and durations of a particular human motion must be approximated in the model system. The primary purpose of this dissertation was to assess aspects of F/E in spinal segments that were relevant to spinal motions in rehabilitation and occupational and recreational activities. Many activities of daily living (ADLs) involve small to moderate amounts of F/E [210, 272], while specific rehabilitation exercises and motion-based therapies (e.g. yoga), certain manual labor tasks, and various sports involve large amounts of F/E

and combined F/E with AT [19, 68, 71, 203]. Replicating these small and large F/E ROM activities *ex vivo* requires selecting moment targets that recapitulate appropriate segmental kinematics. Further, these targets must be translated from human to animal models.

The objective of this project was (1) to relate *in vivo* human F/E kinematics to *in vitro* human kinetics from data by Adams et al. [31], (2) to subsequently relate human kinetic data to rabbit kinetics in order to establish mechanical testing parameters that approximate relevant loading in human ADLs and spine-intensive activities (e.g. rehabilitation, manual labor, recreational sports like tennis, golf, rowing, etc.), and (3) to determine magnitudes of AT to combine with F/E to reflect occupational activities and segmental dysfunction leading to asymmetry.

4.2 PARAMETER DETERMINATION

4.2.1 Loading duration

The goal for the studies in Specific Aim 1 and 2 was simulation of a short activity like a rehabilitation routine or an occupational, recreational, or daily task. The duration of such activities varies [295, 296], but a preconditioning session of 15-20 minutes followed by one hour of repeated cyclic F/E was considered adequately representative.

4.2.2 Flexion/extension moment magnitudes

Identify maximum human lumbar in vivo and in vitro F/E motions

Adams et al. quantified human lumbar segmental motions *in vitro* and *in vivo* in similarly aged spines (Table 5) [31]. They identified segmental F/E movements *in vivo* for L2-3 (10/3°), L3-4 (12/1°) and L4-5 (13/2°). Using standard *in vitro* testing parameters, comparable F/E movements *in vitro*, per level, were L2-3 (9/5.5°), L3-4 (9/4.5°), and L4-5 (12/4°).

Table 5. *In vivo* and *in vitro* human lumbar spine flexion/extension range-of-motion

<i>In vivo</i>				<i>In vitro</i>		
F/E ROM (°)				F/E ROM (°)		
Level	Flexion	Extension	F/E	Flexion	Extension	F/E
L1-2	8	5	13	8	5	13
L2-3	10	3	13	9	5.5	14.5
L3-4	12	1	13	9	4.5	13.5
L4-5	13	2	15	12	4	16
L5-S1	11	5	16	12.5	4.5	17
<i>L1-S</i>	<i>54</i>	<i>16</i>	<i>70</i>	<i>50.5</i>	<i>23.5</i>	<i>74</i>

Data from Adams et al. [31]

Form coefficient for relating in vivo to in vitro F/E motions

As is evident from Table 5, *in vitro* testing underestimates flexion angles, overestimates extension angles, and slightly overestimates overall F/E rotation. These tendencies are quantified in Table 6 by expressing the ratio of *in vitro*-to-*in vivo* ROM. Coefficients in Table 6 serve as a means to convert between *in vivo* and *in vitro* ROM values.

Table 6. Ratio of *in vitro* to *in vivo* flexion/extension range-of-motion

Ratio: In vitro-to-in vivo ROM			
Level	Flexion	Extension	F/E
L1-2	1.00	1.00	1.00
L2-3	0.90	1.83	1.12
L3-4	0.75	4.50	1.04
L4-5	0.92	2.00	1.07
L5-S1	1.14	0.90	1.06
<i>Mean:</i>	<i>0.94</i>	<i>1.47</i>	<i>1.06</i>

Data derived from Adams et al. [31]

F/E angles measured in activities

ADL: Lee et al. measured lumbar spinal motions in activities of daily living. Overall F/E angles (L1-S1) were 4.51°, 4.83°, 10.09°, and 4.68° in level walking, single stair climbing, multiple stair climbing, and stair descent [210]. Alternatively, merging data collected by Jegede et al. [297], which expressed F/E motion in ADLs as a fraction of overall F/E motion, with *in vivo* F/E data collected by Marras et al. [298], Okawa et al. [299], and Lee et al. [300] revealed F/E angles in

ADLs: walking ($6.08 \pm 3.04^\circ$), stair ascent ($9.95 \pm 4.98^\circ$), and stair descent ($7.74 \pm 3.86^\circ$). These angle ranges are representative of motions in activities and exercises that do not require large spinal motions [272]. These angles represent 6.4-18% of maximum F/E ROM [31, 210, 297, 301, 302]

Spine-intensive activities: Spinal lumbar motions involved in motion-based therapies [303], occupations [304], and recreational activities [203] can involve large portions of maximum F/E ROM. Yoga exercises used to treat elderly low back pain patients involved F/E angles that reached a mean 56.5% of maximum F/E motion [303, 305]; younger patients may engage up to 100% of maximum F/E motion [306]. Healthcare workers spent more than 10% of their time at flexion angles 55.5 – 100% of maximum flexion [304]. Large flexion angles are common in other occupations as well [68].

Summary: In general, ADLs involving walking, stair climbing, etc. involve less than 20% of F/E ROM while lumbar-intensive activities involve 50-100% of F/E ROM.

In vitro equivalence of F/E angles: Humans to rabbits

After (i) characterizing the relationship between *in vitro* and *in vivo* ROM and (ii) identifying F/E angles in different activities, *in vivo* ROM in activities can be related to *in vitro* moment-rotation profiles. In particular, the position in the moment-rotation curve that corresponds to F/E angles *in vivo* is functionally important and practically necessary for establishing equivalent loading across species. To translate human *in vivo* angles to human *in vitro* angles, Table 2 can be used directly, which introduces fairly small adjustments. Direct translation of angles between humans and rabbits is not tenable, however, because of different non-linear relationships in moment-rotation curves.

Translation must be made based on the position of the F/E angles with respect to the neutral zone border, i.e. the transition between low stiffness and high stiffness loading. Human lumbar F/E moment-rotation curves for individual segments have low-stiffness regions of 1.4 – 5.0°, representing 12.2-37.1% of the overall curve [307]. Values for L4-5 were 12.2-30.6% of overall motion [307]. By contrast, rabbit lumbar spinal segments have significantly larger low-stiffness regions of 13.8 – 16.9° that comprise 52.2 – 80.0% of the overall motion [281, 282]. It is clear that scaling motions to rabbit spines based only on kinematic equivalence (i.e. simply matching angles by %ROM) would introduce error in amount of loading imparted to tissues based on differences in non-linearity of moment-rotation properties between species. Similar challenges would arise from scaled moment targets.

Connecting the *in vitro* simulated human F/E angles from ADLs and spine-intensive activities with NZ borders in human mechanical tests reveals whether angles are in the low or high stiffness region of moment-rotation curves. *In vitro* simulated ADL F/E motions are at or less than the edge of the low-stiffness neutral zone (Table 7). Conversely, *in vitro* simulated spine-intensive activity F/E motions (58.8-106%) are well within the high-stiffness region of the moment-rotation curve.

To achieve similar loading in rabbit FSUs, NZ width was established in this system. Skeletally mature L4-5 NZW rabbit spinal segments (n=6) tested in the robot testing system had NZ widths (found as described in Section 5.2.2) of $11.07 \pm 2.25^\circ$, representing 57.7% of F/E ROM (Table 8). These results agree with data reported previously [281]. Moment magnitudes spanning the NZ were 0.21 ± 0.05 Nm. Thus, flexion/extension moment targets were set to 0.17/0.05 Nm to reflect F/E angles in ADLs that are within the NZ. To represent spine-intensive activity, F/E angles

were chosen that repeatedly entered the linear region of rabbit FSUs, avoided damage to spinal tissues based on preliminary testing, and corrected for typical *in vitro* overestimation of *in vivo* extension [31]. F/E moment targets that met these criteria were 0.50/0.15 Nm.

Table 7. Human L4-5 F/E ROM in activities

Activity	Human L4-5 ROM (°)			Relative to NZ	
	<i>In vivo</i> ROM (°)	<i>In vitro</i> ROM (°)	%ROM	NZ (°)	NZ (%ROM)
<i>Maximum active ROM</i>	15.00	16.05	100.0	1.8 - 4.5	12.2 - 30.6
ADL (Small ROM) - lower	1.04	1.1128	6.9	<	<
ADL (Small ROM) - upper	2.16	2.3112	14.4	≤	≤
Intense (Large ROM) - lower	8.46	9.0522	56.4	>	>
Intense (Large ROM) - upper	15.00	16.05	100.0	>	>

Maximum ROM data derived from Adams et al., 2006 [31]. Activities of Daily Living (ADL) data further derived from Lee et al., 2011 [210]. Intense spinal activity ROM data obtained from Goncalves et al., 2012 [303] and Le Corroller, et al., 2012 [306]. Neutral zone (NZ) data obtained from White and Panjabi et al., 1990 [308] and Yamamoto et al., 1989 [307].

Table 8. Rabbit flexion/extension moment-rotation properties: Determining moment targets

	NZ (°)	NZ (%ROM)	Moment (Nm)
ADL Approximation: Small ROM	11.07 (2.26)	57.7 (3.0)	0.21 (.05)
Spine-intense Approximation: Large ROM	19.26 (4.20)	57.7 (3.0)	0.66 (.11)

Table 9. F/E moment targets

Approximation	Selected Targets (F/E) Nm
ADL: Small ROM	0.17 / 0.05
Spine-intense Activity: Large ROM	0.5 / 0.15

4.2.3 Axial torsion moment magnitudes

In Specific Aim 2, axial torsion (AT) is coupled with F/E to induce axial asymmetry during repeated F/E movements. A more complete motivation and justification for this combined AT + F/E loading can be found in Section 6.2.2. Briefly, the goal was to compare neutral F/E to asymmetric F/E with mild and severe amounts of coupled AT. Axial asymmetries may arise from (1) active combined bending and twisting in demanding manual labor [68] or (2) segmental dysfunction mediated by connective tissue lesions (e.g. facet-mediated adhesions) [79] or sensorimotor control dysregulation [14, 194]. Torsional movements in the human lumbar spine are small; *in vivo* human lumbar segmental AT motions are 0.9-1.4° (excluding L5-S1) [31]. In *in vitro* mechanical testing, human L3-4 and L4-5 maximal AT motions are 2.1±1.3° and 1.4±1.5° at 10 Nm of applied torque [309]. *In vitro* testing studying effects of torsion on disc mechanics in human lumbar segments applied torques corresponding to 11-40% of failure loading [273].

Matching rabbit torsion to appropriate amounts of torsion in human motions can be based directly on percent of maximum torsion because torsion is linear in moment-rotation properties for both humans and rabbits [281, 310]. Rabbit torsional stiffness and moment-rotation properties are not significantly different from humans [291]. Preliminary testing of n=3 rabbit L4-5 FSUs showed AT failure at 1.91±.04 Nm; a representative load-to-failure plot is shown in Figure 19. Mild to moderate coupled torsion was chosen at 20% of AT failure loading, 0.4 Nm in rabbit L4-5 FSUs, to represent torsional angles within putative normal AT ROM (Small AT). To represent severe, non-injurious coupled torsion that goes to the end ROM observed *in vivo* or simulated *in vitro*, 40% of AT failure, 0.8 Nm in rabbit L4-5 FSUs, was chosen (Large AT).

Table 10. AT torsion moment targets

Coupled AT	Selected Targets (AT) Nm
Small AT	0.4
Large AT	0.8

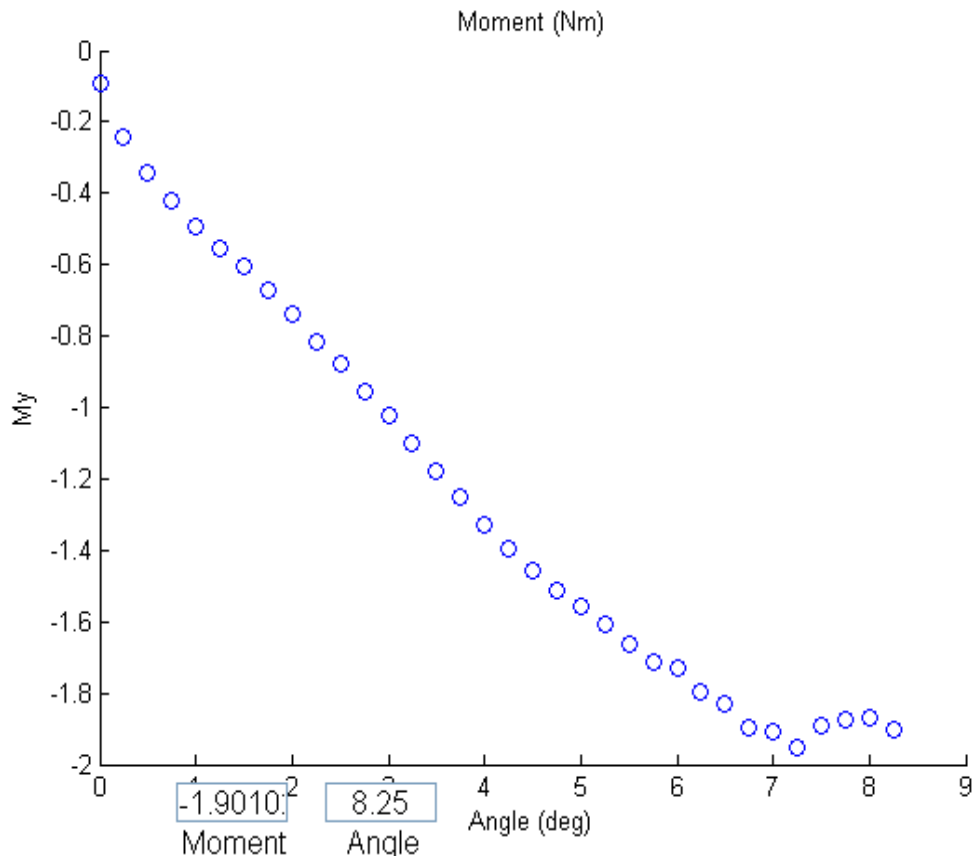


Figure 19. Representative load-to-failure moment-rotation profile for axial torsion

4.2.4 Loading rate

In vivo F/E motion rates are not typically reported directly [210, 311], but motion rates can be calculated. In studies where lumbar motions are presented during gait cycles [210, 311], durations of gait cycle can be used to approximate *in vivo* lumbar F/E motion rates [210, 312, 313]. Using

this approach, F/E motion rates in ADLs involving walking range from 2.83 – 7.96 °/s. F/E motion rates in spine-intensive activities like yoga involve a range of F/E motion rates. Available data suggests F/E lumbar motion rates range from 0.67 – 30 °/s [199].

Approximation of *in vivo* motions using *in vitro* systems typically occurs at slower motion rates than those observed *in vivo* because of the difficulty in safely rotating specimens at high speeds [277]. Determination of the pure moment motion path, which occurs during preconditioning in the robotic testing system employed in these studies, uses an adaptive displacement control (Appendix D.1.2) that operates quasi-statically with steps $\leq 1^\circ$ in size. Kinematic replay of robot joint angles (Appendix D.1.3) from path determination can occur at higher motion rates that better approximate *in vivo* motion rates. Robotic spine testing systems have achieved motion rates of 0.25, 0.35, 0.8, 2, and 6.67 °/s [87, 289, 314-316]. Using the robotic testing system in these studies, F/E motions were replayed at 0.33-0.5 °/s. Thus, while underestimating *in vivo* motion rates, loading rates were comparable to numerous robotic systems used in lumbar spinal loading.

5.0 FLEXION/EXTENSION: RANGE-OF-MOTION & CYCLES

5.1 INTRODUCTION

A common trait observed in patients experiencing back pain is altered kinematics [64]. Trunk motion is governed by the integration of passive, osteoligamentous spinal structures with active musculature. Spinal movements are often coupled, but they are typically simplified to flexion/extension (F/E), axial torsion (AT), and lateral bending (LB)—rotations in the sagittal, transverse, and coronal planes, respectively. Motions in all planes are important in activities of daily life [272] but F/E, in particular, is essential to tasks associated with back injury [270, 317] and can provoke or be altered by back pain [64, 70, 318]. [319]

Motion-based therapies for low back pain often focus on rehabilitation involving F/E movements to improve patient function and restore normal motion patterns [271, 319-321]. Clinical practice suggests a benefit from tailored rehabilitative regimens where parameters of exercise movements like range of motion (ROM), number of cycles, and duration of movements are carefully prescribed [322]. These parameters of F/E are involved in many commonly used rehabilitation strategies [271, 319-321], yet little evidence exists to develop and prescribe exercise protocols for individual patients. More fundamentally, the biological effect of F/E loading parameters on spinal tissues remains largely unknown. The spinal column comprises functional spinal units (FSUs) made up of bony vertebrae that transmit load, an intervertebral disc and facet joints that withstand compression and enable articulation in six degrees-of-freedom (DOF), and numerous spinal ligaments that stabilize segmental motions. In lumbar FSUs, flexion is constrained posteriorly by tension in the posterior ligamentous complex, among which the

ligamentum flavum (LF) factors prominently [86, 87], and anteriorly by the swelling pressure of the disc [87, 323, 324]. A majority of the resistance to extension is provided by discs, but a modest amount (16-40%) is withstood by the facet joints [86-88]. Damage to or degradation of any one of these structures can cause altered segmental mechanics, local instability, and coupled degeneration of joint components/tissues, contributing to back pain [98, 146]. Mechanical loading of spinal tissues can alter biological processes, exacerbating or ameliorating mechanisms underlying degenerative changes and painful symptoms. Therefore, improved knowledge of how motion parameters interact with inflammatory, degenerative, and remodeling processes has the potential to assist rational prescription of exercise.

Biological effects of mechanical loading in discs have been well studied using *ex vivo* organ culture systems. *Ex vivo* systems enable elucidation of the isolated role of applied mechanics within well-controlled environmental conditions. To date, researchers have primarily cultured disc-only explants where bony endplates are removed to maximize culture duration but loading mode is constrained to axial compression [34, 256-259]. Recent advances have explored new loading modes—combined torsion [36] and asymmetric compression [37]—and loaded FSU organ culture [269]. Culturing and loading intact FSUs facilitates *in-situ* loading in physiologic rotations by preserving vertebra, endplates, facets, and spinal ligaments essential to replicating these loading patterns. Further, subjecting preserved FSUs to multi-dimensional loading permits simultaneous evaluation of the biological response in all spinal tissues.

The objective of this study was to determine the effect of spinal F/E on catabolism and inflammation simultaneously in all types of spinal tissue—AF, NP, FC, and LF—in viable FSUs. We hypothesized that larger motions would increase catabolic and inflammatory markers in all

tissues, and smaller motions would reduce catabolic and inflammatory markers in all tissues relative to unloaded controls. We further hypothesized that increasing the number of cycles would elevate catabolic, inflammatory, and structural markers.

5.2 METHODS

5.2.1 Specimen Preparation

Thirty-four lumbar spines were isolated from skeletally mature (>10 months old) New Zealand White rabbits. FSUs were extracted from two levels—L2-3 and L4-5—within two hours of death and dissected to remove musculature and produce clean osteoligamentous segments. FSUs were rinsed in phosphate-buffered saline and were then attached within a temperature- and oxygen-controlled bioreactor for mechanical loading as described previously [269] or placed in static culture as an unloaded control. Loaded FSUs (L4-5) were matched to unloaded control FSUs (L2-3) from the same spine; both FSUs were placed in 10% fetal bovine serum-and 1% penicillin/streptomycin-supplemented Dulbecco's Modified Eagle's Medium including 4.5 g/l glucose with 110 mg/l sodium pyruvate at $37(\pm 0.5)$ °C, 5%/5% O₂/CO₂. Media was pumped through the bioreactor at 1.1 mL/min.

5.2.2 *Ex vivo* Flexion/Extension

The custom-built bioreactor was attached to a serial-linkage robot used previously for *in vitro* flexibility testing of rabbit FSUs [282]. Flexible, silicone and nitrile rubber walls contained media

and permitted free movement of the FSU in six DOF (Figure 20). After reaching steady-state temperature and media flow (~30 min.), FSUs were subjected to three cycles of quasi-static F/E for preconditioning and determination of the segment's pure-moment F/E path [277].

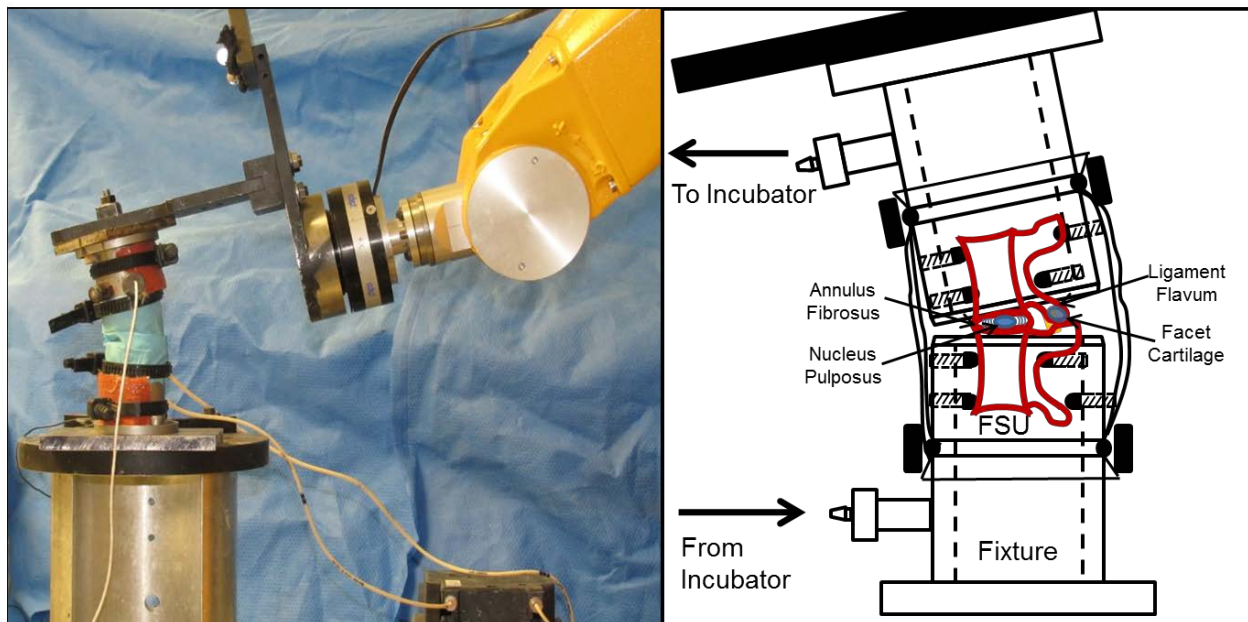


Figure 20. Bioreactor attached to robot testing system circulating media with enclosed, flexed FSU

To test the effect of ROM, FSUs were assigned to small and large groups defined by 0.17/0.05 and 0.5/0.15 Nm moment targets in F/E. Targets were selected so that specimens assigned to small ROM remained within the low stiffness region of the moment-rotation curve (i.e. the neutral zone) and specimens assigned to large ROM entered the high stiffness, linear portion of the curve (i.e. the elastic zone) in flexion and extension (Figure 21). The kinematics of the third path were then replayed for one hour at 0.33°/s.

Because time and loading rate were fixed rather than cycle number, which would differ between large and small ROM, a separate set of experiments was performed to examine the effect of cycle number. FSUs were subjected to large ROM load targets for one hour (1h Cycle), two hours (2h Cycle), or one hour of cycling followed by one hour of static culture (1h Cycle_1h Static). Comparing 1h Cycle to 1h Cycle_1h Static demonstrates the effect of doubling culture duration, and comparing 1h Cycle_1h Static to 2h Cycle isolates the effect of doubling cycles.

Mechanical analyses were performed to characterize the response of FSUs to applied loading. Mean ROM and cycle number were calculated for each group. Work applied to FSUs per cycle, W_{cycle} , was computed by integrating the primary moment at each angle, M_{θ} , with respect to primary angle, θ , in flexion and extension.

Equation 3. Work in flexion/extension per cycle

$$W_{cycle} = \sum_{\theta=\max.\text{extension}}^{\theta=\max.\text{flexion}} M_{\theta} \cdot d\theta + \sum_{\theta=\max.\text{flexion}}^{\theta=\max.\text{extension}} M_{\theta} \cdot d\theta$$

Work was averaged and summed across cycles for cumulative and mean work. Similarly, total and mean energy dissipation (hysteresis, H_{cycle}) were calculated using the difference between loading and unloading curves per cycle.

Equation 4. Hysteresis in flexion/extension per cycle

$$H_{cycle} = \sum_{\theta=\max.\text{flexion}}^{\theta=\max.\text{extension}} M_{\theta} \cdot d\theta - \sum_{\theta=\max.\text{extension}}^{\theta=\max.\text{flexion}} M_{\theta} \cdot d\theta$$

Neutral zone stiffness (NZ_k , Nm/°) and width (NZ_{width} , °) were found using methods described by Smit et al. [325] (Figure 21) (Appendix D.4.4). Briefly, the moment-rotation data were fit with a double sigmoid function to allow stiffness-based demarcation of the neutral zone and elastic zone (i.e. linear region):

Equation 5. Sigmoidal function used for curve-fitting flexion/extension moment-rotation

$$R = \frac{c1}{1 + e^{-(a1+b1*x)}} - \frac{c2}{1 + e^{-(a2+b2*x)}} + d$$

where R is the rotation, a and d represent horizontal and vertical shift parameters, respectively, and b and c reflect the shape of the function. Two functions are added to model the loading and unloading curve. The inflection points—extrema of the second derivative—are used to define the width of the NZ based on the region of minimal stiffness [325]. NZ stiffness was found using a first-order linear fit of the NZ region (Appendix D.4.4). Elastic zone (EZ) stiffness (EZ_k) was calculated in the final three positions ($\sim 10\%$) of the moment-rotation curve.

Equation 6. Elastic zone stiffness

$$EZ_k = \frac{M_f - M_{f=3}}{\theta_f - \theta_{f=3}}$$

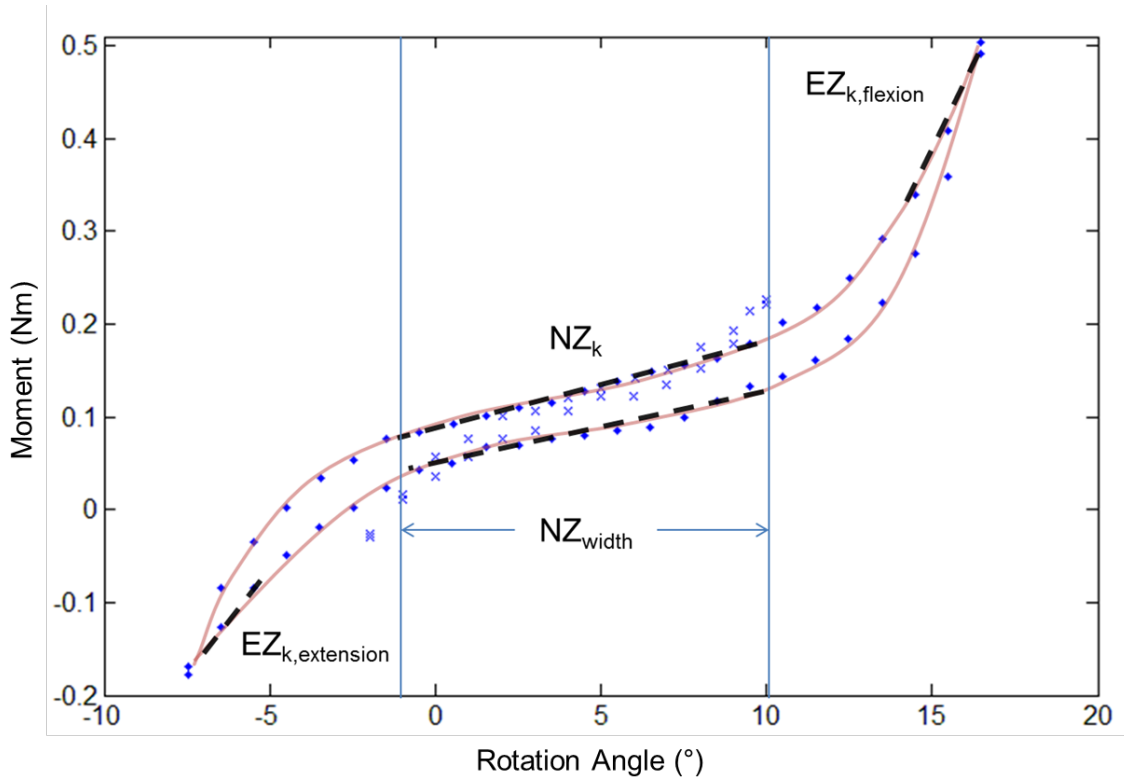


Figure 21. Representative F/E moment-rotations to small (x) and large (o) ROM (curve-fit).

Changes in mechanical measures—primary moment, work, hysteresis, and stiffness—were calculated by normalizing differences between the third cycle and the last cycle by the third cycle of replayed kinematics (Appendices D.4.3 and D.4.5). The third cycle was chosen to allow for preconditioning of the moment-rotation response at the higher loading rate used for kinematic replay. As the chief example, where M_f and $M_{x=3}$ were the moment values for the final and third cycles, primary moment relaxation, $R_{M'}$, was given by:

Equation 7. Primary moment relaxation

$$R_{M'} = \frac{M_f - M_{x=3}}{M_{x=3}}$$

5.2.3 Biological Assessments

Immediately following loading, FSUs were removed from the bioreactor and incubator, and tissues were isolated and stored in RNAlater® (Qiagen, Venlo, ND) at -80°C. To isolate RNA, tissues were minced, homogenized by bead milling (5-10 min.), and extracted using Qiazol Lysis Reagent (Qiagen) and 24:1 chloroform:isoamyl alcohol (Sigma-Aldrich, St. Louis, MO). RNA was then purified using the RNeasy Universal Tissue Kit (Qiagen). Real-time reverse-transcription polymerase chain reaction (RT-PCR) was performed using an iQ5 real-time thermal cycler (BioRad, Hercules, CA) with SYBR green and custom-validated rabbit primers (Table 1) for *matrix metalloproteinase (MMP)-1*, *MMP-3*, *a disintegrin and metalloproteinase with thrombospondin motif (ADAMTS)-5*, *cyclooxygenase (COX)-2*, and *aggrecan (ACAN)*. Sample number varied, based on yield of RNA, by tissue and experimental aim: n=4-5 (NP), n=4-7 (FC), n=5-7 (AF), and n=5-7 (LF) for ROM comparisons, and n=3-5 (all tissues) for additional Cycles groups. Relative gene expression (RGE) between tissues from loaded and unloaded FSUs was

calculated by normalizing to *glyceraldehyde-3-phosphate dehydrogenase (GAPDH)* as a housekeeping gene using the $2^{-\Delta\Delta C_t}$ method [326]. The effect of culture was assessed by also performing RGE between unloaded and *t0* tissues for *MMP-3* and *COX-2* (n=3-5).

Table 11. List of quantitative real-time reverse transcription-polymerase chain reaction primer sequences

Gene	Primer sequences (5'→3') (upper, sense; lower, anti-sense)	GeneBank accession number
<i>MMP-1</i>	GCCTGTCACTCGCAAACC GACCTACGCACCCACACAC	NM_001171139
<i>MMP-3</i>	ACANCAATGGAAATGAAAACCTCTTC CCAGTGGATAGGCTGACANAAA	NM_001082280
<i>ADAMTS-5</i>	CTGTGCCGTGATTGAAGATG CGATACTGGTGAGGATGGATG	XM_002716775
<i>COX-2</i>	CAGGCACCAGACCAAACACTT CACGCAGGTGGAGATGATCTAC	NM_001082388
<i>ACAN-1</i>	GCTACGGAGACAAGGATGAGTTC CGTAAAAGACCTCACCCCTCCAT	XM_002723376
<i>GAPDH</i>	GCTGAGATGATGACCCTTTTGG GATGCTGGTGCCGAGTAC	NM_001082253
ADAMTS, a disintegrin and metalloproteinase with thrombospondin motifs; MMP, matrix metalloproteinase; ACAN, aggrecan; COX, cyclooxygenase; GAPDH, glyceraldehyde 3-phosphate dehydrogenase		

Effects of loading on matrix catabolism were assessed by examining degradation products of aggrecan by Western blotting (Section 1.01(a)(i)Appendix E) in each tissue (n=4 per tissue, per condition). FSUs used for matrix degradation assessment were subjected to repeated F/E as described previously and left to remain in culture for an additional 24 hours from the onset of loading. Tissues from unloaded FSUs were compared to baseline (*t0*) tissues to assess effects of culture. Briefly, proteoglycans were extracted in 4 M guanidine hydrochloride, precipitated in ethanol, and treated with endo-beta-galactosidase (Sigma) and then chondroitinase ABC (Sigma)

for de-glycosylation. Equivalent amounts per weight of tissue were added (30 μ l) in a 10% acrylamide gel. Samples were separated by electrophoresis, transferred to a polyvinyl fluoride membrane, blocked with 5% skim milk, probed with a primary antibody for the aggrecan G1-domain (generously provided by Dr. P. Roughley) [327] and a subsequent secondary anti-rabbit antibody (31460, Thermo Scientific, Waltham, MA), and imaged using the ChemiDoc MP system (BioRad) following chemiluminescence activation. Densitometry quantification was performed using Image Lab Software 5.0 (BioRad); bands from mechanically loaded tissues were normalized by bands from unloaded tissues of the same animal for each tissue. Western blotting reagents were obtained from Thermo/Pierce (Rockford, IL).

5.2.4 Statistical Analysis

One-way independent ANOVA followed by Wilcoxon rank-sum tests with Bonferroni correction were performed to examine the effect of group (small ROM, large ROM/ 1h Cycle, 2h Cycle, 1h Cycle_1h Static) on mechanical properties. Two-way, independent ANOVA was performed for relative gene expression and immunoblotting densitometry to examine the effect of loading and group. Changes between groups were subsequently tested using Wilcoxon rank-sum sum tests with Bonferroni correction. Analyses were performed in MATLAB (The Mathworks, Inc., Natick, MA). Significance was set to $p < 0.05$, and values were expressed as mean \pm standard deviation. Symbol (\dagger) designates a significant effect of loading in the ANOVA ($p < .05$), (#) denotes a significant effect of group in the ANOVA ($p < .05$), and (*) indicates a significant effect of loading in post-hoc tests ($p < .0167$).

5.3 RESULTS

5.3.1 *Ex vivo* Flexion/Extension- Mechanical Characterization

Mechanical description of the loading performed in ROM and cycle number testing is summarized in Table 12 and Table 13. The large ROM group underwent approximately half the number of cycles (31.5 ± 5.7) as the small ROM group (60.9 ± 7.1). The results of the ANOVA testing differences in group (i.e. small ROM, large ROM/1h Cycle, 2h Cycle, and 1h Cycle_1h Static) showed significant effects for cumulative work, mean work, and variation in hysteresis over cycles (F : $p < .0001$, $p < .0001$, and $p = .0298$, respectively). Post-hoc tests revealed that mean and cumulative work were significantly higher in the large ROM group than the small ROM group ($p = .0001$ and $p = .0350$, respectively). In contrast, mean and cumulative hysteresis showed no effect of group. Additionally, variability in hysteresis across cycles, a reflection of repeatable moment-rotation responses, was higher in the small ROM group than the large ROM group ($p = .0035$). The effect of group also significantly influenced change in F/E moment over cycles (F : $p = .0001$), where FSUs subjected to large ROM experienced greater load relaxation ($8.70 \pm 4.11\%$) than the small ROM group ($0.52 \pm 5.12\%$) ($p = .0001$). Differences in neutral zone stiffness and change in stiffness across cycles between all groups were not statistically significant.

Mechanical properties of large ROM groups with varying cycles and durations (i.e. 1h Cycle, 1h Cycle 1h Static, and 2h Cycle) were similar. The 1h Cycle and 1h Cycle_1h Static groups underwent approximately half the number of cycles as the 2h Cycle groups. But, as expected, FSUs in the 2h Cycle group experienced nearly twice the cumulative work ($p = .0159$) and dissipated more than twice the energy compared to 1h Cycle_1h Static FSUs ($p = .0318$). No other differences in work, hysteresis, or primary moment were significant between these groups.

Table 12. Energetics: Mean (SD) work and hysteresis measures per group

Group	Cycles	N	Work (J)				Hysteresis (J)			
			Cumulative	Mean	Stdev	%Change	Cumulative	Mean	Stdev	%Change
Small ROM	60.92 (7.13)	12	147.05 (80.15)	2.42 (1.30)	0.075 (.046)	-0.001 (.107)	33.57 (38.94)	0.565 (.641)	0.023 (.009)	-0.215 (.502)
Large ROM (1h_1xCyc)	31.75 (5.56)	12	191.05 (33.31)	6.18 (1.59)	0.148 (.096)	0.051 (.059)	21.20 (12.38)	0.692 (.455)	0.051 (.031)	0.0155 (.317)
Large ROM (2h_1xCyc)	28.75 (4.57)	4	190.35 (28.29)	6.66 (0.88)	0.125 (.021)	0.043 (.021)	19.71 (7.56)	0.671 (.187)	0.033 (.009)	-0.003 (.128)
Large ROM (2h_2xCyc)	66.40 (7.47)	5	364.00 (28.52)	5.54 (0.79)	0.113 (.083)	0.008 (.069)	41.75 (10.65)	0.631 (.187)	0.042 (.021)	0.199 (.296)

Table 13. Kinetics: Mean (SD) moment-rotation properties and neutral zone stiffness for each group

Group	Moment-Rotation				Neutral Zone Stiffness		
	ROM (°)	Mx (Nm)	Change (Nm)	Relaxation (%)	Stiffness (Nm/°)	Standard Dev.	Relaxation (%)
Small ROM	10.82 (1.84)	0.30 (.06)	0.00 (.02)	0.516 (5.119)	0.027 (.012)	0.0004 (.0002)	-0.003 (.054)
Large ROM (1h_1xCyc)	19.37 (3.48)	0.67 (.04)	0.05 (.03)	8.695 (4.107)	0.016 (.004)	0.0009 (.0005)	0.071 (.111)
Large ROM (2h_1xCyc)	22.07 (3.82)	0.68 (.05)	0.05 (.01)	7.731 (1.839)	0.017 (.009)	0.0004 (.0002)	-0.007 (.016)
Large ROM (2h_2xCyc)	18.55 (2.07)	0.65 (.04)	0.07 (.03)	10.973 (4.484)	0.019 (.003)	0.0008 (.0004)	0.002 (.012)

ROM, range of motion; Mx, x-axis moment (flexion/extension); Change, change in moment; Relaxation, normalized change in parameter

5.3.2 Biological Assessment of Flexion/Extension: Range-of-Motion

Results of the ANOVA assessing real-time RT-PCR of small and large ROM (Figure 22) demonstrated that F/E loading increased *MMP-3* expression in AF ($F: p=.0003$). In post-hoc tests for each group, *MMP-3* expression in the small ROM group in AF was significantly up-regulated (3.32-fold, $p=.0022$). In FC, *COX-2* expression was also significantly up-regulated by F/E loading in the analysis of both groups ($F: p=.0375$), though post-hoc testing did not identify a significant elevation of expression (2.13-fold) with large ROM ($p=.1269$). Results of the ANOVA demonstrated that F/E loading showed a strong trend toward increased *MMP-3* expression in FC ($F: p=.0576$), and post-hoc tests of individual groups pointed to significantly increased *MMP-3* expression in the large ROM group (1.97-fold, $p=.0026$). Similarly, F/E loading in LF increased *MMP-3* and *COX-2* with near significance ($p=.0527$ and $p=.0724$, respectively), though

subsequent post-hoc tests of individual groups did not approach significance. In NP, F/E loading did not show significant changes in *MMP-3*, *COX-2*, and *ACAN* gene expression (*MMP-1* and *ADAMTS-5* not measured). *MMP-3* and *COX-2* expression were elevated in all tissues except for NP *COX-2* expression in unloaded FSUs compared to baseline (*t0*) (Appendix A, Figure 38).

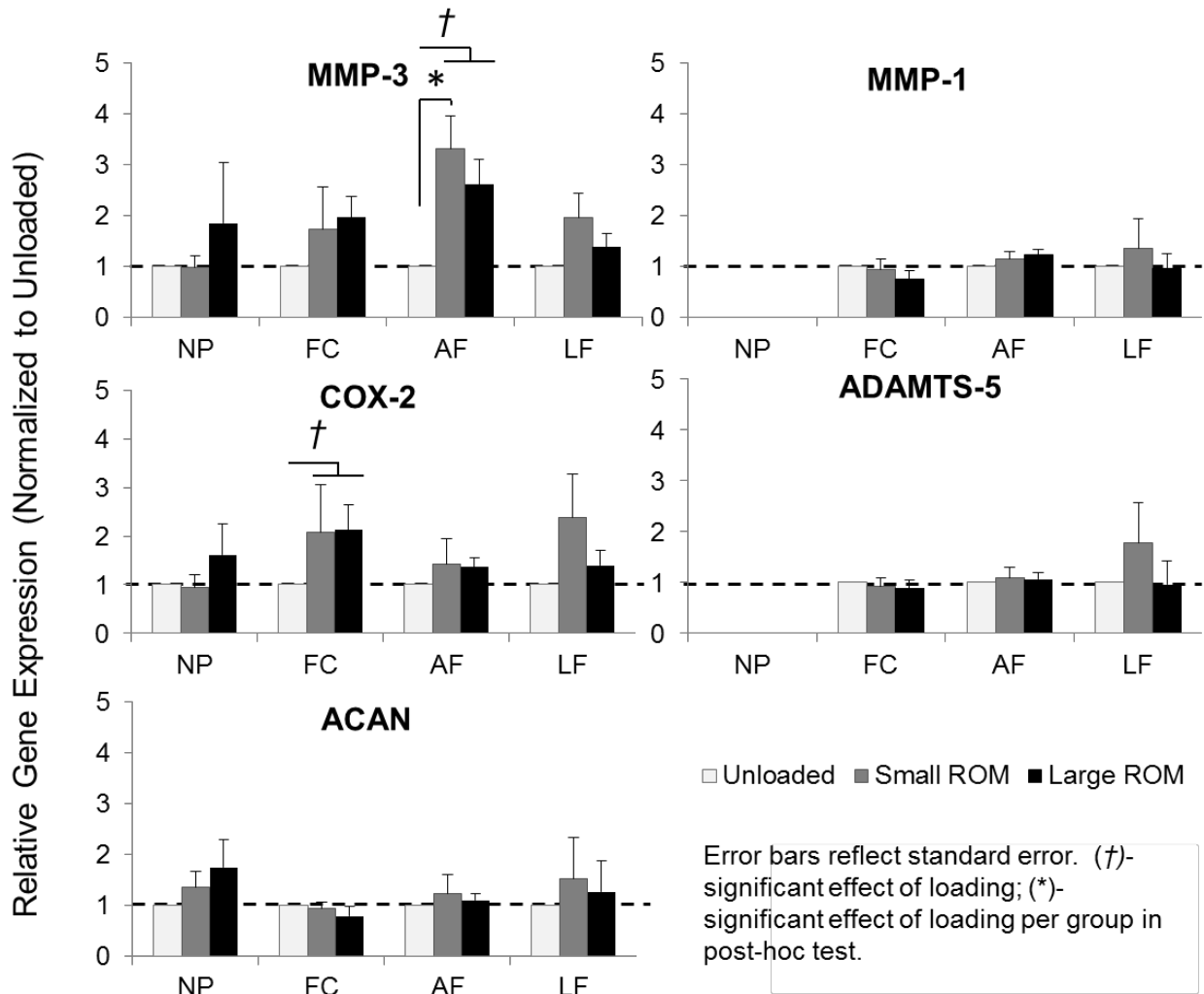


Figure 22. Mean fold (\pm SEM) change in relative gene expression of NP,FC, AF, and LF with loading.

Immunoblotting of aggrecan degradation after F/E (Figure 23) showed that F/E ROM had a significant effect on the MMP-mediated fragments in AF tissue ($p=.0451$) with the large ROM group increasing with loading (1.7-fold). In NP, MMP- and ADAMTS-fragments tended to increase with F/E loading, but trends were not significant ($p=.2034$ and $p=.2059$, respectively) and ROM had no influence. F/E loading tended to increase ADAMTS-fragments in FC ($p=.1718$) compared to unloaded controls irrespective of ROM. MMP-fragments in FC decreased with F/E loading in the small ROM group but increased in the large ROM group; ROM showed a trend of affecting MMP-fragment abundance in FC ($p=.1340$). Aggrecan fragments were not significantly altered by culture compared to baseline ($t0$) (Appendix A, Figure 39). No aggrecan staining was detected in LF.

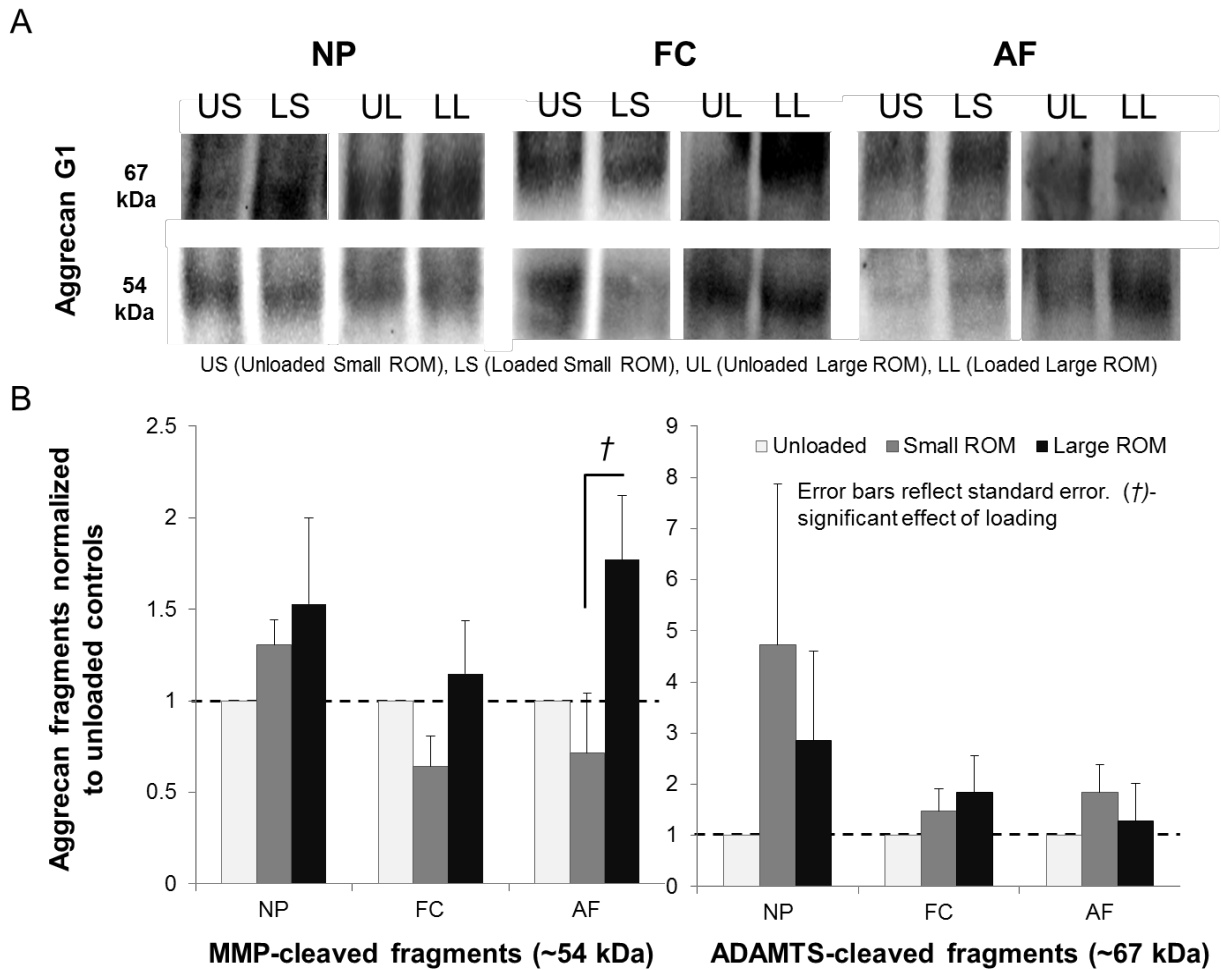


Figure 23. (A) Representative immunoblots against G1 for NP, FC, and AF. (B) Mean (\pm SEM) normalized densitometry for MMP- and ADAMTS-cleaved G1 fragments.

5.3.3 Biological Assessment of Flexion/Extension: Cycles and Duration

Results from the ANOVA of samples subjected to varying durations and cycles (Figure 24) showed that F/E loading had a significant effect on *MMP-3* expression in FC and AF (F : $p=.0176$ and $p=p<.0001$, respectively). Post-hoc testing confirmed elevation of *MMP-3* expression in 1h Cycle in FC ($p=.0022$) and in both 2h Cycle (2.57-fold) and 1h Cycle_1h Static (2.34-fold) in AF compared to unloaded ($p=.0079$ and $p=.0286$, respectively). Similar to ROM analysis, *COX-2*

expression was significantly elevated in FC with F/E loading ($F: p=.0088$). The effect of F/E loading and group were significant for *ACAN* expression ($F: p=.0032$ and $p=.0460$, respectively), and post-hoc testing showed significant increases with F/E loading in 2h Cycle (1.78-fold) and 1h Cycle_1h Static (2.27-fold) ($p=.0286$ and $p=.0286$) and, importantly, significant increases with culture duration ($p=.0242$). The significant increase of *ACAN* expression with culture duration in AF was the only such effect; it was mirrored by a similar trend *ADAMTS-5*, which also regulates aggrecan. FC responded to F/E loading with significant effects on *MMP-1* expression ($F: p=.0262$). *MMP-1* expression in FC was decreased in all groups (14-40%), though effects in individual groups were not significant. LF showed trends of increased *MMP-3* and *COX-2* expression in response to F/E loading ($F: p=.0683$ and $p=.0619$, respectively); however, no effect of culture duration or cycle number were evident. Catabolic and inflammatory gene expression in NP showed no significant effect.

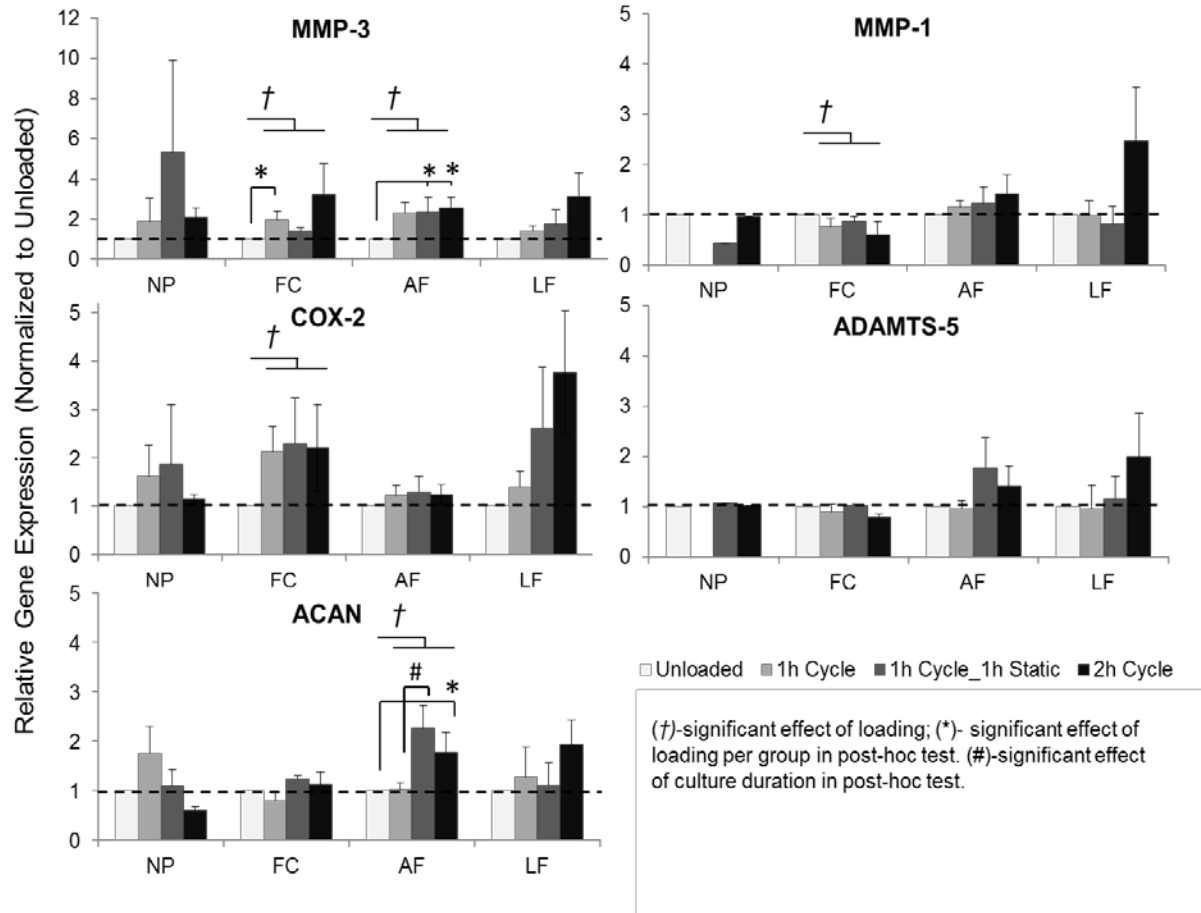


Figure 24. Mean fold change (±SEM) in relative gene expression NP, FC, AF, and LF with loading.

5.4 DISCUSSION

The present study is the first to investigate simultaneous biological responses of disc, facet, and ligamentum flavum to mechanical loading. It provides initial mechanobiological data of how these tissues respond to F/E loading *in-situ*. ROM, an intrinsic feature of F/E relevant to occupational and recreational activities and motion-based therapies, was varied to assess its influence on inflammatory and catabolic markers. Secondly, to isolate the effect of ROM from another F/E

parameter—number of cycles—the duration and cycles of loading were varied in additional experiments. The major findings of this study show a predominantly catabolic response to F/E loading among tissues of the FSU.

The *ex vivo* system developed for this study is the first to be capable of complex, six DOF movements using intact FSUs. Recent research in *ex vivo* disc organ mechanobiology has explored combined compression and torsion [36] and wedge-shaped compression [37]. These systems, along with others recently developed [34, 256, 328], are capable of long-term, diurnal, dynamic loading. However, they are unable to recapitulate physiologic rotational loading, primarily because of the endplate preparation necessary for long-term culture. Further, ligaments and facet joints are removed along with bone in disc explant preparation, so the interaction of FSU components cannot be assessed. Thus, while the samples used in this study are limited to shorter experimental durations [269], this system is capable of examining complex, 6 DOF loading and the role of other tissues in FSUs (i.e. ligaments and facet joints) that are thought to be important in back pain [151, 329] and related degenerative disorders [25, 158, 330].

In physiologic spinal motions, disc, facet joints, and spinal ligaments interact to support loading and restrict motion. Degenerative disorders associated with aging and spinal pathologies may degrade tissue structure in one spinal tissue which in turn negatively affects mechanical loading in other tissues. Facet joint osteoarthritis, for example, is highly associated with disc degeneration [150]. Loss of disc height and segmental hypermobility appear to alter facet loading and lead to degenerative changes of the facet joints [160]. Similarly, altered loading associated with loss of disc height or facet joint degradation may induce hypertrophic processes or buckling in the LF [331]. It is suspected that altered FSU mechanics provoke inflammation [128, 329, 332],

catabolism [249, 333, 334], or compensatory remodeling [250, 333, 335] in these spinal tissues. Development of this system, which preserves intact FSUs and subjects them to complex loading, enables examination of coupled biological responses to altered mechanics in spinal tissues.

Responses to loading were measured after short durations of F/E to approximate exercise sessions or brief activities of daily living. Changes in systemic biological markers with exercise and mechanical loading have been shown to occur rapidly [336-338]. Further, single, brief applications of compression in rat tails have been shown to modulate relative gene expression in discs of biological markers including *MMPs*, *ADAMTSs*, and *ACAN* [339]. Initial biological changes like those measured in the current study cannot be conclusively classified as maintenance, adaptation, or on/off signals without later assessments of matrix catabolism and inflammation [9]. However, the modest magnitude of applied moments and increases in catabolic and inflammatory gene markers in some tissues suggests a remodeling or maintenance response to applied F/E.

In general, F/E loading, regardless of ROM or cycle number, caused an increase in catabolic signaling. In the current study, *MMP-3* proved to be the most responsive gene to F/E loading across different spinal tissues. *MMP-3* is up-regulated early in catabolic processes [340] and has been shown to be responsive to mechanical loading [242, 252]. A collagenase downstream of *MMP-3*, *MMP-1*, was not up-regulated. Mechanically responsive pro-inflammatory changes have been measured by expression of *COX-2* [205, 332]. Elevation of *COX-2*, observed in FC and LF but not disc tissue, was also not dependent on F/E parameter. In extension, FC undergoes combined compression and shear [67]. Both of these loading modes have been shown to provoke increases in *COX-2* expression in chondrocytes [341, 342], but shear stress is a more well-characterized, robust driver of *COX-2* dependent inflammation in chondrocytes [226, 227]. In the current study, *COX-2* expression was elevated to similar levels in small and large ROM, and

compressive loading was not applied, suggesting that compression in FC was relatively low [92], confirmed by Chapter 7.0 , and that shear forces played a larger role in the observed up-regulation of *COX-2* expression. In flexion, LF is a primary resistance band supporting 21-28% and 15-25% of applied flexion moments at mid and end-ROM [86, 87]. Inflammation in general contributes strongly to LF thickening [155, 156], and *COX-2* expression in particular increases with LF thickness [156]. *In vitro* loading of LF fibroblasts revealed a load-responsive increase in pro-inflammatory cytokines via *COX-2* [161]. *Ex vivo* F/E loading in the current study, particularly in groups with greater cycles of loading, showed a similar load-response increase in *COX-2*. Mechanical F/E loading did not influence aggrecan or *ADAMTS-5* gene expression aside from longer loading durations in AF. Aggrecan, the predominant, functional matrix component of disc and cartilage primarily acts to enhance compressive properties of the matrix [130, 131], and *ADAMTS-5*, the most efficient aggrecanase [343], plays a role in aggrecan breakdown and remodeling. Aggrecan and aggrecanases have been shown to be regulated by mechanical compression in disc tissue and cartilage, increasing with magnitude and duration of loading [149, 251, 344, 345]. In the AF, which phenotypically expresses lower amounts of aggrecan than the NP and FC [110], increased ACAN expression may reflect a shift toward an altered, compensatory remodeling to support higher levels of compressive stress [9]. Lack of regulation by F/E loading in pure-moment application suggests little adaptive response from spinal tissues to this loading mode, which may reflect the non-disruptive, physiologic nature, the low magnitudes of compression, or the short duration of the applied loading.

Responses to F/E loading were also measured after 24 h of static culture following loading with the goal of identifying early protein-level changes and net-effects on matrix catabolism. Alteration of aggrecan fragments has been shown to occur following detrimental mechanical

loading and inflammatory stimuli [37, 149, 346]. Long-term compression of caudal discs in rats increased and shifted aggrecan fragment patterns to predominantly MMP-mediated fragmentation in NP and AF [149]. In the current study, large ROM tended to elevate the abundance of MMP-fragments, and small ROM did not. At the level of mRNA expression, the findings were reversed. Lack of synchronicity in response between mRNA and protein expression is not unexpected [347], particularly for a relatively short intervention where protein expression and activation may lag behind gene expression. Aggrecanase-mediated fragments did not appear to be sensitive to F/E loading in any tissues, and this reflects the general lack of load responsiveness observed in ADAMTS-5 mRNA expression. Thus, these findings are similar to previous studies of longer durations and detrimental interventions wherein MMP-fragments show load-responsive increases, especially in the AF [149].

F/E parameters—ROM, cycle number, and culture duration—were varied with the goal of delineating the effect of F/E amplitude on biological markers. However, the effects of ROM and cycles were not broadly significant. Culture duration increased *ACAN* expression in AF, with similar trends mirrored in *ADAMTS-5*, suggesting a delayed, adaptive remodeling response [9]. In a series of investigations by Solomonow et al., researchers identified high loading magnitudes and rates and increased number of cycles of F/E as capable of inducing an inflammatory, tissue-degrading response in supraspinous ligaments over longer time frames *in vivo* [243]. In the current study, increased number of cycles tended to elevate expression of catabolic and pro-inflammatory genes in LF, pointing to a similar role for cycles of F/E in inflammatory remodeling.

While this study takes a first step toward understanding the biological role of loading parameters in spinal tissues, translation of results from this study is limited. Differences in species—in cell populations [267], tissue composition [268], and loading magnitudes [268, 348]—

as well as a lack of systemic factors *ex vivo* limit translation to humans. The lack of adequate compression in this study also reduces its physiologic fidelity. Intradiscal pressures in this bioreactor at the neutral position, 0.13 ± 0.08 MPa [269], is below normal disc pressures in physiologic compression in rabbits [349]. However, all comparisons were made to unloaded controls. Further, while loading rates are comparable to other robotic systems [276], motion rates are slower than those in *in vivo* motions.

To conclude, catabolic, inflammatory, and matrix changes in spinal tissues respond modestly to short durations of F/E loading *ex vivo*. Responses to varying parameters of loading were different in AF, NP, FC, and LF. Prior to using these findings to inform clinical investigations, future experiments need to examine degenerated specimens, introduce inflammatory stimuli, and extend loading durations with axial compression. The combination of viable, intact FSUs attached to a robot-based testing system capable of applying 6 DOF kinematics opens the door for new research directions involving various complex physiologic motions and the coupled mechanobiological interactions of different spinal components.

6.0 COMPLEX LOADING: FLEXION/EXTENSION AND AXIAL TORSION

6.1 INTRODUCTION

A majority of back pain has been classified as being of mechanical origin arising from various spinal structures including intervertebral discs, facet joints, and ligamentum flava [3, 60]. Tasks involving repeated combined bending and torsion are associated with injury and development of back pain [69, 211, 270]. Additionally, high incidence of back pain is linked to exercise and recreational activities that involve complex loading with bending and torsion [70, 71, 350]. Combined axial torsion (AT) and flexion/extension (F/E) has been shown in human cadaveric testing to increase the failure rate of lumbar spines and alter the failure mode from primarily annular rupture to facet joint failure [73]. Biomechanically, the addition of torsion increases loading of lumbar facet joints [89], elevates tensile and compressive stress in the annulus fibrosus (AF) [84, 314], reduces pressure of the nucleus pulposus (NP) [83], and likely increases tension in spinal ligaments of the contralateral side [93]. Results from Section 7.3 corroborate these changes in rabbit FSUs. Repeated, high magnitudes of combined loading clearly alter segmental mechanics leading to increased risk of tissue injury, but it remains unknown how non-destructive combined loading may alter inflammatory and catabolic signaling in loaded spinal tissue.

Chiropractors, osteopathic clinicians, physical therapists, and other practitioners of manual therapy frequently treat “restricted” spinal segments that appear to cause unilateral asymmetries in the axial plane [196, 197]. Restrictions are thought to be mediated by (1) facet adhesions or connective tissue lesions [194, 244] or (2) sensorimotor control dysfunction [14, 194], either of which may manifest radiographically in unequal facet joint spacing [351, 352]. Various manual

therapy techniques seek to mobilize restricted facet joints [79] or to restore normal sensorimotor control [14] and thereby remove aberrant segmental mechanics [353]. In animal studies, static, asymmetric and traumatic loading of facet joints has been shown to induce chronic pain [245] and incite osteoarthritic changes in facets [79, 244]. However, short-term, molecular responses to asymmetric loading in spinal tissues remain unknown. Further, *in vitro* studies and finite element models have shown that asymmetric loading differentially alters the mechanics of left and right facets, compressing facet joints contralateral to the direction of applied torsion and gapping the facet joint ipsilateral to the rotation [85, 354]. Yet, the effects of side on the biological responses to asymmetric loading in facet cartilage have not been studied.

Organ culture systems for spinal mechanobiology have been used extensively to study short-term biological responses to applied loading. Generally, studies have focused exclusively on changes in the intervertebral disc with varying magnitudes, frequencies, and durations of compressive loading [265, 266, 332, 355]. Recently, a system has been developed to examine combined torsion and compression in discs [36]. However, disc organ culture removes posterior components, including facets and spinal ligaments, and modifies end plate thickness in order to maximize culture duration. As a result, physiologic rotations of spinal segments are precluded and the biological effects of *in-situ* loading on extra-discal spinal tissues of intact FSUs remain unstudied.

The objective of this study was to determine the effect of combined AT with F/E on inflammation, catabolism and anabolism simultaneously in multiple spinal tissues—AF, NP, facet cartilage (FC), and ligamentum flavum (LF)—in viable FSUs. It was hypothesized that increasing magnitudes of AT and F/E would increase catabolic and inflammatory markers in all tissues compared to neutral F/E. It was further hypothesized that FC contralateral to the rotation (“compressed”) would increase catabolic and inflammatory markers relative to ipsilateral (“gapped”) FC.

6.2 METHODS

6.2.1 Specimen Preparation

Thirty-six lumbar spines were isolated from skeletally mature (>10 months old) New Zealand White rabbits. FSUs were extracted from two levels—L2-3 and L4-5—within two hours of death and dissected to remove musculature and produce clean osteoligamentous segments. FSUs were rinsed in phosphate-buffered saline and were attached within a flexible-walled, temperature- and oxygen-controlled bioreactor for mechanical loading as described previously [269] or placed in static culture as an unloaded control. Loaded FSUs (L4-5) were matched to unloaded control FSUs (L2-3) from the same spine, and L3-4 tissues were reserved for baseline (*t0*) analyses. Both experimental FSUs were placed in 10% fetal bovine serum-and 1% penicillin/streptomycin-supplemented Dulbecco's Modified Eagle's Medium including 4.5 g/l glucose with 110 mg/l sodium pyruvate at $37(\pm 0.5)$ °C, 5%/5% O₂/CO₂. Media was pumped through the bioreactor at 1.1 mL/min.

6.2.2 *Ex vivo* Combined Loading: Axial Torsion + Flexion/Extension

The custom-built bioreactor was attached to a serial-linkage robot (Staubli RX90, Staubli, Inc., Duncan, SC) with an in-line universal force sensor (UFS Model 90M38A-150, JR3, Inc., Woodland, CA) controlled in MATLAB software. Flexible, silicone and nitrile rubber walls contained media and permitted free movement of FSUs in six DOF (Figure 20) [269]. FSUs were grouped by amount of applied AT—0 Nm (neutral AT), 0.4 Nm (small AT) or 0.8 Nm (large AT)—which reflect lack of, mild (~20% of failure), and severe (~40% of failure) rotations (based on preliminary torsional failure data collected with this system, Section 4.2.3). After reaching steady-state temperature and media flow (~30 min), FSUs were subjected to three cycles of left-sided, quasi-static AT (i.e. superior vertebra rotated to the left). All forces were minimized per rotational step (0.25°) to precondition FSUs and approximate a pure moment AT path [277]. At the final rotated position of the third AT path, FSUs underwent three cycles of F/E to 0.5F/0.15E Nm with force minimization (step size: 1°) to precondition FSUs in the combined AT+F/E orientation. F/E targets were selected so that specimens entered the high stiffness, linear portion of the curve (i.e. the elastic zone) in flexion and extension. The kinematics of the third path were then replayed for one hour at $0.33^\circ/\text{s}$.

6.2.2.1 Mechanical Assessments

Analyses were performed to characterize the mechanical response of FSUs to applied loading. Mean F/E ROM, F/E moment, AT ROM, AT moment, and cycle number were calculated for each loaded FSU per group. Work applied to FSUs per cycle was computed by integrating the primary moment at each angle, M_θ , with respect to primary angle, θ , in flexion and extension (Equation 3).

Work was averaged and summed across cycles for cumulative and mean work. Similarly, total and mean energy dissipation (hysteresis) were calculated using the difference between loading and unloading curves per cycle (Equation 4). Neutral zone (NZ) stiffness (Nm/°) was calculated using methods described by Smit et al. (Equation 5) [325]. Elastic zone (EZ) stiffness was calculated in the final three positions (~10%) of the moment-rotation curve in flexion and extension (Equation 6). Changes in mechanical measures—FE moment, AT moment, work, hysteresis, NZ stiffness, and EZ stiffnesses—across cycles were also calculated by normalizing values from the last cycle to the third cycle of replayed kinematics (Equation 7). The third cycle was chosen to allow for preconditioning of the moment-rotation response at the higher loading rate used for kinematic replay.

6.2.2.2 Biological Assessments

Immediately following loading, FSUs were removed from the bioreactor and incubator, and tissues were dissected and stored in *RNAlater*® (Qiagen, Venlo, ND) at -80°C. To isolate RNA, tissues were minced, homogenized by bead milling, and extracted using Qiazol Lysis Reagent (Qiagen) and 24:1 chloroform:isoamyl alcohol (Sigma-Aldrich, St. Louis, MO). RNA was then purified using the RNeasy Universal Tissue Kit (Qiagen). Real-time reverse-transcription polymerase chain reaction (RT-PCR) was performed using an iQ5 real-time thermal cycler (BioRad, Hercules, CA) with SYBR green and custom-validated rabbit primers (Table 11) for *matrix metalloproteinase (MMP)-1*, *MMP-3*, *a disintegrin and metalloproteinase with thrombospondin motif (ADAMTS)-5*, *cyclooxygenase (COX)-2*, and *aggrecan (ACAN)*. Relative gene expression (RGE) between tissues from loaded and unloaded FSUs was calculated by normalizing to *glyceraldehyde-3-phosphate dehydrogenase (GAPDH)* as a housekeeping gene using the $2^{-\Delta\Delta Ct}$

method [326]. Sample number varied, based on yield of RNA, by tissue and gene: n=4-7 in NP (except for n=3-4 in *ACAN*), n=5-7 in FC, and n=5-8 in AF, and n=5-6 in LF. In FC, left and right samples from loaded FSUs were compared to appropriate left or right-sided, unloaded controls. RGE in FC was expressed per side (Figure 27) and as a mean of the two sides to describe overall effects in FC (Figure 26). The effect of culture was assessed by also performing RGE between unloaded and *t0* tissues for *MMP-3* and *COX-2* (n=3-5).

Western blotting was performed in each tissue (n=4 per tissue, per condition) to examine the effects of loading (1) on matrix catabolism by examining degradation products of aggrecan, which include MMP- and ADAMTS-cleaved fragments that have been shown to increase and shift toward a predominance of MMP-cleaved fragments with detrimental loading [149] and (2) on abundance of chondroadherin (CHAD), a leucine-rich repeat protein involved in matrix organization and cell metabolism that is diminished with catabolic stimuli and abnormal loading in disc [356, 357]. FSUs used for protein assessment were subjected to repeated combined loading as described previously and were left to remain in culture for an additional 24 hours from the onset of loading. Tissues from unloaded FSUs were compared to baseline (*t0*) tissues to assess effects of culture. Briefly, soluble proteins were extracted in 4 M guanidine hydrochloride, precipitated in ethanol, and treated with endo-beta-galactosidase (Sigma) and then chondroitinase ABC (Sigma) for de-glycosylation. Equivalent amounts per weight of tissue were added (30 μ l) in a 10% acrylamide gel. Samples were separated by electrophoresis, transferred to a polyvinyl fluoride membrane, blocked with 5% skim milk, probed with (a) a primary antibody for the aggrecan G1-domain (generously provided by Dr. P. Roughley) [327] and a subsequent secondary goat anti-rabbit antibody (31460, Thermo Scientific, Waltham, MA) or (b) a mouse polyclonal primary antibody against the C-terminus of CHAD (H00001101-A01, Novus Biologicals,

Littleton, CO) and a subsequent secondary goat anti-mouse antibody (314030, Pierce/Thermo Scientific, Rockford IL). Immunoblots were imaged using the ChemiDoc MP system (BioRad) following chemiluminescence activation. Densitometry quantification was performed using Image Lab Software 5.0 (BioRad); bands from mechanically loaded tissues were normalized to bands from unloaded tissues of the same animal for each tissue. Western blotting reagents were obtained from Pierce/Thermo Scientific.

6.2.3 Statistical Analysis

One-way independent ANOVA followed by Wilcoxon rank-sum tests with Bonferroni correction were performed to examine the effect of group (Neutral F/E, Small AT+F/E, and Large AT+F/E) on mechanical properties. Two-way, independent ANOVA was performed for relative gene expression and immunoblotting densitometry to examine (1) the effect of loading and group in all tissues and (2) the effect of side (i.e. left vs right) and group in loaded FC. Significant effects were subsequently queried using Wilcoxon rank-sum sum tests with Bonferroni correction. Analyses were performed in Matlab 2013a. Significance was set to $p < 0.05$, and values were expressed as mean \pm standard deviation unless noted otherwise. Symbol (\dagger) designates a significant effect of loading ($p < .05$), (#) denotes a significant effect of group ($p < .05$), (*) indicates a significant effect of loading in post-hoc tests ($p < .0167$), and (\ddagger) denotes a significant effect of group in post-hoc tests ($p < 0.0167$).

6.3 RESULTS

6.3.1 Mechanical Response: Axial Torsion + Flexion/Extension

Examining F/E moment-rotation properties (Table 14), results of the ANOVA confirmed that there was no effect of torsion on mean F/E ROM or moment magnitudes, but relaxation of F/E moments were significantly influenced by group ($F: p=.0193$). Less relaxation of F/E moments (Moment-Rotation Relaxation) occurred in torsion groups ($3.62\pm 3.69\%$ and $5.88\pm 5.39\%$ in small and large AT, respectively) compared to neutral ($8.62\pm 4.16\%$) (Figure 25.A); individual differences between Neutral F/E and Small AT+F/E and Neutral F/E and Large AT+F/E approached significance ($p=.0303$ and $p=.0684$, respectively). Similarly, change in flexion stiffness across cycles ($20.42\pm 23.12\%$ decrease) was significantly different across groups ($F: p=.0143$) with a greater relaxation of flexion stiffness in Neutral F/E than small or large torsion groups (Figure 25.B) ($3.46\pm 6.73\%$ or $6.85\pm 5.87\%$, respectively). No significant differences in stiffness and no relaxation in neutral zone or extension stiffness were observed.

Table 14. Moment-rotation and stiffness properties for F/E

Group	Moment-Rotation			Neutral Zone Stiffness		Flexion Stiffness		Extension Stiffness	
	ROM (°)	Mx (Nm)	‡Relaxation (%)	Stiffness (Nm/°)	Relaxation (%)	Stiffness (Nm/°)	‡Relaxation (%)	Stiffness (Nm/°)	Relaxation (%)
Neutral FE	19.16 (3.32)	0.672 (0.034)	8.62 (4.16)	0.017 (0.004)	2.24 (14.0)	0.077 (0.022)	20.42 (23.12)	0.080 (0.015)	8.54 (11.13)
Small AT+FE	21.62 (2.35)	0.696 (0.052)	3.62 (3.69)	0.016 (0.003)	-1.29 (5.10)	0.062 (0.013)	3.46 (6.73)	0.081 (0.016)	7.04 (3.88)
Large AT+FE	19.68 (3.26)	0.671 (0.044)	5.88 (5.39)	0.018 (0.004)	3.23 (5.50)	0.065 (0.011)	6.85 (5.87)	0.078 (0.012)	8.03 (5.70)

‡-Significant effect of group ($F, p<.05$)

The AT moment-rotation response during F/E cycling was also measured (Table 15). As expected, differences in mean AT ROM were significantly different across and between all groups at each of three positions: maximum flexion, maximum extension, and mid-FE ($p < .0001$ for all comparisons). Interestingly, Neutral F/E torsional moments relaxed (decreased) at all positions ($10.07 \pm 23.15 - 22.01 \pm 22.60\%$), Small AT+F/E torsional moments changed little ($0.34 \pm 4.76 - 2.41 \pm 3.83\%$), and Large AT+F/E torsional moments actually increased ($4.32 \pm 3.98 - 8.08 \pm 3.81\%$) across cycles. Differences in AT moment relaxation between all groups were significant ($p < .0001$ for all comparisons).

Table 15. AT properties at extremes and middle of F/E

Group	Axial Torsion - Flexion			Axial Torsion - Extension			Axial Torsion - Mid Path		
	ROM (°)	My (Nm)	Relaxation (%)	ROM (°)	My (Nm)	Relaxation (%)	ROM (°)	My (Nm)	Relaxation (%)
Neutral FE	0.06 (0.15)	0.159 (0.066)	-22.01 (22.60)	0.04 (0.05)	0.125 (0.078)	-10.08 (23.16)	0.33 (0.54)	0.204 (0.045)	-18.57291335
Small AT+FE	1.42 (0.55)	0.390 (0.131)	0.34 (4.76)	-1.16 (0.57)	0.484 (0.086)	2.41 (3.84)	1.28 (0.43)	0.447 (0.058)	1.65 (3.16)
Large AT+FE	3.75 (0.70)	0.586 (0.120)	4.34 (3.98)	-3.43 (0.84)	0.761 (0.100)	8.08 (3.81)	3.35 (0.75)	0.644 (0.081)	6.47 (3.42)

All differences between groups were significant ($U, p < .0167$)

Changes in energy applied to and dissipated by FSUs are listed in Table 4. Cumulative work was higher in small and large torsion groups ($291.83 \pm 92.57\%$ and $297.90 \pm 69.22\%$, respectively) than the neutral group ($210.21 \pm 59.19\%$) ($F: p = .0140$) (Figure 25.C). Post-hoc tests showed differences to be significant between Neutral F/E and Large AT+F/E ($p = .0038$) and approached significance between neutral and Small AT+F/E ($p = .0336$). Further, group had a significant effect on the change in work across cycles ($F: p = .0123$) (Figure 25.D). Relaxation in work across cycles ($4.68 \pm 6.60\%$) was evident in Neutral F/E but not in either torsion group ($-0.35 \pm 3.33\%$ and $-1.15 \pm 4.34\%$ for small and Large AT+F/E, respectively). These differences in

work relaxation were statistically significant for neutral compared to Large AT+F/E ($p=.0091$) and nearly significant for neutral compared to Small AT+F/E ($p=.0246$). The effect of group on hysteresis parameters was not significant.

Table 16. Work and hysteresis properties for flexion/extension per and across cycles

Group	Work (J)					Hysteresis (J)		
	Cycles	N	†Cumulative	Mean	† Change(%)	Cumulative	Mean	Change (%)
Neutral FE	32.25 (5.25)	11	220.52 (66.78)	7.08 (2.66)	4.65 (6.34)	24.36 (17.17)	0.80 (0.62)	-19.79 (80.74)
Small AT+FE	34.17 (4.61)	12	291.83 (92.57)	8.52 (2.34)	-0.35 (3.33)	22.97 (7.52)	0.69 (0.24)	11.10 (15.50)
Large AT+FE	36.62 (4.79)	13	*297.90 (69.23)	8.30 (2.33)	*-1.15 (4.54)	29.41 (14.40)	0.79 (0.32)	6.35 (12.70)

†-Significant effect of group ($F, p<.05$), *-significant difference compared to Neutral FE

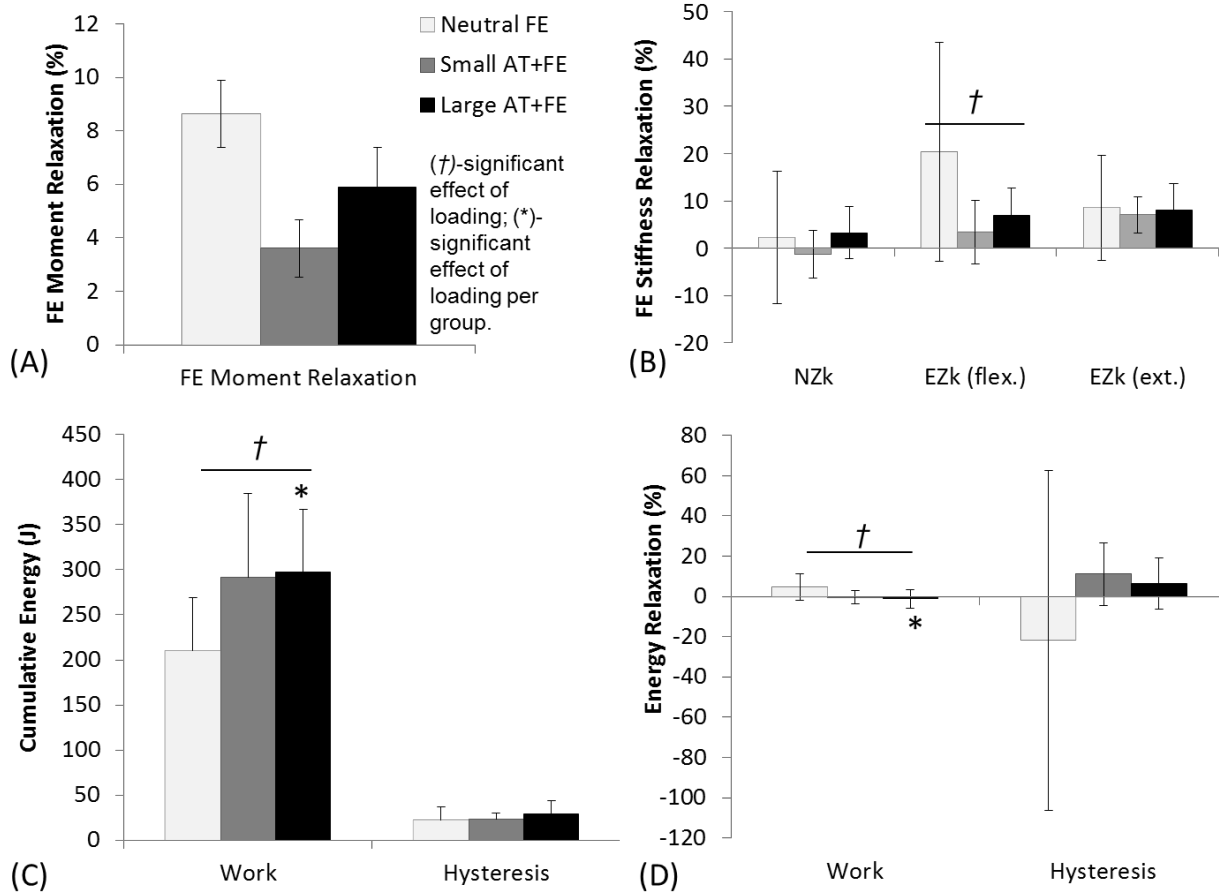


Figure 25. Mean (\pm SEM) mechanical responses in AT+F/E: (A) Relaxation of F/E moments, (B) Relaxation of F/E NZk, EZk flexion, and EZk extension, (C) Cumulative work and hysteresis, and (D) Relaxation of work and hysteresis.

6.3.2 Biological Response: Relative Gene Expression

Relative gene expression showed significant effects of loading across tissues (Figure 26). Loading had a significant effect on *COX-2* and *MMP-3* expression in all tissues, *ACAN* in AF and FC, *MMP-1* in AF, and *ADATMS-5* in LF. Post-hoc tests showed that Large AT+F/E increased *COX-2* mRNA expression in all spinal tissues: 1.60-fold in AF ($p=.0005$), 1.74-fold in NP ($p=.0169$), 2.97-fold in FC ($p=.0476$), and 4.86-fold in LF ($p=.0022$). Further, Large AT+F/E significantly up-regulated *MMP-1* in AF (2.30-fold, $p=.0002$), *MMP-3* in FC (2.43-fold, $p=.0169$), and

ADAMTS-5 in LF (2.32-fold, $p=.0022$). Small AT+F/E loading also increased *COX-2* expression in NP (1.77-fold, $p=.0476$), FC (3.42-fold, $p=.0022$), and LF (2.38-fold, $p=.0476$). Neutral F/E only had a significant effect of loading in FC on *MMP-3* expression (1.97-fold increase, $p=.0058$). *MMP-3* and *COX-2* expression were generally elevated in tissues. In contrast, NP *COX-2* expression in unloaded FSUs was not increased compared to baseline ($t0$) (Appendix A, Figure 38).

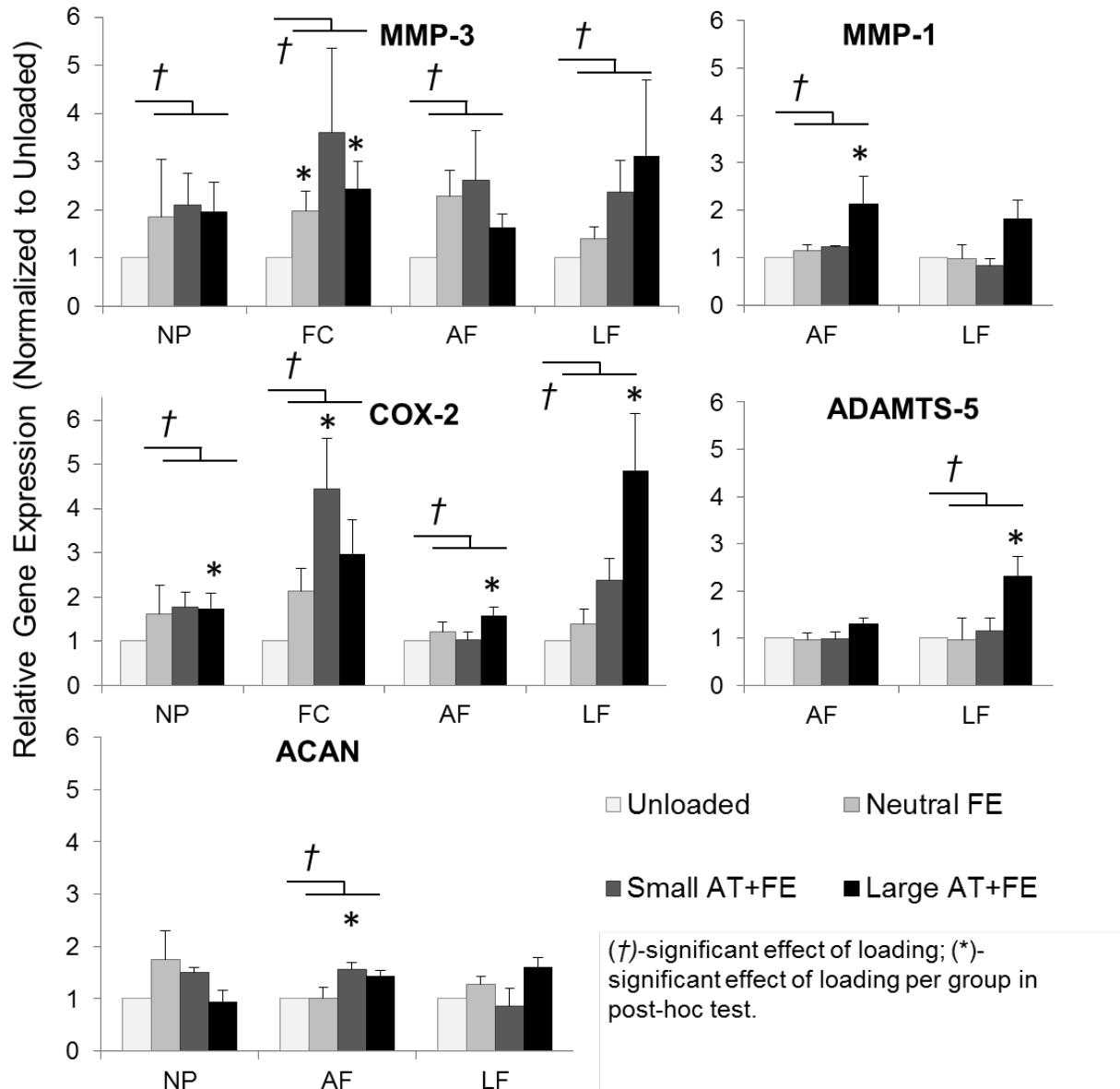


Figure 26. Mean fold change (±SEM) in relative gene expression NP, FC, AF, and LF with loading.

Comparing the effects of loading on left (gapped) and right (compressed) FC (Figure 27) confirmed a significant effect of loading across groups for *MMP-3* and *COX-2*. Mean left FC expression was higher than mean right-sided expression for both *MMP-3* and *COX-2*. Post-hoc tests confirmed significant elevation of *COX-2* in left FC in both torsion groups ($p=.0022$ and

$p=.0286$ in Small AT+F/E and Large AT+F/E, respectively). Left FC *COX-2* expression was significantly higher than right-sided expression, and a similar trend was evident for *MMP-3* ($F: p=.1589$).

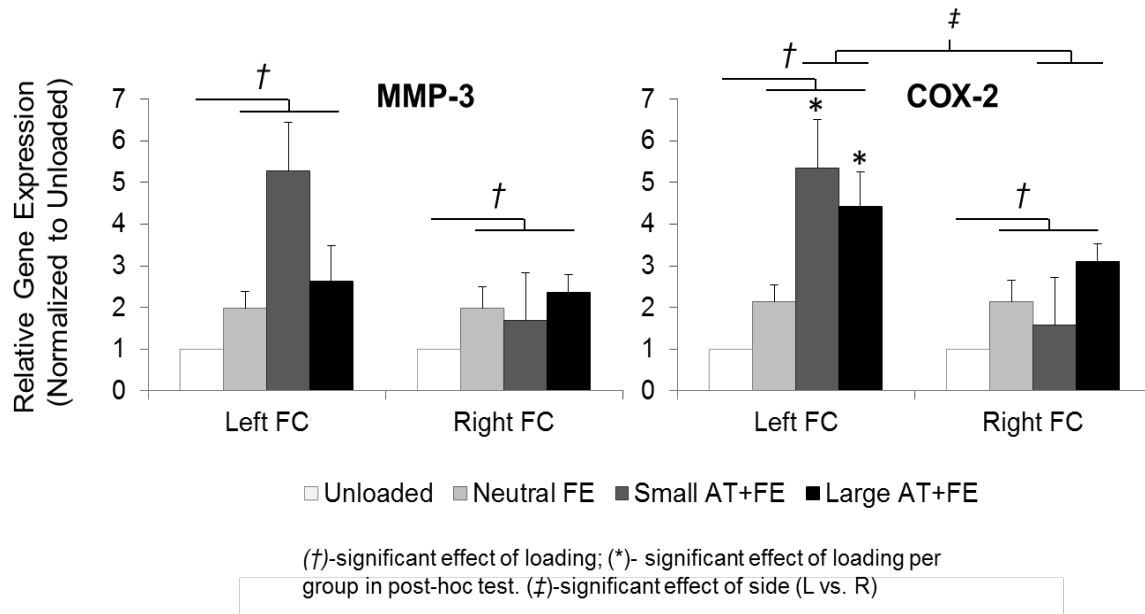


Figure 27. Mean (\pm SEM) fold change in relative gene expression of left and right FC with loading

6.3.3 Biological Response: Western Blotting

In ADAMTS-cleaved fragments (~67 kDa), neither loading nor the amount of axial torsion had a significant effect on fragment abundance in any tissues, but torsion groups tended to have fewer fragments (Figure 28). In FC, this effect of torsion showed a strong trend ($F: p=.0880$). For MMP-cleaved fragments (~54 kDa), loading tended to elevate fragments in NP ($F: p=.0880$), but no other effects in other tissues approached significance. When comparing fragment abundance

between left and right FC (Figure 29), no difference was observed for MMP-cleaved fragments. Aggrecan fragments were not significantly altered by culture compared to baseline (*t0*) (Appendix A, Figure 39).

Immunoblotting performed for CHAD (~36 kDa) showed that each tissue responded significantly to loading (Figure 28). The NP manifested a significant reduction in CHAD with loading in both torsion groups ($p=.0286$ each), and, conversely, the AF showed increased CHAD with loading in both torsion groups ($p=.0286$ each). FC tissue showed a significant effect of group, with both torsion groups tending to have less CHAD than neutral FC ($p=.1333$). Comparing left and right FC tissue similarly revealed a significant effect of group on CHAD abundance ($p=.0500$) (Figure 29); the decrease in CHAD in right FC compared to neutral FC approached significance ($p=.0571$). Differences in CHAD between sides were not present in Small AT+F/E but were prominent, though not significant, in Large AT+F/E. On the left (gapped) side, CHAD was similarly reduced regardless of the amount of torsion, but on the right (compressed) side, CHAD was further reduced more in the Large AT+F/E. CHAD expression in unloaded culture compared to baseline (*t0*) increased 4.56 ± 3.11 -fold in NP, 2.11 ± 1.49 -fold in AF, and decreased by $51.8 \pm 31.5\%$ in FC (Appendix A, Figure 40).

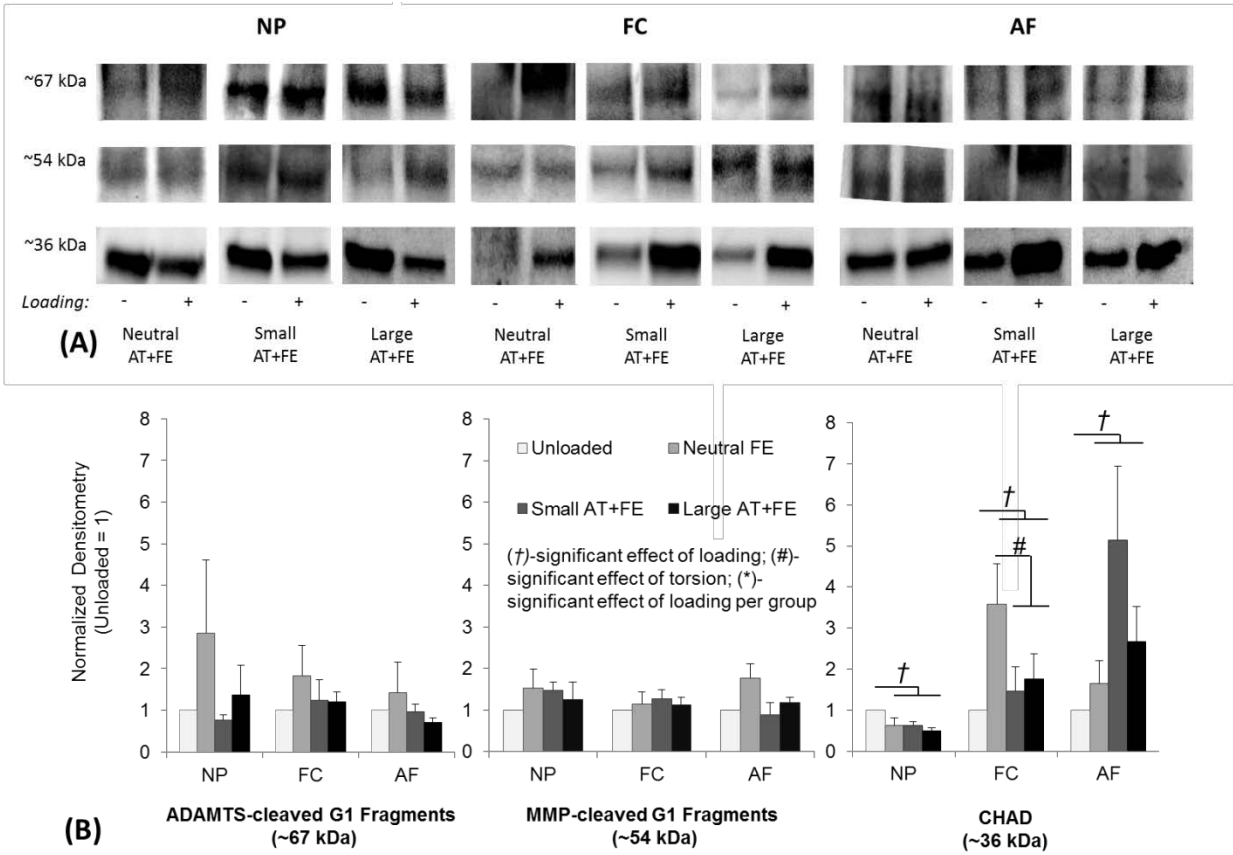


Figure 28. (A) Representative immunoblots against G1 fragments and CHAD for NP, FC, and AF. (B) Mean (\pm SEM) normalized densitometry for each protein per tissue.

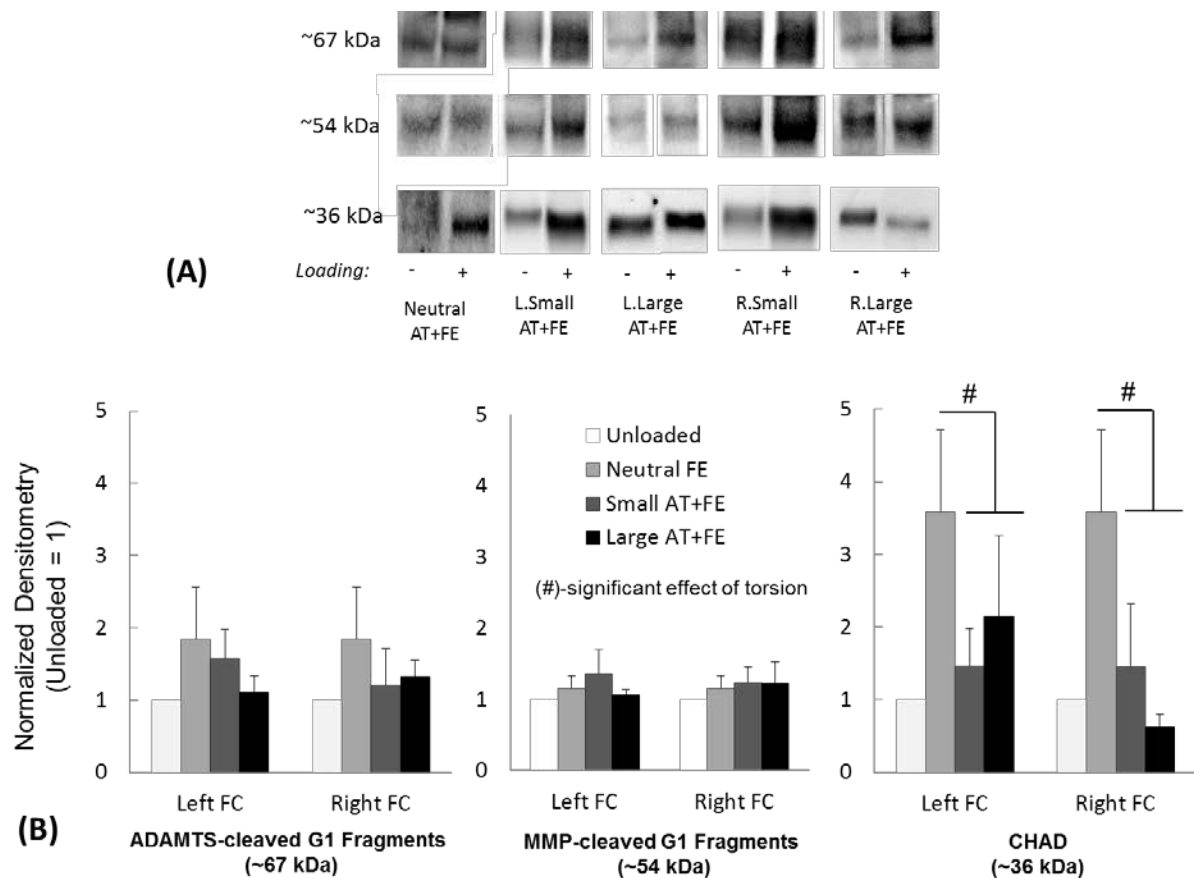


Figure 29. (A) Representative immunoblots against G1 fragments and CHAD are shown for left (L) and right (R) facet cartilage (FC) with loading. (B) Mean (±SEM) normalized densitometry for each protein per side of FC per group across samples.

6.4 DISCUSSION

This study examined biological responses of multiple spinal tissues to varying amounts of torsion in non-destructive, combined axial torsion and flexion/extension of functional spinal units *ex vivo*. The goal of this study was to assess how axial asymmetries alter biological and mechanical responses to short durations of flexion/extension movements, which are involved in a variety of occupational, recreational, and rehabilitative activities [70, 71, 270, 271, 319]. The major findings reveal a primarily pro-inflammatory response to coupled torsion in F/E across spinal tissues, with

catabolic increases in AF and LF. In FC, which is differentially loaded in left-sided axial torsion, pro-inflammatory changes were higher in gapped, left facets than compressed, right facets. Mechanically, load relaxation did not occur in combined AT and F/E groups as it did in Neutral F/E. The observations in this *ex vivo* model point to a role for altered mechanics associated with axial asymmetries in driving pro-inflammatory, catabolic processes in spinal tissues that may play a role in the onset and progression of tissue damage and degeneration associated with complex loading.

Treating restricted or rotated spinal segments and restoring normal, symmetric joint mechanics is an important tenant of manual therapy [196, 197]. Facet adhesions may develop through hypomobility or abnormal loading [79, 244] and lead to mal-alignment of spinal segments, degenerative changes in facet joints, and development of painful symptoms [79, 244, 245]. Alternatively, unilateral segmental restriction diagnosed clinically may result from sensorimotor control dysfunction, which may reflect altered, detrimental spinal mechanics [195]. Spinal manipulation and other forms of manual therapy frequently apply axial rotational and complex loading to rotated spinal segments with the intent of mobilizing restricted facet joints or disrupting mal-adaptive neural signaling to restore normal segmental mechanics [14, 79]. Radiological evidence demonstrates that manipulation preferentially “gaps” the facet on the side of contact and reduces facet joint spacing on the non-contact side [351, 352]. In the model used in this study, the right facet joint, whose inferior facet surface is rotated toward its superior surface and held in torsion during repeated F/E, is intended to represent a “restricted” facet during activity. Surprisingly, pro-inflammatory changes in the left (gapped) FC were significantly higher than those in right FC. Loss of CHAD, likely reflecting a catabolic response with implications for altered matrix organization and metabolism [357, 358], was similarly reduced by torsion in FC of

both sides, but the trend showed more depletion on the right side. Thus, both results confirm a more favorable response of neutral alignment in activities involving F/E. However, pro-inflammatory gene expression suggests that asymmetric facet joint spacing may be more damaging on the non-contact side, and protein changes reflecting matrix damage suggest added degenerative changes on the restricted, contact side.

Mechanical changes known to occur in facet joints with combined AT and F/E coupled with well-characterized chondrocyte responses to loading provide a possible basis for these biological responses. Combined loading elevates facet joint forces measured in compressed facet joints and presumably decompresses gapped facets entirely [85, 89]. Articular cartilage reacts to lack of compression with pro-inflammatory, matrix degrading responses that include elevation of inflammatory mediators and loss of matrix components [221-224]. High levels of compression can also provoke a similar, detrimental response [225]. Thus, a possible interpretation suggests that, in the gapped joint, decompression of FC [85] led to consistent, comparable high expression of inflammatory markers (*COX-2* expression) and loss of matrix components (CHAD) in both torsion groups. At the same time, in the compressed facet joint, moderately increased facet forces in Small AT+F/E likely led to CHAD depletion but showed no effect on *COX-2* expression compared to Neutral F/E. In Large AT+F/E, facet forces increase further [85], and added compression may have led to more severe CHAD depletion and the modest increase in inflammatory signaling observed relative to Neutral F/E. These interpretations cannot be confirmed by our data; future studies must establish a relationship between joint level motions and FC mechanics (in particular, characterizing the unknown role of shear forces) and investigate how FC mechanics modulate local inflammation and matrix homeostasis.

Coupled torsion with F/E altered FSU mechanics and elevated pro-inflammatory signaling in all tissues. Adding AT to F/E increased work applied to FSUs for comparable rotations, reflecting elevated moments and forces throughout the motion path in torsion groups. Coupled torsion also prevented relaxation of F/E and AT moments, applied work, and flexion stiffness across cycles, demonstrating a difference in the energy imparted to FSUs and the loads sustained by tissues of the FSU. Elevation of *COX-2* expression in all tissues in nearly all torsion groups, alongside the evident lack of up-regulation of *COX-2* in neutral F/E for any tissue, points to a pro-inflammatory response of tissues to the altered mechanics of asymmetric loading. *In vitro* studies with cell types from each tissue have shown elevation of *COX-2* expression in response to high load magnitudes [161, 204, 205, 359], and increased *COX-2* expression is associated with the initiation and progression of degenerative processes in each tissue [127, 156, 360]. Clinically, *COX-2* is common target of therapeutics for back pain. Thus, sustained higher levels of segmental loading and elevated *COX-2* expression with coupled torsion demonstrate broadly detrimental effects of asymmetric loading in tissues of the FSU.

Certain spinal tissues manifested a catabolic response to coupled torsion in F/E. The LF, which acts as a primary tension bands in resisting flexile moments, increased catabolic expression with increasing amounts of torsion. Increased tensile forces in LF resulting from combined flexion and torsion may be inferred [361]. Thus, *MMP-3* expression in LF, which showed a trend of increasing expression with increasing coupled torsion, appears to be sensitive to magnitudes of loading. This notion is strengthened by studies that show elevated *MMP-3* expression in LF samples (Park, 2009; Oh, 2009) obtained from surgical patients with degenerative conditions involving altered spinal loading and *in vitro* experiments that applied varying magnitudes of tensile stretch to ligament fibroblasts [362]. Expression of *MMP-1* in AF (non-significantly in LF) and

ADAMTS-5 in LF did not show an effect in Small AT+F/E; instead, expression increased only in Large AT+F/E. Elevation of expression for *MMP-1*, a collagenase, in collagen-rich tissue like AF, alongside increased *ACAN* expression, suggests that increased compressive and tensile stresses in AF induced by large coupled torsional moments triggered tissue remodeling. Elevation of *ADAMTS-5*, a highly efficient aggrecanase, without significant elevation of *ACAN* expression in LF suggests a dysregulation of proteoglycan metabolism similar to previous findings in diseased ligamentous tissue [363, 364]

Coupled torsion and F/E altered anabolic responses differentially in NP and AF. A trend of decreased *ACAN* expression and CHAD abundance with coupled torsion in NP may reflect reduced intradiscal pressure in the NP [83]. However, given increased CHAD with unloaded culture, reduced CHAD with loading may mark a return to baseline (*t0*) levels. The opposite trends in *ACAN* expression and CHAD abundance in AF indicate an adaptive remodeling to increased and altered stress in the AF with combined loading [84].

Translation of results from this study is principally limited by use of a healthy animal model *ex vivo*. A unilateral facet restriction was simulated mechanically by asymmetric rotation in otherwise healthy spines, which likely differ in their mechanical and biological environment from spines with prolonged segmental abnormalities. Differences in cell populations [267], tissue composition [268], loading magnitudes [268, 348], and segmental anatomy along with lack of systemic factors *ex vivo* limit translation of rabbit FSUs to humans. However, scaled torsional and compressive mechanical properties are similar between rabbit and human lumbar spines [268, 291]. Intradiscal pressures in this bioreactor at the neutral position, 0.13 ± 0.08 MPa

[269], are below normal disc pressures in physiologic compression in rabbits [349], which may influence the load magnitudes and distribution among tissues of the FSU. To account for this, all comparisons were made relative to unloaded controls.

The FSU mechanobiological testing system used in this study investigates, for the first time *ex vivo*, cellular and molecular responses to *in situ* loading involving combined spinal rotations. Previous systems remove vertebral and posterior structures, including facets and spinal ligaments, and modify the cartilage endplate to promote metabolite exchange [258, 365]. The capability of the current system, in examining complex, six DOF loading and the simultaneous biological responses of facets and ligaments, is aimed to address questions relating to rotational movements, segmental alignment, and manual and physical therapy, all of which involve segmental mechanics and the influence posterior structures. The pro-inflammatory response to asymmetric F/E in all tissues, most pronounced in FC and LF, may contribute to the onset and progression of tissue damage and degeneration associated with asymmetric loading. FC changes with torsion—elevated pro-inflammatory and catabolic gene expression and reduced chondroadherin abundance—support clinical paradigms that seek to restore neutral axial alignment. Surprisingly, pro-inflammatory changes were significantly higher in ipsilateral, gapped FC. Future studies will explore the mechanisms of differential responses among FC, clarifying the mechanical environments of facet joints, and aim to simulate interventions in the model system as a therapeutic intervention.

7.0 MECHANICAL CONTRIBUTION OF FSU COMPONENTS

7.1 INTRODUCTION

Interpretation of biological changes in Chapters 5.0 and 6.0 relied on numerous experimental and computational studies that described the mechanical role of individual FSU components in flexion/extension (F/E) and axial torsion (AT) [86, 87, 91-93]. Experimental descriptions of mechanical contributions of spinal components to segmental loading typically involve a serial resection of joint structures with repeated intact kinematics [87, 277, 366, 367]. The changes in primary moment with each cut provide insight in to the contribution of individual structures to applied moments. Robotic systems used in joint research can replay intact kinematic motion paths to determine the role of spinal components in 6 DOF loading [285]. Gillespie and Dickey utilized a robotic system to characterize the percent contribution of spinal components to F/E moments [87], but only one study has been performed using human lumbar segments, and it did not involve replayed kinematics, only repeated displacement control [86]. No such testing of any kind has been performed in rabbit spinal segments to permit full interpretation of the current findings in Chapter 5.0 . Further, characterization of the contribution of forces/moments in spinal structures in complex loading remains unstudied experimentally in lumbar spines in general, preventing full characterization of the current findings in Chapter 6.0.

The experimental approach to determine the percent contribution of each structure to physiologic rotations relies on the principle of linear superposition, namely, that the percent moment contributions of components sum linearly [284, 285]. Thus, the percent contribution of

each structure to primary moment resistance is defined by the change in primary moment with each cut, i , normalized by the intact moment, M_{intact} ,

Equation 8. Percent moment contribution

$$\% \text{ Moment} = \frac{M_i - M_{i-1}}{M_{intact}}$$

Applying serial resection in the context of assumed linear superposition permits experimental determination of how spinal structures are loaded *in-situ*.

The objective of this study was to illuminate biological findings in Chapters 5.0 and 6.0 by determining how F/E moments and forces were distributed in spinal components of rabbit lumbar FSUs in (i) neutral F/E and (ii) coupled AT with F/E. The goal of this analysis was (1) to quantify the role of key structures (LF, facet joints (FJ), and intervertebral disc) in F/E moment resistance and (2) to quantify the effects of AT on the role of key structures in F/E. To achieve this goal, a serial reaction of spinal structures in replayed intact kinematics of neutral and axially rotated F/E was performed in rabbit lumbar FSUs.

7.2 METHODS

Specimen preparation: Lumbar L4-5 NZW rabbit (Female, age 10-12 mo.) FSUs were attached within novel fixtures as previously described in Section 3.2.2. Bioreactor fixtures were used without intervening rubber membranes to permit access to spinal structures. Specimens were kept moist throughout testing by frequent spraying of 0.9% NaCl. FSUs attached to fixtures were mounted within the robot spine testing system as described previously (Section 3.2.2.1).

Protocol: Fresh/frozen FSUs (n=4) were subjected to F/E moment targets of 0.5/0.15 Nm in neutral axial positions (neutral F/E) or with coupled axial rotations (AT+F/E) using AT targets of 0.8 Nm (the same as Large AT+F/E from 6.2.2). Experimental methods for applying coupled AT are described in greater detail in Section 6.2.2 and Appendix D.1. FSUs were cycled three times to moment targets using adaptive displacement control ('Pathseek') for preconditioning (Section 6.2.2). The third motion path was saved as the intact path to be replayed. These methods were consistent with previous testing for biological outcomes (Section 6.2.2).

After replay of the intact motion path, FSUs were serially resected in a posterior-to-anterior manner. Experimental interventions were performed as follows: the (1) supraspinous and interspinous ligaments (SSL/ISL) were resected, (2) ligamentum flava were resected, (3) facet capsules and facets cartilage were removed, and (4) discs were punctured antero-laterally with a 16G needle in to the NP [368]. Needle puncture depressurizes discs [369]; however, the relative size of the 16G needle to disc height in rabbit lumbar discs indicates that sufficient annular damage occurred with puncture to influence annular properties as well [370]. Nonetheless, depressurization of the NP is predicted to be the primary change as a result of this injury [369]. For each replayed state, after waiting five minutes, the robot system replayed intact kinematics three times. Neutral F/E was followed five minutes later by AT+F/E. The use of three 'Replay' paths and the delay between states and conditions allowed for reduction of viscoelastic effects.

Analysis: Percent contribution of each resected structure to primary moments was calculated using Equation 8 (p. 133) Equation 8. Percent moment contribution. Mean normalized moments and contributions to moment resistance were calculated. Additionally, mean changes in forces with resection were presented as a secondary outcome. Forces and moments were measured at and about the origin of the local anatomical coordinate system based on center-of-rotation

measurements (Section 3.4.2). In rabbit FSUs, forces and moments were measured at the mid-disc height, centered, posterior third of the disc. Measured forces (and moments) are those that act on (or about) that position in the local anatomical coordinate system, so changes in force reflect changes in *in-situ* loading in the disc that can be attributed to the resected tissue. It also follows that structures that cause pure moment loading about the COR have minimal effect on measured forces.

7.3 RESULTS

Contribution to F/E Moments: A representative F/E moment-rotation plot (SSL/ISL not pictured) is shown in Figure 30 illustrating the change in F/E curves with resection of each structure.

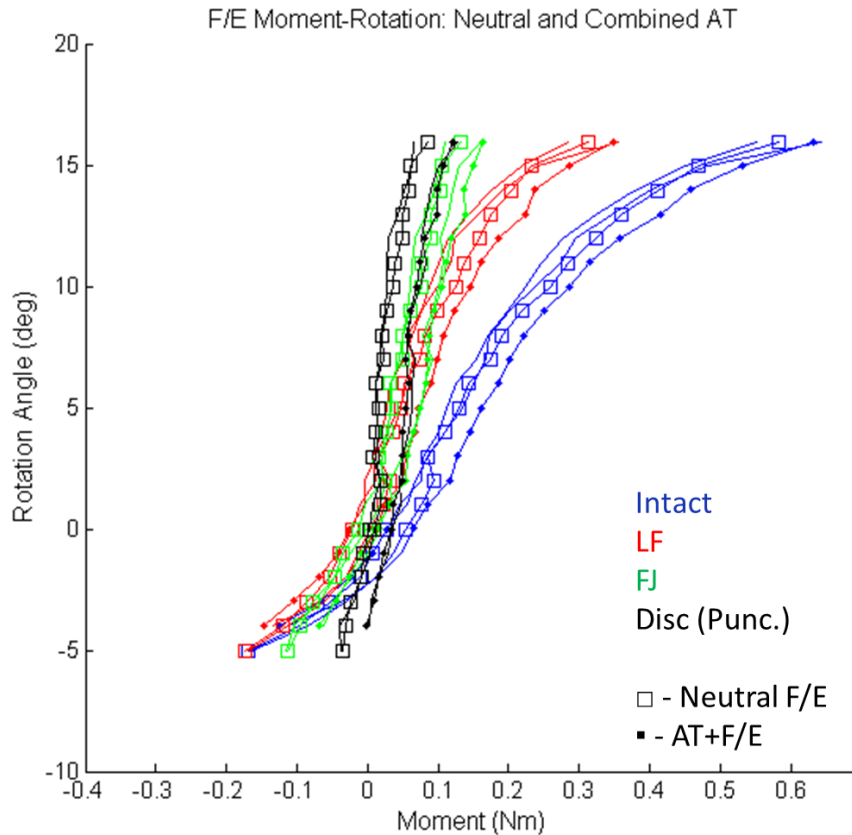


Figure 30. Representative F/E moment-rotation curve with serial resection of FSU components

Normalized flexion moments per structure in Neutral F/E and AT+F/E are presented in Figure 31. The percent contribution to F/E moments per structure are presented in Table 17. Flexion moments clearly declined with increasing resection of structures, and differences between Neutral F/E and AT+F/E in terms of how flexion moment changed with resection were small. The LF was the predominant contributor to flexion moment resistance (Table 17). FSUs subjected to AT+F showed an increased role of the disc in flexion compared to those in neutral flexion. In neutral extension, changes in moment with LF resection were negative (not included

in Figure 31). Facets contributed to $10.9 \pm 3.44\%$ of the extension moment. The addition of AT generally increased the role of resected structures to extension resistance; the role of facets ($39.72 \pm 12.86\%$) increased 3.65-fold over Neutral F/E (Table 17).

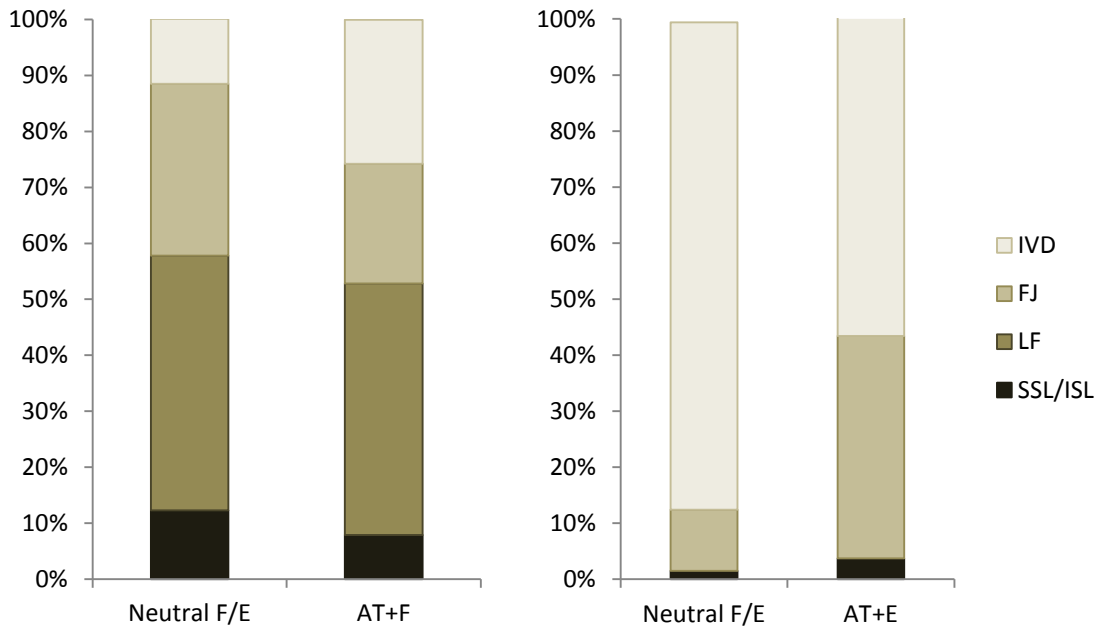


Figure 31. Percent flexion (left) and extension (right) moment resistance per structure in Neutral and AT+F/E

Table 17. Percent contribution to F/E moments by resected structures in Neutral F/E and AT+F/E

		SSL/ISL		LF		FJ		Disc (Puncture)		Disc (Remainder)	
Direction	Alignmen t	Mea n	SD	Mean	SD	Mea n	SD	Mean	SD	Mean	SD
Flexion	Neutral	12.27	0.9 8	45.45	9.01	30.71	25.2 0	2.85	3.29	8.73	9.62
	AT + F	7.90	0.4 7	44.94	5.99	21.40	3.80	4.24	1.00	21.52	10.11
Extensio n	Neutral	1.55	0.0 4	16.24	1.81	10.93	3.44	26.11	15.24	77.64	4.23
	AT + E	3.74	1.8 7	-8.79	4.50	39.72	12.8 6	26.50	20.81	38.82	7.76

Finally, the percent moment resistance in flexion per structure in rabbit FSUs is compared to other species—human lumbar (Human-L) and porcine lumbar (Porcine-L) [86, 87]—and spinal regions—human cervical (Human-C) [371]. The role of the LF is larger in rabbit lumbar spines than other lumbar spines; its role is more similar to that in the human cervical spine. Also, the role of the disc in rabbit lumbar neutral flexion is lower than all other models. The addition of torsion makes the role of the disc equivalent to other lumbar models.

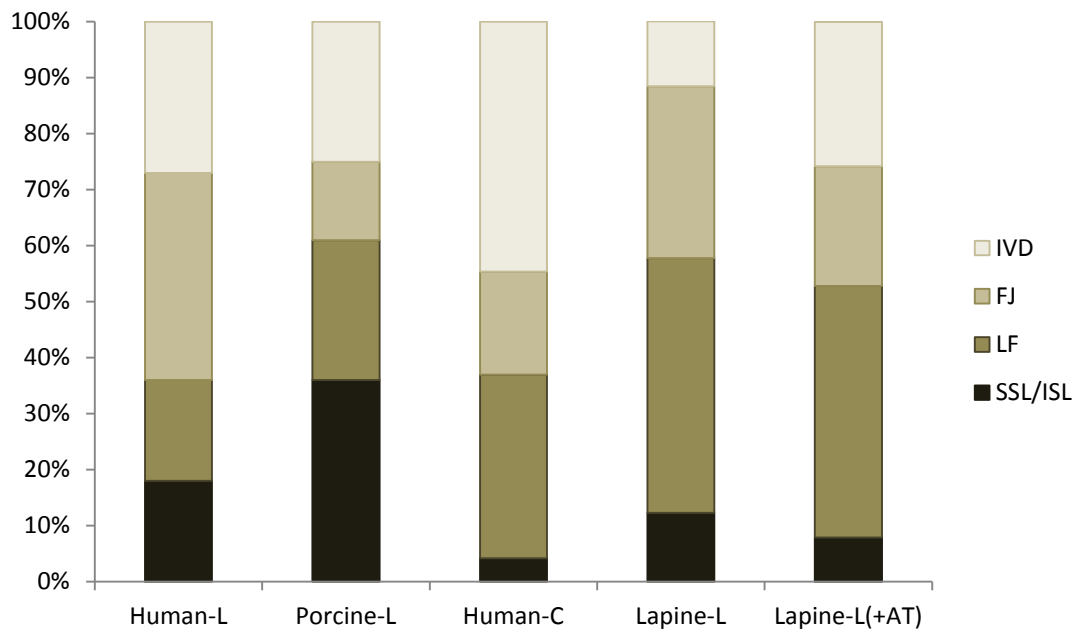


Figure 32. Distribution of FSU component loading (percent contribution) in flexion in different species

Changes in resultant force magnitudes: Figure 33 illustrates that spinal ligaments in neutral F/E caused little to no change in forces experienced in the disc. As Table 17 shows, the LF played an important role in flexion moment resistance but does not influence forces in the disc. The addition of AT caused an increase in force (~13.1% body weight (BW)) with LF resection. This reflects the lack of pure moment loading with AT and suggests higher overall loading in LF with

torsion. Most notably, resection of facets led to increases in force magnitudes in extension (4.77±4.84 and 11.98±3.83 in Neutral F/E and Large AT+F/E, respectively). These changes in force indicate that facets restricted forces in extension. This change in force was >2.5-fold higher with coupled AT. The orientation of the force vector is described below (Figure 34).

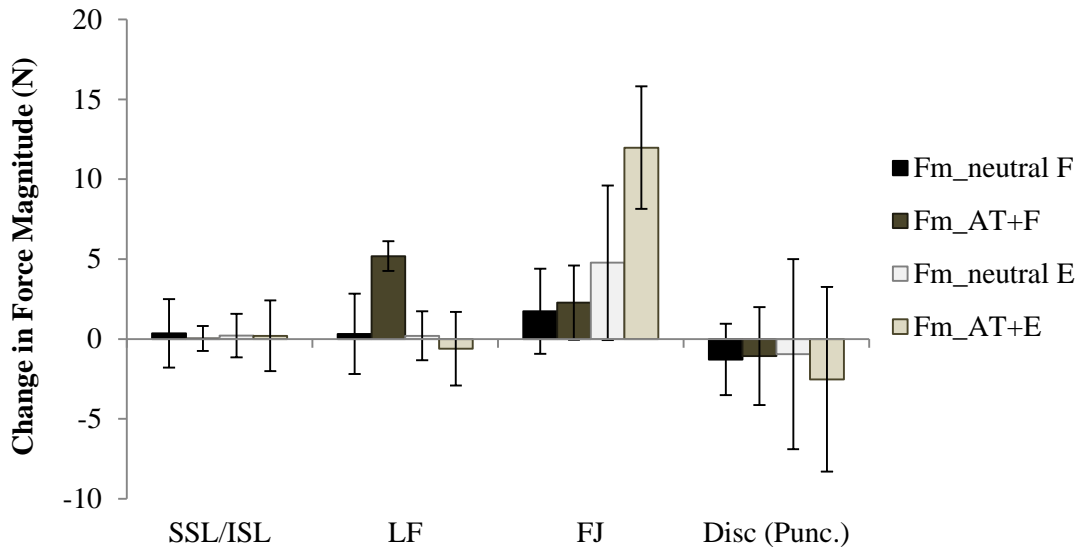


Figure 33. Changes in resultant force magnitudes in neutral F/E and AT+F/E with serial resection

Change in Component Forces: Changes in magnitude of component forces with resection of spinal structures are shown in Figure 34 and Figure 35. Examining changes in force components permits visualization of the orientation of the force vectors ($F_{z, \text{Medial-Lateral}}$, $F_{y, \text{Superior-Inferior}}$, $F_{z, \text{Anterior-Posterior}}$) in flexion (F) and extension (E)) acting on the LCS origin. In general, changes in component forces are larger in Large AT+F/E (Figure 35) than Neutral F/E (Figure 34). In Large AT+F/E, F_x changes with facet resection show a medial-lateral force (5.93±1.44 N) toward the right, the direction of facet compression with combined AT. This suggests that rotation to the right caused compression in the right facet joint, and this compression was present in both flexion and

extension. A small amount of compressive force (F_{y_E}) is also evident in extension, and this compressive force is apparently larger in Large AT+F/E (-3.56 ± 2.10 N) than Neutral F/E (-1.08 ± 2.14 N). The small amount of compressive forces generated in extension likely reflects lack of applied compression; pure moment testing has relatively small facet forces in extension [67, 89]. Most notably, changes in F_z , observed in flexion and extension, are the largest among component forces. Anterior shear forces were ~50% higher in extension than flexion, and two times higher in Large AT+F/E (6.62 ± 5.03 N and 12.90 ± 3.84 N in flexion and extension) than Neutral F/E (9.10 ± 4.78 N and 4.00 ± 3.12 N in flexion and extension). They demonstrate that facets resist a large anterior (“shear”) force because facet removal exposes the disc COR origin to high amounts of anterior force.

Changes with SSL/ISL and disc forces are generally small in size with a large amount of error. The trend of decreased force components for all directions with disc puncture suggests that disc depressurization reduces all forces in FSUs. The trend toward uniform slight negative changes in component forces reinforces that conception that needle puncture depressurized discs.

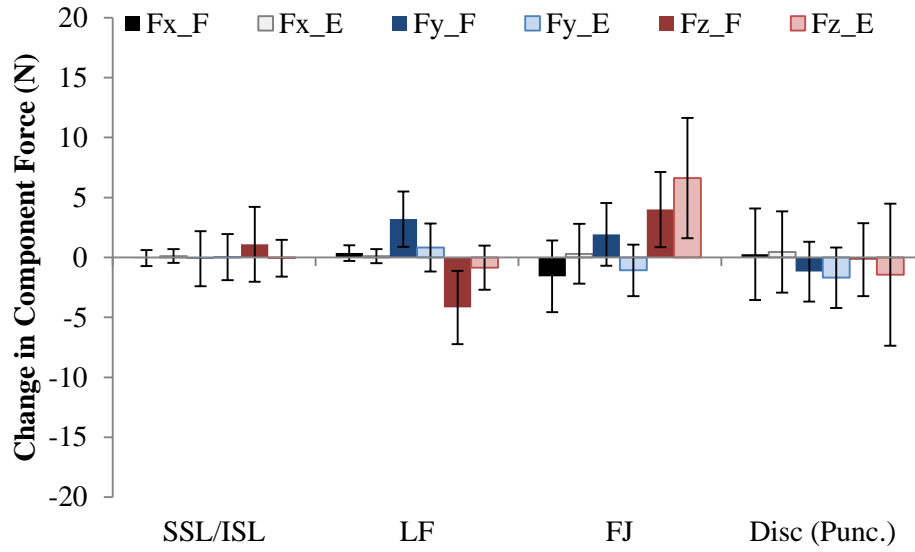


Figure 34. Change in component forces with serial resection of FSU structures in Neutral F/E

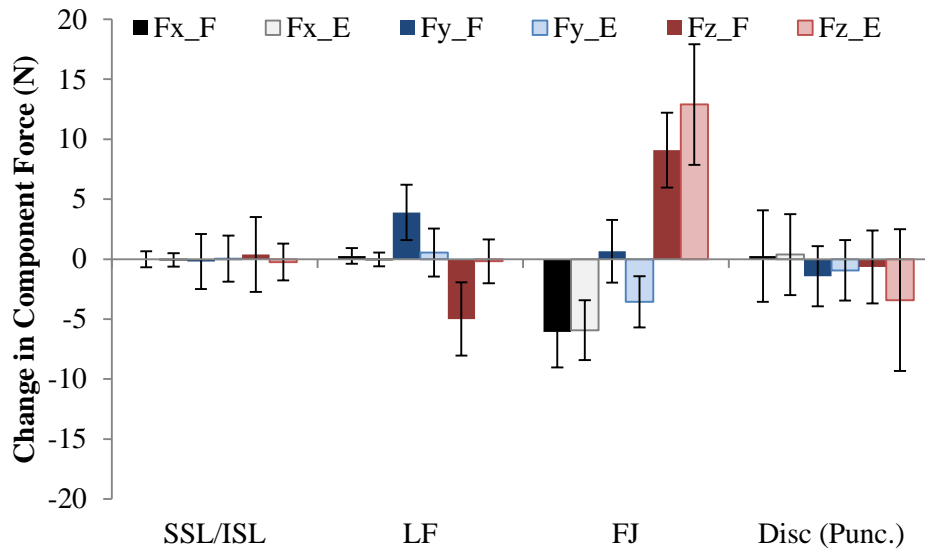


Figure 35. Change in component forces with serial resection of FSU structures in Large AT+F/E

7.4 DISCUSSION

This study quantified the mechanical role of important spinal structures in rabbit lumbar FSUs in neutral and axially rotated F/E. It identified the predominant role of the LF in flexion moment resistance and the disc in extension moment resistance. The addition of torsion to F/E increased the role of facets in extension moment resistance and increased the forces associated with facet joints in extension (Figure 35). These findings shed light on mechanobiological studies in Chapters 5.0 and 6.0 assessing biological changes in spinal tissues subjected to neutral and combined F/E by (1) clarifying the role individual tissues play in F/E moment resistance and (2) describing how this role changes with combined AT.

7.4.1 Neutral F/E

This study identified the role spinal structures play in F/E moment resistance under *in vitro* loading. Other studies of human and large animal lumbar spines have also identified the prominence of the LF in flexion moment resistance [86, 87, 366]; however, in this rabbit study, the contribution of the LF in flexion was higher than in other species. In addition to its importance in various spinal pathologies [156, 372], the distinction of the LF in terms of its large mechanical role in flexion supports selection of LF for mechanobiological analysis over other components of the posterior ligamentous complex. The LF was the only structure that showed any sensitivity to cycles of F/E (increased catabolic and pro-inflammatory gene expression), and its large role in flexion may contribute to its load-responsive changes.

In neutral extension, results were distorted by a violation of the principle of superposition in that moments increased after LF resection. The negative response in this study of the LF in extension obscures and may distort the role of facets and disc as determined using Equation 8. As calculated, facets played a small role in moment resistance. This proportion of moment resistance in extension falls low but within the published *in vitro* range (3-41% contribution) [27, 67, 88]. It has been shown that increased compression increases facet joint forces and pressure [88, 92], so lack of applied compression likely underlies this low contribution to extension loading. Additionally, changes in force due to facet resection (~13.1% BW) compare to BW-normalized human facet joint forces (2.0-16.8% BW). Modest increases in *MMP-3* and *COX-2* gene expression in neutral F/E (Figure 22 and Figure 24) reflect the putative small-to-modest mechanical role of facets in extension. Thus, the degree of facet contribution to extension supports examination of biological responses in facet cartilage under neutral extension, even in the absence of applied compression.

At the same time, the contribution of the disc to flexion resistance is smaller in rabbits than other species, and the contribution of the disc to extension resistance is larger in rabbits [87, 373]. This difference in the role of the disc may reflect lack of compression in rabbit FSUs. Compression would presumably increase the role of the facets in extension [67], thereby decreasing the role of the disc in flexion [80], thus reducing the role of posterior spinal ligaments (especially the LF). The small role of the disc in flexion may contribute to the relatively small biological changes observed in the disc, particularly the NP in repeated F/E (Section 5.3.2). In flexion, as well as in extension, the small negative force change with disc puncture reflects depressurization. Using the change in force components following needle puncture as a measure

of pressurization, flexion did not pressurize discs more than in extension. This small change might be more evident if axial compression had been applied to discs, increasing the amount of NP pressurization during F/E [374]

As indicated previously, the result in extension raises questions about the contribution of the LF to extension. It is also possible that removal of the LF tension band dramatically shifted the preferred COR anteriorly or somehow increased specimen stiffness. Such a shift could increase the extension moment and exaggerate the role of the disc. It is more likely, however, that results in extension reflect incomplete loading in extension. The extension moments in three of four FSUs did not go substantially beyond the transition point from low stiffness to high stiffness. This incomplete loading, which leaves FSUs in the neutral zone, likely explains the increase in extension moment with LF resection because loading in the neutral zone is more variable than that in the linear elastic zone and could increase after resection. The current characterization reflects loading used in this dissertation research. Moreover, the mechanical differences between neutral F/E and AT + F/E remain relevant to how the mechanical environment changed between the two types of loading and contributed to different biological responses. Thus, some caution is required in interpreting the role of the disc and facets in extension.

7.4.2 Combined loading: AT+F/E

Combined loading (AT+F/E) had a notable effect on the distribution of moment resistance among FSU structures. Combined loading had the largest effect on facets in extension. The nearly four-fold increase in contribution to extension resistance by facets indicates that facet involvement in AT+F/E represents a high level of physiologic loading. Moreover, the change in forces with facet resection in AT+F/E increased to nearly 24.5% BW. This value is higher than human lumbar

facet forces measured in extension or axial torsion (<20% BW) [89, 91, 375], but less than facet forces predicted in sustained anterior shear or compression, which reached as high as 100% BW [92]. Force vector data showed anterior, right-lateral, compressive orientation in keeping with rotational loading and support of an anterior shear force predicted by recent computational models of facet forces [67, 92]. Thus, the facet involvement in AT+F/E likely represents a high level of physiologic loading but does not exceed limits of facet loading likely to cause injury. Understanding this high degree of facet loading in extension helps to explain how axial torsion elicited a strong pro-inflammatory and pro-catabolic response in facet cartilage after a relatively short duration of loading (Section 6.3.2). Inflammatory and catabolic gene expression matched the higher level of loading with coupled AT.

Coupled torsion in F/E also affected the mechanical response in LF. In flexion, Large AT+F/E caused a change in force with LF resection to increase from near zero N in Neutral F/E to 5.19 ± 0.93 N (~11% BW). This modest change in force suggests increased loading with AT+F/E. The role of the LF in combined AT+F/E had not been described in any model system, so this provides important mechanical data for interpreting biological results. It is possible that the elevated force associated with the LF in coupled torsion contributes to the higher pro-inflammatory and pro-catabolic responses with AT+F/E (Section 6.3.2) compared to neutral F/E (Section 5.3.2).

The large increase in the role of facets in extension moment resistance was matched by a reduced contribution of the disc to extension resistance compared to neutral F/E (~63% decrease). It is reasonable that increased facet engagement, evidenced by higher *in-situ* forces (almost 3-fold increase), reduced loading in the disc at extremes of F/E. Reduced NP pressurization has been reported with applied AT [83], so it is possible that extension with added axial torsion also results

in lower intradiscal pressure, which influences both AF and NP mechanics [83, 84, 376]. This altered load distribution relative to neutral F/E could underlie different biological responses observed in disc tissue, particularly the AF, with combined loading.

7.4.3 Limitations

Connecting these results with biological changes in Chapter 5.0 and Chapter 6.0 neglects differences in testing: ambient temperature, lack of a fluid-filled environment, and fresh/frozen storage. These differences could have small influence on mechanical properties in spinal segments [377]. Because facet resection was performed bilaterally, the separate mechanical roles of left and right sides in AT+F/E were not elucidated. Instead, the net effect of AT on F/E mechanics was characterized. The change in resultant force vector with bilateral facet joint resection indicated an anterior, lateral, compressive force that reflects the strong engagement of the right facet. The disc puncture in this study does not adequately isolate NP depressurization from AF injury because of the large needle diameter used. Disc puncture in this context represents a disc injury that combines depressurization and annular injury, and while depressurization is certainly the larger influence [369, 378], rigorous distinct assessment of NP and AF are not appropriate. It is also important to appreciate that moments and forces measured by the UFS are based on a prescribed local anatomical (or joint) coordinate systems and point of action [284, 285]. Thus, error in alignment and positioning of the specimen or COR estimate could influence values of moments and forces. However, the adaptive nature of the robotic control and error tolerance shown in Section 3.4.2 mitigate these concerns. It is also critical that the testing system and fixture stiffness be high enough to remain unaffected by reduced specimen stiffness with resection. It is possible that the elevation of extension moments and large drop in flexion moments following LF resection in

neutral F/E is an artifact of inadequate system stiffness. This seems unlikely, however, because of the small moments applied and relatively low stiffness of rabbit FSUs in F/E. The analysis of percent contribution of each structure to primary moment resistance relies on the principle of linear superposition. It has been pointed out that this principle does not hold perfectly in spinal segments [87, 373], and interactions between structures and viscoelastic effects can cause coupling. While apparent interaction of spinal structures casts doubt on the application of this assumption in spinal segments, this limitation has generally small effects and is accepted in the literature [288, 373, 379]. The results of LF resection in incomplete extension reflect a violation of this assumption that may result from viscous effects in the disc within the neutral zone.

7.4.4 Conclusions

In summary, this study addressed the question of how spinal structures were loaded in rabbit FSUs in neutral F/E and combined AT + F/E. The salience of the LF in flexion resistance was confirmed, and coupled torsion elevated *in-situ* loads in flexion. The addition of torsion to F/E greatly increased the amount of facet loading and its contribution to extension resistance. The disc played a relatively small role in flexion and a relatively large role in extension resistance. Torsion reduced the contribution of the disc to extension and increased its role in flexion. These findings support mechanobiological analysis of each of these spinal tissues because of their mechanical importance in F/E and their differential mechanical response to coupled torsion. The degree of biological responsiveness matched well with the mechanical role of tissues in moment resistance.

7.4.5 Acknowledgements

The assistance of Mr. Robert Tisherman in helping with experimental testing and data analysis is gratefully acknowledged.

8.0 REGRESSION ANALYSIS: CORRELATING MECHANICAL AND BIOLOGICAL RESPONSES

8.1 INTRODUCTION

A primary purpose of mechanobiology is to characterize the response of cells to stimuli that arise or change due to mechanical factors. In numerous fields, researchers have presented theories that attempt to understand cellular responses in their relation to applied loading, macroscopic mechanical properties, cellular mechanical properties, and models of mechanotransduction [380, 381]. In cartilaginous tissues of the spine, unifying theories for explaining cellular behavior in terms of mechanics are less developed [9, 30]. It is clear that cells in these tissues respond to changes in their mechanical environment, and these responses mediate degenerative processes [30, 98]. Multi-scale modeling has sought to connect cellular responses to changes in the micro-environment with applied macroscopic loading [108, 109, 112, 382], but applying these findings to complex loading scenarios seen *in vivo* and accounting for the enormous variation in cells and their surrounding matrix across species, age, and degree of degeneration is daunting. Instead, relating macroscopic mechanical responses of spinal segments to biological changes in spinal tissues provides a simpler, more measurable, more readily translatable approach to connecting biology and mechanics.

In spine research, few attempts have been made to link mechanical or structural properties, particularly at the macroscopic scale, with cellular responses [383-385]. Studies have focused exclusively on relating material properties of isolated spinal tissue to biochemical composition with the goal of relating tissue mechanics and composition. In contrast, a recent exploratory study

sought to understand cellular responses to mechanical loading by correlating mechanical parameters of axially compressed spinal segments with changes in relative gene expression [386]. The authors found that late-stage creep parameters significantly and highly ($R>0.7$) correlated with *MMP-3* expression in AF. Because of the importance of other loading modes in spinal motions, it is of interest to understand similar relationships between segmental mechanics and biological responses in complex, rotational loading.

To account for variation in cellular responses across different loading modes seen *in vivo* (e.g. flexion, rotation, and compression), unifying mechanical factors that scale across loading modes must be established. These can include measured properties like compressive pressurization [387], predicted responses such as fluid flows and stress magnitudes [108, 112, 388, 389], or calculated energetic properties like applied energy (work) or dissipated energy (hysteresis) [390, 391]. Work reflects a summation of loading over a movement; it integrates the amount of applied load with the amount of movement. Thus, it can be applied in any degree-of-freedom (DOF) or mode of loading. Because movement and loading are readily measured or approximated, work serves as a translatable metric to *in vivo* scenarios [392]. In fact, rehabilitation science utilizes work to characterize loading in human movements at other joints [393, 394]. When applied to tissues of the spine, the deformation of each structure and proportion of load sustained by each structure during the movement must be considered. Like work, hysteresis measures a change in energy and can be applied in any loading mode. Unlike work, however, hysteresis characterizes the non-elastic response of a spinal segment. In FSUs, the segment as a whole and each structure, though principally the NP [395], behave in a viscoelastic manner exhibiting energy

dissipation. Energetic properties can be calculated in spinal segments as candidate mechanical parameters that may enable comparisons between types of loading for assessment of mechanical and biological responses.

Biological responses to rotational loading were explored using a novel *ex vivo* mechanobiology testing system (Chapters 5.0 and 6.0). Flexion/extension (F/E) with and without axial torsion (AT) was applied to FSUs over short durations (< 2 hours). These loading modes are involved in daily activities, rehabilitation exercises, and occupational tasks [68]. Segmental mechanical response parameters like range-of-motion (ROM), stiffness, and load relaxation, which have been characterized thoroughly in cadaveric spine testing and may be estimated during *in vivo* activities [210, 297, 396-400], have good utility as candidate mechanical predictors of biological responses. Alongside segmental mechanics, relative gene expression was calculated for inflammatory (*COX-2*), catabolic (*MMP-1*, *-3*, *ADAMTS-5*), and anabolic (*ACAN*) gene markers in annulus fibrosus (AF), nucleus pulposus (NP), facet cartilage (FC), and ligamentum flavum (LF). Specifically, the mechanical responses (as calculated in Section 5.2.2) included the amount of rotational deformation in F/E and AT, given by range-of-motion in flexion (ROM_f), extension (ROM_e), and axial rotation (aROM). Neutral zone stiffness (NZ_k) provides insight in to the amount of tissue laxity (Equation 5) and may reflect the extent of age-related or degenerative changes in the tissues of the FSU [401, 402]. Cumulative and mean work and hysteresis were calculated for FSUs (Equation 3 and Equation 4). Changes in mechanical properties across cycles of loading were calculated (Equation 7); these describe how FSUs adjust to loading, and these changes may also reflect age-related or degenerative changes in tissue [403, 404].

It would be clinically beneficial to understand relationships between mechanical factors and predicted biological responses to those factors. In such a paradigm, measurable mechanical factors like flexion and axial ROM or total work in exercise might be monitored and used to predict changes in catabolism and anabolism. Characterizing the relationship between mechanical factors of spinal segments with biological changes provides clinical utility to design of motion-based therapies and prediction of injurious modes of loading.

The objective of this analysis is to perform multiple regression analysis on F/E mechanobiology data from spinal segments. The goals are (1) to identify the most important mechanical variables (i.e. those that account for the most variation), (2) to seek to quantify their association with biological responses (relative gene expression) in each of the spinal tissues analyzed, and (3) to look for differences in modeling results between tissues and genes. The basic premise is to determine the amount of variation in biological responses that can be attributed to mechanical factors.

8.2 METHODS

Linear multiple regression was employed to relate mechanical factors as input variables (i.e. predictors) to dependent biological variables (i.e. outputs). Relative gene expression, calculated using the $2^{-\Delta\Delta C_t}$ method comparing loaded to unloaded tissues, of pro-inflammatory (*COX-2*), catabolic (*MMP-1*, *-3*, and *ADAMTS-5*) and anabolic (*ACAN*) genes was used as the regression model output. Relative gene expression was chosen as the biological output because it provides direct insight in to various cellular responses, its range is theoretically large, and its sample size in the present data set was largest. All available genes measured in each tissue for each specimen

were used by pooling all experimental groups from previous aims. The mean of left and right FC gene expression was used for samples subjected to combined torsion and flexion/extension. Mechanical factors were calculated for each of N=45 tests. A total of N=37 mechanical factors (see Table 16) were entered in to the analysis.

Table 18. List of predictors and outcomes for multiple regression

<u>Classification</u>	<u>Predictors</u>	<u>Mean</u>	<u>SD</u>	<u>Outcomes</u>	<u>Mean</u>	<u>SD</u>
Energetic Properties	Work Cumulative (J)	240.68	85.37	Relative	<i>AF_MMP-1</i>	1.45 0.94
	Work Mean (J)	6.23	2.52	Gene	<i>AF_MMP-3</i>	2.11 1.35
	Work Change (J)	0.08	0.32	Expression	<i>AF_ADAMTS-5</i>	1.23 0.57
	Work Relaxation (%)	0.01	0.07		<i>AF_COX-2</i>	1.27 0.70
	Hysteresis Cumulative (J)	30.31	21.84		<i>AF_ACAN</i>	1.46 0.73
	Hysteresis Mean (J)	0.74	0.41		<i>FC_MMP-1</i>	0.73 0.34
	Hysteresis Change (J)	0.07	0.14		<i>FC_MMP-3</i>	2.20 1.64
	Hysteresis Relaxation (%)	0.03	0.33		<i>FC_ADAMTS-5</i>	0.92 0.34
FE Moment-Rotation	ROMf (°)	14.42	3.77		<i>FC_COX-2</i>	2.46 1.65
	ROME (°)	-3.43	2.47		<i>FC_ACAN</i>	0.84 0.45
	Mxf (Nm)	0.46	0.12		<i>NP_MMP-3</i>	2.32 3.53
	Mxe (Nm)	0.14	0.08		<i>NP_COX-2</i>	1.61 1.21
	Mxf Change (Nm)	0.03	0.03		<i>NP_ACAN</i>	1.17 0.76
	Mxe Change (Nm)	0.01	0.02		<i>LF_MMP-1</i>	1.40 1.23
	Mxf Relaxation (%)	5.92	5.46		<i>LF_MMP-3</i>	2.33 2.17
	Mxe Relaxation (%)	-4.38	62.03		<i>LF_ADAMTS-5</i>	1.61 1.29
	NZk (Nm/°)	0.02	0.01		<i>LF_COX-2</i>	2.86 2.37
	NZk Change (Nm/°)	0.01	0.01		<i>LF_ACAN</i>	1.40 1.01
	NZk Relaxation (%)	0.01	0.03			
AT Moment-Rotation	aROMf (°)	-1.02	1.51			
	aROME (°)	-0.92	1.41			
	aROMmidfe (°)	-0.97	1.46			
	Myf (Nm)	-0.21	0.25			
	Mye (Nm)	-0.27	0.33			
	Mymidfe (Nm)	-0.25	0.29			
	Myf Change (Nm)	-0.01	0.07			
	Mye Change (Nm)	-0.02	0.07			
	Mymid Change (Nm)	-0.01	0.07			
	Myf Relaxation (%)	53.91	877.70			
	Mye Relaxation (%)	-449.45	2781.0			
	Mymid Relaxation (%)	-62.69	341.97			
Covariates	Cycles (n)	42.66	15.34			
	Age (mo.)	14.22	5.77			

8.2.1 Mechanical Factor Reduction

All redundant factors were consolidated to avoid correlation between predictors. Consolidation included choosing one variable to represent change in that parameter across cycles (i.e. choosing normalized changes over changes in actual magnitude). Also, to permit possible insights in to differences in flexion and extension, which load tissues differently, flexion and extension variables were considered separately, and overall measures of F/E (ROM_{fe}, Mx_{fe}) were excluded. Because of the presence of multicollinearity in a dataset of applied, measured, and calculated mechanical factors, autocorrelation analysis was performed to identify correlated factors and remove unwanted redundancy that increases error in regression model coefficients. Briefly, an autocorrelation matrix was created from *R*-values from simple Pearson's correlation between each factor and all other factors. Variables were considered to be highly correlated if $R > 0.75$. Using a rule to retain as many mechanical factors in the data set as possible, correlated variables were removed. That is, if correlated pairs of variables included x - y and x - z , then x was removed and y and z were retained.

8.2.2 Principal Component Analysis

To identify the variables that accounted for the most variation in the mechanical response and enter only these mechanical factors as predictors in the multiple regression analysis, principal component analysis (PCA) was performed on the remaining factors. Single-value decomposition was performed using Matlab (R2013) on standardized variables (to account for magnitude differences among variables) to identify the principal components. Varimax rotation was applied to maximize the unique contribution of original variables to each principal component and enable

interpretation of the first principle component [405]. Eigenvalues associated with each principal component and the amount of variation in the data set accounted for by each principal component were calculated. Principal components with eigenvalues greater than 1 were selected (Kaiser rule). Original variables were then correlated with the coefficients of the principal components using Pearson correlation. For this study, factors that (1) had correlations $R > 0.6$, (2) were among the two factors mostly highly correlated with that principal component, and (3) were not correlated with the other factors within that principal component ($R > 0.6$) were chosen.

8.2.3 Multiple Regression-Part I: Hierarchical Entry Rationale

Linear multiple regression was performed using a hierarchical approach with ordered groups of predictors formed *a priori*. Final predictor variables were clustered in to four groups representing different aspects of FSU mechanical responses: (a) Energetics properties, (b) F/E moment-rotation properties, (c) AT properties, and (d) Relaxation of parameters. The ordering of predictors was based on an order of presumed importance of mechanical predictors to each tissue within the FSU. Previous research and mechanical theory point to different mechanical roles and responses of each tissue in F/E and combined AT and F/E loading, so the order of entry of groups was based on a rationale specific to each tissue (see Table 19).

Table 19. Tissue-specific order of predictor groups

Tissue	Predictor Group Order
AF	1) AT Moment-rotation > 2) Energetic properties > 3) F/E Moment-rotation > 4) Relaxation
FC	1) AT Moment-rotation > 2) F/E Moment-rotation > 3) Energetic properties > 4) Relaxation
NP	1) Energetic properties > 2) Relaxation > 3) F/E Moment-rotation > 4) AT Moment-rotation
LF	1) F/E Moment-rotation > 2) Energetic properties > 3) AT Moment-rotation > 4) Relaxation

AF: The order of entry was chosen to be (1) AT properties, (2) energetic properties, (3) F/E moment-rotation properties, and (4) relaxation of parameters. The primary role of AF across loading modes is torsional resistance [81], so AT properties were entered in to the regression model first. Because the AF supports compression in flexion [40, 406] and resists extension moments through tension on the posterior side [367] (thus always resisting loading in the direction of movement), energetic properties, which integrate loading with movement, were considered second. By the same rationale, F/E ROM and NZ stiffness similarly influence AF, but these properties are thought to be regulated by the interaction of many tissues [87, 367, 379], and the serial resection study in rabbit FSUs showed that the disc was a small contributor to flexion resistance, so F/E property variance is less likely to be reflected specifically in biological changes in AF. Finally, relaxation of parameters was placed last because moment relaxation is governed largely by other joint structures [87].

FC: The following entry order was used: (1) AT properties, (2) F/E moment-rotation properties, (3) Energetic properties, and (4) Relaxation of parameters. The results of the serial resection study (Section 7.3) combined with previous research make it clear that lumbar facet loading increases dramatically with axial rotation [85, 89], supporting the choice of AT properties as a reasonable first group. Secondly, facets contribute largely to resistance of extension moments [67, 93, 407], so F/E moment properties are entered next. Both energetics and relaxation, particularly as they relate to extension, have been considered to be important in describing facet mechanics [85, 89, 408, 409], but it is unclear which is more so. To be consistent with the order of entry of predictors in AF and LF models, energetic parameters were entered earlier and relaxation parameters were entered afterward.

NP: The order of predictor variable entry for NP was the following: (1) Energetic properties, (2) Relaxation of parameters, (3) F/E moment-rotation properties, and (4) AT properties. Because the NP is a viscous structure that plays a central role in the absorption and dissipation of forces in FSUs, energetic properties were entered in to the model first [92, 410]. For similar reasons, the NP influences time-dependent changes of FSU mechanics [404], so the relaxation of parameters was entered in to the model second. This relative ordering of energetic and relaxation parameters is also consistent with the other tissues. In pure moment testing where compression is not applied to FSUs, the NP plays a small role in F/E moment-rotation properties [411]. The serial resection study supports this diminished role of the NP in F/E in this dissertation as NP depressurization had only a small effect on F/E moment resistance. Finally, while some evidence suggests NP may be depressurized by AT [83], without applied compression, the effect of AT on NP pressurization is expected to be minimal.

LF: The order was (1) F/E moment-rotation, (2) Energetic properties, (3) AT properties, and (4) Relaxation of parameters. Numerous studies, including the serial resection study in Chapter 7.0, confirm that the LF primarily resists flexion moments and may influence NZ stiffness [86, 87]. Spinal ligaments have been shown to be responsive to cycles and rates of loading [243], so energetics properties like cumulative work are expected to influence LF mechanobiology. While the LF is not generally thought to play a measurable role in AT resistance [412], combined loading may recruit LF fibers on the contralateral side and consequently alter LF mechanics [93]. Resection of the LF in Chapter 7.0 in AT+F/E showed a small increase in force with added AT that may reflect increased tension in LF. Finally, while the LF influences flexion relaxation, it does not generally influence extension moments or

extension relaxation. Because relaxation of extension moments exclusively constituted this category after PCA, this category was placed last as it is unlikely for this relaxation property to influence LF biology.

8.2.4 Multiple Regression-Part II: Final Regression

Hierarchical linear multiple regression analysis was performed using SPSS® Statistics 22.0 (IBM Corporation, Armonk, NY). A sequential regression method was performed in two steps [413]. In the first step, all of the mechanical factors were entered in to the model as groups in the order described per tissue for all genes (Table 19). The effect size and significance of each predictor variable were assessed, and predictors that were important to the model were retained for a second, final regression (individual coefficient weights $\beta > 0.3$ with significance values $p < .20$) analysis that focused on the most relevant predictors [413]. Liberal cutoff values of $\beta > 0.3$, a small-to-moderate model weight [413], and $p < .20$, twice that of typical low significance thresholds [413], was used at this intermediate stage to include variables that could contribute to the final model (final significance was set to $p < .05$), but whose partial correlation may have been diminished from the influence of many predictors ($n=8$). Predictors were then entered in the final model by the order of their importance to the initial model (β -size and associated p -value), and the resulting regression analysis was assessed. Significance of the model was determined using an F-statistic, the ratio of variability accounted for by the linear model divided by random variability about the mean of the data. The number of predictors and sample size, which influence the significance of regression results, are accounted for in the F-statistic. The overall size of the relationship (or effect size) between the model and outcomes was given by R (< 0.2 being negligible, $0.2-0.4$ being small, $0.4-0.6$ being moderate, and > 0.6 being large effects), the amount of variance accounted for by the

model was given by R^2 , and generalizability of findings to a broader population was given by Adjusted R^2 . Adjusted R^2 , which is less than or equal to R^2 , indicates a predicted reduction in explained variation when the model is applied to the population as a whole. If Adjusted R^2 values are close to R^2 values, then findings are considered generalizable.

Each model was also analyzed for contribution of individual predictors. The coefficients, standard errors of coefficients, standardized coefficients, significance of coefficients, and simple linear correlations (Pearson) were calculated per predictor in the model. Simple linear correlations show the relationship between a predictor and outcome without the influence of any other predictor variable. Model coefficients (B) describe the effect of individual predictors while holding other predictors constant. Standardized coefficient values, β , describe the magnitude of the relationship between individual predictors and model effects on biological outcomes in standard deviation units. Thus, they relate the change in a given predictor normalized by its variability to the effect on a standardized outcome, i.e. how many standard deviations the outcome will change for a given change of one standard deviation in the predictor. Predictors with significant coefficients were reported and discussed per model.

Assumptions of multiple regression were assessed by (1) ensuring lack of multicollinearity by autocorrelation of predictors (Pearson's $R < 0.75$) and checking that mean variable inflation factors (VIFs) were close to 1, (2) checking for independence of errors by confirming that standardized residuals were normally distributed, and (3) inspecting the assumptions of linearity and homoscedasticity by assessing spread and shape in plots of standardized predicted values vs. standardized residuals. Initial regression analysis showed assumptions of homoscedasticity, linearity, and independence of errors were not met in all tissues for all genes, so relative gene expression was transformed using a log function. A log transform of outcome data enabled

assumptions of multiple regression to be met. To permit more facile interpretation of model weights, which explain the weighted relationship of a predictor to a change in the outcome, model coefficients were reverse-transformed. Expressing coefficients' effects on gene expression data in a linear scale makes comparison with previous experimental data easier. Finally, sensitivity of model outcomes to order-of-entry was also checked by using a hierarchical scheme across all tissues that entered variables in to the model based on their order in principal component analysis.

8.3 RESULTS

8.3.1 Data Reduction: Autocorrelation

The overall reduction process for predictors is depicted in Figure 36. Eliminating known redundancies and performing autocorrelation reduced the number of predictor candidates from $n=37$ to $n=15$. The autocorrelation matrix is displayed in Appendix C.1. Mean work was highly correlated with flexion ROM and moments ($R=0.797$, $R=0.792$, respectively), and relaxation in work across cycles was also highly correlated with change in flexion moments across cycles ($R=0.794$). Also, cumulative hysteresis was highly correlated with mean hysteresis ($R=0.823$) while cumulative work and mean work did not show as high of a degree of correlation ($R=0.660$). All AT ROM and moment factors were highly correlated ($R=0.841-0.994$), and AT moment relaxation factors were also highly correlated ($R=0.831-0.986$). The retained variables are listed in Table 20 and Figure 36.

Table 20. Mechanical factors not correlated or redundant to other factors

Autocorrelation Results: Non-correlated Factors			
Work Cumulative	ROMf	aROMmidfe	Cycles
Hysteresis Mean	ROME	Mymidfe Relax.	Age
Hysteresis Relax.	MxF		
	MxE		
	Mxf Relax.		
	Mxe Relax.		
	NZk		
	NZk Relax.		

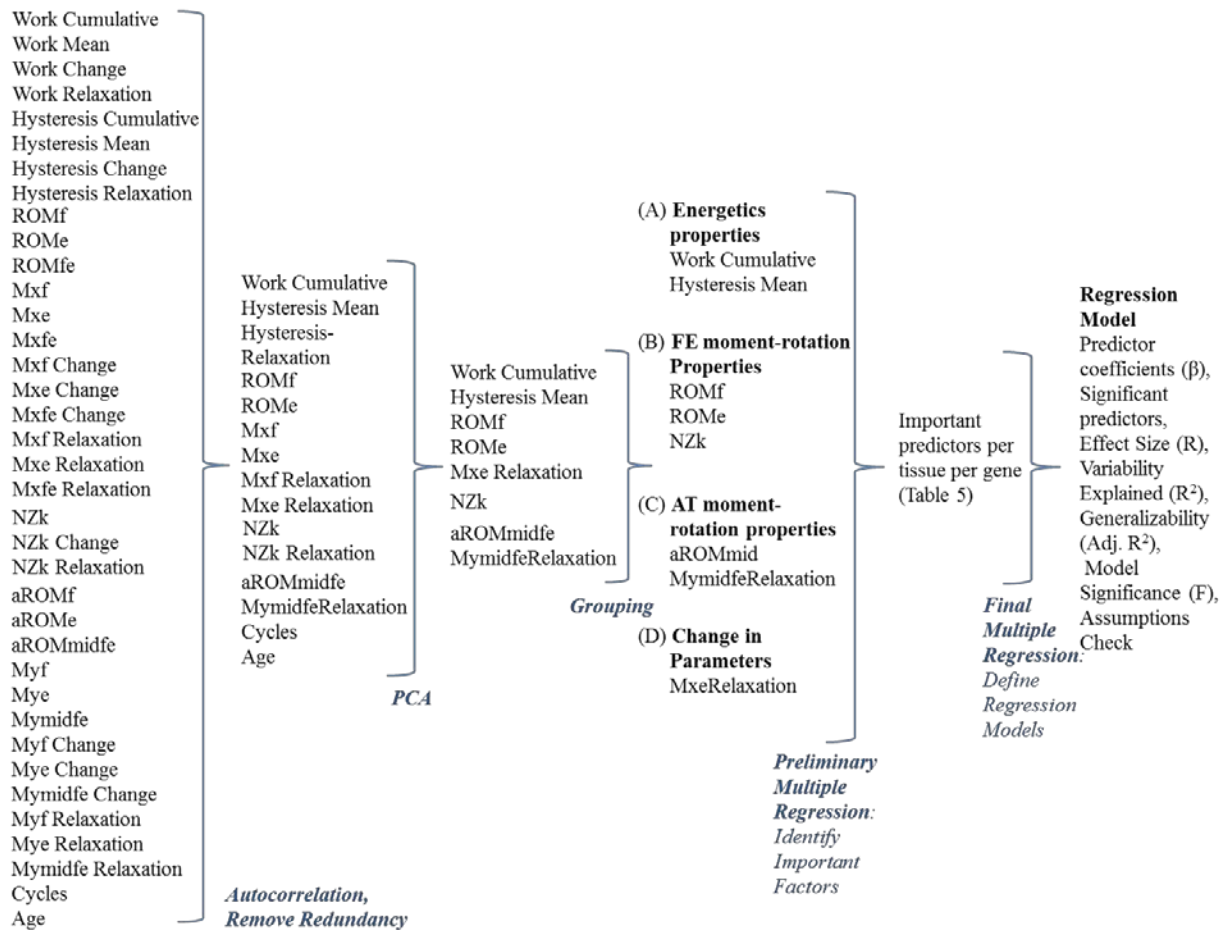


Figure 36. Overview of data reduction and sequential multiple regression

8.3.2 Principal Component Analysis

Results of the PCA analysis are displayed in Figure 37 and Table 21. A total of $n=5$ principal components (PCs) exceeded the minimum threshold (Kaiser rule): eigenvalues > 1.0 [413]. The first PC (PC1) had large correlations (>0.6) with flexion properties and energetic properties: flexion moments ($R=.901$), flexion ROM ($R=.806$), cumulative work ($R=.752$), and hysteresis relaxation ($R=.627$). The second PC (PC2) was highly associated with other portions of the F/E moment-rotation curves: extension moments ($R=.835$), extension ROM ($R=.814$), NZ stiffness ($R=.715$), and Cycles ($R=.699$). The third PC (PC3) was associated with change in parameters across cycles; relaxation of extension moments ($R=.764$) and relaxation of NZ stiffness ($R=.904$) were correlated with PC3. The fourth PC (PC4) was associated with AT properties; AT ROM ($R=.667$) and AT moment relaxation ($R=.614$) were correlated with PC4. Finally, the fifth PC (PC5) correlated highly with only one original variable, mean hysteresis ($R=.818$). By selecting the two most highly correlated variables with each PC and applying a strict autocorrelation rule of $R>0.6$ among variables within a PC, a total of $n=8$ variables were ultimately selected (see Table 21). Final predictors included F/E Moment Rotation properties—ROMf, ROMe, and NZk, AT moment-rotation properties—aROM and MyRelaxation, Energetic properties—Cumulative Work, Mean Hysteresis, and Relaxation in parameters, MxeRelaxation (also includes MyRelaxation, but it was grouped with AT moment-rotation properties to avoid double-entry in to the model).

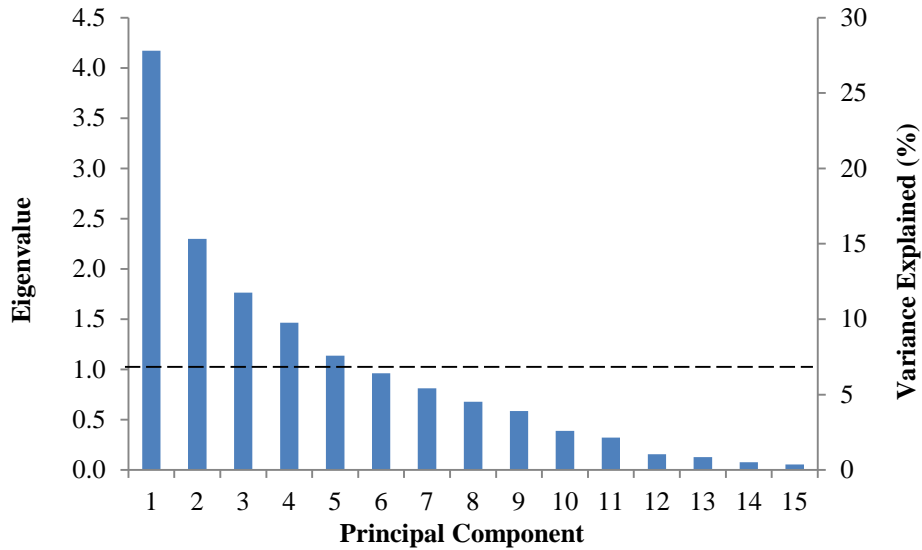


Figure 37. Principal component eigenvalues and percent variance explained per principal component.

Table 21. Uncorrelated ($R < .6$) mechanical factors correlated with PCs ($R > 0.6$) with highest R values

Principal Component	Mechanical Factor Grouping			
	Energetics	FE Properties	AT Properties	Relaxation
1	Work Cumulative	ROMf		
2		ROME, NZk		
3				Mxe Relax.
4			aROM, My Relax.	
5	Hysteresis Mean			

8.3.3 Multiple Regression—Part I: Important Predictors Identified

Table 22 summarizes the important predictors and their coefficient p-values that were identified by the preliminary multiple regression across all tissues and genes. The factors that contributed

importantly ($\beta > 0.3$, $p < 0.2$) to preliminary multiple regression are listed alongside their model coefficient significance. All tissue and gene combinations except for FC MMPs yielded important predictors.

Table 22. Predictors identified in preliminary regression ($\beta > 0.3$, $p < 0.2$) with p-values

Tissue	<i>MMP-1</i>		<i>MMP-3</i>		<i>ADAMTS-5</i>		<i>COX-2</i>		<i>ACAN</i>	
	Predictor	<i>p</i>	Predictor	<i>p</i>	Predictor	<i>p</i>	Predictor	<i>p</i>	Predictor	<i>p</i>
AF	Work Cumulative	0.16	aROM	0.059	NZk	0.133	ROMf	0.087	Hysteresis Mean	0.064
					MyRelax	0.153	MxeRelax	0.134	MyRelax	0.161
									Work Cumulative	0.133
									ROMf	0.132
FC	no important predictors		no important predictors		NZk	0.073	Work Cumulative	*0.007	aROM	*0.024
					aROM	0.152	MyRelax	*0.013	Work Cumulative	0.126
							aROM	0.107	MyRelax	0.188
NP	no RGE available		ROMe	0.159	no RGE available	Hysteresis Mean	0.126	MxeRelax.	0.118	
						ROMe	0.164	NZk	0.131	
								ROmf	0.142	
LF	Work Cumulative	0.069	ROMf	0.104	NZk	0.061	aROM	*0.014	NZk	0.054
	NZk	*0.023			ROMf	0.178	ROMf	0.073		
	ROMf	0.071			MyRelax	0.119	NZk	*0.046		
							MyRelax.	0.056		

t- $p < .10$, * $p < .05$, ** $p < .01$; NS-Non-significant or trending ($p > .10$) coefficients; x-no relative gene expression data available. **Bold**- $p < .05$

8.3.4 Multiple Regression—Part II: Summary in All Tissues

Reduced sets of important predictors were examined in subsequent, final regressions. Of the possible 18 biological outcomes (four tissues and five genes per tissue with no *MMP-1* and

ADAMTS-5 data collected for NP), nine had significant regression models ($F, p < .05$) and one had a model that showed a strong trend ($F, p = .096$) (Table 23). In general, the magnitude of the correlation of mechanical predictors with biological outcomes was moderate in size with R values in significant models ranging from 0.368–0.710 (Table 6). Overall model significance was most frequent in AF with all genes except *COX-2* showing significant or nearly significant regression models. However, the amount of variance predicted by models was only modest—13.5–32.3% of the variation in AF biological responses was accounted for by mechanical predictors. By comparison, 31.9–50.4% of variation in biological outcomes was accounted for by significant regression models in FC and LF. Also, FC and LF models were both significant for three of the five genes (*ADAMTS-5*, *COX-2*, and *ACAN* in FC and *MMP-1*, *ADAMTS-5*, and *COX-2* in LF). No regression models were significant in the NP.

Table 23. R-values and significance of final regression models

<u>Tissue</u>	<i>MMP-1</i>	<i>MMP-3</i>	<i>ADAMTS-5</i>	<i>COX-2</i>	<i>ACAN</i>
AF	*0.445	*0.368	†0.393	0.229	*0.569
FC	.	.	*0.653	*0.624	*0.629
NP	x	0.116	x	0.206	0.478
LF	*0.609	0.175	*0.564	*0.710	0.284

*-Significant model, $F, p < .05$ †-Trending model, $F, p < .10$

x-no relative gene expression data available

.-no important predictors identified in Part I

Significant individual predictor coefficients are summarized in Table 24. Across models for all tissues and genes, five mechanical predictors were significant: Work Cumulative, NZk, aROM, MyRelaxation, and ROMf. Predictors that showed trends toward significance include Hysteresis Mean and MxeRelax. Thus, only ROME, among the final set of predictors, showed no correlation with outcomes. Standardized coefficients ranged between $\beta = 0.643$ –5.083 for all

significant predictors. Standardized coefficients were consistently large (>1.0) for NZk in LF across biological responses ($\beta=1.961-5.083$) with the largest value for NZk in *COX-2* expression. Other significant predictors with large weights were Work Cumulative and aROM in AF, aROM in FC, and ROMf and My Relaxation in LF (see Table 24 for β -values).

Table 24. Summary of significant predictors and their standardized coefficients (β)

Tissue	<i>MMP-1</i>		<i>MMP-3</i>		<i>ADAMTS-5</i>		<i>COX-2</i>		<i>ACAN</i>			
	Predictor	β	Predictor	β	Predictor	β	Predictor	β	Predictor	β		
AF	Work Cumulative	*1.78	aROM	-*1.33	MyRelax	†-.54	NS	.	ROMf	†1.03		
					NZk	†-.52			MyRelax	*-.65		
									Hysteresis Mean Work Cumulative	†-.52		
FC	NS	.	NS	.	NZk	*-.69	Work Cumulative	*-.77	aROM	*-2.29		
									MyRelax	*-.73	MyRelax.	†1.909
									aROM	*.59	Work Cumulative	†1.907
NP	NS	.	NS	.	NS	.	NS	.	MxeRelax	†5.95		
LF	NZk Work Cumulative	*1.96 †1.17	NS	.	NZk	*1.99	ROMf	*5.08	NS	.		
											ROMf	*2.60
											MyRelax	*1.53
											aROM	*.64

*-Significant coefficients $p < .05$, †-Coefficient trends $p < .10$, NS-Non-significant or trending ($p > .10$) coefficients
x-no relative gene expression data available

The effect of varying hierarchical order-of-entry did not change significant results. In the alternative hierarchical approach where predictors were entered based on their relevance in principal component analysis, no changes in significant models or significant predictors occurred (data not shown). The assumption of lack of multicollinearity was upheld very well within the

reduced, transformed data set. Autocorrelation among predictors was low ($R < .75$), individual VIF values did not approach 10, and mean VIF values per regression were generally very close to 1. The assumption of independent errors, verified by assessing normality of standardized residuals, was generally upheld. Assumptions of linearity were generally upheld; standardized predicted value vs. standardized residuals showed little evidence of underlying curves or shapes. Assumptions of homoscedasticity were valid in all tissues (Appendices C.2.1 and C.6).

8.3.5 Tissue-Specific Regression Analysis

Results of individual multiple regressions are organized by tissue and listed in tables in the sections below. Significant models are reported and explained in each section. The constant (vertical offset) in each regression model is included in equations.

8.3.6 Annulus Fibrosus (AF)

Regression models were significant (or nearly so) in four of five biological outcomes in AF (Table 25). Only *COX-2* expression was not well predicted by regression analysis. Small to moderate effects were evident with $R=0.368-0.569$, indicating 13.5–32.3% of the biological variation explained by models. AT moment-rotation properties (aROM, MyRelaxation) and Work Cumulative were significant predictors (Table 26). Of these, aROM and Work Cumulative were large ($\beta > 1$). Individual models are discussed below.

Table 25. Description of regression models for AF

AF						
Gene	F	N	Predictors	R	R ²	Adjusted R ²
<i>MMP-1</i>	*5.942	26	1	0.445	.198	.165
<i>MMP-3</i>	*5.649	38	1	0.368	.136	.112
<i>ADAMTS-5</i>	†2.556	31	2	0.393	.154	.094
<i>COX-2</i>	.910	36	2	0.229	.052	-.005
<i>ACAN</i>	*3.470	34	4	0.569	.324	.230

*-Significant coefficients $p < .05$; †-Coefficient trends $p < .10$

Table 26. Description of model predictors for AF

AF						
Gene	Predictor	B	SE(B)	β	Sig.	R
<i>MMP-1</i>	Work Cumulative	.001	.001	* 1.789	.023	*0.445
<i>MMP-3</i>	aROM	-.115	.047	* -1.335	.023	*-0.368
<i>ADAMTS-5</i>	NZk	-.995	19.549	†-.520	.091	-0.216
	MyRelax.	.000	.000	†-.548	.069	†-.249
<i>COX-2</i>	ROMf	-.015	.015	-.337	.301	-0.188
	MxeRelax	-.001	.002	-.259	.448	-0.143
<i>ACAN</i>	Hysteresis Mean	-.203	.122	†-.521	.058	*-.364
	Work Cumulative	-.001	.001	†-.534	.093	-0.158
	ROMf	.023	.013	†1.036	.079	0.136
	MyRelax	-.000	.000	* -.657	.013	†-.244

*-Significant coefficients $p < .05$, †-Coefficient trends $p < .10$,
 B-coefficient weight, SE(B)-standard error of B, β -standardized coefficient, Sig.-p-value
 of t-test, R-univariate correlation

8.3.6.1 MMP-1

Results: Preliminary regression analysis identified Work Cumulative as the only important predictor of *MMP-1* expression in AF ($\beta=1.623$, $p=.142$). As is seen in Table 26, using Pearson's correlation, Work Cumulative is significantly, positively correlated with *MMP-1* expression ($R=0.445$). Regression analysis (single variable) confirmed this significant relationship, $R^2=0.198$, $F(1, 26)=5.942$ ($p=.023$) (Table 25). Adjusted R^2 was 0.033 less than R^2 , indicating a predicted 3.3% reduction in explained variation in the population as a whole. Thus, these findings are considered generalizable. The significant standardized coefficient, $\beta=1.789$, $p=.023$, indicates a large, positive effect of Work Cumulative on *MMP-1* expression.

$$MMP1_{AF} = 1.5 \times 10^{-3} * (Work\ Cum.\ J) + 0.622$$

Interpretations: Cumulative work presumably describes the summation of repeated compression in flexion and tension in extension that AF undergoes in cyclic F/E. *MMP-1* expression in AF has shown sensitivity to repeated tensile stretch and to abnormal compression [37, 204]. Thus, it is reasonable to suppose that cumulative work, which aggregates induced tensile and compressive stresses in the AF, is positively related to *MMP-1* expression. In the model, cumulative work has a moderate effect on predicted changes in *MMP-1* expression. A change of one standard deviation in Work Cumulative (85 J) elicits an increase in *MMP-1* of 1.789 standard deviations (1.68-fold increase). This represents a sizable change in work over 1 hour and a modest-to-large change in *MMP-1* expression in the data set which itself showed a small range. Thus, by itself, Work Cumulative accounts for a small amount of variability in *MMP-1* expression. However, the sequential regression analysis does identify a mechanical

factor, among many considered, that relates significantly to *MMP-1* expression. Given that only one mechanical factor comprises the model, it is not surprising that more than 80% of the *MMP-1* response remains unexplained.

8.3.6.2 MMP-3

Results: Preliminary regression analysis showed aROM to be the only salient predictor of the *MMP-3* response in AF ($\beta=-1.117$, $p=.072$). Simple Pearson's correlation (Table 26) showed aROM to be significantly negatively correlated with *MMP-3* expression ($R=-.368$). Regression analysis (single variable) confirmed this significant relationship, $R^2=0.136$, $F(1, 38)=5.649$ ($p=.023$) (Table 25). These findings are generalizable; Adjusted R^2 was 0.024 less than R^2 , indicating a predicted 2.4% reduction in explained variation in the population as a whole. A significant, large $\beta=-1.335$ (Table 26) denotes that an increase in aROM leads to a sizable decrease in *MMP-3*.

$$MMP3_{AF} = 2.197 - 0.115 * (aROM \text{ }^\circ)$$

Interpretations: This model identifies the only significant effect of a mechanical predictor on *MMP-3* expression in this study. In real terms, a decrease of 1.45° AT in repeated F/E leads to a predicted 1.80-fold increase in *MMP-3* expression. This is a fairly large amount of AT for a less than 2-fold increase in *MMP-3* expression. *MMP-3* expression in FSUs subjected to Large AT+F/E manifested 70% lower *MMP-3* expression levels than neutral F/E for a nearly 3° difference in AT angle. The model does not account for this accurately, but the regression only accounts for 13.6% of the overall variability in *MMP-3* expression. Axial torsion elevates circumferential stress in AF [81, 369, 378] and may increase compressive stress as well [83, 84]. Previous studies have shown that tensile stretch and compression can up-regulate *MMP-3* expression in AF cells, and tensile stretch can both increase or decrease expression based

magnitude of stretch [204, 242]. In disc-only models, axial torsion is associated with increased *MMP-3* expression [36, 209]. In this model, increased aROM was associated with a moderate decrease in *MMP-3* expression ($\beta=-1.335$), which is opposite from what was expected. A possible explanation is that the range of axial torsion magnitudes coupled with F/E moments applied to FSUs in this study did not cause AF stresses to reach the threshold for *MMP-3* activation seen in previous studies. It is also likely that there are regional differences in the AF response based on torsion, but gene expression is a global average insensitive to regional variation.

8.3.6.3 ADAMTS-5

Results: Multiple regression showed a trend toward predicting *ADAMTS-5* expression ($F, p=.096$) with NZk and MyRelaxation. Both variables had small, negative simple correlations with *ADAMTS-5* expression ($R=-.216, -.249$, respectively), though the correlation with NZk was not significant, and the correlation with MyRelaxation showed only a trend ($p=.089$). In multiple regression, after adjusting for the influence of the other predictor, each predictor maintained a small-to-moderate negative weight on *ADAMTS-5* expression reflected in $\beta=-.520$ ($p=.091$) and $\beta=-.548$ ($p=.069$) for NZk and My Relaxation, respectively (Table 26). The model explained 15.4% of *ADAMTS-5* expression variability, $R^2=0.154$, $F(2, 31) = 2.556$, $p=.096$.

$$ADAMTS5_{AF} = 1.385 - 0.995 * \left(NZk \frac{Nm}{\circ} \right) - 1.9x10^{-4} * (My Relax. \%)$$

Interpretations: The regression model showed trends of increasing neutral zone stiffness and moment relaxation with decreased *ADAMTS-5* expression. Changes of 55% of the mean NZk or 545% of the mean MyRelaxation predict modest decreases of 29.5% and 31.1%, respectively, in *ADAMTS-5* expression. This suggests that a decrease in stress in the AF across repeated F/E may be associated with reduced *ADAMTS-5* expression. Previous studies provide little insight in

to the role of mechanics in regulating *ADAMTS-5* in AF [66, 414, 415], but findings with *ADAMTS-4* point to a positive relationship between aggrecanase gene expression and stress magnitudes [36, 416] which support the findings of the model. Increased NZ stiffness is also associated with reduced *ADAMTS-5* expression, but it is unclear how NZ stiffness relates to AF mechanics. Previous studies explain how AF mechanics influence NZ width and elastic zone stiffness, but the AF's role in NZ stiffness is considered negligible [417]. Increased NZ stiffness may reflect degenerative changes in other structures like the NP or LF, which are known regulators of NZ stiffness and stiffen with degeneration [87, 121, 141, 331, 418]. The consequence of a stiffer NZ, regardless of the cause, cause altered load distribution in the FSU and reduced stress in the AF. This reduced stress in the AF could reasonably relate to lower *ADAMTS-5* expression. In any case, the model explains only a small amount of the variation in *ADAMTS-5* expression in AF, and effects of individual predictors on the outcome were quite modest.

8.3.6.4 ACAN

Results: Four predictors entered the final regression model for *ACAN* expression in AF (Table 26). MyRelaxation, Work Cumulative, Hysteresis Mean, and ROMf were all important predictors ($\beta, p < .20$) in preliminary regression analysis, with the most importance for Hysteresis Mean ($\beta = -.610, p = .064$) and the least importance for MyRelaxation ($\beta = .509, p = .161$). In simple regressions (Table 26), Hysteresis Mean was significantly, negatively correlated with *ACAN* expression ($R = -.364, p = .017$), and MyRelaxation showed a trend of negative correlation with *ACAN* expression ($R = -.244, p = .083$). Work Cumulative was also negatively correlated with the outcome, but its effect was small ($R = -.158$) and insignificant ($p = .187$). ROMf was positively correlated with *ACAN* expression, although it too was not significant ($p = .222$). Combining these variables in multiple regression yielded a significant model that explained the largest variance in biological

outputs for AF, $R^2=.324$, $F(4, 34)=3.470$, $p=.020$. A decrease of 0.093 in the Adjusted R^2 suggests a small mitigation of the generalizability of the model. The coefficients of the model matched the sign of their simple relationships with *ACAN* expression: Hysteresis Mean ($\beta=-.521$, $p=.058$), Work Cumulative ($\beta=-.534$, $p=.093$), and My Relaxation ($\beta=-.657$, $p=.013$) were negatively related to *ACAN* expression, and ROMf ($\beta=1.036$, $p=.079$) was positively related with the outcome.

$$ACAN_{AF} = 1.507 - .203 * (Hysteresis\ Mean\ J) - 1.1 \times 10^{-3} * (Work\ Cum.\ J) + .022 * (ROMf\ ^\circ) - 3.5 \times 10^{-4} * (My\ Relax.\ \%)$$

Interpretations: This model explains more than 30% of the variability in *ACAN* expression, and even though it uses four predictors, generalizability (based on Adjusted R^2) is good. While it is difficult to relate each of these mechanical predictors to AF mechanics, the results do not seem to adhere to the notion that increased *ACAN* expression in AF tissue is an adaptive response to elevated compression [9, 248]. My Relaxation increased, which denotes decreased torsional loading across cycles and putative lower AF compressive stresses [84], with increasing *ACAN* expression. Energetic predictors also showed associations of decreased energy applied (cumulative work) and energy dissipated (hysteresis) with increased *ACAN* expression. It is expected that sustained torsional moments, which presumably elevate compressive stress [84] in the AF, would increase *ACAN* expression [36, 206, 344]. Similarly, it is assumed that increased applied and dissipated energy relate, at least partially, to elevated compressive loading and fluid pressurization. *ACAN* expression in AF is not like NP or FC because of lower aggrecan amounts. It is expected that *ACAN* expression would increase in AF in response to compressive stimuli, but the model does not agree with these expectations, nor, in fact, do simple regressions of each of these factors with *ACAN* expression. On the other hand, ROMf is positively associated with *ACAN*

expression. If increased ROMf adds to compression in AF, then elevated *ACAN* expression with increased ROMf is reasonable. Nonetheless, given the assumption that tensile loading regulates collagen expression and compressive loading regulates proteoglycan expression, the expectation for increased proteoglycan expression based on how these predictors relate to compressive loading is not met.

8.3.7 Facet Cartilage (FC)

Regression models were significant in *ADAMTS-5*, *COX-2*, and *ACAN* expression in FC (Table 27). Gene expression is an average of left and right FC. A uniform, large amount of variation was accounted for in these biological responses to loading ($R=0.624-0.653$); specifically, 38.9-42.6% of the variation in biological responses is explained by these models. Significant predictors included aROM, My Relaxation, NZk, and Work Cumulative (Table 28). The strongest individual predictor of a biological response was aROM in *ACAN* expression ($\beta=-2.290$), and this predictor factored in to each significant model in FC. In addition to aROM, My Relaxation and Work Cumulative were both involved in significant *COX-2* and *ACAN* models. NZ stiffness ($\beta=-.699$) was important in explaining variation in *ADAMTS-5* expression. No predictors emerged from preliminary regression analysis as being important ($p<.20$) in explaining variation in *MMP-1* and *MMP-3* expression. Significant models are discussed below.

Table 27. Description of regression models for FC

FC						
Gene	F	N	Predictors	R	R ²	Adjusted R ²
MMP-1	no important ($p < .20$) predictors					
MMP-3	no important ($p < .20$) predictors					
ADAMTS-5	*5.578	18	2	.653	.427	.350
COX-2	**5.088	28	3	0.624	.389	.312
ACAN	*3.715	21	3	0.629	.396	.289

Table 28. Description of model predictors for FC

FC						
Gene	Predictor	B	SE(B)	β	Sig.	R
MMP-1	no important ($p < .20$) predictors					
MMP-3	no important ($p < .20$) predictors					
ADAMTS-5	aROM	.180	.129	.525	.123	*0.401
	NZk	-1.000	811.444	*-.699	.019	**-.570
COX-2	Work Cumulative	-.004	.001	*-.777	.002	*-.335
	MyRelax	-.001	.000	*-.733	.005	-.231
	aROM	.112	.055	*.597	.036	.096
ACAN	aROM	-.111	.033	*-2.29	.005	*-.454
	Work Cumulative	.001	.001	†1.907	.063	.056
	My Relax.	.024	.011	†1.909	.056	.132

*-Significant coefficients $p < .05$, **- $p < .01$; †-Coefficient trends $p < .1$

B-coefficient weight, SE(B)-standard error of B, β -standardized coefficient, Sig.-p-value of t-test, R-univariate correlation

8.3.7.1 ADAMTS-5

Results: Preliminary regression analysis identified aROM ($\beta = -1.495$, $p = .163$) and NZk ($\beta = -1.967$, $p = .073$) as important predictors of ADAMTS-5 expression in FC. Table 28 shows that, in simple regression, aROM is significantly positively correlated ($R = .401$, $p = .050$) and NZk is significantly

negatively correlated ($R=-.570, p=.007$) with *ADAMTS-5* expression. When entered in to the final regression model, a significant, large amount of variation is explained: $R^2=0.427, F(2, 18)=5.578$ ($p=.015$) (Table 27). Adjusted R^2 was 0.076 less than R^2 , indicating a predicted 7.6% reduction in explained variation in the population as a whole. NZk had a significant, moderate negative weight in the model ($\beta=-.699, p=.019$), indicating that specimens exhibiting higher neutral zone stiffness were linked to decreased *ADAMTS-5* expression in FC. aROM did not factor significantly in to the regression model.

$$ADAMTS5_{FC} = 1.572 - .180 * (aROM \text{ }^\circ) - 1.00 * (NZk \text{ Nm/}^\circ)$$

Interpretations: This model predicts a large amount of the variation (42.7%) in *ADAMTS-5* expression. *ADAMTS-5* expression decreased or did not change in FC in the sample data set: 0.60-1.01-fold change in relative expression. An increase of 55% of the mean NZk leads to an expected 22.6% decrease in *ADAMTS-5* expression, which represents over half of its range from the experimental data. The model indicates that increased stiffness of the NZ is correlated with reduced gene expression. It is possible that FSUs with higher NZ stiffness, whatever the cause, have less engagement of facet joints in extension because other, stiffer tissues take up more of the moment resistance [92, 419]. Reduced FC compression could plausibly lead to reduced *ADAMTS-5* expression [420, 421]. Another possible explanation for this relationship posits that age-related or degeneration-mediated changes in FSUs with stiffer neutral zones cause a diminished *ADAMTS-5* response [401, 422].

8.3.7.2 COX-2

Results: Three predictors entered the final regression model for *COX-2* expression in FC (Table 28). Work Cumulative, MyRelaxation, and aROM were all important predictors ($\beta, p<.20$) in preliminary regression analysis. The most important predictor, based on preliminary regression

coefficient significance, was Work Cumulative ($\beta=-.146, p=.007$) followed by MyRelaxation ($\beta=-.460, p=.013$) and aROM ($\beta=.504, p=.107$). In simple regressions (Table 28), Work Cumulative ($R^2= -.335, p=.041$) and MyRelaxation ($R^2=-.231, p=.119$) are negatively, moderately correlated with *COX-2* expression but aROM is weakly, positively correlated with the outcome ($R^2=.096, p=.313$). Combining these variables in multiple regression yielded a significant model that explained a large amount of variance in *COX-2* expression in FC, $R^2 = .389, F(3, 28) = 5.088, p=.007$. The results of the model were considered to be generalizable based on an Adjusted R^2 that was 0.076 less than R^2 . All coefficients in the model were significant, positive, of similar weights ($\beta=.597-.777$), and matched the sign of their simple relationships with *COX-2* expression.

$$COX2_{FC} = 5.145 + .112 * (aROM^\circ) - 7.4 \times 10^{-4} * (My\ Relax.\ %) - .004 * (Work\ Cum.J)$$

Interpretations: In FC, cumulative work, AT moment relaxation, and axial ROM were significantly associated with *COX-2* expression (averaged between right and left FC). Increases in axial ROM were associated with increases in *COX-2* expression, suggesting more asymmetric rotation of the FSU in F/E is linked to higher *COX-2* expression. Decompression and supra-normal compression of cartilage, reflecting changes in gapped and compressed facets with torsion, can both lead to pro-inflammatory changes in cartilage [342, 423]. In this model, an increase of 1.45° leads to a 98% increase in *COX-2* expression, which reflects a modest relationship between the predictor and output. Additionally, more AT moment relaxation was associated with elevated *COX-2* expression, indicating that FSUs which decreased more from their initial AT moment tended to have higher pro-inflammatory gene expression. Specifically, the model projects that FSUs which experienced 100% more relaxation would have 35.4% less *COX-2* expression; this effect is relatively small given the required magnitude of relaxation to see the effect. Also, specimens with less cumulative work tended to have higher *COX-2* expression. Holding other

predictors constant, an increase of 85 J (35% of mean Work Cumulative) is expected to reduce expression by 127.9%. The effect of aROM on the model agrees with theoretical expectations of increased compression and decompression causing *COX-2* up-regulation [342], but My Relaxation and Work Cumulative act on pro-inflammatory gene expression in a manner not anticipated.

8.3.7.3 ACAN

Results: Preliminary regression analysis yielded aROM, Work Cumulative, and My Relaxation as important predictors ($\beta = -.639, p=.024; \beta = .502, p=.126$, and $\beta = .373, p=.188$, respectively). Predictors aROM had a significant, moderate negative correlations with *ACAN* expression ($R = -.454, p=.019$), and Work Cumulative and My Relaxation had very small positive correlations with *ACAN* ($R = .056, p=.405$ and $R = .132, p=.285$, respectively). In multiple regression, the model explained nearly 40% of the variation in *ACAN* expression in FC (Table 27), $R^2 = .629, F(3,21) = 3.715, p=.032$. There was a modest loss of generalizability in this model described by a 0.107 decrease between R^2 and Adjusted R^2 . All predictors had large effects on *ACAN* expression ($\beta = 1.907-3.796$). After adjusting for the influence of Work Cumulative and My Relaxation, aROM factored significantly and largely in influencing model predictions of *ACAN* expression; increases of one standard deviation in aROM would reduce *ACAN* expression by 3.796 standard deviations ($p=.005$). The partial correlation effects of My Relaxation and Work Cumulative were not significant but were nearly so ($p=.056$ and $p=.063$, respectively).

$$ACAN_{FC} = 0.585 - .111 * (aROM^\circ) + 2.56 \times 10^{-4} * (My\ Relax.\ \%) + 1.1 \times 10^{-3} * (Work\ Cum.\ J)$$

Interpretations: The relationship that emerges from this model is a large, negative effect of axial torsion rotation angle on *ACAN* expression in FC. Fixing other factors, for a given increase in aROM of 0.73°, *ACAN* expression is expected to decrease by 49.8%. This model accounts for

39.6% of the variation in *ACAN* expression, and axial torsion properties have large weights in the model. Dramatic reduction of anabolic expression in FC (mean expression of both facets) with torsion suggests that altered FC mechanics in torsion dampen anabolic expression. In left-sided axial torsion, FC on the left side is gapped, and FC on the right side is compressed [85, 354]. The gapped FC experiences depressurization (i.e. loss of compression), the compressed side experiences increased compression [85], and both sides have altered shear loading during F/E [67]. De-compression, excessive compression, and elevated shear loading in chondrocytes can reduce anabolic expression [423, 424], confirming the relationship described by the regression model. In contrast, holding other factors constant, increased cumulative work or moment relaxation predicted increased *ACAN* expression. The large effect of cumulative work leading to increased compression agrees with expectations below damaging loading magnitudes or durations [9].

8.3.8 Nucleus Pulposus (NP)

No regression models were significant in relating mechanical factors to gene expression responses in NP (Table 29). Mechanical factors describing extension were important predictors from the preliminary regression analysis for *MMP-3*, *COX-2*, and *ACAN*. NP is the only tissue where extension properties emerged as important from the preliminary regression analysis while no models were significant in the final analysis. *ACAN* expression showed a trend of an individual predictor, MxeRelaxation ($p=.100$), significantly influencing a model (Table 30). This was the only incidence of extension moment relaxation (or an extension property at all) contributing to prediction of biological responses, albeit insignificant.

Table 29. Description of regression models for NP

NP						
<u>Gene</u>	<i>F</i>	<i>N</i>	<i>Predictor</i>	<i>R</i>	<i>R</i> ²	<i>Adjusted R</i> ²
<i>MMP-1</i>	no gene expression available					
<i>MMP-3</i>	.353	28	1	.116 ^a	.013	-.025
<i>ADAMTS-5</i>	no gene expression available					
<i>COX-2</i>	.442	23	2	0.206	.042	-.053
<i>ACAN</i>	1.085	15	3	0.478	.228	.018

*-Significant coefficients $p < .05$ †-Coefficient trends $p < .10$

Table 30. Description of model predictors for NP.

NP						
<u>Gene</u>	<u>Predictor</u>	B	SE(B)	β	Sig.	R²
<i>MMP-1</i>	no RGE available					
<i>MMP-3</i>	ROMe	.027	.046	.305	.558	.116
<i>ADAMTS-5</i>	no RGE available					
<i>COX-2</i>	Hysteresis Mean	.193	.255	.489	.446	.188
	ROMe	.013	.035	.217	.706	.116
<i>ACAN</i>	MxeRelax	.007	.004	†5.958	.100	.292
	NZk	4.634E+22	8.263E+15	6.173	.182	-.048
	ROMf	.054	.045	2.346	.258	.044

*-Significant coefficients $p < .05$; †-Coefficient trends $p < .10$

B-coefficient weight, *SE(B)*-standard error of *B*, *β*-standardized coefficient, *Sig.*-*p*-value of *t*-test, *R*-univariate correlation

8.3.8.1 ACAN

Results: MxeRelaxation, NZk, and ROMf were important predictors in the preliminary regression analysis with coefficient significance of $p=.118$, $p=.131$, and $p=.142$, respectively. MxeRelaxation showed a positive, weak but insignificant correlation with ACAN expression, while NZk and ROMf did not weakly or significantly correlate with ACAN expression (Table 30). In multiple regression, MxeRelaxation had a strong positive effect on predicted ACAN expression ($\beta=5.958$, $p=.100$). The other factors did not significantly impact the model. The model itself

predicted 47.8% of the variability in ACAN expression (Table 29), but it was not significant and not generalizable (Adjusted $R^2 = .018$).

$$ACAN_{NP} = -.665 + 6.95 \times 10^{-3} * (Mxe\ Relax.\ \%) + 4.6 \times 10^{-22} * \left(NZk \frac{Nm}{\circ} \right) + .054$$

$$* (ROMf\ \circ)$$

Interpretations: Because the model is not significant or generalizable, its impact is limited. A decrease in MxeRelaxation of 10.4% (less relaxation) leads to a 75.7% increase in ACAN expression. Given the size of relaxation and range of ACAN modulation in FSU loading, this is a large effect. The trend of reduced extension moment relaxation (or sustained extension moments across cycles of loading) with increased ACAN expression is a reasonable result. Extension moments are born to a large extent by NP [87, 88, 92]; sustained extension moments indicate higher average loading (less load dissipation) and less load dissipation, a process in which the NP plays a prominent role [418]. Higher pressurization in NP cells, within a window of physiologic pressure magnitudes, elicits increases in ACAN expression [98, 425]. So, increased ACAN expression with reduced load dissipation could represent an adaptive, anabolic response.

8.3.9 Ligamentum Flavum (LF)

Regression models were significant in *MMP-1*, *ADAMTS-5* and *COX-2* expression in LF (Table 31). In these models, a large amount of variation, $R=0.537-0.710$, reflecting 31.9-50.4% of the variation in biological responses, was explained by mechanical predictors. Significant predictors included NZk, ROMf, aROM, and MyRelaxation. NZk was a large, significant predictor in each significant model. LF was the only tissue in which ROMf was a significant predictor. Significant models are discussed below. *MMP-3* and *ACAN* expression in LF were not predicted by regression model factors.

Table 31. Description of regression models for LF

LF						
Gene	<i>F</i>	N	Predictors	<i>R</i>	<i>R</i> ²	Adjusted <i>R</i> ²
<i>MMP-1</i>	**4.900	29	3	0.609	.370	.295
<i>MMP-3</i>	.856	29	1	.175 ^a	.031	-.005
<i>ADAMTS-5</i>	*4.052	30	3	.564	.319	.240
<i>COX-2</i>	**5.848	28	4	0.71	.504	.418
<i>ACAN</i>	2.377	29	1	0.284	.081	.047

*-Significant coefficients $p < .05$ †-Coefficient trends $p < .10$

Table 32. Description of model predictors for LF

LF						
Gene	Predictor	B	SE(B)	β	Sig.	R
<i>MMP-1</i>	NZk	2.20E+06	754.256	* 1.961	.037	†.296
	Work Cumulative	.002	.001	†1.171	.074	**497
	ROMf	.041	.025	1.273	.123	.178
<i>MMP-3</i>	ROMf	.026	.028	.497	.363	.175
<i>ADAMTS-5</i>	NZk	6.57E+10	1671.209	* 4.024	.011	*.357
	ROMf	.000	.000	1.763	.038	.149
	MyRelax	.058	.026	.972	.190	.056
<i>COX-2</i>	aROM	-.186	.072	* -.643	.007	**458
	NZk	3.89E+14	1.389E+4	* 5.083	.002	.142
	MyRelax	.001	.000	* 1.532	.035	.112
	ROMf	.090	.030	* 2.605	.008	†.256
<i>ACAN</i>	NZk	-1.00	282.674	-.481	.135	†-.284

Significant coefficients $p < .05$ †-Coefficient trends $p < .10$

B-coefficient weight, SE(B)-standard error of B, β -standardized coefficient, Sig.-p-value of t-test, R-univariate correlation

8.3.9.1 MMP-1

Results: Preliminary regression analysis identified NZk ($\beta=.967$, $p=.023$), Work Cumulative ($\beta=.390$, $p=.069$), and ROMf ($\beta=.473$, $p=.071$) as important predictors of *MMP-1* expression in LF. Table 32 shows that Work Cumulative is significantly, largely, and positively correlated with *MMP-1* ($R=.497$, $p=.003$). NZk and ROMf are moderately positively correlated ($R=-.296$, $p=.060$ and $R=.178$, $p=.178$, respectively). In multiple regression, only NZk was significant as a predictor of *MMP-1* ($\beta=.471$, $p=.037$), but Work Cumulative was close to significance ($\beta=.337$, $p=.074$). Both predictors had positive weights in the model, indicating that increases in neutral zone stiffness and cumulative work related to expected increases in *MMP-1*

expression. The size of the weights was modest, but the model was able to account for 37.0% of the variation in *MMP-1* expression in LF, $R^2 = .370$, $F(3, 29) = 4.900$, $p = .008$. Adjusted R^2 was 0.076 less than R^2 , indicating good generalizability to the population as a whole.

$$MMP1_{LF} = -0.409 + 2.2 \times 10^6 * \left(NZk \frac{Nm}{\circ} \right) + 1.8 \times 10^{-3} * (Work\ Cum.\ J) + .041 \\ * (ROMf \circ)$$

Interpretations: As NZk increases in LF, *MMP-1* expression increases moderately ($\beta = 0.471$). A 55% increase in NZk elicits from the model a 44.2% increase in *MMP-1* expression. Given the small responses in *MMP-1* in LF to F/E and the small variation in NZk, this effect is modest. The influence of Work Cumulative is even smaller, but it also has a positive weight in the model. Within these small changes, NZk, and to a lesser extent, Work Cumulative, explain over a third of the variability in *MMP-1* expression. This model suggests that additional tensile loading—reflected in energy imparted to the LF in flexion or in higher tensile forces in stiffer FSUs—leads to projected higher expression of *MMP-1* in these tissues. Studies examining ligament fibroblasts have identified variable sensitivity of *MMP-1* to tensile loading [426, 427], but *MMP-1* mediated remodeling in response to tensile loading has been observed in ligaments *in vivo* [428]. In the context of these previous findings, the relationship of Work Cumulative and NZk to *MMP-1* expression in LF is tenable and enlightening.

8.3.9.2 ADAMTS-5

Results: NZk ($\beta = .695$, $p = .061$), ROMf ($\beta = .335$, $p = .178$), and My Relaxation ($\beta = .310$, $p = .119$) were important predictors following preliminary regression analysis (Table 32). Each predictor was weakly to moderately positively correlated to ADAMTS-5 expression in simple correlation, though only NZk showed a significant correlation ($p = .027$). In multiple regression,

NZk was a strong, significant predictor of ADAMTS-5 expression ($\beta=4.024$, $p=.002$), and ROMf was less so but also significant ($\beta=1.763$, $p=.038$). My Relaxation was not significant ($\beta=.972$, $p=.093$). Both significant predictors had positive weights in the model, indicating that increases in neutral zone stiffness and flexion angle led to expected increases in ADAMTS-5 expression in LF. The size of the weights was moderate and the model was able to account for 31.9% of the variation in ADAMTS-5 expression in LF, $R^2 = .319$, $F(3, 30) = 4.502$, $p=.017$ (Table 31). Adjusted R^2 was 0.079 less than R^2 , indicating a predicted 7.9% reduction in explained variation in the population as a whole. This suggests a small loss in generalizability in this model.

$$ADAMTS_{LF} = -.380 + 6.5 \times 10^{10} * \left(NZk \frac{Nm}{\circ} \right) + 3.5 \times 10^{-3} * (My Relax. \%) + 0.058$$

$$* (ROMf \circ)$$

Interpretations: This model significantly relates NZk and ROMf to changes in ADAMTS-5 expression, and in so doing accounts for a modest amount of variation in ADAMTS-5 changes with F/E. Increases of NZk by ~55% of the mean or increases of ROMf angle by 3.77° lead to 61.4 or 40.4% increases in ADAMTS-5 expression, respectively. A strong, positive relationship between NZk and ADAMTS-5 expression was evident, which is expected. Higher magnitudes of loading in LF have been shown to provoke inflammation [161] and proteoglycan metabolism dysregulation in ligamentous tissue [363]. The LF, which plays a prominent mechanical role throughout the NZ and in flexile moment resistance [86, 87], could be stiffer in stiffer FSUs. In this case, LF tissues would likely experience higher forces in stiffer FSUs and in those with greater amounts of flexion. So, an association between stiffer NZk and greater ROMf with higher ADAMTS-5 expression is reasonable. Alternatively, if other tissues like the NP are

responsible for stiffer NZk, then it is likely that LF tissue would be stress-shielded and experience reduced loading. Reduced loading could provoke catabolic expression as a part of adaptive, structural remodeling [9].

8.3.9.3 COX-2

Results: Four predictors entered the final regression model for COX-2 expression in LF (Table 32); MyRelaxation, aROM, NZk, and ROMf were all important predictors ($\beta > 0.3$, $p < .20$) in preliminary regression analysis, with the most importance for aROM ($p = .014$) and the least importance for MyRelaxation ($p = .073$). In simple regressions (Table 32), all variables had positive correlations with COX-2 expression, but only aROM had a large, significant correlation ($R = .458$, $p = .007$). Combining these variables in multiple regression yielded a significant model that explained the largest variance in biological outputs for LF, $R^2 = .504$, $F(4, 28) = 5.848$, $p = .002$ (Table 31). Adjusted R^2 was 0.086 less than R^2 , indicating a predicted 8.6% reduction in explained variation in the population as a whole. This suggests a small loss in generalizability in this model, probably reflected in a relatively high predictor-to-sample size ratio. NZk had the largest weight in the model, and MyRelaxation had the least influence on the outcome.

$$COX2_{LF} = -.592 + .186 * (aROM \text{ }^\circ) + 3.9 \times 10^{14} * \left(NZk \frac{Nm}{\text{ }^\circ} \right) + 1.0 \times 10^{-3} * (My \text{ Relax. } \%) \\ + 0.089 * (ROMf \text{ }^\circ)$$

Interpretations: The individual contribution of each predictor was small to moderate; modest changes in predictors separately effected 104.2 – 185.7% increases in COX-2. Added together, however, they accounted for a majority of COX-2 expression changes in LF. This is the only model in all tissues and genes to account for a majority of the biological variation in a gene. Results of Section 7.3 corroborate this expectation in rabbit lumbar FSUs. Increases in each of

these parameters point to elevated tensile loading in LF. Increased axial ROM putatively increases tensile loading in the contralateral portion of the LF during asymmetric motions [93] although regional assessment of gene expression was not performed. Increased NZ stiffness suggests greater tensile loading of LFs during each cycle of loading [87]. Higher flexion ROM is indicative of greater LF involvement in moment resistance [86, 87]. Less relaxation of AT moments suggests a maintaining of higher loading in the LF [93]. As each of these parameters putatively increased loading in LF, COX-2 expression increased.

8.3.10 Comparisons Across Tissues

As noted, significant LF and FC models had higher R values (0.564-0.710) than AF models (0.368-0.569). In particular, the *COX-2* response in LF was best predicted by mechanical factors; just over half of its variability (50.4%) can be attributed to mechanical factors. *MMP-1* in LF, *COX-2* in FC, *ACAN* in FC, and *ADAMTS-5* in FC were also well described by regression models; 37.1%, 39.0%, 39.6%, and 42.6% of the variation in responses, respectively, was accounted for in these analyses. NP did not have significant regression models, and this agrees with mechanical studies showing small changes in NP pressurization with bending and torsion [411]. This also likely reflects the absence of axial compression applied to rabbit FSUs.

The ability of mechanics to predict changes in expression of particular genes also varied across tissues. *ADAMTS-5* expression was consistently well-described in regression models across tissues (3 of a possible 3 tissues had models $p < .10$). Variation in *MMP-1* (2 of 3), *COX-2* (2 of 4), and *ACAN* (2 of 4) was significantly accounted for models in two tissues each. Models explaining *MMP-3* expression were only significant in one tissue (1 of 4), and its effect ($R < .368$) was considerably smaller than other genes. Intriguingly, variability in *ADAMTS-5* expression,

which was relatively small, was consistently accounted for by mechanical factors in all tissues, but variability in *MMP-3* expression, which was much larger, was poorly accounted for by mechanical factors across tissues. The other genes demonstrated a moderate amount of tissue-specificity in their relation to mechanical predictors.

Mechanical predictors also showed noteworthy patterns across tissues. In LF, NZk and ROMf were important predictors in the preliminary regression analysis in 4 of 5 and 3 of 5 genes, respectively (see Table 22). In final regression analysis, NZk was a significant predictor for each significant model in LF (3 of 3) and ROMf was significant in 2 of 3 models (Table 24). In FC, aROM emerged from preliminary analysis as an important predictor in 3 of 5 genes (Table 22), and it remained salient as a significant predictor in significant models in FC (2 of 3) (Table 24). Interestingly, NZk was also a significant factor in all *ADAMTS-5* models across tissues (Table 24). NZk demonstrated specificity as a significant predictor in AF and FC for *ADAMTS-5* only. Work Cumulative was a significant predictor in both significant models for *MMP-1* expression, and AT moment-rotation predictors were significant in both significant models for *COX-2* expression and multiple models in AF and FC. Predictors in *ACAN* across tissues were consistently related to relaxation properties.

8.4 DISCUSSION

Linear multiple regression showed that mechanical predictors accounted for moderate to large amounts of variation ($R=0.4-0.6$ being moderate, $R>0.6$ being large) in relative gene expression for pro-inflammatory, catabolic, and anabolic markers in viable spinal segments loaded *ex vivo* in flexion/extension (F/E) and combined F/E with axial torsion (AT). Models explained up to 50.4%

of the variability in outcomes, which, given the wide age range in rabbits used in this study, the inclusion of males and females, and the short duration and mild nature of the mechanical intervention, is quite remarkable. The first goal of the study was to identify the most important mechanical parameters and use them to drive regression analysis. The second aim was to develop models that explain variation in gene expression with mechanical predictors and compare the ability of mechanical parameters to predict biological responses across tissues and genes. A corollary of the second aim was to identify those predictors that best describe biological responses to obtain insight in to what mechanical factors truly associate with biological changes. The major findings of the analysis highlighted that mechanical predictors had a greater influence on biological response in FC and LF than AF and NP. Regression also uncovered important mechanical predictors—F/E NZk, AT properties, and cumulative work—as important variables in predicting biological responses across tissues.

Identifying differences between tissues based on the ability of mechanical predictors to account for variation in biological responses describes differential mechanosensitivity among FSU tissues subjected to the same applied loading. In pure moment F/E and AT + F/E, FC and LF show greater effects of mechanical loading on biological responses than AF and NP. This finding underscores the importance of examining spinal tissues beyond the disc, particularly in rotational loading. Considering the demonstrated mechanosensitivity of disc tissues to compression parameters [22], the observed differential mechanosensitivity in F/E and AT+F/E points to (i) how spinal movements in different DOF differentially load tissues in spinal segments (seen in Chapter 7.0) and (ii) how biological responses depend on the DOF of loading. Comparing the mechanosensitivity of disc tissues in this study shows that the AF is more responsive to rotational loading than the NP. This result agrees with previous studies that have shown the AF to experience

large changes in stress in F/E and AT, particularly in the posterior region [80, 429, 430]. Compressive stress or intradiscal pressure in the NP can change dramatically in flexion [431] as well, and to lesser extent in extension and AT [83, 432], but disc puncture (which included AF damage in addition to NP depressurization), showed only small effects of NP pressurization in F/E. Changes in stress in the AF may be larger [430] and, more importantly, lack of applied axial compression reduces NP pressure [374], which likely alters NP mechanosensitivity and limits translation of these results.

Different genes exhibit different amounts sensitivity to mechanical loading. While mechanical loading can modulate cell metabolism and regulate genes non-specifically, ample evidence points to gene, tissue, and loading parameter specificity in mechanoregulation [22, 30]. In this analysis, sensitivity of specific gene expression to mechanical predictors, measured by model significance (Table 23), was not specific to gene categories: pro-inflammatory, catabolic, and anabolic. However, considering only significant regression models, *COX-2* expression demonstrated the highest dependence on mechanical predictors. Mechanics has proven to influence *COX-2* expression specifically in chondrocytes and LF fibroblasts [161, 433]. The largest differences in genes were between *ADAMTS-5*, explained by regression models in 3-of-3 tissues, and *MMP-3*, explained by regression models in only one tissue. This finding sheds new light on the role of *ADAMTS-5* in spinal tissues, which is largely under-studied in mechanobiology [30]. It also suggests an on/off regulation of *MMP-3*, which was up-regulated by loading in all tissues but not, apparently, modulated by mechanical variation. This kind of response in *MMP-3* is not evident in disc compression studies [204, 257]. On the whole, mechanical regulation of gene expression was specific to combinations of individual genes and tissues.

This study identified the most important mechanical parameters among the set of candidate predictors and assessed their contribution to significant models of gene expression. The primary results of PCA cleanly reflect theoretical expectations. PCA identified ROM_f and ROM_e as parameters correlated with the first two principal components; this intuitive result confirms the simple expectation that, in tissues subject to applied, repeated flexion/extension, mechanical parameters describing flexion and extension should matter most. Cumulative work reflects both F/E moments and movements, so its eminence in the data set is also reasonable if less obvious. Interestingly, biological responses were not consistently or strongly related to flexion or extension ROM in multiple regression but were consistently and strongly related to cumulative work, particularly in MMP-1 expression. It appears then that applied energy better accounts for biological changes in response to loading than changes in response to motion amplitudes. PCA also uncovered the importance of neutral zone stiffness among mechanical factors. Neutral zone stiffness influences the amount of loads experienced in tissues throughout the majority of motion paths. Stiff tissues increase loads experienced in that tissue and alter loads experienced in other tissues of the FSU. It is possible that this variation in loads experienced by tissues throughout the bulk of cyclic loading underlies the reason for the consistent importance of NZ_k in significant regression models. PCA revealed the secondary importance of relaxation of parameters and axial torsion properties in the data set. While less important to variation in the mechanical predictors than flexion and extension ROM, axial torsion responses much more consistently related to biological outcomes. Small amounts of axial rotation, which reflect asymmetries, have a strong influence on biological outcomes. This result echoes findings from Specific Aim 2. Thus, movements in flexion and extension account

for large amounts of variation in mechanical data, but these amplitudes of movement are not strong predictors of biological change. Rather, cumulative work, neutral zone stiffness, and axial rotation account for much of the biological variation.

Translating these mechanical predictors to other loading modes requires mechanical parameters that are insensitive to DOF. A goal of this regression model was to identify mechanical response parameters that could be generalized to other loading modes and serve as a basis for comparison across these modes. Energetic properties—work and hysteresis—represent energy applied to or dissipated from spinal segments, which does not depend on DOF. In this study, cumulative work and mean hysteresis per cycle emerged from preliminary analysis as important predictors, but their influence in biological outcomes was limited. Cumulative work was more important than mean hysteresis as a model predictor (mean hysteresis was not a significant predictor in any model), though it was not broadly significant across tissues or genes. Thus, an attempt to broadly explain biological variation in response to applied loading through energetic properties is not supported by these data. Instead, cumulative work proves to be instructive in explaining biological responses in *MMP-1* expression in AF and LF where positive relationships between Work Cumulative and gene expression is illuminating [204, 427, 428].

Similarly, it was hypothesized that change in mechanical parameters (e.g. moments) across cycles would vary with samples and serve as predictors that could translate across DOF. This phenomenon of load relaxation reflects a certain adaptation to loading by FSUs wherein, by means of tissue composition and interaction of multiple tissues, constantly applied movements are supported by reduced tissue loading. This adaptation is generally thought to be advantageous, potentially lowering risk of injury [403, 434] and attenuating mechanical stimuli [112, 382, 435]. Relaxation parameters influenced aggrecan metabolism (*ADAMTS-5* and/or *ACAN* expression) in

disc tissue and pro-inflammatory signaling in FC and LF; relaxation parameters were significant in 2 of 5 AF (*ADAMTS-5*, *ACAN*), 2 of 5 FC (*COX-2*, *ACAN*), 1 of 3 NP (*ACAN*), and 1 of 5 LF (*COX-2*) models. Load dissipation is governed principally by NP hydration and NP-AF interactions [410, 411]. Thus, it is reasonable that in these tissues moment relaxation relates to aggrecan metabolism, which directly influences tissue hydration and time-dependent changes in tissue pressurization [436]. The influence of time-dependent changes in loading in FC and LF on pro-inflammatory changes is more obscure; however, a possible interpretation is that the ability to adapt to repeated loading could mollify or exacerbate pro-inflammatory changes in these tissues [403, 434]. In general, relaxation parameters were consistently but not strongly associated with biological changes, limiting their utility.

Translating these results to clinical application is appealing, but additional testing and an expanded framework are required prior to doing so. The limitations of species, simplified loading modes, lack of physiologic compression, and lack of systemic factors certainly prevent immediate translation to humans. Even acknowledging those limitations, much of the variation in gene expression remains unexplained, so model predictions are fairly inaccurate. Furthermore, relative gene expression describes initial molecular responses within cells; numerous levels of regulation occur between transcription and functional protein activity that can modify the ultimate biological response. The scope of testing must also be expanded and more complex models introduced to discover and describe the likely non-linear relationship between most mechanical parameters and biological responses [437]. Clinically, routine measurement of the most useful mechanical predictors, like neutral zone stiffness and axial torsion, is impractical if not impossible. Nevertheless, the relationships identified between mechanical predictors and

biological responses takes an initial step toward quantifying the effects of multi-dimensional loading on spinal tissues to quantitatively assist recommendations for injury prevention and rehabilitation exercises.

Multiple regression is subject to a number of limitations. The order of predictor entry will always influence regression results in datasets where multicollinearity exists to any extent. However, evidence for a strong effect of order does not exist. The type of predictors that were significant for each tissue did not reflect the assumed order in the hierarchical entry. Multiple regression is also not used to test hypotheses or identify causal relationships; instead, it predicts associations between multiple variables that can be used to understand variations within data, cautiously extrapolate to larger populations, and motivate experimental testing.

8.4.1 Conclusions

The primary motivation for performing multiple regression was to investigate whether mechanical responses can predict biological responses and how this predictive capacity varied across tissues and genes. In a general sense, as in Specific Aims 1 and 2, experiments are designed based on applied mechanics. Samples are grouped based on applied mechanics, and changes in biological responses are assessed based on these groups. Different samples may have different mechanical properties, related to tissue damage, age-related changes, or inadvertent pre-loading, and so respond differently to the same applied mechanics. Understanding the link between mechanical responses and biological responses provides insight in to how tissue responses (related to function or properties instead of group), affects cellular and molecular behavior. While a majority of the variation in biological responses remains unexplained by mechanical predictors, multiple regression did uncover a number of important relationships: (1) neutral zone stiffness (NZk) and

LF catabolism and inflammation, (2) neutral zone stiffness and aggrecan metabolism (*ADAMTS-5*) in all spinal tissues, (3) axial torsion and anabolism in FC, and (4) cumulative work and *MMP-1* expression in LF and AF. Given (i) the small amount of variability (<30%) in disc degeneration that mechanics is thought to account for *in vivo* [438] and (ii) the use of macroscopic mechanical parameters rather than cellular level parameters to describe cell-based biological changes, the amount of variation explained by mechanical factors is remarkable if not surprising.

9.0 DISCUSSION

9.1 SUMMARY

This work has provided the field of spine and orthopaedic research with a novel experimental platform for simultaneous biological assessment of multiple spinal tissues in intact spinal segments subjected to 6 DOF loading. Previous systems have examined axial compression and axial torsion only, so the investigation of pure flexion/extension and combined rotations—flexion/extension with axial torsion—represents an important advancement in mechanobiology of the disc and spine. Moreover, the preservation of osteoligamentous FSUs with intact endplates and posterior structures ensures *in-situ* load transmission in the disc that has not been achieved previously. Most importantly, retention of facet joints and posterior ligaments enables simultaneous biological assessment of facet cartilage and ligamentum flavum, tissues that are implicated in degenerative spinal disorders, along with intervertebral disc. Mechanical loading of intact FSUs in 6 DOF accompanied by evaluation of mechanical and biological responses in multiple tissues opens frontiers in studying tissue interactions and novel simulations of physiologic and injurious loading.

This study demonstrated the feasibility of attaching the bioreactor system previously developed for axial testing to a robotic testing system capable of 6 DOF loading. The control and precision of the robotic testing system were sufficient in the context of the loads and displacements involved in rotational loading of rabbit FSUs. Rigid fixation of FSUs in the bioreactor fixtures was demonstrated in flexion/extension and axial torsion. Because epoxy fixation, the conventional fixation means used for orthopaedic joint mechanics, is exothermic and inhibits metabolic exchange between media and tissue, it could not be used. Consequently, an alternative fixation

method that relied on 16 rubber-capped screws for fixation was implemented, which limited damage to spinal tissues during mechanical testing. Rotational movements in these DOF were also unrestricted by bioreactor components. Methods were developed for fixture attachment to the robot and measurement and placement of the center-of-rotation (COR). Enclosing FSUs in media-filled dialysis membranes, which passively concentrates proteins (>2 kDa) in small volumes of conditioned media, did not prevent rigid fixation or contribute to measured moments. Integration of the bioreactor system with the robot testing system permitted repeatable mechanical testing of rabbit FSUs in rotational DOF.

Load-based testing protocols were developed for flexion/extension in rabbit spines to reasonably approximate *in vivo* segmental motions relevant to human spinal motions. While rabbits and humans are anatomically quite similar in the lumbar spine, the non-linear stiffness of moment-rotation responses in flexion/extension showed notable differences. Because motion in activities of daily living and spine-intensive activities in humans apparently occur in low and high stiffness regions of spinal loading, respectively, moment targets in rabbits were chosen relative to the transition from low-stiffness to high-stiffness regions. Moment targets at or below the transition point represented human spinal motions in many daily activities, and moment targets in the high-stiffness region represented occupational, recreational, or rehabilitative activities with large spinal motions. Selecting torsion magnitudes in rabbits to simulate coupled axial torsion in humans was simpler because moment-rotation curves are linear for both species. Moment targets were based on the same percentage of failure moments. A loading rate of 0.33°/s was applied during cycling, similar to other robotic systems [87, 276], and a one hour duration of loading was chosen to be representative of a rehabilitation exercise routine or an occupation task [295, 296].

Biological changes in neutral flexion/extension were generally catabolic and relatively modest. Significant changes in catabolic and pro-inflammatory gene expression with loading were between 2 and 3.5-fold increases. Only AF (*MMP-3* and *ACAN*) and FC (*MMP-1*, *-3*, and *COX-2*) showed significant effects of loading, although catabolic and pro-inflammatory gene expression in LF evidenced trends of up-regulation with loading. Immunoblotting for aggrecan fragment yielded variable results, but comparing means showed generally higher fragment abundance in loaded tissue. Because gene expression was not uniformly up-regulated, it is unlikely that changes are due to a general uptick in metabolic activity; instead, these changes may be part of an adaptive remodeling response to loading [9]. Differences in individual groups or resulting from loading parameters—ROM or cycle number—were few. ROM had a significant effect only on MMP-cleaved aggrecan fragments in AF, and cycle number showed a trend toward elevated *MMP-3* and *COX-2* gene expression in LF. Based on the biological outcomes measured in this study, variations of ROM magnitude and cycle number within physiologic bounds for short durations at low loading rates showed negligible to small effects. Thus, small and large ROM, simulations of ADLs and spine-intensive activities, did not show expected differences. It may be that healthy spines respond similarly to a range of amplitudes within a broad envelope of physiologic motion. Injured or degenerating spines might show greater sensitivity to ROM. It is also likely that longer durations, higher magnitudes of loading or loading rate, or more sensitive biological outcomes are required to observe significant effects of F/E parameters in healthy spines. In any case, F/E loading compared to unloaded static conditions tended to modestly up-regulate catabolic expression. Coupling torsion to flexion/extension simulated (i) segmental axial asymmetries treated clinically by manual and motion-based therapies or (ii) combined loading associated with potentially damaging activities.

In this model of asymmetric loading, FSUs with small and large magnitudes of coupled torsion showed elevated pro-inflammatory responses to loading in all spinal tissues. Pro-catabolic changes were also evident in AF and LF with the large magnitude of torsion. Previous studies indicated that coupled torsion with F/E elevates facet forces in the compressed facet [91] (supported by mechanical data in Section 7.3), alters regional loading in the compressed facet [91], and removes compression in cartilage in the gapped facet [91, 354]. Intriguingly, while pro-inflammatory and pro-catabolic expression was elevated in both facets, pro-inflammatory changes were higher in gapped facets and did not show sensitivity to magnitude of torsion. In contrast, chondroadherin was depleted in compressed facets and decreased with increased magnitudes of torsion. These results demonstrate the detrimental effect of asymmetric movements in all spinal tissues. Clinically, they suggest that segmental asymmetries, whatever their origin, and occupational tasks involving sustained twisting with bending, negatively influence both ipsi- and contralateral facets. In general, these findings point to a strong role for altered mechanics associated with axial asymmetries in driving pro-inflammatory, catabolic processes in spinal tissues that may contribute to the onset and progression of tissue damage and degeneration associated with complex loading.

Serial resection of FSU structures combined with (i) replayed intact kinematics and (ii) measured changes in primary moments with each cut addressed the question of how spinal structures in rabbit FSUs contributed to neutral F/E and combined AT + F/E moment resistance. In neutral F/E, the salience of the LF in flexion resistance was confirmed. In extension, rabbit lumbar facets were found to play a minor role in extension moment resistance, similar to human lumbar facets. The disc played a relatively small role in flexion and a relatively large role in extension resistance. The addition of torsion to F/E greatly increased the contribution of facets to

extension resistance and increased the changes in forces associated with facets (mean of both sides). Coupled torsion reduced the contribution of the disc to extension and increased its contribution in flexion. It also modestly elevated forces associated with the LF in flexion. These findings furnish initial direct evidence of the effect of combined loading on force/moment distribution in lumbar FSUs. The prominence of each of the structures in supporting F/E moments supports biological analysis of each of these spinal tissues. Structures that contributed most in flexion and extension, the LF and FC (particularly in AT+F/E), respectively, were most biologically responsive. While it is tempting to generalize that the tissues most mechanically loaded in a particular loading mode are most biologically responsive, different tissues may have different thresholds for various biological responses. Nonetheless, because tissues with a larger contribution to loading correlated with higher mechanosensitivity in this study, the results of this dissertation suggest that greater mechanical involvement in a particular DOF elicits a greater response. These results reinforce the need to quantify mechanical contributions of tissues in musculoskeletal systems in conjunction with biological assessments. They also confirm the importance of evaluating biological responses in non-disc tissues that play primary roles in mechanical support of F/E and AT.

Multiple regression analysis uncovered relationships between mechanical predictors and biological responses that varied based on tissue and gene. Mechanical predictors accounted for more variation in gene expression in FC and LF than AF and NP, highlighting the overall importance of non-disc tissue—FC and LF—in rotational loading. Lack of significant mechanical models in NP likely results from lack of axial compression in these studies. Regression models most consistently and significantly predicted *ADAMTS-5* expression across tissues and most infrequently and poorly predicted *MMP-3* expression. It is clear that the same applied loading to

FSUs regulated biological processes in separate spinal tissues differently, and that the biological markers measured in this study were more sensitive to flexion/extension loading in non-disc tissue. Principal component analysis confirmed the primary importance of flexion and extension ROM and revealed the importance of cumulative work, neutral zone stiffness, moment relaxation, and axial torsion properties in accounting for most of the variation in mechanical responses. Some patterns emerged between individual predictors and tissues or genes: neutral zone stiffness was a significant predictor of *ADAMTS-5* (across tissues) and LF gene expression (across genes); axial torsion properties were significant in *COX-2* (across tissues) and FC and AF gene expression (across genes); cumulative work was significant for *MMP-1* expression, and flexion ROM was significant in LF gene expression. Interestingly, among the mechanical predictors that accounted for the most variation in mechanical responses, including flexion and extension ROM and cumulative work, neutral zone stiffness most consistently accounted for variation in biological responses. Variation in neutral zone stiffness, which was not correlated with age, may reflect altered distribution of loading in FSUs and within specific spinal tissues, like the LF, that underlies its predictive capacity. In general, mechanical predictors accounted for a moderate-to-large amount of variation in biological responses confirming the importance of mechanical regulation of biological responses.

9.2 LIMITATIONS

The testing and experimentation performed in this project has a number of limitations. First, the motion rates of kinematic replay, while dynamic, are slower than *in vivo* motions, and loading rate may influence biological responses in spinal tissues [265, 439]. This limitation could be overcome

by altered robotic control methods that allow for continuous dynamic movements [440]. Second, lack of axial compression in flexion/extension and axial torsion, while permitting mechanistic insight in to the isolated role of these rotations, fails to recapitulate *in vivo* loading. Lack of compression likely influences mechanobiology in NP primarily [410] and FC secondarily [67]. This limitation could be addressed by adding axial compression to the bioreactor using the current robotic control scheme. In that case, control FSUs would require axial compression as well.

Other limitations are more difficult to overcome without significant development. The current fixation system for securing FSUs within the bioreactor was not rigid in AP translation. This lack of rigidity was magnified by a small ROM with poor resolution in that DOF, which made experimental testing unachievable with this system. Overcoming these limitations would require a more rigid fixation scheme and a different robotic testing system capable of higher precision and resolution. Additionally, the duration of studies involving intact FSUs is limited by decrease in viability in disc tissue after 24 hours [441]. While the insertion of tunnels through vertebral bodies to promote metabolic exchange in disc tissue seems to be reasonable *prima facie*, preliminary testing did not show improvement in NP cell viability [441]. Thus, in the current model with short durations (<24 hours) of loading, only acute biological responses to mechanical loading can be detected. This prevents the assessment of spinal tissues exposed to prolonged loading or evaluation of most regenerative therapies, but it does provide a wide range of valuable biological data about the response to initial bouts of simulated activity, exercise, or injury in the form of mRNA expression, protein translocation, matrix fragmentation, cell metabolism, and cell viability. Longer experimental durations may likely be achieved (i) by pre-mortem heparinization of animals or, in a less likely solution, (ii) by increased removal of cancellous bone with careful endplate thinning achieved through vertebral bodies.

As is the case in every biological study, the outcomes chosen represent only a small portion of the broad gamut of potential biological markers. Additional outcomes could broaden the understanding of how *in-situ* loading influences spinal tissue. In particular, studying the effects of loading on cell metabolism, fate, and viability would be instructive [66, 165, 250]. The outcomes selected in this study were relevant to features of degenerative disorders but were not chosen based on common cell signaling pathways. Cell signaling pathways including ERK, Akt [442], MAPK [228] and NFkB (unpublished data from our lab) have been implicated in mechanical loading and could be assessed in spinal tissues to provide more mechanistic insights in to the effects of loading on biological responses.

Aggrecan fragment analysis showed a high degree of variability that rendered it somewhat insensitive to the mechanical loading applied in this study. Initial evidence for aggrecan fragment changes with mechanical loading occurred following long-term (8 week) compression. One week of asymmetric compression in organ culture altered aggrecan fragments in the annulus fibrosus [37]. This study is the first to measure aggrecan fragments after mechanical loading in timeframes less than several days. Moreover, the G1 primary antibody was raised in rabbits and applied to rabbit tissue, generated significant background signal. MMP-cleaved bands were generally distinct from background and consistent between samples, but ADAMTS-cleaved bands were less distinguishable and more variable between samples. No differences with loading or between groups were evident in ADAMTS-cleaved bands, though they did show trends of decreased abundance in FSUs subjected to coupled torsion. MMP-cleaved fragments were significantly different in AF between small and large ROM, but changes with loading were generally small. Longer durations of culture, more severe forms of loading, or alternative animal models are likely required to detect consistent differences in aggrecan fragments.

The serial resection study showed unexpected results in extension that likely reflect incomplete loading in extension. The extension moments in three of four FSUs did not go beyond the transition point from low stiffness to high stiffness. This incomplete loading which leaves FSUs in the neutral zone likely explains the increase in extension moment with LF resection. Loading in the neutral zone is more variable than that in the linear elastic zone. The consequence is inaccurate characterization of the role of structures at full amplitudes of neutral extension. The addition of axial torsion caused the same FSUs to enter the linear region, and so changes in extension moments were consistent and agreed with theoretical expectations. However, this characterization reflects loading used in this dissertation research. Moreover, the mechanical differences between neutral F/E and AT+F/E remain relevant to how the mechanical environment changed between the two types of loading and contributed to different biological responses.

Regression models uncovered patterns and relationships in biological and mechanical variables, but their predictive capacity is limited and untested. Despite the prevalence of significant models explaining biological variation based on mechanical predictors, large amounts of variation in biological responses remain unexplained. This limits the accuracy of the model. Additional testing samples were not performed at intermediate amounts of mechanical loading to confirm predictive models, although this could be done in the future. Finally, for some regression models, the relatively small number of samples used to generate the models relative to the number of predictors limited its generalizability as reflected in the Adjusted R^2 value.

9.3 BROADER IMPACTS & FUTURE DIRECTIONS

The novel experimental system developed and tested in this dissertation has the potential to impact basic and applied research in spine and orthopaedic studies. Immediate extensions of this work include investigations of additional spinal tissues and analysis of conditioned media. The cartilage endplate (CEP) plays an important role in compressive loading of the disc, and CEP defects and degenerative changes have been associated with disc degeneration and symptoms of back pain [146, 147]. Isolation of CEP from rabbit FSUs has been demonstrated by the author [443], and CEP from all FSUs in loaded in Specific Aims 1 and 2 have been collected and stored at -80°C. The role of other ligamentous structures could also be investigated. The facet capsule is a richly innervated structure with mechanoreceptors and nociceptive neurons [67] that plays an important role in restricting flexion in rabbit FSUs (~30%, Table 17) and contributes to bending and torsion as well [87, 373]. While its degenerative pathology is distinct from the other spinal tissues and would require alternative outcomes for assessment [67], its response to *ex vivo* mechanical loading in intact FSUs is relevant in short-term loading [67, 444, 445] and remains unstudied. Finally, supraspinous ligaments, though not mechanically important under the applied loading in this dissertation (Table 17), were subjected to repeated flexion/extension *in vivo* in feline models and showed acute inflammatory responses to loading with increased numbers of cycles and faster loading rates [243]. Examining the inflammatory and catabolic response of supraspinous ligaments to flexion/extension in intact FSUs to confirm previous findings and place them in the context of changes in other spinal tissues would add to spine mechanobiology research by probing the relationship between mechanical prominence of a structure in a given loading mode and the resulting biological response.

Analysis of conditioned media from organ culture can serve as a screening stage in the search for specific, sensitive biomarkers related to spinal disorders *in vivo*. Because of the high degree of non-specificity of MRI for most symptomatic spinal disorders [446], the variability in patient response to treatments of back pain [53], and the numerous but ill-defined sub-groups within back pain patients [58], serum or urine-based biomarkers that could improve diagnosis and prognosis are desired [447]. To have utility, biomarkers must be specific to spinal disorders and have sufficient sensitivity for detection and range for longitudinal measurement throughout treatment. Because of the similarities of disc degeneration, facet osteoarthritis, and ligamentum flavum hypertrophy with other inflammatory and degenerative conditions of the musculoskeletal system [448, 449], identifying systemic biomarkers specific to spinal tissues or spinal disorders has been difficult. Comparing conditioned media from healthy and degenerated FSUs subjected to neutral flexion/extension and axial torsion with flexion/extension (Specific Aim 2), which showed detrimental effects of mechanical loading in spinal tissues, could identify proteins uniquely or significantly elevated in conditioned media from loaded samples. This type of *ex vivo* analysis excludes systemic factors and focuses on proteins (>2 kDa) that are released from spinal tissues. As a result, it can also be used to vet candidate biomarkers thought to arise from spinal tissues; if proteins are not detectable in small volumes of conditioned media immediately surrounding spinal tissues, it is unlikely that they will be measurable in serum *in vivo*. Conditioned media from within the inner dialysis membrane that encloses FSUs was collected from Specific Aims 1 and 2 and can be used for such future analyses.

Future studies using FSUs could explore a number of permutations with relevance to basic science and clinical research. Most simply, different forms of spinal injuries could be simulated, and their effects on acute mechanical and biological changes could be assessed. These injuries

could include needle punctures or rim lesions to simulate small annular tears, annular defects to induce nucleus pulposus herniation, or ligament transection in the posterior ligamentous complex to simulate ligament rupture or injury. The mechanical consequences of injury could be assessed simultaneously with biological changes within damaged structures as well as in neighboring tissues and the surrounding media. Integrating this data could improve understanding of the initial response to spinal injury in directly and indirectly impacted tissues, provide a platform for evaluating the effect of injury severity on biological markers, and assist in identification of candidate biomarkers specific to certain injuries [81]. Furthermore, FSUs from rabbit models of disc degeneration could be studied and compared to non-degenerated FSUs to test how degeneration affects biological responses to flexion/extension and complex loading. Finally, inflammatory mediators could be introduced to media within the dialysis membrane to simulate an inflammatory milieu and test how parameters of mechanical loading interact with inflammation in intact FSUs.

While lack of long-term culture and removal of systemic influences (e.g. the immune system) *ex vivo* prevents complete assessment of therapeutic interventions like tissue engineered constructs, stem cell therapy, or gene therapy, early effects of some interventions may be assessed. Small molecules (e.g. glucosamine, LinkN), which can diffuse in to spinal tissues [262, 450], and their interaction with different forms of mechanical loading could be assessed with and without degeneration or injury to FSUs. Alternatively, different forms of manual therapy could be applied to FSUs in culture. Although their analgesic effect is thought to largely occur through neurophysiologic signaling that involves intact peripheral and central nervous systems [194],

direct mechanosensitive, analgesic effects of manual therapy in spinal tissues may occur [193, 451, 452]. Coupling inflammatory conditions or detrimental loading with simulated manual therapy, which could be parameterized based on amplitudes, rates, and durations of movements, could explore if and how direct effects in spinal tissues occur.

The full potential of this system to influence orthopaedic rehabilitation would be realized by improved robotic control and extension to other musculoskeletal joints. In the current iteration of this system, relatively simple motions were applied using adaptive displacement control combined with kinematic replay. However, control of robotic systems has improved to the point where continuous, dynamic control of musculoskeletal joints at *in vivo* motion rates is possible [440]. Using new control methods and new robotic systems, the *ex vivo* mechanobiology system could be used to simulate spinal motions in exercise regimes or a series of occupational tasks with greater fidelity. Experiments could be constructed (i) to evaluate biological responses to different types of exercise routines or occupational tasks or (ii) to assess biological responses to the same set of motions given differing amounts of degeneration, injury, or mal-alignment.

Moreover, the bioreactor developed for this study is not limited to rabbits or to spinal segments; it could be readily modified to test other animal models and other musculoskeletal joints. *Ex vivo* mechanical loading and biological assessment of viable, intact knees, hips, and other diarthrodial joints has not been performed. Assessment of simultaneous, early biological responses to varying loading parameters *ex vivo* in tissues of diarthrodial joints could potentially open a new area of investigation in the basic science of joint physiology. Understanding the relationship between how synovium, synovial fluid, menisci, cartilage, and ligamentous tissue respond to applied loading in the context of normal physiology and injury, asymmetry, or arthritis could elucidate protective and detrimental effects of loading. Specifically, this system could also

address aspects of current questions such as how meniscal tears influence the mechanical and biological response to loading of surrounding structures. Also, simulations of different forms and parameters of exercise and activities (e.g. walking, running, squatting, etc.) could be studied in diarthrodial joints like the knee and hip. These extensions of the mechanobiological testing system could introduce a system that scales to multiple musculoskeletal joints, improves understanding of the physiologic response and interactions among tissues to applied loading, and provides orthopaedic rehabilitation with a tool to evaluate early biological responses to motion simulations *ex vivo*.

The system developed in this dissertation fulfills an important role in translational research from benchtop-to-bedside. *In vitro* cellular studies supply information for outcomes to assay the *ex vivo* system, which in turn provides loading conditions and interactions to be examined mechanistically at the cellular level. Similarly, biological changes in and interactions between spinal tissues, identified candidate serum biomarkers and screened therapeutics tested *ex vivo* can be introduced to *in vivo* animal models to improve outcome targets. Similarly, effects of loading parameters and tissue interactions, along with outcomes from animal studies, can inform trials (e.g. specific vs. non-specific exercise in back pain patients) in human studies. The ultimate goal of this translational process is to improve clinical practice by clarifying the role of mechanics in disease and treatment to permit rationally prescribed manual and motion-based therapies and improve integration of these therapies in orthopaedic care.

APPENDIX A

UNLOADED CULTURE VS. BASELINE

A.1 INTRODUCTION

Throughout this dissertation, all biological responses—relative gene expression and protein densitometry from Western blots—compare loaded tissues to time-matched, cultured unloaded tissues from adjacent spinal segments. This method of normalization controls for variation between animals and with time in culture. What remains unclear using this method alone is the effect of culture conditions on biological outcomes compared to baseline (t_0). So, tissues from unloaded cultured FSUs were normalized to tissues isolated at baseline (t_0) to address how unloaded culture influences baseline expression values and to assess whether loading expression levels show the same trend or return toward baseline values.

A.2 METHODS

Methods are described in detail 5.2.3 and 6.2.2.2. First, for relative gene expression, *MMP-3* and *COX-2* expression between tissues (NP n=5, FC n=5, and AF n=2-3) from unloaded and *t0* spinal segments were calculated using $2^{-\Delta\Delta C_t}$ referencing *GAPDH* as a housekeeping gene. The time in unloaded organ culture for transcriptional outcomes was ~2 hours. Second, protein amount of MMP- and ADAMTS-cleaved aggrecan fragments and of CHAD in unloaded tissues (n=3-5 of NP, FC, and AF) were normalized to protein amounts at baseline (*t0*). The time in unloaded culture for protein outcomes was ~24 hours.

A.3 RESULTS

The effect of organ culture on inflammatory and catabolic relative gene expression in NP, FC and AF is shown in Figure 38. Neutral F/E (Large ROM) and Large AT+F/E relative to baseline are included for comparison. Unloaded culture shows a trend toward up-regulation of *MMP-3* expression in all tissues and *COX-2* in FC and AF. Mean *MMP-3* expression changes the most in NP (4.00-fold increase) and the least in AF (1.44-fold increase). *COX-2* expression in NP is unaffected by organ culture (12% decrease). Changes in *COX-2* expression in FC with culture (4.31-fold increase) show trends toward elevated expression; changes in AF betray high variability.

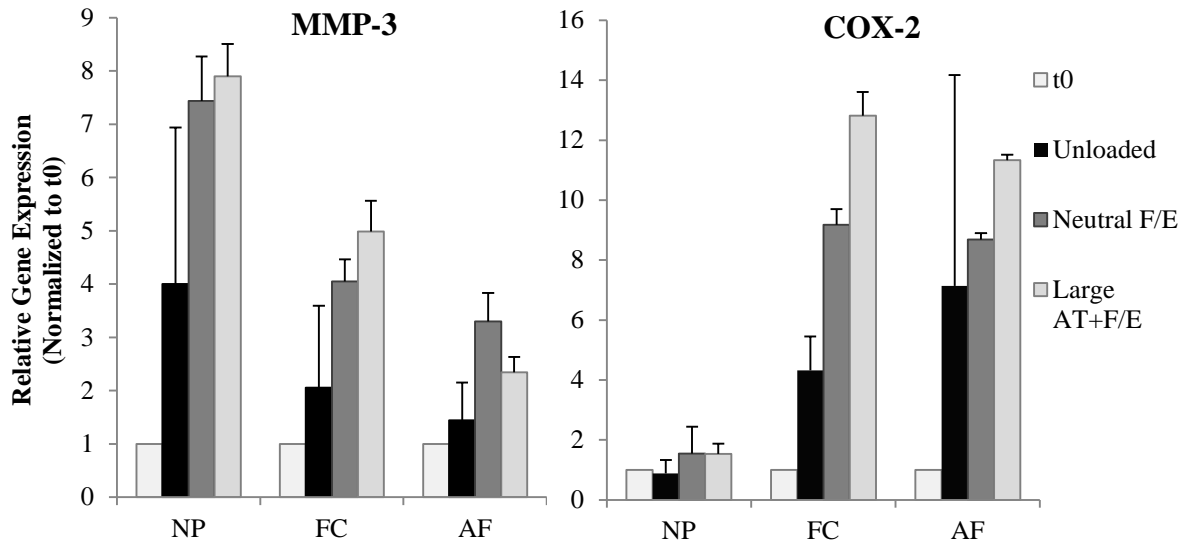


Figure 38. Relative gene expression in NP, FC, and AF of MMP-3 and COX-2 normalized to *t0*

The effect of unloaded culture on aggrecan fragments in spinal tissues is depicted in Figure 39. Neutral F/E (Large ROM) and Large AT+F/E relative to baseline are included for comparison. MMP-fragments in AF show variable differences in cultured FSUs relative to baseline (*t0*) with a mean decrease of $18 \pm 35\%$ in unloaded, cultured samples. ADAMTS-fragments in AF are similarly quite variable. Aggrecan fragments show a trend of increasing with culture relative to intact in FC; MMP- and ADAMTS-fragments increase $35 \pm 51\%$ and $28 \pm 37\%$, respectively. In contrast to FC, aggrecan fragments decrease in NP tissue in unloaded culture. MMP- and ADAMTS-fragments decrease, quite similarly and consistently, by $15 \pm 19\%$ and $25 \pm 16\%$, respectively.

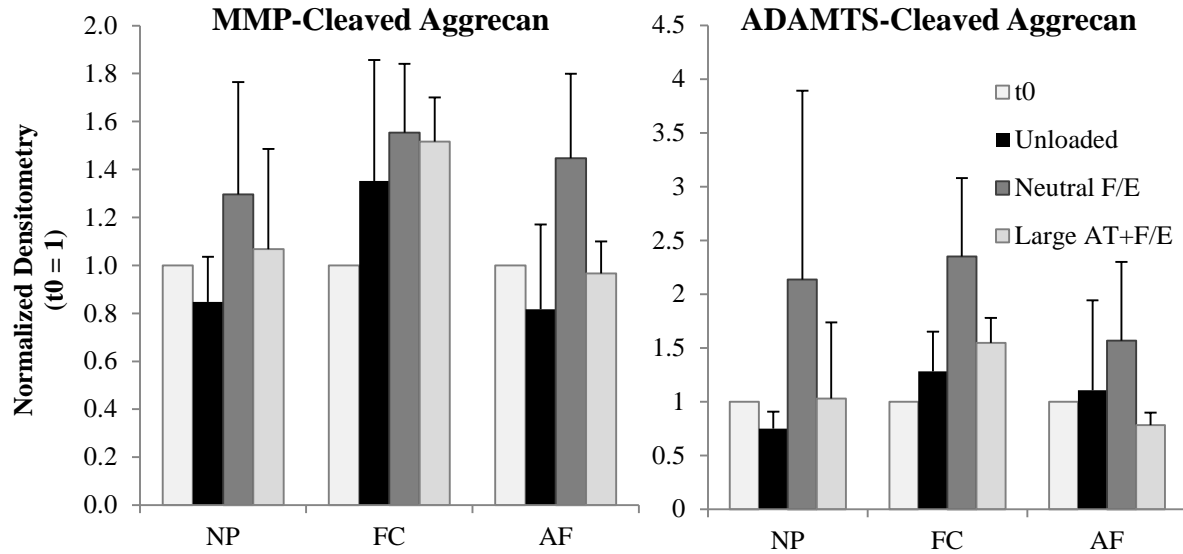


Figure 39. MMP-cleaved (left, ~54kDa) and ADAMTS-cleaved (right, ~67kDa) aggrecan fragments in cultured tissues normalized to baseline.

Changes in CHAD expression with unloaded organ culture are shown in Figure 40. Neutral F/E (Large ROM) and Large AT+F/E relative to baseline are included for comparison. Changes in expression with culture were larger than those seen with aggrecan fragments. In NP, expression increased 4.56 ± 3.11 -fold, and in the AF, it increased 2.11 ± 1.49 -fold. In contrast, CHAD expression decreased in FC with culture by $51 \pm 32\%$.

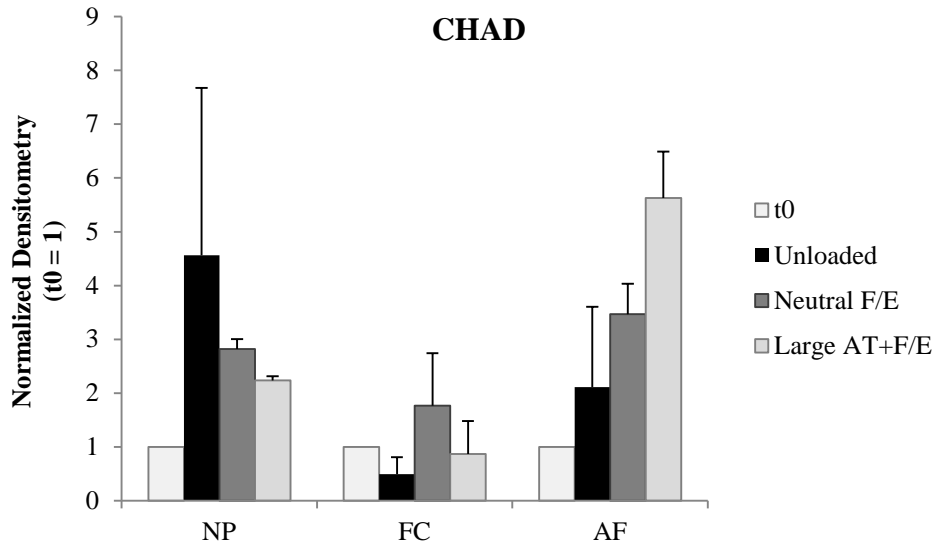


Figure 40. CHAD expression (~36kDa) in spinal tissues in normalized to *t0*

A.4 DISCUSSION

The effect of organ culture showed how the passage of time in culture influenced relative gene expression and protein expression relative to baseline values. The short term culture (~2 hours) used for transcriptional analysis showed modest increases in catabolic and pro-inflammatory gene expression in all tissues except for *COX-2* expression in NP. Other studies comparing inflammatory and catabolic gene expression in unloaded tissues compared to baseline have observed increased expression [220, 453, 454]. Longer culture durations (~24 hours) used to describe protein level responses to mechanical loading showed more variability in the effect of culture. Aggrecan fragment abundance in all tissues changed little (<35%) with culture but CHAD abundance increased by as much as 456% in NP. Changes in aggrecan fragment

abundance with long-term dynamic compression were only modest [149], so it is expected that short-term changes compared to baseline would be small. CHAD expression increases have not been observed in spinal studies previously [356, 357].

The chief utility of characterizing the effect of organ culture on baseline gene and protein expression is to classify responses to mechanical loading in culture (i.e. the differences between loaded culture and unloaded culture) as similar to or different from changes relative to baseline (i.e. the differences between loaded culture and baseline (t_0)). *MMP-3* and *COX-2* gene expression increased in all loaded tissues compared to unloaded tissues in culture. Because the effect of unloaded culture broadly elevated expression compared to baseline levels, the effect of mechanical loading further elevated expression away from baseline levels. The only exception was in NP *COX-2* expression where the trend of up-regulation was mitigated by comparison to baseline.

Trends in protein outcomes were maintained or mitigated when normalized to baseline in aggrecan fragments but not in CHAD. The mechanical responses in MMP- and ADAMTS-cleaved aggrecan fragments in F/E loading generally remained the same whether comparisons were made to baseline or unloaded tissues. In contrast, trends for CHAD in NP and FC were reversed and altered when compared to baseline. While CHAD in loaded NP was reduced relative to the high amount of CHAD expressed in unloaded NP samples, CHAD in loaded NP is higher than baseline levels (~2.5-2.75 fold increase). In FC, comparisons of loaded relative to unloaded FC showed that torsion reduced CHAD compared to neutral F/E, but CHAD levels in torsion groups were still higher than unloaded FC. Comparisons with baseline CHAD levels show that torsion group levels are similar to baseline (control). This suggests that FSUs subjected to torsion are more similar to baseline than those subjected to pure moment F/E. Previous trends in the AF are maintained compared to baseline. In contrast to NP and FC, load-responsive increases in CHAD in AF are in

addition to increases in CHAD with unloaded culture. Thus, unloading appears to have profound effects on CHAD in NP and FC tissue. A paucity of research on CHAD makes interpretation of increased expression seen in AF difficult as only CHAD depletion has been observed [356, 357], but it is possible that increased CHAD represents anabolic or protective remodeling.

To conclude, transcriptional changes with loading observed in Specific Aims 1 and 2 represent perturbations away from expression levels at t_0 . In contrast, load-responsive protein expression changes in many tissues were mitigated by comparison to baseline. Loading trends are reversed for CHAD in NP when compared to baseline and amplified in AF. These results help to interpret changes with loading reported in Specific Aims 1 and 2.

APPENDIX B

EFFECT OF AGE ON BIOLOGICAL OUTCOMES

B.1 INTRODUCTION

Spines from rabbits with a wide range of ages (8-33 m.o. / 13.8 ± 5.8 m.o.) were included in this research project. To promote consistency of results, skeletally immature rabbits were excluded (<8 m.o.) [455]. Nonetheless, because of the variability introduced by a broad age range, the effect of age was analyzed to see if it influenced (i) biological responses to loading and (ii) biological outcomes in unloaded samples.

B.2 METHODS

The primary motivation of this study was to determine to what extent age affected the biological responses to applied loads in spinal tissues. To address this concern, simple Pearson correlation was performed per gene for each tissue (1) between relative gene expression (loaded vs. unloaded) and age and (2) between normalized protein levels (loaded densitometry normalized to unloaded densitometry) and age. A secondary goal of this analysis was to query whether age influenced aggrecan and CHAD expression in spinal tissues apart from the effect of loading. This question was addressed by similarly using simple Pearson correlation between raw densitometry values of

unloaded tissues and age. For both aims, Pearson’s rho and associated p-values are reported. Correlations with $R>0.3$ and $p<0.2$ were considered very weakly correlated. Significant correlations were defined by $p<.05$.

B.3 RESULTS

Correlations between age and load-responsive changes in relative gene expression are summarized in Table 33. Only two correlations, *MMP-1* expression in AF and *COX-2* expression in LF (Figure 41), have $R>0.3$ and $p<0.2$, and neither is statistically significant. Therefore, correlations of age with relative gene expression for load effects are, at most, weak and insignificant.

Table 33. Simple correlation (Pearson’s *R*) of age with relative gene expression for the effect of loading

		Gene				
Tissue	Correlation	MMP-1	MMP-3	ADAMTS-5	COX-2	ACAN
AF	<i>R</i>	0.317	-0.100	-0.140	0.203	-0.213
	<i>p</i>	0.107	0.545	0.445	0.229	0.220
NP	<i>R</i>	.	-0.222	.	-0.072	0.276
	<i>p</i>	.	0.247	.	0.738	0.339
FC	<i>R</i>	.	0.159	.	0.017	-0.119
	<i>p</i>	.	0.391	.	0.931	0.606
LF	<i>R</i>	0.106	-0.052	-0.007	0.319†	-0.004
	<i>p</i>	0.578	0.784	0.969	0.097	0.982
p < 0.2 are shaded, †-p<0.1						

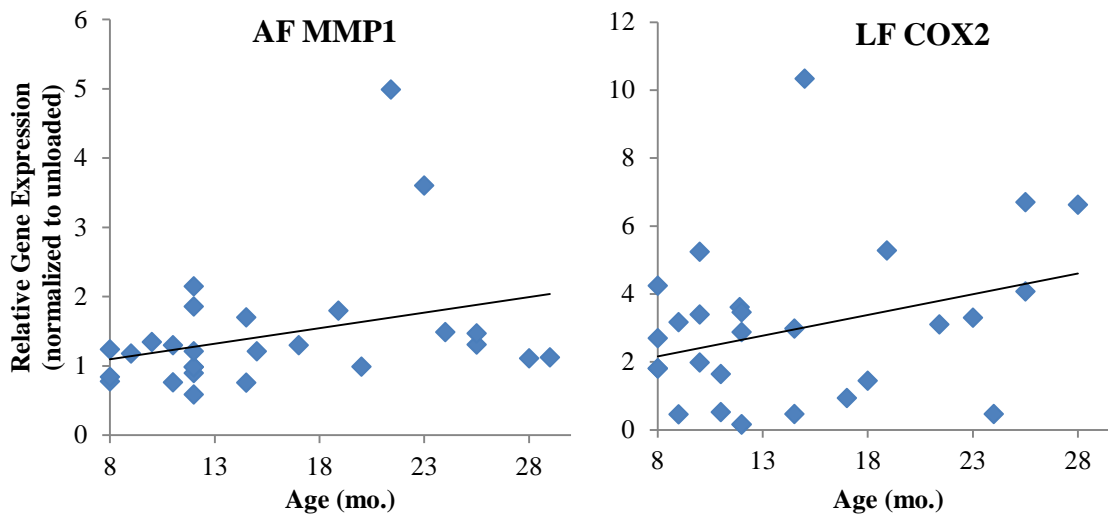


Figure 41. Age vs. Relative Gene Expression: The two strongest correlations between age and load responsive changes in gene expression

Correlations of age with (1) the raw densitometry for protein expression of outcomes in unloaded tissues only and (2) the load response in protein outcomes are shown in Table 34. No load response correlations were significant ($p > 0.249$ for all tissues and proteins). Raw densitometry of protein outcomes were correlated with age in NP for each outcome ($p < 0.2$); these correlations are illustrated in Figure 42, Figure 43, and Figure 44. Both types of aggrecan fragments increase with age, and CHAD decreases with age. Correlations of ADAMTS-cleaved fragments were significant ($p = .042$), and correlations of MMP-cleaved fragments approached significance ($p = .082$).

Table 34. Correlations of age with protein outcomes (1) raw densitometry of unloaded (only) and (2) load response (normalized to unloaded)

Protein		Correlation	Tissue		
			NP	FC	AF
G1: MMP- cleaved fragment	Raw Dens.	<i>R</i>	0.448†	0.110	0.313
		<i>p</i>	0.082	0.686	0.271
	Loaded vs. Unloaded	<i>R</i>	-0.095	0.306	0.046
		<i>p</i>	0.726	0.249	0.864
G1: ADAMTS- cleaved fragment	Raw Dens.	<i>R</i>	0.528*	0.133	0.147
		<i>p</i>	0.042	0.628	0.615
	Loaded vs. Unloaded	<i>R</i>	-0.287	-0.216	-0.013
		<i>p</i>	0.300	0.422	0.961
CHAD	Raw Dens.	<i>R</i>	-0.447	-0.233	-0.138
		<i>p</i>	0.168	0.517	0.668
	Loaded vs. Unloaded	<i>R</i>	-0.128	-0.254	0.213
		<i>p</i>	0.707	0.451	0.507

p < 0.2 are shaded, †-p<0.1, *-p<0.05

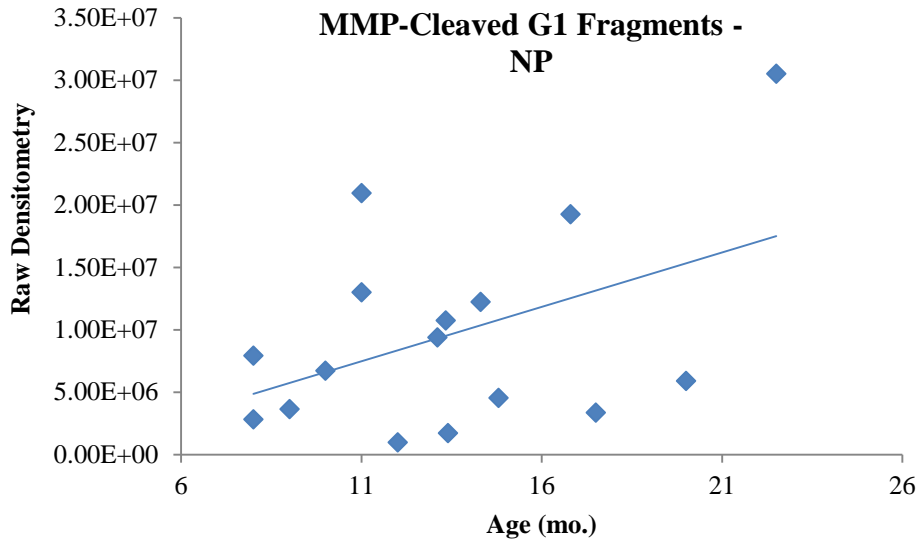


Figure 42. Correlation of age with MMP-cleaved aggrecan raw densitometry values in NP

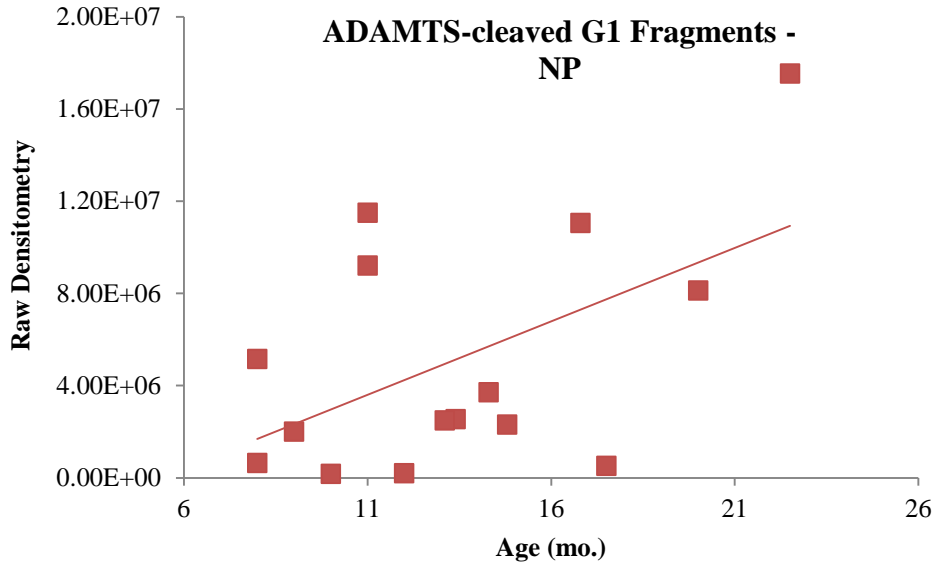


Figure 43. Correlation of age with ADAMTS-cleaved aggrecan raw densitometry values in NP

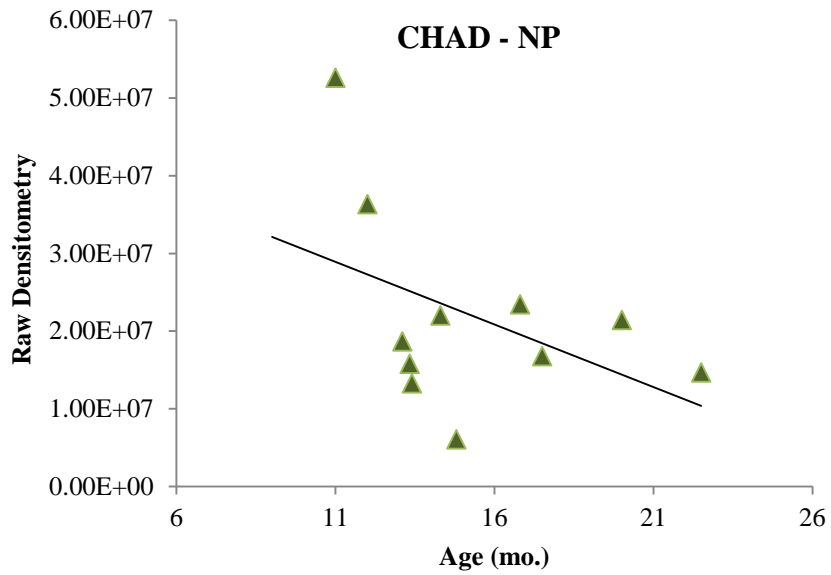


Figure 44. Correlation of age with CHAD raw densitometry values in NP

B.4 DISCUSSION

Age in skeletally mature NZW rabbits does not have a significant effect on biological responses to mechanical loading applied in Specific Aims 1 and 2. No correlations between load-responsive relative gene expression or protein expression were significant, and all effect sizes were small or negligible ($R < 0.319$). Correlations between age and protein abundance in unloaded tissue did show significant results that describe the effect of aging on spinal tissues in healthy skeletally mature rabbits. Generally, the NP is the first spinal tissue (and one of the first tissues in the body) to demonstrate degenerative effects of age in humans and other mammals [147, 166, 246, 456]. These results reflect that paradigm in that the NP showed significant (or nearly significant) increases in aggrecan fragmentation and decreases in CHAD abundance, but AF and FC showed no changes approaching significance. Further, aggrecan breakdown is a hallmark of early degeneration [327, 456], and the elevated levels of fragments in older tissues suggest that early degenerative changes had begun in older rabbits. CHAD depletion has been observed with degeneration and abnormal loading in spinal asymmetries [356, 457], so loss of CHAD with age in rabbits further supports the idea that early degeneration of the NP occurs in rabbits with aging.

APPENDIX C

LINEAR MULTIPLE REGRESSION

More detailed results from the second step of the sequential regression are shown here. Output from SPSS tabulating the Model Summary, ANOVA results and Coefficients are presented in tables per tissue and per gene. The Model Summary shows how the variability accounted for by the model improves (R , Change in R^2) with each added variable from the results of the first step of the regression analysis (Table 22). The variables added in each model are presented in the first column of the Coefficients Table, and their weight (B), standard error (SE), standardized weight (β), t -value from a Student's t -test (t), p -value from the test (significance), partial correlation values, and collinearity statistics are shown. Finally, ANOVA tables illustrate model significance with each variable added. For each of these tables, the effect of each added variable with each step is evident. Additionally, results from tests of the assumptions of multiple regression are shown in (1) histograms of standardized residuals and (2) standardized residuals vs. standardized predicted value plots (generated in SPSS). These show tests of the assumptions of independent error (residuals should be normally distributed), linearity and homoscedasticity (data should be randomly and evenly dispersed or spread without underlying shapes or clustering).

C.2 PRINCIPAL COMPONENT ANALYSIS

Table 35. Principal Component Analysis: Eigenvalues and variance explained

<u>PC</u>	<u>Eigenvalue</u>	<u>Variance Explained</u>
1	4.169164739	27.7944316
2	2.300206818	15.33471212
3	1.76361428	11.75742853
4	1.463758883	9.758392553
5	1.136885904	7.579239358
6	0.961958094	6.413053958
7	0.812048881	5.413659206
8	0.67770067	4.518004468
9	0.58576343	3.905089533
10	0.389920388	2.59946925
11	0.323447388	2.156315922
12	0.155979158	1.039861056
13	0.127544417	0.850296112
14	0.077399203	0.515994684
15	0.054607748	0.364051654

Table 36. Simple correlation of original predictors with principal components

Orgin. Predictors	Principal Component (Absolute Value)				
	PC 1	PC 2	PC 3	PC 4	PC 5
WorkCum	0.752064	0.220132	0.351424	0.0076866	0.0314571
HysteresisMean	0.33725	0.260302	0.014535	0.0141195	0.8176816
HysteresisRelax	0.626612	0.151782	0.202264	0.0505621	0.1443871
ROMfMean	0.80602	0.435965	0.037301	0.3608294	0.0099175
ROMeMean	0.315328	0.814065	0.307256	0.1489292	0.1592257
MxfMean	0.901174	0.349848	0.374472	0.2934666	0.0839054
MxeMean	0.185241	0.835618	0.224021	0.0065823	0.1422405
MxfRelaxRelax	0.0373	0.321556	0.002609	0.5461371	0.0112159
MxeRelaxRelax	0.266049	0.384245	0.764435	0.0497733	0.2477114
AROMmidMean	0.391522	0.135522	0.308668	0.6665297	0.1696801
MymidRelax	0.043324	0.366447	0.307761	0.6141728	0.0829438
NZMean	0.368351	0.714779	0.213467	0.2210544	0.4645159
NZRelax	0.232293	0.242156	0.903626	0.1611218	0.1360785
Cycles	0.504658	0.699162	0.006657	0.4867177	0.3206097
Age	0.360869	0.077043	0.109792	0.4843183	0.5367919

C.2.1 Matlab Code for PCA

```
%Rob Hartman - 05/17/14
%PCA for multiple regression across all groups (SA1 & 2)

%save location
fileLocation = 'Z:\Ortho Research 3\FergusonLab\Students\Hartman,
Robert\Biological Outcomes\RNA\PCR\Summary\Stats\';
% fileLocation = 'C:\Users\Rob\Documents\MATLAB\Statistics\RGE_summary\';

%Contains RGE data ('RGE_all' is raw, 'RGE' is analyzed)
load([fileLocation, 'rFSU_RGESABoth_NumerOrder_051214b.mat']); %wo-with
outliers; no-no outliers
clear RGE

tissueStr = {'AF', 'FC', 'NP', 'LF'};
geneStr = {'MMP1', 'MMP3', 'ADAMTS5', 'COX2', 'AGC'};

regressStr = {'PCA', 'PCA_Std'};

% p = 8; %predictor matrix column; 1 := cycles, end:= age

%Difference b/w RGE per gene & Per comparison & keep track of N
%RGE_all structure AF(2:6), FC(7:11), NP(12:16), LF(17:21); genes:
MMP1>MMP3>ADAMTS5>COX2>AGC

%read in mechanical predictor data
analysisDate = '_051714'; %Bivariate correlation down sizing: chose %change
(i.e. relax.) and flex & ext but not f/e
fileLocation = 'Z:\Ortho Research 3\FergusonLab\Students\Hartman,
Robert\Biological Outcomes\RNA\PCR\Summary\Stats\';
% fileID = [fileLocation, 'mechanicalPredictors', analysisDate, '.xlsx'];
% workSheetStr =
{'Work_Hysteresis', 'MomentRotation_FE', 'AxialRotation', 'NZEZ', 'Covariates'};
workSheetStr = {'PostAutoCorrData'}; %variables that remain after examining
and accounting for autocorrelation

%read in Predictor variables from Excel file
for i=1:size(workSheetStr,2)
    mechanicalPredictors.(workSheetStr{i}) =
xlsread([fileLocation, 'MechPredictorsAll', analysisDate, '.xlsx'], workSheetStr{
i});
end

%form groups
for j = 1:size(RGE_all,1) %for the number of rows in RGE_all, i.e. number of
samples
    RGE.(regressStr{1}).Values(j,:) = RGE_all(j,1:(size(RGE_all,2)-1));
%date and 3 genes per tissue
end
```

```

%%%%can modify 'MechPredictors' to be 'mechanicalPredictors.x'%%%%
    %from xlsx file
%
    RGE.(regressStr{1}).Predictors(j,:) = MechPredictors(j,2:end);
%---grouping by type of predictor---
%
    RGE.(regressStr{1}).Predictors(j,:) =
mechanicalPredictors.workSheetStr{1}; %energetics
%
    RGE.(regressStr{1}).Predictors(j,:) =
mechanicalPredictors.workSheetStr{2}; %moment/rotation
%
    RGE.(regressStr{1}).Predictors(j,:) =
mechanicalPredictors.workSheetStr{3}; %NZk
%
    RGE.(regressStr{1}).Predictors(j,:) =
[mechanicalPredictors.Cycles mechanicalPredictors.workSheetStr{1}
mechanicalPredictors.Age]; %energetics + cycle + age
%
    RGE.(regressStr{1}).Predictors(j,:) =
[mechanicalPredictors.Cycles mechanicalPredictors.workSheetStr{2}
mechanicalPredictors.Age]; %moment/rotation + cycle + age
%
    RGE.(regressStr{1}).Predictors(j,:) =
[mechanicalPredictors.Cycles mechanicalPredictors.workSheetStr{3}
mechanicalPredictors.Age]; %NZk + cycle + age
%---reduced number of predictors-----
    %w/o 'cycles' and 'age'
%
    cols = [2 6 7 11]; RGE.(regressStr{1}).Predictors(j,:) =
mechanicalPredictors.workSheetStr{1}(:,cols); %energetics
%
    cols = [4 7 10 13]; RGE.(regressStr{1}).Predictors(j,:) =
mechanicalPredictors.workSheetStr{2}(:,cols); %moment/rotation
%
    cols = [2 5]; RGE.(regressStr{1}).Predictors(j,:) =
mechanicalPredictors.workSheetStr{3}(:,cols); %NZk
    %w/ 'cycles' and 'age'
%
    cols = [2 6 7 11]; RGE.(regressStr{1}).Predictors(j,:) =
[mechanicalPredictors.Cycles mechanicalPredictors.workSheetStr{1}(:,cols)
mechanicalPredictors.Age]; %energetics + cycle + age
%
    cols = [4 7 10 13]; RGE.(regressStr{1}).Predictors(j,:) =
[mechanicalPredictors.Cycles mechanicalPredictors.workSheetStr{2}(:,cols)
mechanicalPredictors.Age]; %moment/rotation + cycle + age
%
    cols = [2 5]; RGE.(regressStr{1}).Predictors(j,:) =
[mechanicalPredictors.Cycles mechanicalPredictors.workSheetStr{3}(:,cols)
mechanicalPredictors.Age]; %NZk + cycle + age
%----alternative groupings-----
%
    %change in mechanics: work (mag:%), hyst (mag:%),
moment(Nm)(f:e:fe), moment(%) (f:e:fe), NZ(mag:%)
%
    RGE.(regressStr{1}).Predictors(j,:) =
[mechanicalPredictors.workSheetStr{1}(:,5:6)
mechanicalPredictors.workSheetStr{1}(:,10:11)... %change in energetics, mag:%
%
    mechanicalPredictors.workSheetStr{2}(:,8:13)
mechanicalPredictors.workSheetStr{3}(:,4:5)];
%
    %redcued to avoid collinearity (%'s, FE combined)
%
    RGE.(regressStr{1}).Predictors(j,:) =
[mechanicalPredictors.workSheetStr{1}(:,6)
mechanicalPredictors.workSheetStr{1}(:,11)... %change in energetics, mag:%
%
    mechanicalPredictors.workSheetStr{2}(:,10)
mechanicalPredictors.workSheetStr{2}(:,12)
mechanicalPredictors.workSheetStr{3}(:,5)];
%
    %magnitudes (not change across cycles)
%
    RGE.(regressStr{1}).Predictors(j,:) =
[mechanicalPredictors.workSheetStr{1}(:,2:4)
mechanicalPredictors.workSheetStr{1}(:,7:9)... %change in energetics, mag:%

```

```

%           mechanicalPredictors.workSheetStr{2}(:,2:7)
mechanicalPredictors.workSheetStr{3}(:,2:3)];
% %----all variables-----
%           %if using all worksheets, all variables
%           RGE.(regressStr{1}).Predictors.mechanicalPredictors(:, :) =
[mechanicalPredictors.(workSheetStr{1})(:,2:end)
mechanicalPredictors.(workSheetStr{2})(:,2:end) ...
%           mechanicalPredictors.(workSheetStr{3})(:,2:end)
mechanicalPredictors.(workSheetStr{4})(:,2:5)
mechanicalPredictors.(workSheetStr{5})(:,2:end)]; %2:5 omits the EZ zone
%           %if using only post-autocorrelation variables
RGE.(regressStr{1}).Predictors.mechanicalPredictors(:, :) =
mechanicalPredictors.(workSheetStr{1})(:,2:end);

% %----hierarchical - user defined/selected, from 'all variables' in section
above-----
%           RGE.(regressStr{1}).Predictors(j, :) =
[mechanicalPredictors.Cycles mechanicalPredictors.workSheetStr{1}
mechanicalPredictors.Cycles mechanicalPredictors.workSheetStr{2}...
%           mechanicalPredictors.Cycles
mechanicalPredictors.workSheetStr{3} mechanicalPredictors.Age];
%           end
% end

%-----Auto-correlation analysis-----
% % % % % % %---correlations: bivariate correlations of all predictors
variables; ignore tissue/gene groupings of predictors
% % % % % % for ii =
1:size(RGE.(regressStr{1}).Predictors.mechanicalPredictors,2)
% % % % % %         for jj =
1:size(RGE.(regressStr{1}).Predictors.mechanicalPredictors,2)
% % % % % %         %form an nxn matrix where n is number of predictors that
calculates correlations between every permutation of predictor variables
% % % % % %         [RGE.(regressStr{1}).Predictors.rho(ii,jj),
RGE.(regressStr{1}).Predictors.rhoP(ii,jj)] =
corr(RGE.(regressStr{1}).Predictors.mechanicalPredictors(:,ii),RGE.(regressStr{1}).Predictors.mechanicalPredictors(:,jj),'type','Pearson');
% % % % % %         end
% % % % % % end
%-----

% % % % % % %---univariate correlations of each predictor with each
tissue/gene
% % % % % % tissueGeneCtr = 1;
% % % % % % for i = 1:size(tissueStr,2) %samples
% % % % % %         for j = 1:size(geneStr,2) %genes per tissue
% % % % % %
% % % % % %         tissueGeneStr = [tissueStr{i},geneStr{j}];
% % % % % %         tissueGeneCtr = tissueGeneCtr + 1; %first iteration-it's
2
% % % % % %
% % % % % %         dummyRGE = RGE.(regressStr{1}).Values(:,tissueGeneCtr);
% % % % % %         dummyRGE(isnan(dummyRGE)) = 0; %convert NaNs to 0's
% % % % % %         %---consolidate matrix, remove 0's rows - dates not in
group

```

```

% % % % % %           indexAll = find(dummyRGE ~= 0);
% % % % % %           dummyRGE = dummyRGE(indexAll,:);
% % % % % %           %performing univariate correlations w/ consolidated
mechanical predictors
% % % % % %           for ii =
1:size(RGE.(regressStr{1}).Predictors.mechanicalPredictors,2)
% % % % % %
[RGE.('UniCorr').(tissueStr{i}).(geneStr{j}).rho(ii),RGE.('UniCorr').(tissueS
tr{i}).(geneStr{j}).p(ii)] =
corr(dummyRGE,RGE.(regressStr{1}).Predictors.mechanicalPredictors(indexAll,ii
));
% % % % % %           end
% % % % % %           clear dummyRGE indexAll
% % % % % %           end
% % % % % %           end
% % % % % %           tissueGeneCtr = 0;
% % % % % %           for i = 1:size(tissueStr,2) %samples
% % % % % %           for j = 1:size(geneStr,2) %genes per tissue
% % % % % %           tissueGeneCtr = tissueGeneCtr + 1;
% % % % % %           for ii =
1:size(RGE.(regressStr{1}).Predictors.mechanicalPredictors,2)
% % % % % %           if
RGE.('UniCorr').(tissueStr{i}).(geneStr{j}).p(ii) < 0.1
% % % % % %           RGE.('UniCorr').P(tissueGeneCtr,ii) =
RGE.('UniCorr').(tissueStr{i}).(geneStr{j}).p(ii);
% % % % % %           RGE.('UniCorr').Rho(tissueGeneCtr,ii) =
RGE.('UniCorr').(tissueStr{i}).(geneStr{j}).rho(ii);
% % % % % %           end
% % % % % %           %-----
%---perform PCA of predictor variables on a gene/tissue basis?---
%PCA on raw data
%centering subtracts the mean so that PC's point in the direction of maximal
variance w/o undue influence of the mean
[RGE.(regressStr{1}).Predictors.(regressStr{1}).coeff,RGE.(regressStr{1}).Pre
dictors.(regressStr{1}).score,RGE.(regressStr{1}).Predictors.(regressStr{1}).
latent,...

RGE.(regressStr{1}).Predictors.(regressStr{1}).tsquared,RGE.(regressStr{1}).P
redictors.(regressStr{1}).explained,RGE.(regressStr{1}).Predictors.(regressSt
r{1}).mu]...
=
pca(RGE.(regressStr{1}).Predictors.mechanicalPredictors,'algorithm','svd','ce
ntered','on'); %exclude the date variable in the first column
RGE.(regressStr{1}).Predictors.(regressStr{1}).nPC = 9; %number of PC
determined above cutoff

%PCA on standardized X - based on autocorrelation: sum of eigenvalues is
number of variables

```

```

[RGE.(regressStr{1}).Predictors.(regressStr{2}).coeff,RGE.(regressStr{1}).Pre
dictors.(regressStr{2}).score,RGE.(regressStr{1}).Predictors.(regressStr{2}).
latent,...

RGE.(regressStr{1}).Predictors.(regressStr{2}).tsquared,RGE.(regressStr{1}).P
redictors.(regressStr{2}).explained,RGE.(regressStr{1}).Predictors.(regressSt
r{2}).mu]...
=
pca(zscore(RGE.(regressStr{1}).Predictors.mechanicalPredictors),'algorithm','
svd','centered','on'); %exclude the date variable in the first column
RGE.(regressStr{1}).Predictors.(regressStr{2}).nPC = 5; %number of PC
determined above cutoff

%score:= data in the princ. comp. space (row-observation; col-PC)
%returns rotated coefficients to maximize unique contribution of original
variables to each principal component and the transformation matrix,T, by
%which one should be able to align 'scores' (and other 'pca' matrices)
[RGE.(regressStr{1}).Predictors.(regressStr{2}).coeffVr,
RGE.(regressStr{1}).Predictors.(regressStr{2}).Tvr] =
rotatefactors(RGE.(regressStr{1}).Predictors.(regressStr{2}).coeff(:,1:RGE.(r
egressStr{1}).Predictors.(regressStr{2}).nPC),'Method','varimax');
RGE.(regressStr{1}).Predictors.(regressStr{2}).score_Tvr =
RGE.(regressStr{1}).Predictors.(regressStr{2}).score(:,1:RGE.(regressStr{1}).
Predictors.(regressStr{2}).nPC) *
RGE.(regressStr{1}).Predictors.(regressStr{2}).Tvr;

%interpret principle components by correlating with original predictor
variables
for ii = 1:size(RGE.(regressStr{1}).Predictors.mechanicalPredictors,2)
%number of PC determined above cutoff
    for jj = 1:RGE.(regressStr{1}).Predictors.(regressStr{2}).nPC

RGE.(regressStr{1}).Predictors.(regressStr{2}).Data_PC_correlation.rho(ii,jj)
=
corr(RGE.(regressStr{1}).Predictors.mechanicalPredictors(:,ii),RGE.(regressSt
r{1}).Predictors.(regressStr{2}).score(:,jj));

RGE.(regressStr{1}).Predictors.(regressStr{2}).Data_PCvr_correlation.rho(ii,j
j) =
corr(RGE.(regressStr{1}).Predictors.mechanicalPredictors(:,ii),RGE.(regressSt
r{1}).Predictors.(regressStr{2}).score_Tvr(:,jj));
    end
end

%output of PCA copied to mechanicalPredictors_BCDS_031914\PCA_standardized
%result of PCA and interpretation and downsizing permitted by bivariate
%correlation of all predictors - avoiding collinearity
% indxBivC_PCA = [1 5 9 10 13 14 15 17]; %WorkCum HystCum Mxf Mxe dMxf dMxe
NZk dNzk
predVarStr = {'WorkCum','Hyst','ROMf','ROME','dMxe','NZk','aROM','dMy'};
%can I reat this in from MechPredictorAll*.xls ???
indxBivC_PCA =
1:1:size(RGE.(regressStr{1}).Predictors.mechanicalPredictors,2); %+ dHyst Age
% predVarStr = {'WorkCum','HystCum','Cycles','Age'};
% indxBivC_PCA = [1 5 18 19]; %+ dHyst Age

```

```

RGE.(regressStr{1}).Predictors.(regressStr{2}).finalPredictors =
RGE.(regressStr{1}).Predictors.mechanicalPredictors(:,indxBivC_PCA);
PredictorVar =
RGE.(regressStr{1}).Predictors.(regressStr{2}).finalPredictors;

%----multiple regression in Matlab-----
% % % % %replace NaN's with 0's
% % % % % for i = 1:size(regressStr,2)-1 %number of groups
% % % %     RGE.(regressStr{1}).Values(isnan(RGE.(regressStr{i}).Values)) =
0;
% % % % %
RGE.(regressStr{i}).Predictors(isnan(RGE.(regressStr{i}).Values)) = 0;
% % % % % end
% % % % %
% % % % %consolidate matrix, remove 0's rows - dates not in group
% % % % % for i = 1:size(regressStr,2)-1 %number of groups
% % % %     RGE.(regressStr{1}).IndexAll =
find(RGE.(regressStr{i}).Values(:,1) ~= 0);
% % % %     RGE.(regressStr{1}).Values =
RGE.(regressStr{i}).Values(RGE.(regressStr{i}).IndexAll,:);
% % % %
RGE.(regressStr{1}).Predictors.mechanicalPredictors(RGE.(regressStr{1}).Index
All,:) =
RGE.(regressStr{i}).Predictors.mechanicalPredictors(RGE.(regressStr{i}).Index
All,:);
% % % % % end
% % % % %
% % % % %
% % % % %count N per gene per group (non-NaN's per column)
% % % % %form Values in by tissue and by gene (under group)
% % % % % for i = 1:size(regressStr,2) %groups
% % % % % predictors are not separated by tissue and gene (apply across
tissue &
% % % % % gene combinations)
% % % %     colIndx = 1;
% % % %     for j = 1:size(tissueStr,2) %samples
% % % %         for k = 1:size(geneStr,2) %genes per tissue
% % % %             colIndx = colIndx+1; %columns 2 thru 10
% % % %             RGE.(regressStr{i}).(tissueStr{j}).(geneStr{k}).Values =
RGE.(regressStr{i}).Values(:,colIndx);
% % % %
RGE.(regressStr{i}).(tissueStr{j}).(geneStr{k}).Predictors.mechanicalPredicto
rs = RGE.(regressStr{i}).Predictors.mechanicalPredictors; %copy Predictor to
each tissue/gene combination
% % % %     end
% % % %     end
% % % % % end
% % % % %
% % % % %remove 0 values per tissue per gene, get N per ...
% % % % % for i = 1:size(regressStr,2) %groups
% % % % %     for j = 1:size(tissueStr,2) %samples
% % % % %         for k = 1:size(geneStr,2) %genes per tissue
% % % % %             ctr = 1;
% % % % %             for ii =
1:size(RGE.(regressStr{i}).(tissueStr{j}).(geneStr{k}).Values,1) %find
indices of predictor rows that don't have corresponding RGE values

```

```

% % % %           if
RGE.(regressStr{i}).(tissueStr{j}).(geneStr{k}).Values(ii) == 0 %row where
RGE value is missing
% % % %
RGE.(regressStr{i}).(tissueStr{j}).(geneStr{k}).predictorDeleteIndx(ctr) =
ii; %indices (rows) to delete
% % % %           ctr = ctr+1;
% % % %           end
% % % %           end
% % % %           %remove rows w/ zero RGE values
% % % %
RGE.(regressStr{i}).(tissueStr{j}).(geneStr{k}).PredictorVar =
removerows(RGE.(regressStr{i}).(tissueStr{j}).(geneStr{k}).Predictors.mechani
calPredictors,'ind',RGE.(regressStr{i}).(tissueStr{j}).(geneStr{k}).predictor
DeleteIndx);
% % % %           %contract RGE values vector to remove non-zero values
% % % %
RGE.(regressStr{i}).(tissueStr{j}).(geneStr{k}).Values((RGE.(regressStr{i}).(
tissueStr{j}).(geneStr{k}).Values)==0) = [];
% % % %           %store size per tissue per gene
% % % %           RGE.(regressStr{i}).(tissueStr{j}).(geneStr{k}).N =
size(RGE.(regressStr{i}).(tissueStr{j}).(geneStr{k}).Values,1); %get N per
group
% % % %
% % % %           end
% % % %           end
% % % %           end
% % % %
% % % % %---correlations: bivariate correlations of each predictor w/ RGE---
% % % % for i = 1:size(regressStr,2) %groups
% % % %     for j = 1:size(tissueStr,2) %samples
% % % %       for k = 1:size(geneStr,2) %genes per tissue
% % % %         for ii =
1:size(RGE.(regressStr{i}).(tissueStr{j}).(geneStr{k}).PredictorVar,2)
% % % %           %perform linear correlation of each predictor with
each tissue/gene RGE
% % % %           %correlation rho is 1xn vector w/ values for each
predictor (how does each predictor correlate w/ that RGE)
% % % %
[RGE.(regressStr{i}).(tissueStr{j}).(geneStr{k}).rho(ii),
RGE.(regressStr{i}).(tissueStr{j}).(geneStr{k}).rhoP(ii)] =
corr(RGE.(regressStr{i}).(tissueStr{j}).(geneStr{k}).PredictorVar(:,ii),RGE.(
regressStr{i}).(tissueStr{j}).(geneStr{k}).Values,'type','Pearson');
% % % %           end
% % % %
% % % %           %make linear regression data structure
% % % % for i = 1:size(regressStr,2)
% % % %     for j = 1:size(tissueStr,2) %samples
% % % %       for k = 1:size(geneStr,2) %genes per tissue
% % % %
RGE.(regressStr{i}).(tissueStr{j}).(geneStr{k}).multiRegress.tbl =

```



```

% % % analysisDate = '051214';
% % % fileLocation = 'Z:\Ortho Research 3\FergusonLab\Students\Hartman,
Robert\Biological Outcomes\RNA\PCR\Summary\Stats\';
% % %
% % % cellPredictorStr = {'allMechanics'}; %add age, others
% % % % cellAnovaMx = {'B2'};
% % %
% % % for i = 1:size(regressStr,2)
% % %     for j = 1:size(tissueStr,2) %samples
% % %         for k = 1:size(geneStr,2) %genes per tissue
% % %             if
RGE.(compareStr{1}).(tissueStr{j}).(geneStr{k}).anovaMatrix ~= 0
% % %
RGE.(regressStr{i}).(tissueStr{j}).(geneStr{k}).multiRegress.tbl =
[RGE.(regressStr{i}).(tissueStr{j}).(geneStr{k}).Values
RGE.(regressStr{i}).(tissueStr{j}).(geneStr{k}).PredictorVar]; %variable to
write
% % %             tissueGeneStr = [tissueStr{j},geneStr{k}]; %sheet name
% % %             cellLabelStr =
{'tissueGeneStr','Cycles','Work_Cum','Hysteresis_Cum','Net_Energy','fROM','eROM
','ROM','Age'};
% % %
xlswrite([fileLocation,'RGE_multiRegress',analysisDate,'.xlsx'],cellLabelStr,
tissueGeneStr,'A1:I1');
% % %
xlswrite([fileLocation,'RGE_multiRegress',analysisDate,'.xlsx'],RGE.(regressS
tr{i}).(tissueStr{j}).(geneStr{k}).multiRegress.tbl,tissueGeneStr,'A2');
% % % %             end
% % %         end
% % %     end
% % % end
%-----

```

C.3 REGRESSION RESULTS: ANNULUS FIBROSUS

C.3.1 MMP-1

Model Summary^b

Model	R	R Square	Adjusted R Square	Std. Error of the Estimate	Change Statistics				
					R Square Change	F Change	df 1	df 2	Sig. F Change
1	.445 _a	.198	.165	.11588	.198	5.943	1	24	.023

a. Predictors: (Constant), WorkCum

b. Dependent Variable: logMMP1_AF

ANOVA^a

Model	Sum of Squares	df	Mean Square	F	Sig.
1 Regression	.080	1	.080	5.943	.023 _b
Residual	.322	24	.013		
Total	.402	25			

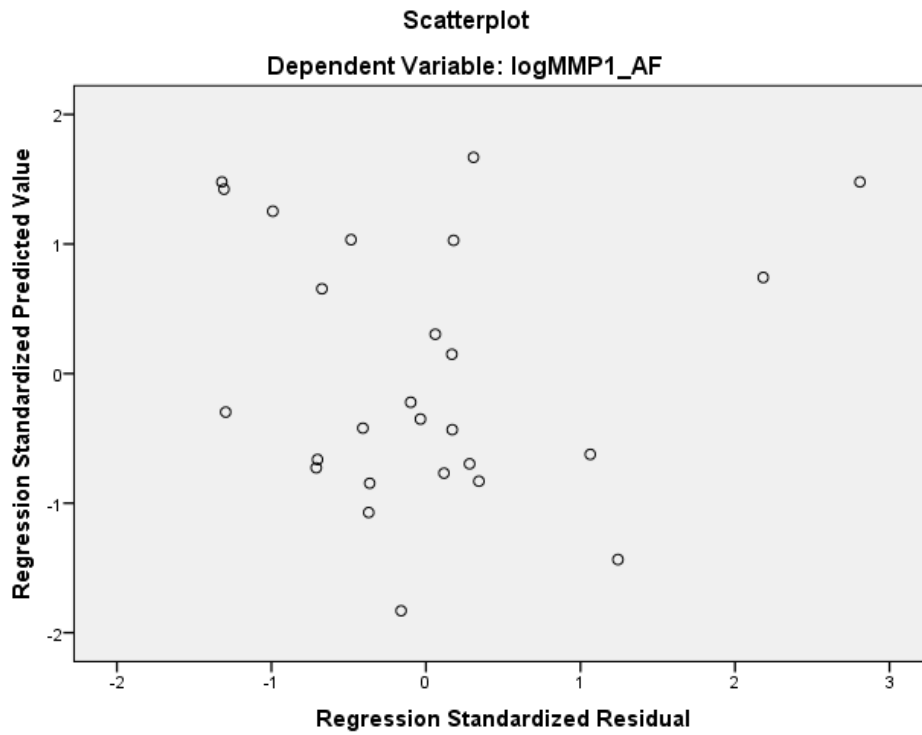
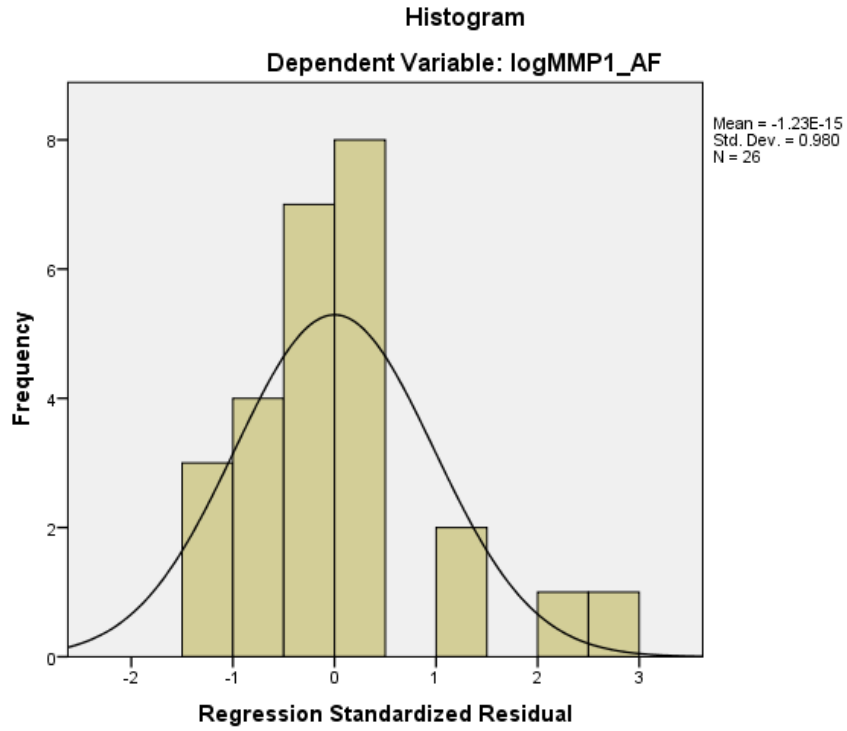
a. Dependent Variable: logMMP1_AF

b. Predictors: (Constant), WorkCum

Coefficients^a

Model	Unstandardized Coefficients		Standardized Coefficients	t	Sig.	Collinearity Statistics	
	B	Std. Error	Beta			Tolerance	VIF
1 (Constant)	.210	.069		3.054	.005		
WorkCum	.001	.000	.445	2.438	.023	1.000	1.000

a. Dependent Variable: logMMP1_AF



C.3.2 MMP-3

Model Summary^b

Model	R	R Square	Adjusted R Square	Std. Error of the Estimate	Change Statistics				
					R Square Change	F Change	df 1	df 2	Sig. F Change
1	.368 ^a	.136	.112	.18362	.136	5.649	1	36	.023

a. Predictors: (Constant), AROMmidMean

b. Dependent Variable: logMMP3_AF

ANOVA^a

Model		Sum of Squares	df	Mean Square	F	Sig.
1	Regression	.190	1	.190	5.649	.023 ^b
	Residual	1.214	36	.034		
	Total	1.404	37			

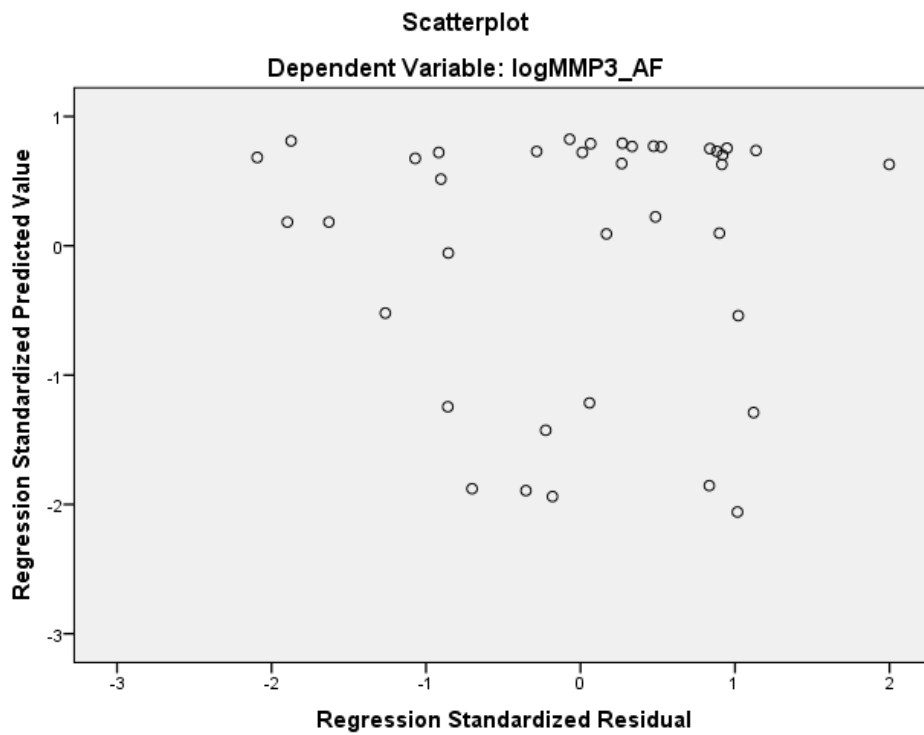
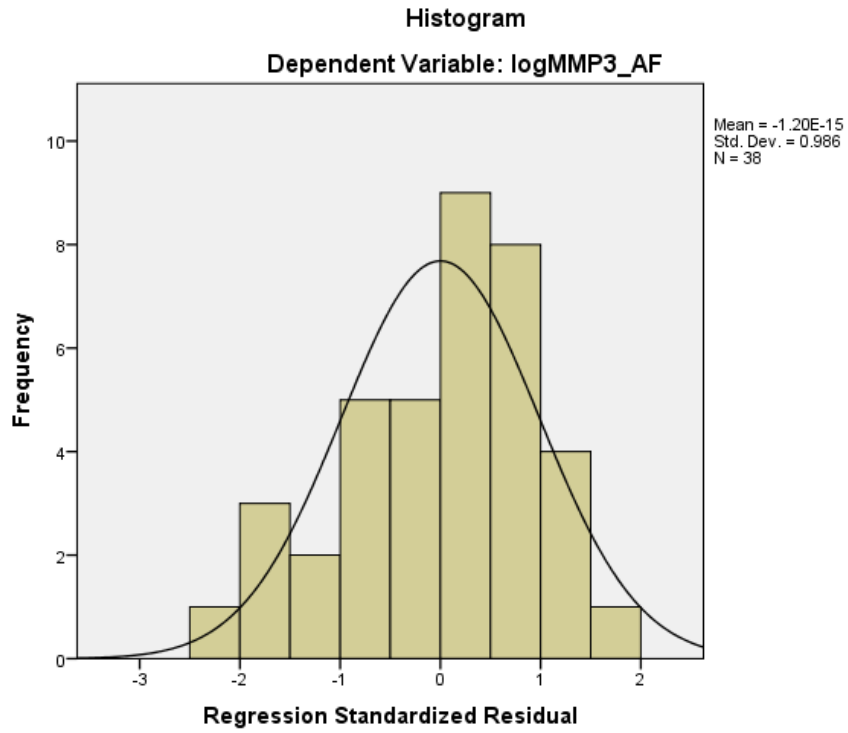
a. Dependent Variable: logMMP3_AF

b. Predictors: (Constant), AROMmidMean

Coefficients^a

Model		Unstandardized Coefficients		Standardized Coefficients	t	Sig.	Collinearity Statistics	
		B	Std. Error	Beta			Tolerance	VIF
1	(Constant)	.505	.037		13.515	.000		
	AROMmidMean	.047	.020	.368	2.377	.023	1.000	1.000

a. Dependent Variable: logMMP3_AF



C.3.3 ADAMTS-5

Model Summary^c

Model	R	R Square	Adjusted R Square	Std. Error of the Estimate	Change Statistics				
					R Square Change	F Change	df 1	df 2	Sig. F Change
1	.216 ^a	.046	.014	.09506	.046	1.413	1	29	.244
2	.393 ^b	.154	.094	.09111	.108	3.574	1	28	.069

a. Predictors: (Constant), NZMean

b. Predictors: (Constant), NZMean, MymidRelax

c. Dependent Variable: logADAMTS5_AF

ANOVA^a

Model	Sum of Squares	df	Mean Square	F	Sig.
1 Regression	.013	1	.013	1.413	.244 ^b
Residual	.262	29	.009		
Total	.275	30			
2 Regression	.042	2	.021	2.556	.096 ^c
Residual	.232	28	.008		
Total	.275	30			

a. Dependent Variable: logADAMTS5_AF

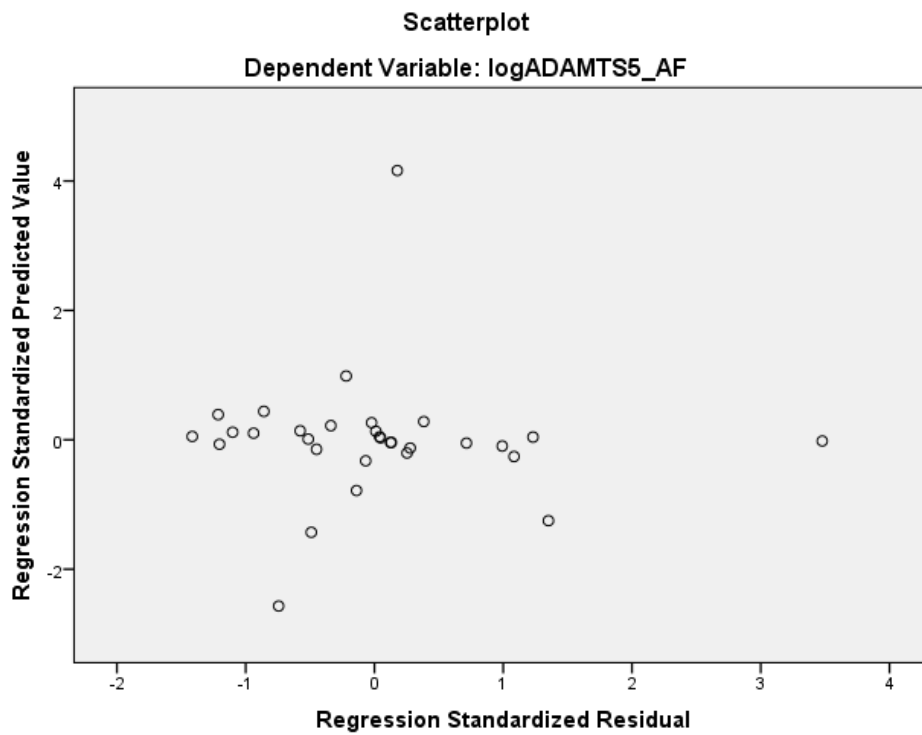
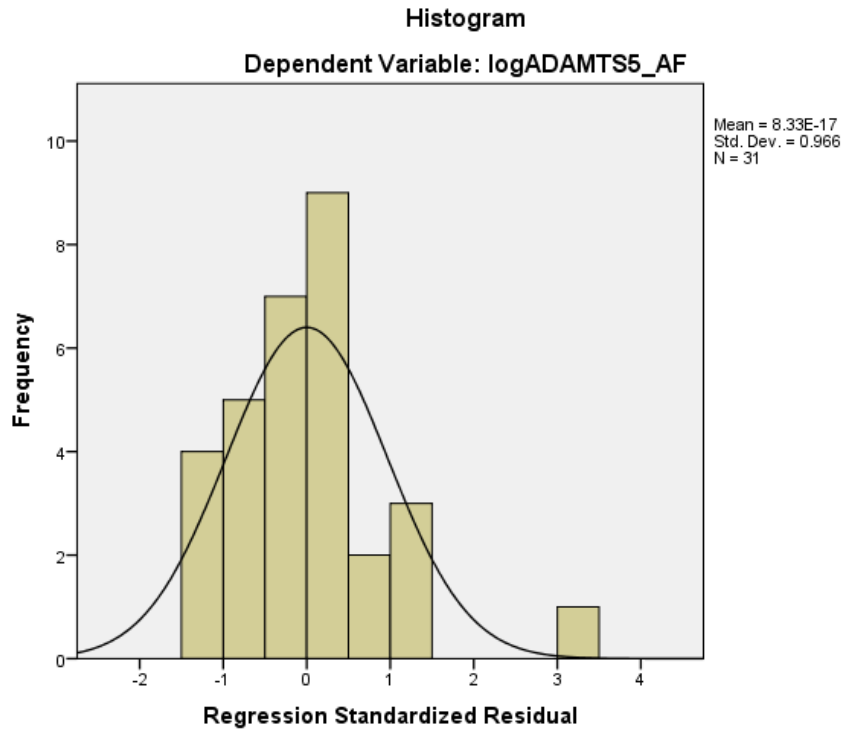
b. Predictors: (Constant), NZMean

c. Predictors: (Constant), NZMean, MymidRelax

Coefficients^a

Model	Unstandardized Coefficients		Standardized Coefficients	t	Sig.	Collinearity Statistics	
	B	Std. Error	Beta			Tolerance	VIF
1 (Constant)	.368	.032		11.655	.000		
NZMean	-1.553	1.306	-.216	-1.189	.244	1.000	1.000
2 (Constant)	.378	.031		12.307	.000		
NZMean	-2.299	1.313	-.319	-1.751	.091	.910	1.099
MymidRelax	.	.000	-.344	-1.890	.069	.910	1.099

a. Dependent Variable: logADAMTS5_AF



C.3.4 COX-2

Model Summary^c

Model	R	R Square	Adjusted R Square	Std. Error of the Estimate	Change Statistics				
					R Square Change	F Change	df 1	df 2	Sig. F Change
1	.188 ^a	.035	.007	.13470	.035	1.245	1	34	.272
2	.229 ^b	.052	-.005	.13552	.017	.589	1	33	.448

a. Predictors: (Constant), ROMfMean

b. Predictors: (Constant), ROMfMean, MxeRelax

c. Dependent Variable: logCOX2_AF

ANOVA^a

Model		Sum of Squares	df	Mean Square	F	Sig.
1	Regression	.023	1	.023	1.245	.272 ^b
	Residual	.617	34	.018		
	Total	.639	35			
2	Regression	.033	2	.017	.910	.413 ^c
	Residual	.606	33	.018		
	Total	.639	35			

a. Dependent Variable: logCOX2_AF

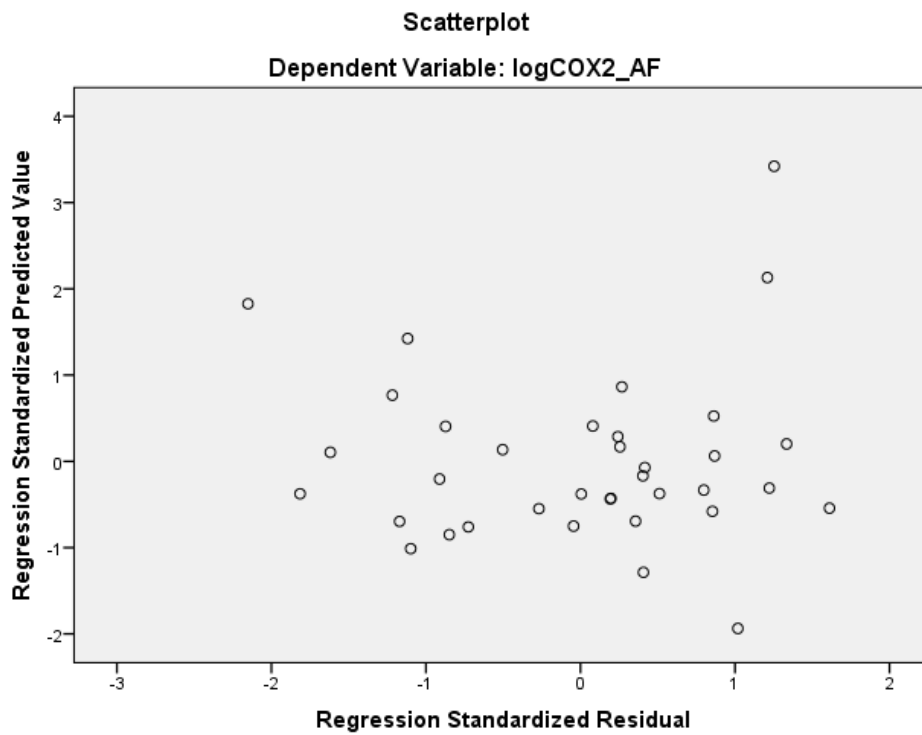
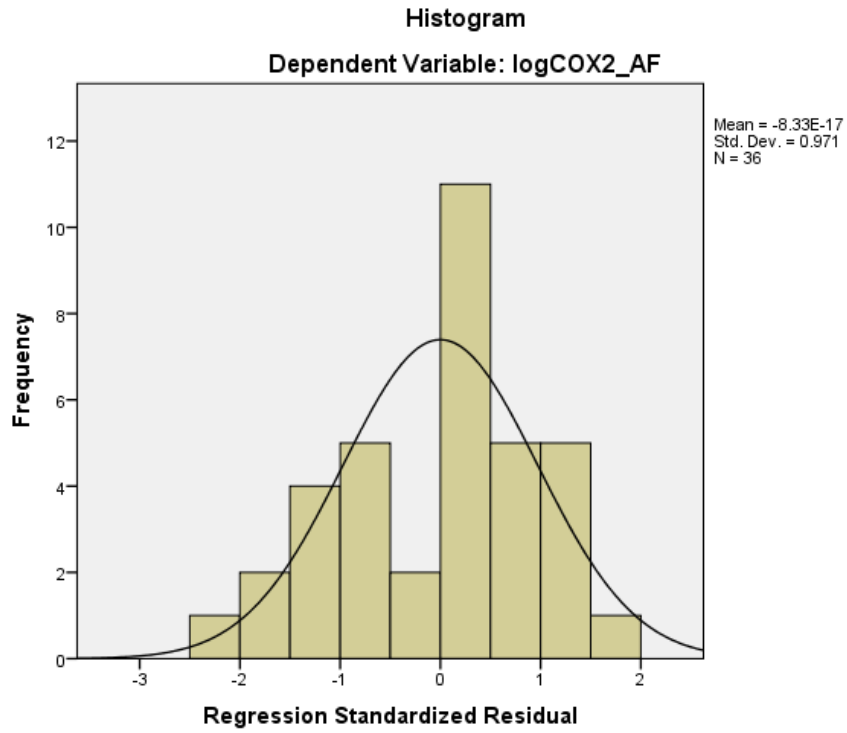
b. Predictors: (Constant), ROMfMean

c. Predictors: (Constant), ROMfMean, MxeRelax

Coefficients^a

Model		Unstandardized Coefficients		Standardized Coefficients	t	Sig.	Collinearity Statistics	
		B	Std. Error	Beta			Tolerance	VIF
1	(Constant)	.443	.098		4.525	.000		
	ROMfMean	-.007	.006	-.188	-1.116	.272	1.000	1.000
2	(Constant)	.440	.099		4.464	.000		
	ROMfMean	-.007	.006	-.178	-1.050	.301	.995	1.005
	MxeRelax	-.001	.001	-.130	-.767	.448	.995	1.005

a. Dependent Variable: logCOX2_AF



C.3.5 ACAN

Model Summary^e

Model	R	R Square	Adjusted R Square	Std. Error of the Estimate	Change Statistics				
					R Square Change	F Change	df 1	df 2	Sig. F Change
1	.364 ^a	.133	.106	.10997	.133	4.900	1	32	.034
2	.367 ^b	.135	.079	.11160	.002	.070	1	31	.793
3	.400 ^c	.160	.076	.11180	.025	.890	1	30	.353
4	.569 ^d	.324	.230	.10201	.164	7.033	1	29	.013

- a. Predictors: (Constant), HysteresisMean
- b. Predictors: (Constant), HysteresisMean, WorkCum
- c. Predictors: (Constant), HysteresisMean, WorkCum, ROMfMean
- d. Predictors: (Constant), HysteresisMean, WorkCum, ROMfMean, MymidRelax
- e. Dependent Variable: logACAN_AF

ANOVA^a

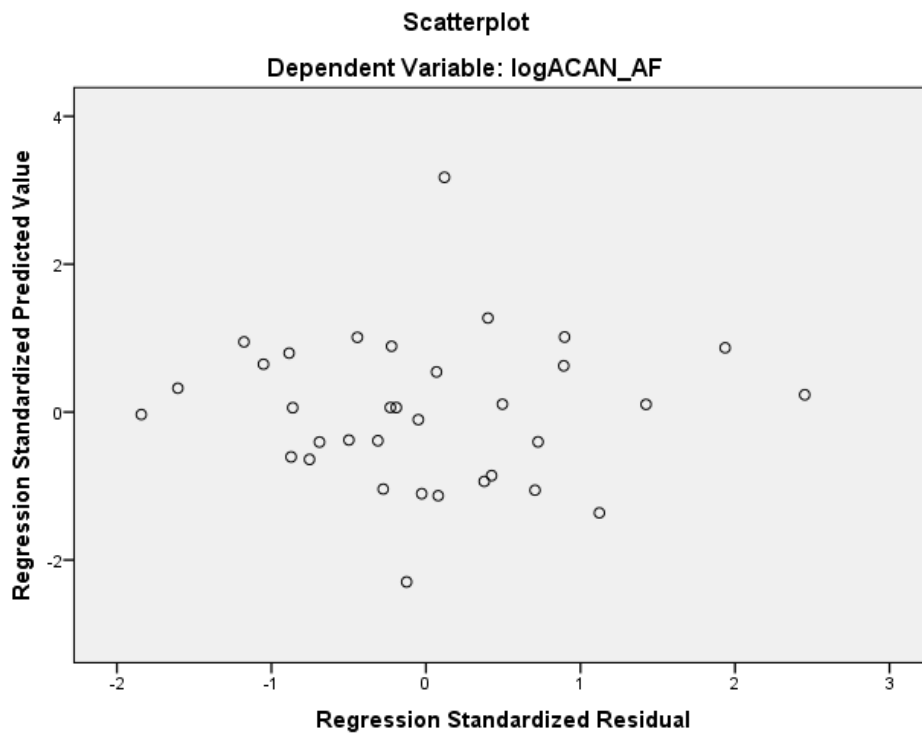
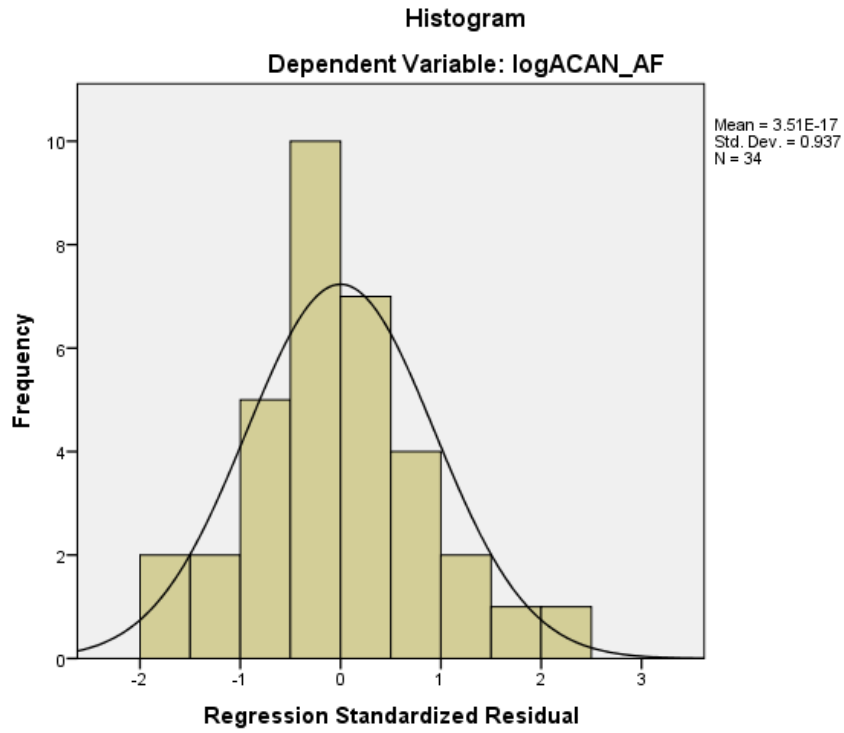
Model	Sum of Squares	df	Mean Square	F	Sig.
1 Regression	.059	1	.059	4.900	.034 ^b
Residual	.387	32	.012		
Total	.446	33			
2 Regression	.060	2	.030	2.414	.106 ^c
Residual	.386	31	.012		
Total	.446	33			
3 Regression	.071	3	.024	1.900	.151 ^d
Residual	.375	30	.012		
Total	.446	33			
4 Regression	.144	4	.036	3.470	.020 ^e
Residual	.302	29	.010		
Total	.446	33			

- a. Dependent Variable: logACAN_AF
- b. Predictors: (Constant), HysteresisMean
- c. Predictors: (Constant), HysteresisMean, WorkCum
- d. Predictors: (Constant), HysteresisMean, WorkCum, ROMfMean
- e. Predictors: (Constant), HysteresisMean, WorkCum, ROMfMean, MymidRelax

Coefficients^a

Model	Unstandardized Coefficients		Standardized Coefficients	t	Sig.	Collinearity Statistics	
	B	Std. Error	Beta			Tolerance	VIF
1 (Constant)	.457	.041		11.037	.000		
HysteresisMean	-.112	.051	-.364	2.214	.034	1.000	1.000
2 (Constant)	.470	.065		7.228	.000		
HysteresisMean	-.108	.054	-.350	1.985	.056	.899	1.112
WorkCum	#####	.000	-.047	-.265	.793	.899	1.112
3 (Constant)	.405	.095		4.281	.000		
HysteresisMean	-.103	.055	-.333	1.875	.071	.890	1.124
WorkCum	.000	.000	-.101	-.545	.590	.812	1.231
ROMfMean	.005	.006	.166	.943	.353	.903	1.107
4 (Constant)	.399	.086		4.619	.000		
HysteresisMean	-.098	.050	-.319	1.972	.058	.889	1.125
WorkCum	.000	.000	-.331	1.740	.093	.644	1.554
ROMfMean	.010	.005	.309	1.823	.079	.812	1.231
MymidRelax	.000	.000	-.465	2.652	.013	.759	1.318

a. Dependent Variable: logACAN_AF



C.4 REGRESSION RESULTS: FACET CARTILAGE

C.4.1 ADAMTS-5

Model Summary^c

Model	R	R Square	Adjusted R Square	Std. Error of the Estimate	Change Statistics				
					R Square Change	F Change	df 1	df 2	Sig. F Change
1	.401 ^a	.161	.108	.07282	.161	3.067	1	16	.099
2	.653 ^b	.427	.350	.06217	.266	6.949	1	15	.019

a. Predictors: (Constant), AROMmidMean

b. Predictors: (Constant), AROMmidMean, NZMean

c. Dependent Variable: logADAMTS5_FC

ANOVA^a

Model		Sum of Squares	df	Mean Square	F	Sig.
1	Regression	.016	1	.016	3.067	.099 ^b
	Residual	.085	16	.005		
	Total	.101	17			
2	Regression	.043	2	.022	5.578	.015 ^c
	Residual	.058	15	.004		
	Total	.101	17			

a. Dependent Variable: logADAMTS5_FC

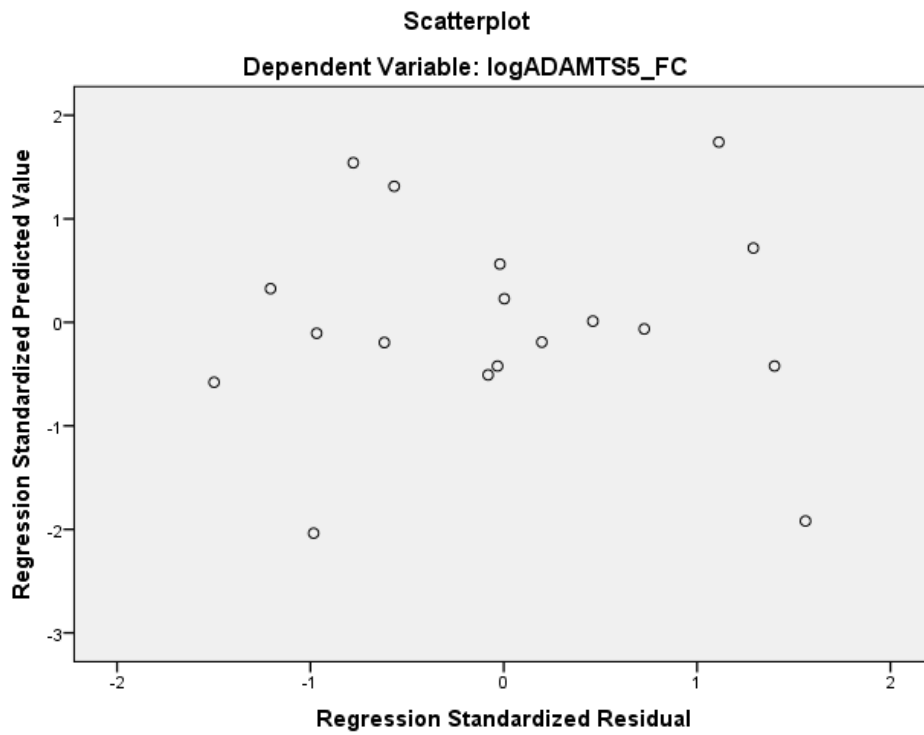
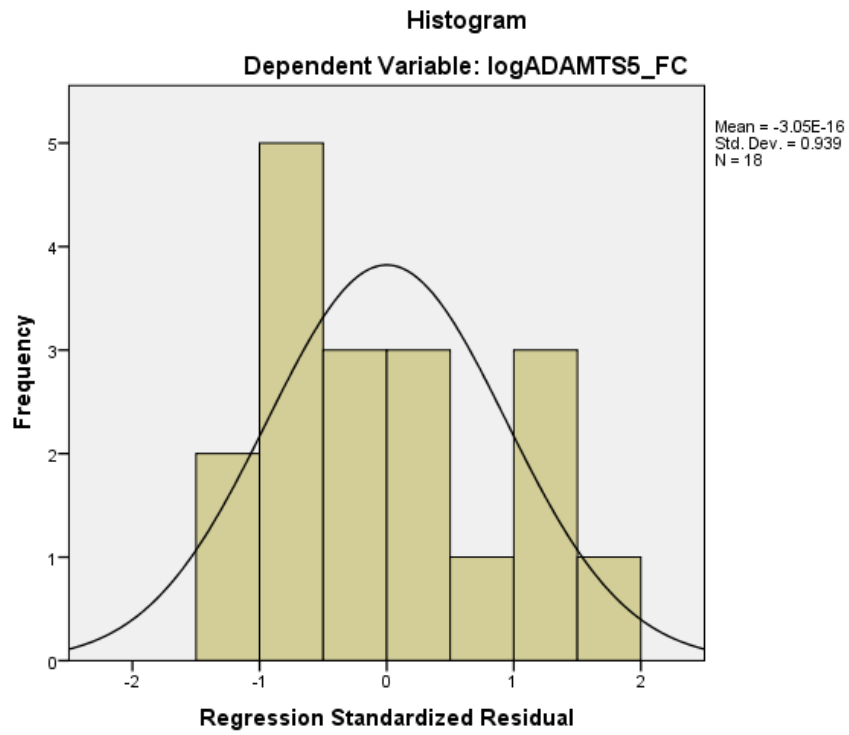
b. Predictors: (Constant), AROMmidMean

c. Predictors: (Constant), AROMmidMean, NZMean

Coefficients^a

Model		Unstandardized Coefficients		Standardized Coefficients	t	Sig.	Collinearity Statistics	
		B	Std. Error	Beta			Tolerance	VIF
1	(Constant)	.265	.018		14.424	.000		
	AROMmidMean	-.107	.061	-.401	-1.751	.099	1.000	1.000
2	(Constant)	.410	.057		7.148	.000		
	AROMmidMean	-.086	.053	-.323	-1.634	.123	.978	1.023
	NZMean	-7.670	2.910	-.521	-2.636	.019	.978	1.023

a. Dependent Variable: logADAMTS5_FC



C.4.2 COX-2

Model Summary^d

Model	R	R Square	Adjusted R Square	Std. Error of the Estimate	Change Statistics				
					R Square Change	F Change	df 1	df 2	Sig. F Change
1	.335 ^a	.112	.078	.20177	.112	3.294	1	26	.081
2	.512 ^b	.263	.204	.18755	.150	5.092	1	25	.033
3	.624 ^c	.389	.312	.17428	.126	4.952	1	24	.036

a. Predictors: (Constant), WorkCum

b. Predictors: (Constant), WorkCum, MymidRelax

c. Predictors: (Constant), WorkCum, MymidRelax, AROMmidMean

d. Dependent Variable: logCOX2_FC

ANOVA^a

Model	Sum of Squares	df	Mean Square	F	Sig.
1 Regression	.134	1	.134	3.294	.081 ^b
Residual	1.059	26	.041		
Total	1.193	27			
2 Regression	.313	2	.157	4.452	.022 ^c
Residual	.879	25	.035		
Total	1.193	27			
3 Regression	.464	3	.155	5.088	.007 ^d
Residual	.729	24	.030		
Total	1.193	27			

a. Dependent Variable: logCOX2_FC

b. Predictors: (Constant), WorkCum

c. Predictors: (Constant), WorkCum, MymidRelax

d. Predictors: (Constant), WorkCum, MymidRelax, AROMmidMean

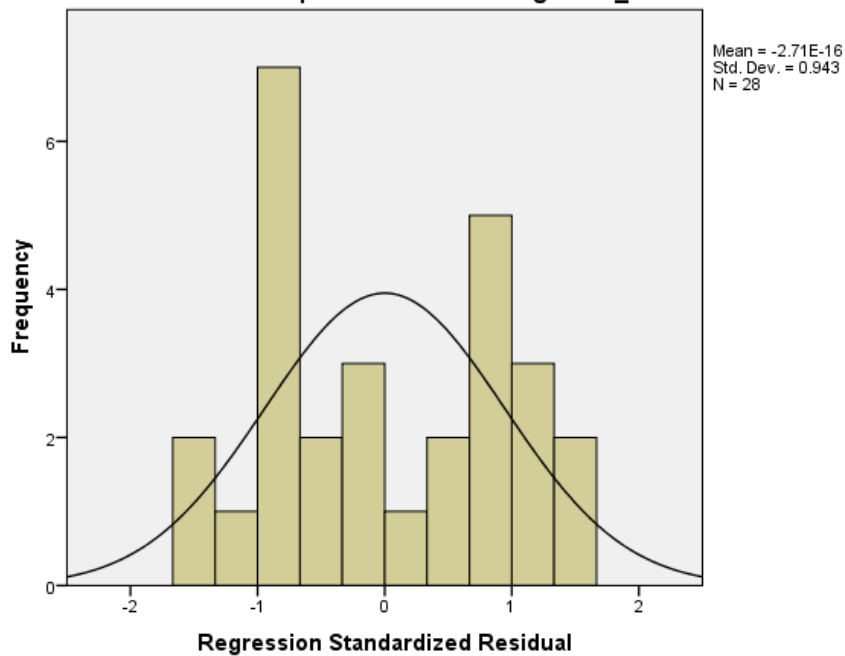
Coefficients^a

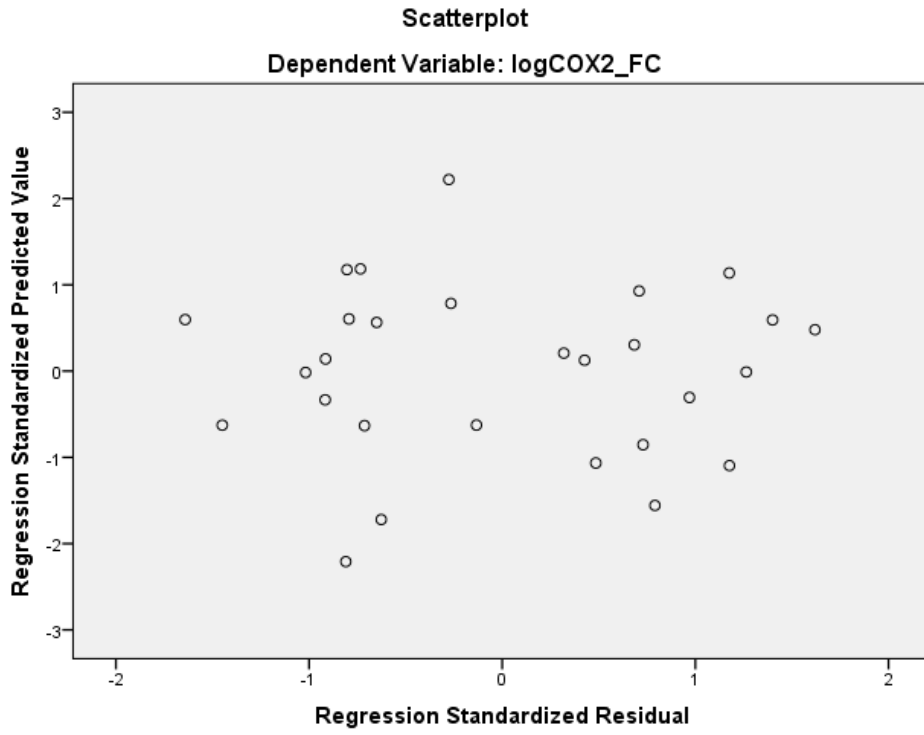
Model	Unstandardized Coefficients		Standardized Coefficients	t	Sig.	Collinearity Statistics	
	B	Std. Error	Beta			Tolerance	VIF
1 (Constant)	.695	.119		5.861	.000		
WorkCum	-.001	.000	-.335	-1.815	.081	1.000	1.000
2 (Constant)	.768	.115		6.685	.000		
WorkCum	-.001	.000	-.495	-2.665	.013	.855	1.170
MymidRelax	.000	.000	-.419	-2.257	.033	.855	1.170
3 (Constant)	.789	.107		7.360	.000		
WorkCum	-.002	.000	-.652	-3.496	.002	.733	1.364
MymidRelax	.000	.000	-.573	-3.082	.005	.736	1.358
AROMmidMean	-.052	.023	-.395	-2.225	.036	.808	1.237

a. Dependent Variable: logCOX2_FC

Histogram

Dependent Variable: logCOX2_FC





C.4.3 ACAN

Model Summary^d

Model	R	R Square	Adjusted R Square	Std. Error of the Estimate	Change Statistics				
					R Square Change	F Change	df 1	df 2	Sig. F Change
1	.454 ^a	.206	.164	.09373	.206	4.925	1	19	.039
2	.496 ^b	.247	.163	.09380	.041	.971	1	18	.337
3	.629 ^c	.396	.289	.08642	.149	4.206	1	17	.056

- a. Predictors: (Constant), AROMmidMean
- b. Predictors: (Constant), AROMmidMean, WorkCum
- c. Predictors: (Constant), AROMmidMean, WorkCum, MymidRelax
- d. Dependent Variable: logACAN_FC

ANOVA^a

Model		Sum of Squares	df	Mean Square	F	Sig.
1	Regression	.043	1	.043	4.925	.039 ^b
	Residual	.167	19	.009		
	Total	.210	20			
2	Regression	.052	2	.026	2.944	.078 ^c
	Residual	.158	18	.009		
	Total	.210	20			
3	Regression	.083	3	.028	3.715	.032 ^d
	Residual	.127	17	.007		
	Total	.210	20			

- a. Dependent Variable: logACAN_FC
- b. Predictors: (Constant), AROMmidMean
- c. Predictors: (Constant), AROMmidMean, WorkCum
- d. Predictors: (Constant), AROMmidMean, WorkCum, MymidRelax

Coefficients^a

Model	Unstandardized Coefficients		Standardized Coefficients	t	Sig.	Collinearity Statistics	
	B	Std. Error	Beta			Tolerance	VIF
1 (Constant)	.288	.023		12.296	.000		
AROMmidMea n	.030	.014	.454	2.219	.039	1.000	1.000
2 (Constant)	.239	.055		4.328	.000		
AROMmidMea n	.035	.014	.517	2.411	.027	.910	1.099
WorkCum	.000	.000	.211	.985	.337	.910	1.099
3 (Constant)	.200	.054		3.693	.002		
AROMmidMea n	.046	.014	.681	3.195	.005	.782	1.278
WorkCum	.000	.000	.463	1.991	.063	.656	1.524
MymidRelax	.000	.000	.464	2.051	.056	.695	1.439

a. Dependent Variable: logACAN_FC

C.5 REGRESSION RESULTS: NUCLEUS PULPOSUS

C.5.1 MMP-3

Model Summary^b

Model	R	R Square	Adjusted R Square	Std. Error of the Estimate	Change Statistics				
					R Square Change	F Change	df 1	df 2	Sig. F Change
1	.116 ^a	.013	-.025	.27039	.013	.353	1	26	.558

a. Predictors: (Constant), ROMeMean

b. Dependent Variable: logMMP3_NP

ANOVA^a

Model	Sum of Squares	df	Mean Square	F	Sig.
1 Regression	.026	1	.026	.353	.558 ^b
Residual	1.901	26	.073		
Total	1.927	27			

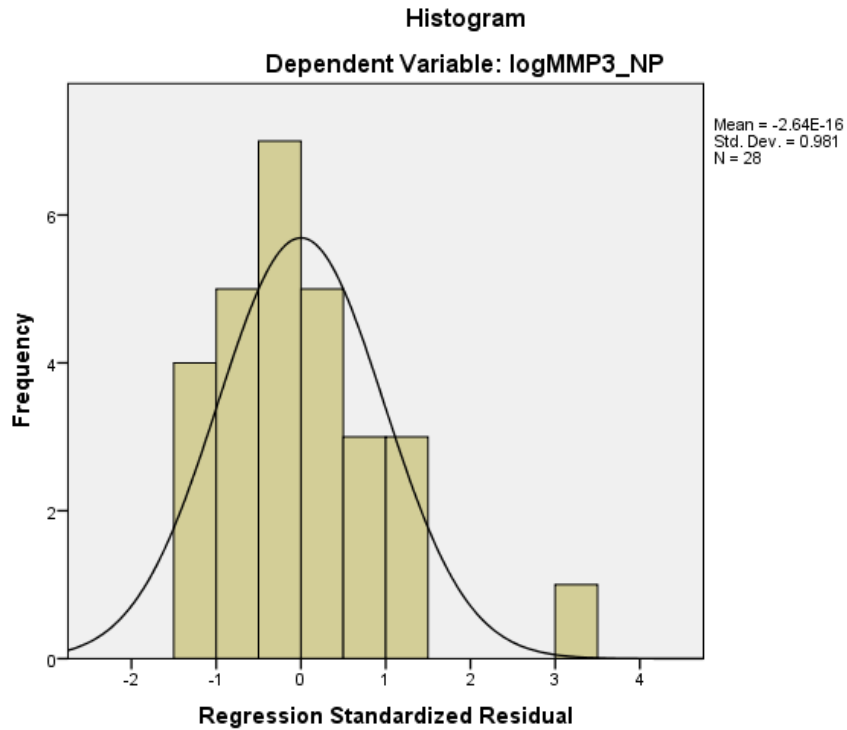
a. Dependent Variable: logMMP3_NP

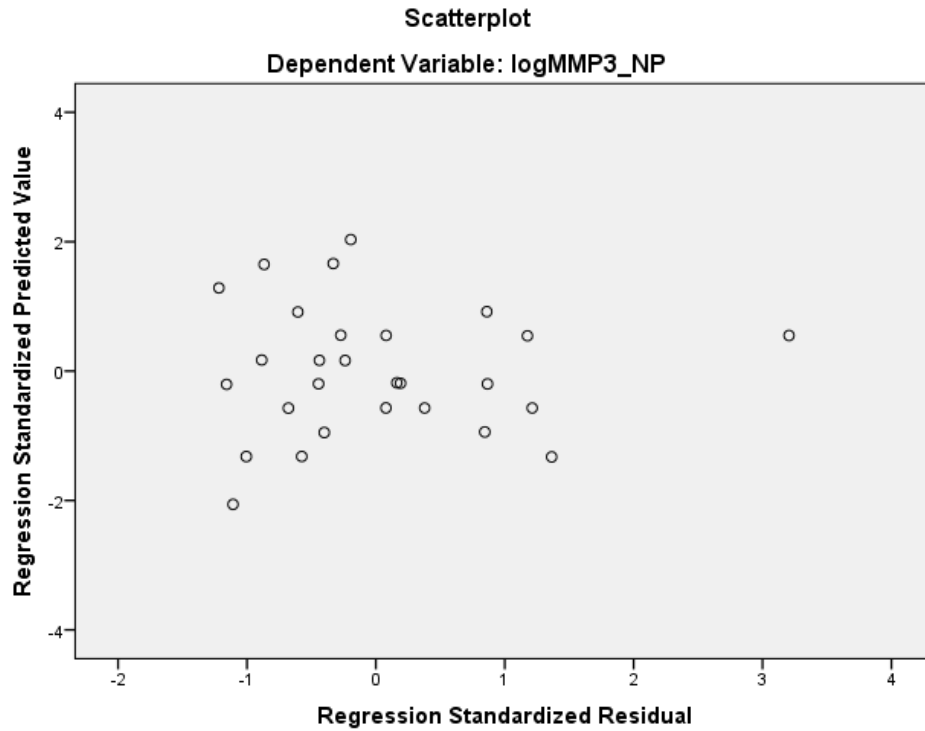
b. Predictors: (Constant), ROMEan

Coefficients^a

Model	Unstandardized Coefficients		Standardized Coefficients	t	Sig.	Collinearity Statistics	
	B	Std. Error	Beta			Tolerance	VIF
1 (Constant)	.456	.084		5.423	.000		
ROMEan	.012	.019	.116	.594	.558	1.000	1.000

a. Dependent Variable: logMMP3_NP





C.5.2 COX-2

Model Summary^c

Model	R	R Square	Adjusted R Square	Std. Error of the Estimate	Change Statistics				
					R Square Change	F Change	df 1	df 2	Sig. F Change
1	.188 ^a	.035	-.011	.17603	.035	.769	1	2	.391
2	.206 ^b	.042	-.053	.17972	.007	.147	1	2	.706

a. Predictors: (Constant), HysteresisMean

b. Predictors: (Constant), HysteresisMean, ROMEan

c. Dependent Variable: logCOX2_NP

ANOVA^a

Model	Sum of Squares	df	Mean Square	F	Sig.
1 Regression	.024	1	.024	.769	.391 ^b
Residual	.651	21	.031		
Total	.675	22			
2 Regression	.029	2	.014	.442	.649 ^c
Residual	.646	20	.032		
Total	.675	22			

a. Dependent Variable: logCOX2_NP

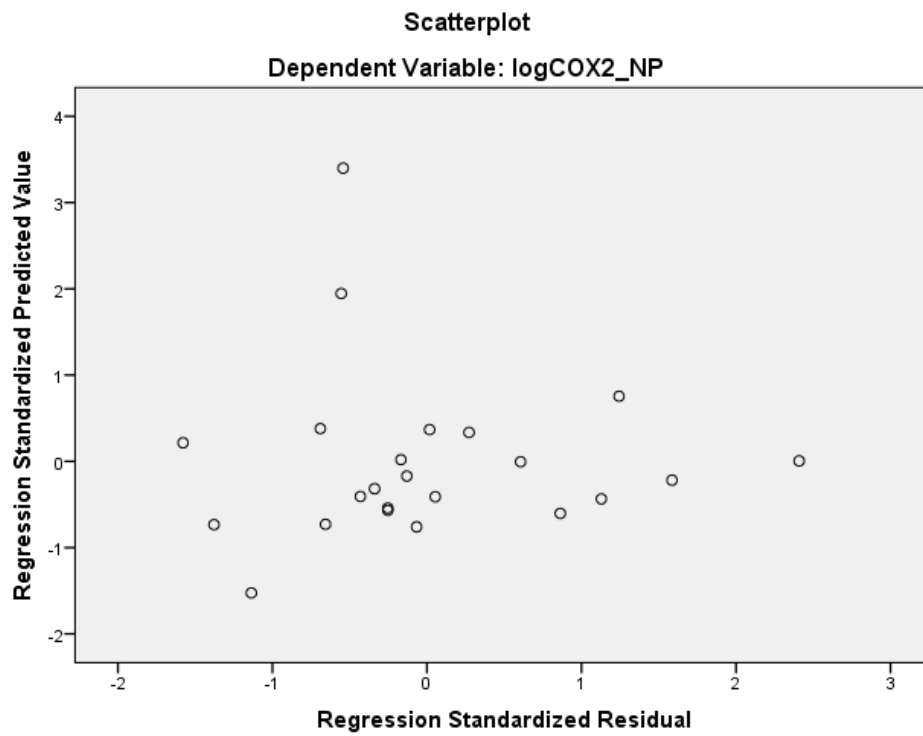
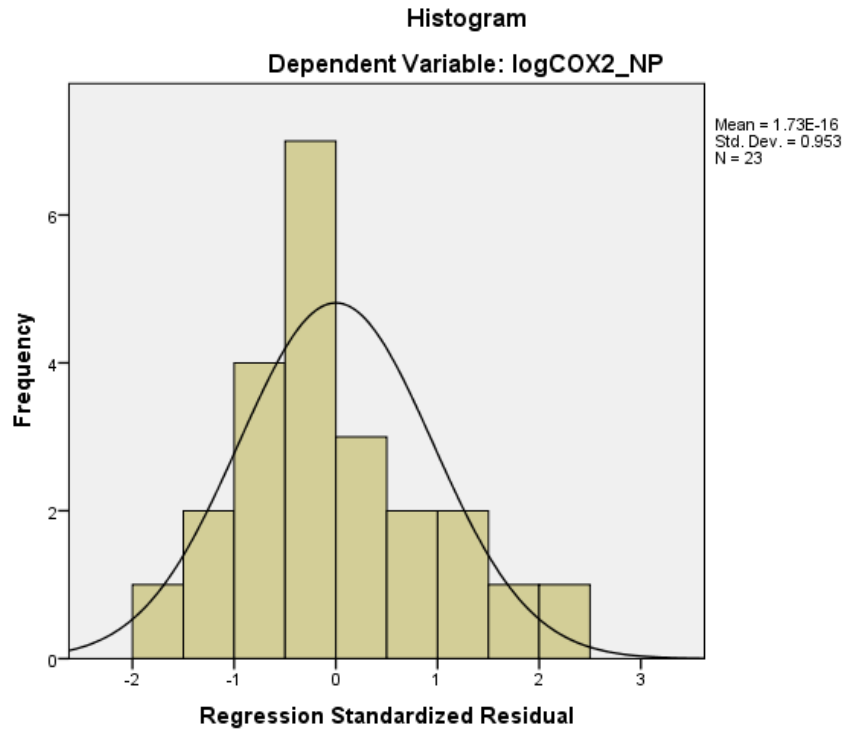
b. Predictors: (Constant), HysteresisMean

c. Predictors: (Constant), HysteresisMean, ROMEan

Coefficients^a

Model	Unstandardized Coefficients		Standardized Coefficients	t	Sig.	Collinearity Statistics	
	B	Std. Error	Beta			Tolerance	VIF
1 (Constant)	.316	.082		3.856	.001		
HysteresisMean	.083	.095	.188	.877	.391	1.000	1.000
2 (Constant)	.340	.104		3.252	.004		
HysteresisMean	.077	.099	.173	.777	.446	.968	1.033
ROMEan	.006	.015	.085	.383	.706	.968	1.033

a. Dependent Variable: logCOX2_NP



C.5.3 ACAN

Model Summary^d

Model	R	R Square	Adjusted R Square	Std. Error of the Estimate	Change Statistics				
					R Square Change	F Change	df 1	df 2	Sig. F Change
1	.292 _a	.086	.015	.14581	.086	1.216	1	13	.290
2	.359 _b	.129	-.017	.14814	.043	.595	1	12	.456
3	.478 _c	.228	.018	.14561	.100	1.421	1	11	.258

a. Predictors: (Constant), MxeRelax

b. Predictors: (Constant), MxeRelax, NZMean

c. Predictors: (Constant), MxeRelax, NZMean, ROMfMean

d. Dependent Variable: logACAN_NP

ANOVA^a

Model		Sum of Squares	df	Mean Square	F	Sig.
1	Regression	.026	1	.026	1.216	.290 ^b
	Residual	.276	13	.021		
	Total	.302	14			
2	Regression	.039	2	.019	.886	.438 ^c
	Residual	.263	12	.022		
	Total	.302	14			
3	Regression	.069	3	.023	1.085	.396 ^d
	Residual	.233	11	.021		
	Total	.302	14			

a. Dependent Variable: logACAN_NP

b. Predictors: (Constant), MxeRelax

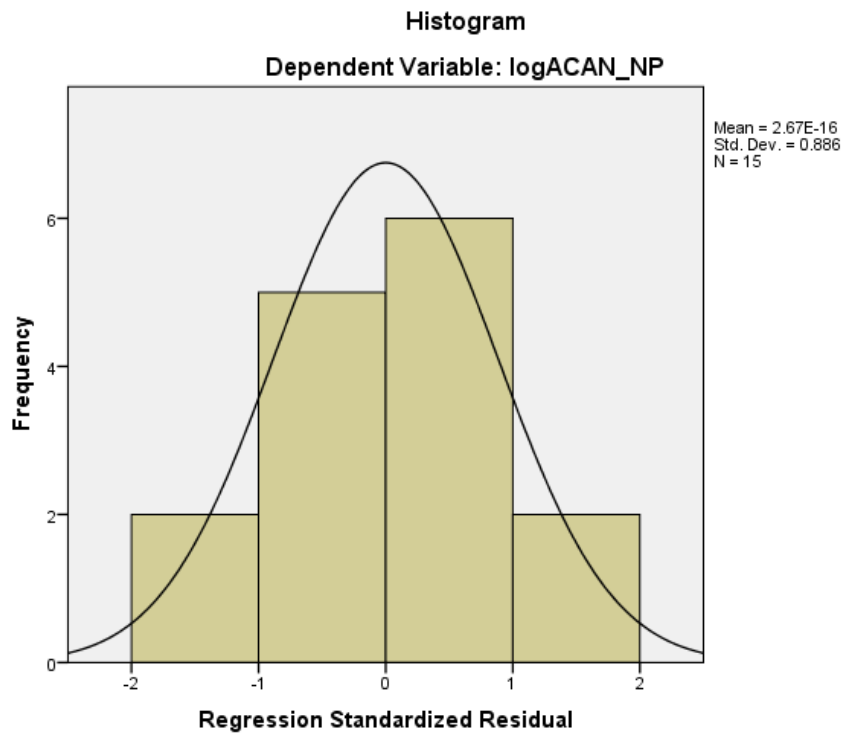
c. Predictors: (Constant), MxeRelax, NZMean

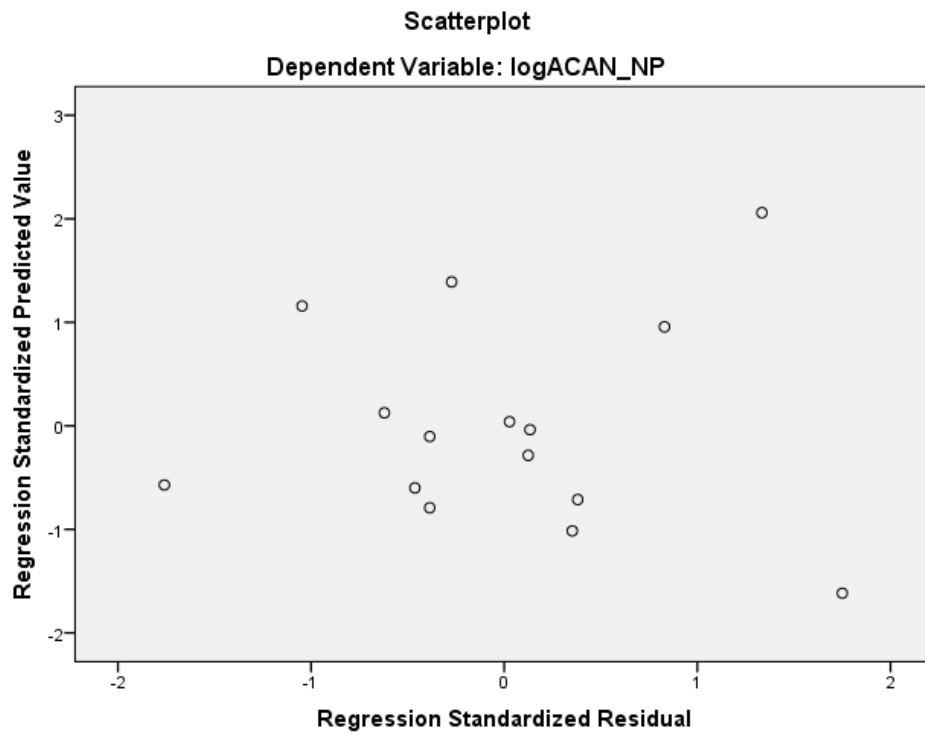
d. Predictors: (Constant), MxeRelax, NZMean, ROMfMean

Coefficients^a

Model	Unstandardized Coefficients		Standardized Coefficients	t	Sig.	Collinearity Statistics	
	B	Std. Error	Beta			Tolerance	VIF
1 (Constant)	.296	.038		7.860	.000		
MxeRelax	.001	.001	.292	1.103	.290	1.000	1.000
2 (Constant)	.161	.179		.899	.387		
MxeRelax	.002	.001	.487	1.319	.212	.534	1.873
NZMean	7.532	9.769	.284	.771	.456	.534	1.873
3 (Constant)	-.475	.562		-.846	.416		
MxeRelax	.003	.002	.842	1.794	.100	.318	3.144
NZMean	22.666	15.917	.856	1.424	.182	.194	5.148
ROMfMean	.023	.019	.525	1.192	.258	.362	2.760

a. Dependent Variable: logACAN_NP





C.6 REGRESSION RESULTS: LIGAMENTUM FLAVUM

C.6.1 MMP-1

Model Summary^d

Model	R	R Square	Adjusted R Square	Std. Error of the Estimate	Change Statistics				
					R Square Change	F Change	df 1	df 2	Sig. F Change
1	.296 ^a	.088	.054	.18201	.088	2.591	1	27	.119
2	.553 ^b	.306	.253	.16175	.219	8.188	1	26	.008
3	.609 ^c	.370	.295	.15713	.064	2.550	1	25	.123

a. Predictors: (Constant), NZMean

b. Predictors: (Constant), NZMean, WorkCum

c. Predictors: (Constant), NZMean, WorkCum, ROMfMean

d. Dependent Variable: logMMP1_LF

ANOVA^a

Model		Sum of Squares	df	Mean Square	F	Sig.
1	Regression	.086	1	.086	2.591	.119 _b
	Residual	.894	27	.033		
	Total	.980	28			
2	Regression	.300	2	.150	5.734	.009 ^c
	Residual	.680	26	.026		
	Total	.980	28			
3	Regression	.363	3	.121	4.901	.008 _d
	Residual	.617	25	.025		
	Total	.980	28			

a. Dependent Variable: logMMP1_LF

b. Predictors: (Constant), NZMean

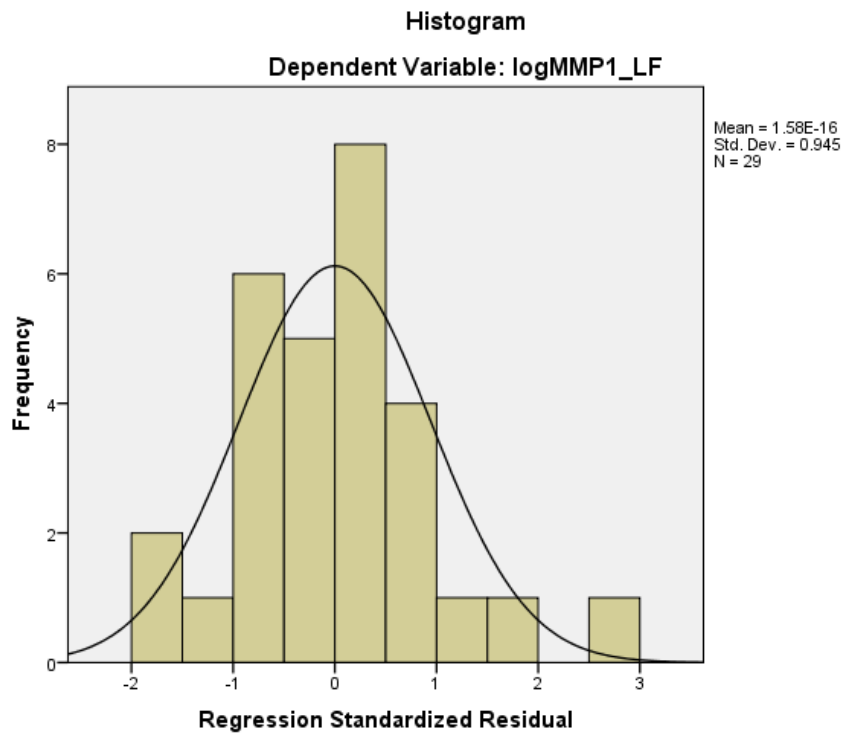
c. Predictors: (Constant), NZMean, WorkCum

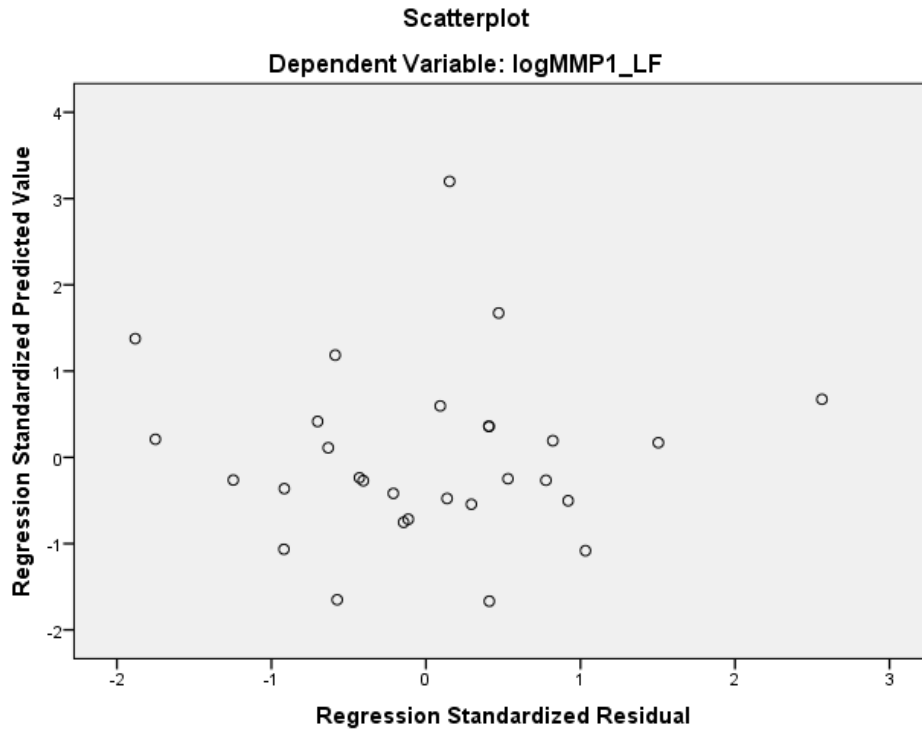
d. Predictors: (Constant), NZMean, WorkCum, ROMfMean

Coefficients^a

Model	Unstandardized Coefficients		Standardized Coefficients	t	Sig.	Collinearity Statistics	
	B	Std. Error	Beta			Tolerance	VIF
1 (Constant)	.253	.063		4.038	.000		
NZMean	3.980	2.473	.296	1.610	.119	1.000	1.000
2 (Constant)	.010	.102		.094	.926		
NZMean	3.282	2.211	.244	1.485	.150	.988	1.012
WorkCum	.001	.000	.470	2.861	.008	.988	1.012
3 (Constant)	-.228	.179		-1.278	.213		
NZMean	6.342	2.878	.471	2.203	.037	.550	1.817
WorkCum	.001	.000	.337	1.867	.074	.775	1.291
ROMfMean	.017	.011	.357	1.597	.123	.505	1.979

a. Dependent Variable: logMMP1_LF





C.6.2 MMP-3

Model Summary^b

Model	R	R Square	Adjusted R Square	Std. Error of the Estimate	Change Statistics				
					R Square Change	F Change	df 1	df 2	Sig. F Change
1	.175 ^a	.031	-.005	.24579	.031	.856	1	27	.363

a. Predictors: (Constant), ROMfMean

b. Dependent Variable: logMMP3_LF

ANOVA^a

Model	Sum of Squares	df	Mean Square	F	Sig.
1 Regression	.052	1	.052	.856	.363 ^b
Residual	1.631	27	.060		
Total	1.683	28			

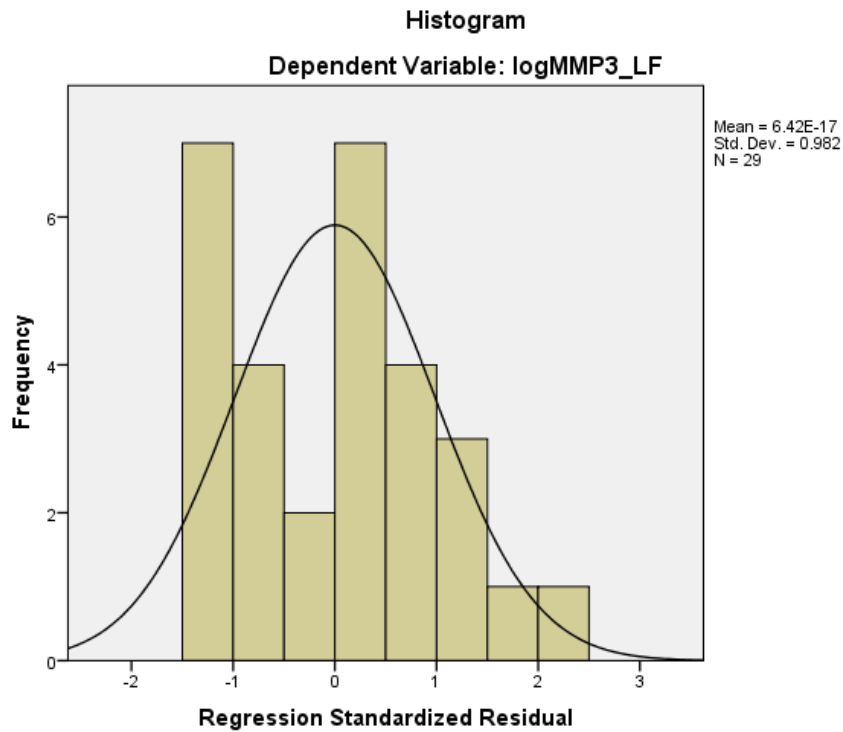
a. Dependent Variable: logMMP3_LF

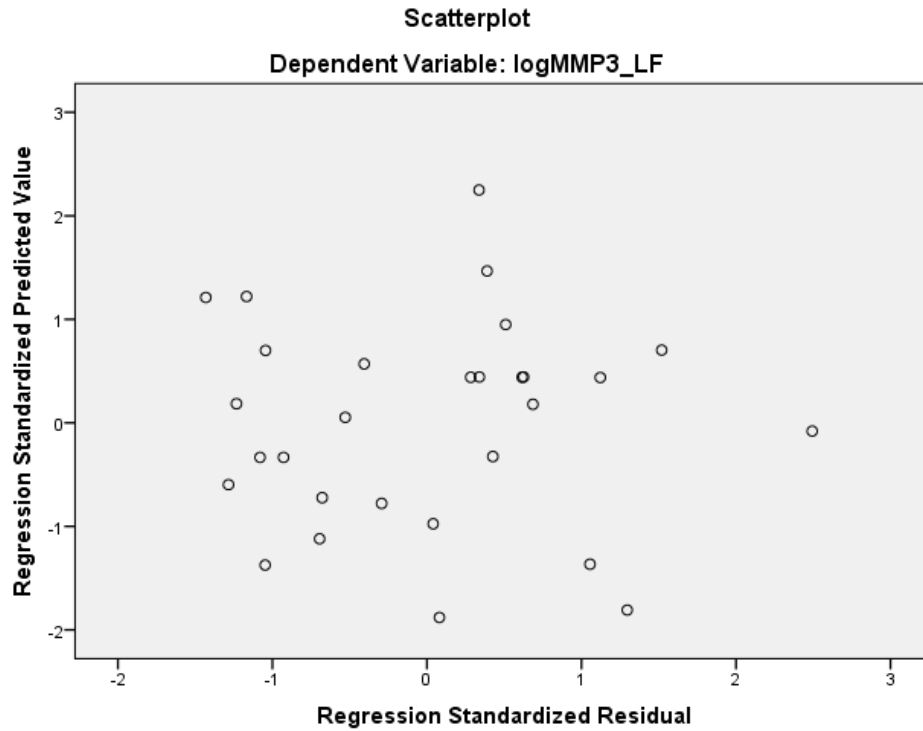
b. Predictors: (Constant), ROMfMean

Coefficients^a

Model	Unstandardized Coefficients		Standardized Coefficients	t	Sig.	Collinearity Statistics	
	B	Std. Error	Beta			Tolerance	VIF
1 (Constant)	.293	.177		1.654	.110		
ROMfMean	.011	.012	.175	.925	.363	1.000	1.000

a. Dependent Variable: logMMP3_LF





C.6.3 ADAMTS-5

Model Summary^d

Model	R	R Square	Adjusted R Square	Std. Error of the Estimate	Change Statistics				
					R Square Change	F Change	df 1	df 2	Sig. F Change
1	.357 ^a	.127	.096	.20048	.127	4.080	1	28	.053
2	.440 ^b	.194	.134	.19624	.066	2.223	1	27	.148
3	.564 ^c	.319	.240	.18383	.125	4.769	1	26	.038

a. Predictors: (Constant), NZMean

b. Predictors: (Constant), NZMean, MymidRelax

c. Predictors: (Constant), NZMean, MymidRelax, ROMfMean

d. Dependent Variable: logADAMTS5_LF

ANOVA^a

Model		Sum of Squares	df	Mean Square	F	Sig.
1	Regression	.164	1	.164	4.080	.053 ^b
	Residual	1.125	28	.040		
	Total	1.289	29			
2	Regression	.250	2	.125	3.241	.055 ^c
	Residual	1.040	27	.039		
	Total	1.289	29			
3	Regression	.411	3	.137	4.052	.017 ^d
	Residual	.879	26	.034		
	Total	1.289	29			

a. Dependent Variable: logADAMTS5_LF

b. Predictors: (Constant), NZMean

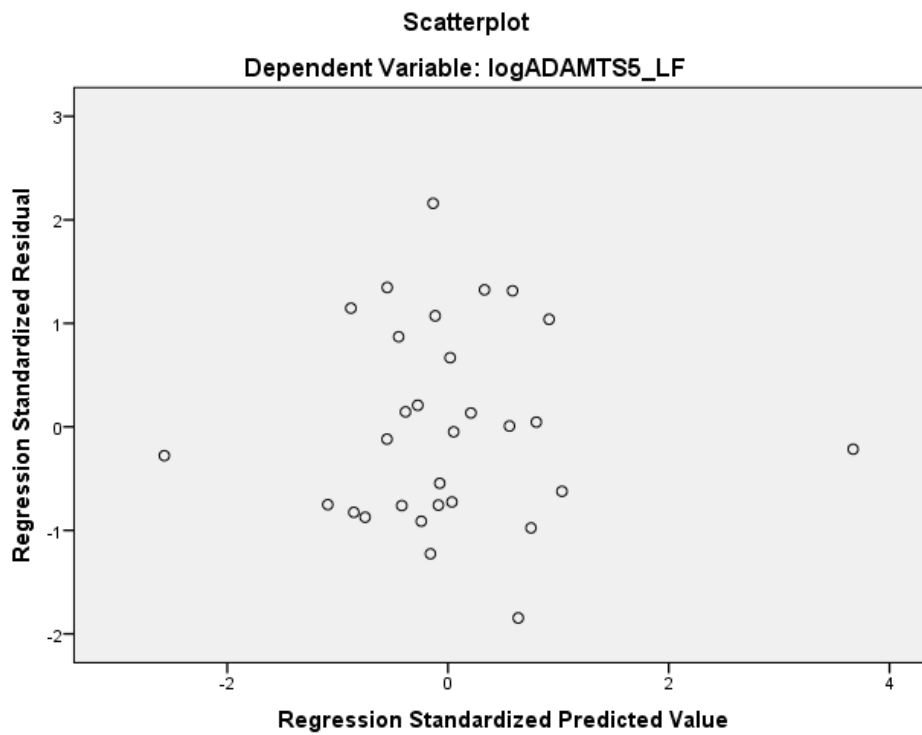
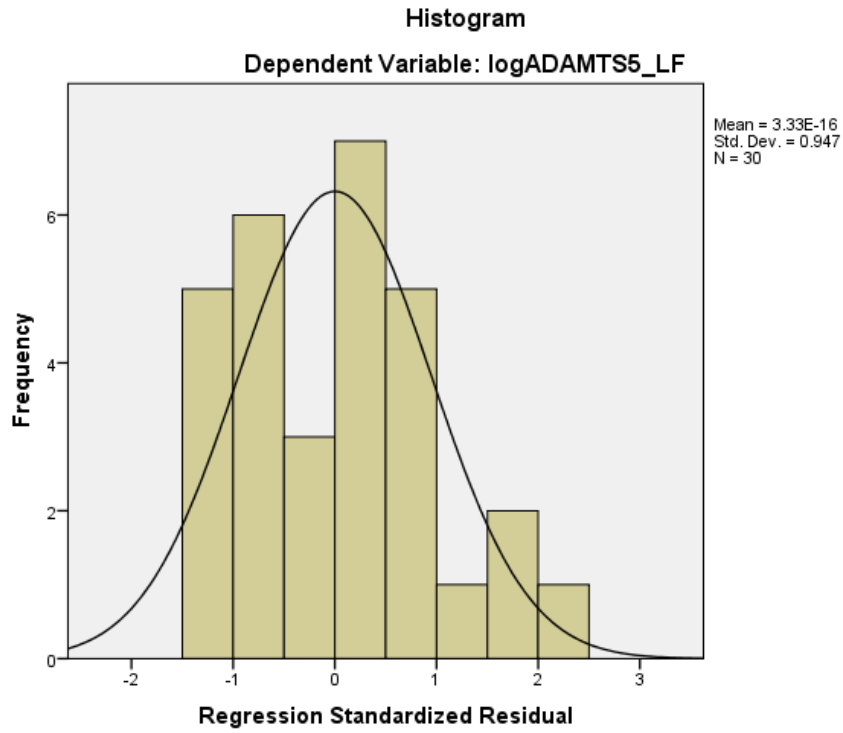
c. Predictors: (Constant), NZMean, MymidRelax

d. Predictors: (Constant), NZMean, MymidRelax, ROMfMean

Coefficients^a

Model	Unstandardized Coefficients		Standardized Coefficients	t	Sig.	Collinearity Statistics	
	B	Std. Error	Beta			Tolerance	VIF
1	(Constant)	.240	.068		.002		
	NZMean	5.499	2.722	.357	2.020	.053	1.000
2	(Constant)	.229	.067		.002		
	NZMean	6.641	2.773	.431	2.395	.024	.924
	MymidRelax	.000	.000	.268	1.491	.148	.924
3	(Constant)	-.207	.210		-.990	.331	
	NZMean	10.810	3.223	.701	3.354	.002	.600
	MymidRelax	.000	.000	.295	1.747	.093	.919
	ROMfMean	.024	.011	.441	2.184	.038	.642

a. Dependent Variable: logADAMTS5_LF



C.6.4 COX-2

Model Summary^e

Model	R	R Square	Adjusted R Square	Std. Error of the Estimate	Change Statistics				
					R Square Change	F Change	df 1	df 2	Sig. F Change
1	.458 ^a	.210	.179	.23859	.210	6.897	1	26	.014
2	.514 ^b	.264	.206	.23473	.055	1.863	1	25	.184
3	.566 ^c	.320	.235	.23037	.055	1.956	1	24	.175
4	.710 ^d	.504	.418	.20091	.184	8.552	1	23	.008

- a. Predictors: (Constant), AROMmidMean
 b. Predictors: (Constant), AROMmidMean, NZMean
 c. Predictors: (Constant), AROMmidMean, NZMean, MymidRelax
 d. Predictors: (Constant), AROMmidMean, NZMean, MymidRelax, ROMfMean
 e. Dependent Variable: logCOX2_LF

ANOVA^a

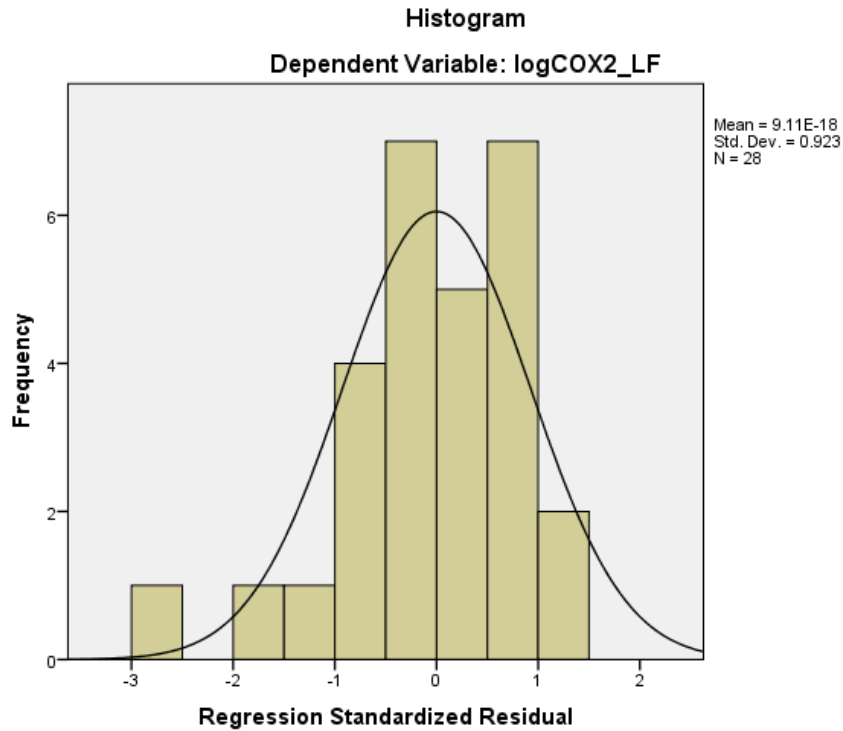
Model	Sum of Squares	df	Mean Square	F	Sig.
1 Regression	.393	1	.393	6.897	.014 ^b
Residual	1.480	26	.057		
Total	1.873	27			
2 Regression	.495	2	.248	4.494	.022 ^c
Residual	1.377	25	.055		
Total	1.873	27			
3 Regression	.599	3	.200	3.763	.024 ^d
Residual	1.274	24	.053		
Total	1.873	27			
4 Regression	.944	4	.236	5.848	.002 ^e
Residual	.928	23	.040		
Total	1.873	27			

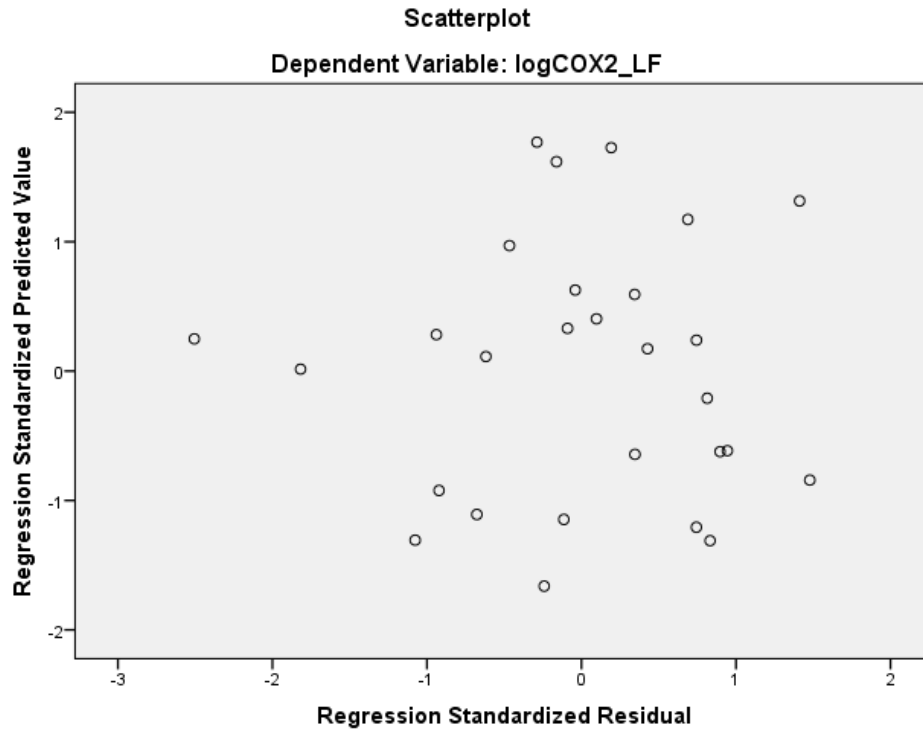
- a. Dependent Variable: logCOX2_LF
 b. Predictors: (Constant), AROMmidMean
 c. Predictors: (Constant), AROMmidMean, NZMean
 d. Predictors: (Constant), AROMmidMean, NZMean, MymidRelax
 e. Predictors: (Constant), AROMmidMean, NZMean, MymidRelax, ROMfMean

Coefficients^a

Model	Unstandardized Coefficients		Standardized Coefficients	t	Sig.	Collinearity Statistics	
	B	Std. Error	Beta			Tolerance	VIF
1 (Constant)	.442	.055		8.020	.000		
AROMmidMean	-.091	.035	-.458	-2.626	.014	1.000	1.000
2 (Constant)	.339	.093		3.638	.001		
AROMmidMean	-.100	.035	-.503	-2.881	.008	.964	1.038
NZMean	4.438	3.251	.238	1.365	.184	.964	1.038
3 (Constant)	.285	.099		2.886	.008		
AROMmidMean	-.101	.034	-.507	-2.957	.007	.963	1.038
NZMean	7.333	3.804	.394	1.928	.066	.678	1.475
MymidRelax	.000	.000	.282	1.398	.175	.698	1.433
4 (Constant)	-.389	.246		-1.580	.128		
AROMmidMean	-.089	.030	-.448	-2.965	.007	.946	1.057
NZMean	14.590	4.143	.784	3.522	.002	.435	2.300
MymidRelax	.000	.000	.404	2.234	.035	.661	1.513
ROMfMean	.037	.013	.557	2.924	.008	.594	1.682

a. Dependent Variable: logCOX2_LF





C.6.5 ACAN

Model Summary^b

Model	R	R Square	Adjusted R Square	Std. Error of the Estimate	Change Statistics				
					R Square Change	F Change	df 1	df 2	Sig. F Change
1	.284 ^a	.081	.047	.18053	.081	2.377	1	27	.135

a. Predictors: (Constant), NZMean

b. Dependent Variable: logACAN_LF

ANOVA^a

Model	Sum of Squares	df	Mean Square	F	Sig.
1 Regression	.077	1	.077	2.377	.135 ^b
Residual	.880	27	.033		
Total	.957	28			

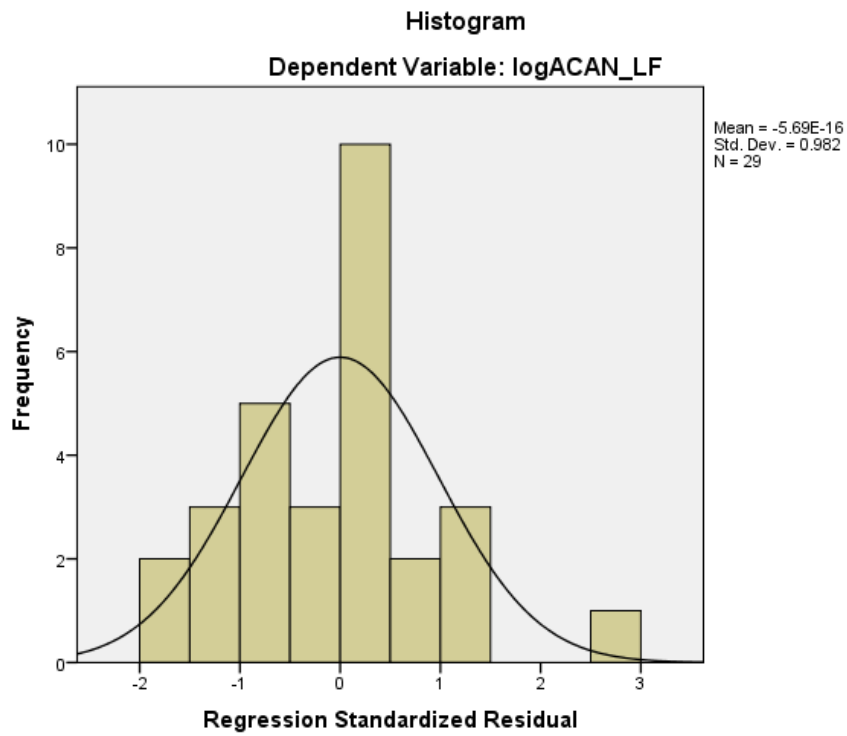
a. Dependent Variable: logACAN_LF

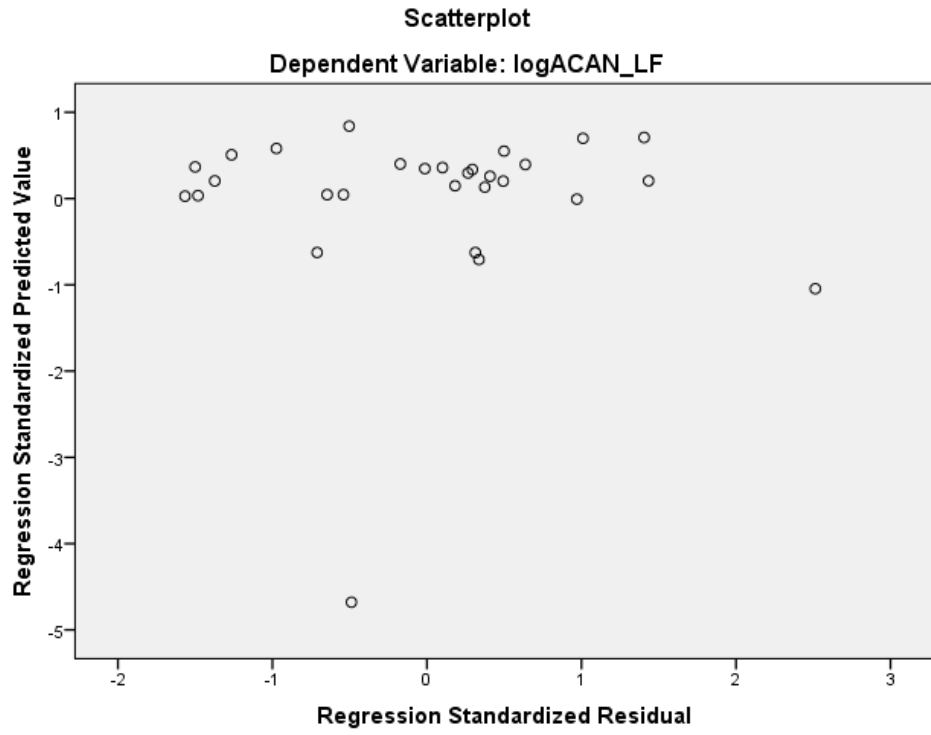
b. Predictors: (Constant), NZMean

Coefficients^a

Model	Unstandardized Coefficients		Standardized Coefficients	t	Sig.	Collinearity Statistics	
	B	Std. Error	Beta			Tolerance	VIF
1 (Constant)	.415	.062		6.683	.000		
NZMean	-3.782	2.453	-.284	-1.542	.135	1.000	1.000

a. Dependent Variable: logACAN_LF





APPENDIX D

MATLAB CODE - MECHANICS

The overview of Matlab code is summarized in Figure 45. Each component of the robotic control, kinematic tracking, and post-hoc analysis is described in the following sections.

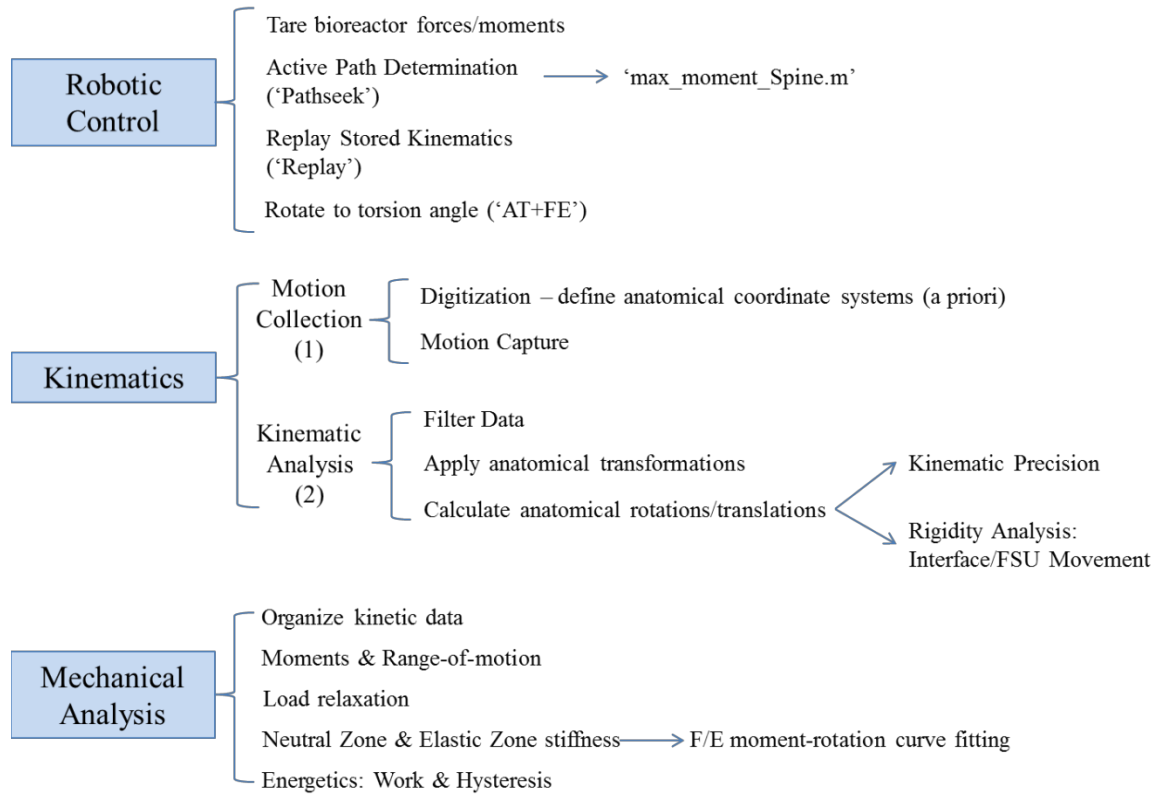


Figure 45. Overview of Matlab Code

D.1 ROBOT TESTING SYSTEM CONTROL

D.1.1 Tare Bioreactor Force/Moments

Because the bioreactor was assembled in sterile conditions and attached to the robot as a unit, the weight and contribution of the superior fixture had to be determined a priori and loaded in to the robot control program ahead of testing. The script, 'boltup_Spine.m' (below) was used to determine the influence of the superior fixture, and variables, 'w_mg', 'avg', 'x0', 'y0', 'z0', 'final_tare' were loaded in to the workspace.

Boltup_Spine.m

```
% boltup_accuracy
%controller moves robot into #pp1-6
%function to read forces/moments at each #pp
pause on;
final_tare = [0,0,0,0,0,0];

% Disable buttons on GUI until boltup_Spine.m is done running
buttons_Spine(guihandles, 'off');

pp(1,1:6) = [0,-45.001,135.001,0,-.001,-180.001];
pp(2,1:6) = [0,-45.001,135.001,0,-.001,-.001];
pp(3,1:6) = [0,-45.001,135.001,0,-.001,90.001];
pp(4,1:6) = [0,-45.001,135.001,0,-.001,-90.001];
pp(5,1:6) = [0,-45.001,135.001,0,-90.001,-90.001];
pp(6,1:6) = [0,-45.001,135.001,0,90.001,-90.001];

% % set transformation for COR from UFS face (remember that the UFS has a
left-hand rule, so positive z axis points toward the robot)
% trans_ufst = [1,round(x1*1000/0.0254), 2,round(y1*1000/0.0254), 3,round(-
(z1-0.045)*1000/0.0254), 4,round(rx1*32768/180), 5,round(ry1*32768/180),
6,round(rz1*32768/180),0];
% b = matj3pci('set_transforms', 0, 'trans_ufst', 13, 0);
%
% % use transformation
% b = matj3pci('use_transforms', 0, 0);
%
% % only use pause if updating COR
% pause(1);
```

```

for p = 1:6

    ok = 0;
    flag = 6.1;
    fprintf(port1,'%f\n', [ok, flag]);
    fprintf(port1,'%f\n', pp(p,1:6));

    done_moving = fscanf(port1);
    done_moving2 = sscanf(done_moving, '%f');

    pause(1);

    get_loads;
    pp_fin(1:3,p)=fm_ufs(1:3)';
    pp_min(1:3,p)=fm_ufs(4:6)';
    cg_fin(1:3,p)=fm_ufs(1:3)';
    cg_min(1:3,p)=fm_ufs(4:6)';

end

ok = 0;
flag = 6.1;
fprintf(port1,'%f\n', [ok, flag]);
fprintf(port1,'%f\n', pp(3,1:6));

done_moving = fscanf(port1);
done_moving = sscanf(done_moving, '%f');

% FSU forces/moments=UFS forces/moments[]-avg[]-fixture wt[]
favgx = (pp_fin(1,3)+pp_fin(1,4)+pp_fin(1,5)+pp_fin(1,6))/4;
favgy = (pp_fin(2,1)+pp_fin(2,2)+pp_fin(2,5)+pp_fin(2,6))/4;
favgz = (pp_fin(3,1)+pp_fin(3,2)+pp_fin(3,3)+pp_fin(3,4))/4;
mavgx = (pp_min(1,1)+pp_min(1,2))/2;
mavgy = (pp_min(2,3)+pp_min(2,4)+pp_min(2,5)+pp_min(2,6))/4;
mavgz = (pp_min(3,3)+pp_min(3,4)+pp_min(3,5)+pp_min(3,6))/4;

avg = -[favgx favgy favgz mavgx mavgz];
avg_dig(2) = avg(2)*16384/20/4.44;
avg_dig(3) = avg(3)*16384/50/4.44;

% FSU forces/moments=UFS forces/moments[]-avg[]-fixture wt[]
cg_favgx = (cg_fin(1,3)+cg_fin(1,4)+cg_fin(1,5)+cg_fin(1,6))/4;
cg_favgy = (cg_fin(2,1)+cg_fin(2,2)+cg_fin(2,5)+cg_fin(2,6))/4;
cg_favgz = (cg_fin(3,1)+cg_fin(3,2)+cg_fin(3,3)+cg_fin(3,4))/4;
cg_mavgx = (cg_min(1,1)+cg_min(1,2))/2;
cg_mavgy = (cg_min(2,3)+cg_min(2,4)+cg_min(2,5)+cg_min(2,6))/4;
cg_mavgz = (cg_min(3,3)+cg_min(3,4)+cg_min(3,5)+cg_min(3,6))/4;

% Calculate the center of gravity and mass of top fixture.

% 3 and 4 : d = z
% 3 : dz = -mx/fy
% 4 : dz = -mx/fy

```

```

fy_cg3 = -cg_fin(2,3) + cg_favgy;
fy_cg4 = -cg_fin(2,4) + cg_favgy;
mx_cg3 = -cg_min(1,3) + cg_mavgx;
mx_cg4 = -cg_min(1,4) + cg_mavgx;
momarm_z1 = -(mx_cg3/fy_cg3)*1000;
momarm_z2 = -(mx_cg4/fy_cg4)*1000;
momarm_z = (momarm_z1 + momarm_z2)/2;
z0 = momarm_z/1000;

% 1 and 2 : d = y
% 1 : dy = -mz/fx
% 2 : dy = -mz/fxfy_cg3 = cg_fin(2,3);
fx_cg1 = -cg_fin(1,1) + cg_favgx;
fx_cg2 = -cg_fin(1,2) + cg_favgx;
mz_cg1 = -cg_min(3,1) + cg_mavgz;
mz_cg2 = -cg_min(3,2) + cg_mavgz;
momarm_y1 = -(mz_cg1/fx_cg1)*1000;
momarm_y2 = -(mz_cg2/fx_cg2)*1000;
momarm_y = (momarm_y1 + momarm_y2)/2;
y0 = momarm_y/1000;

% 5 and 6 : d = x
% 5 : dx = -my/fz
% 6 : dx = -my/fzfy_cg3 = cg_fin(2,3);
fz_cg5 = -cg_fin(3,5) + cg_favgz;
fz_cg6 = -cg_fin(3,6) + cg_favgz;
my_cg5 = -cg_min(2,5) + cg_mavgy;
my_cg6 = -cg_min(2,6) + cg_mavgy;
momarm_x1 = -(my_cg5/fz_cg5*1000);
momarm_x2 = -(my_cg6/fz_cg6*1000);
momarm_x = (momarm_x1 + momarm_x2)/2;
x0 = momarm_x/1000;

% mass = 3(-fy), 4(fy), 1(-fx), 2(fx), 5(-fz), 6(fz)
mass_calc = ((-fy_cg3) + (fy_cg4) + (-fx_cg1) + (fx_cg2) + (-fz_cg5) +
(fz_cg6))/6;
mass_calc = -mass_calc;
w_mg = [0 0 mass_calc]';

get_loads;
fm_tare6;
final_tare = fm_tcs;

filename = ['c:\Robot Current\temp\temp ', date];
save(filename, 'w_mg', 'avg', 'x0', 'y0', 'z0', 'final_tare');

if abs(w_mg(3)) < 10 | abs(w_mg(3)) > 35
    error('Error: Load cell is not recording properly - rerun boltup or
testei.exe');
else
    msgbox('The Load Cell is ready for use!')
end

% Disable buttons on GUI until boltup_Spine.m is done running
buttons_Spine(guihandles, 'on');

```

D.1.2 Active path determination ('Pathseek')

The control interface, active path determination ('Pathseek'), and force/moment minimization code are published by Dr. Kevin Bell in his doctoral dissertation (Appendix A.1 – A.2) [458]. All code was written initially by Dr. Bell for humans; modifications made for this dissertation for rabbit testing are marked by 'RAH' (author's initials). A version of the script that controls robot motions when moment targets are reached, 'Max_moment_spine.m,' is presented here. This version was modified for loop path determination of unequal moment targets in positive and negative directions, with variable step-sizes permitted.

Motion control scheme when moment targets are reached: Max_moment_Spine.m:

```
% max_moment_Spine.m
% max moment loop
% Kevin Bell
% 3/18/2005 - modified by RAH (7/12)

% Determines whether & how to modify robot motion based on (1) max load

%asymmetric load targets - added by RAH 7/6/12
%'max_mom' is from GUI
% max_mom_pos = max_mom; %used default max load target for start pos
% max_mom_neg = .1; %!!!this value will over-ride GUI 'start neg' max load
target; need to modify max load target for start neg
% %comment out line 11 & 61

% Max moment
if loctarget_value == 0
    if posloop == 1 %going in positive direction (based on start pos/neg
radio button in GUI)
        % Loop to determine if max_mom or max_force is appropriate
        for i = 1:6
            if motion(i) == 1 %motion is 0 for all non-primary DOF; this
selects only primary DOF
                if i < 4
                    max_load = max_force; %set max_load to max force
                    step_down_load = max_load - (max_load*.1); %calculate
load at which smaller steps will be taken
                else
                    max_load = max_mom;
                    step_down_load = max_load - (max_load*.1);
                end
            end
        end
    end
end
```

```

end

%if on final leg of loop path, enter first part where
%step_down_load is around 0 rather than around target (max_mom)
if pathsequence == 1 && path_counter == sequencenum && final_loop ==
1
    %for final leg of loop paths leave load target ('max_mom')
unchanged but begin smaller step
    %sizes close to 0Nm to ensure that you land on 0 deg
    %
    display('final loop')
    step_down_load = (max_load*.1); %close to 0 Nm
    if (fm_tcs(1))*motion(1) > (max_load) | (fm_tcs(2))*motion(2) >
(max_load) | (fm_tcs(3))*motion(3) > (max_load) | (fm_tcs(4))*motion(4) >
(max_load) | (fm_tcs(5))*motion(5) > (max_load) | (fm_tcs(6))*motion(6) >
(max_load)
        dir_flag = 1;
        disp('***** CHANGING DIRECTION *****')
        continue % change direction
    elseif (abs(fm_tcs(1))*motion(1) < (step_down_load) ||
(abs(fm_tcs(2))*motion(2) < (step_down_load) || (abs(fm_tcs(3))*motion(3) <
(step_down_load) || (abs(fm_tcs(4))*motion(4) < (step_down_load) ||
(abs(fm_tcs(5))*motion(5) < (step_down_load) || (abs(fm_tcs(6))*motion(6) <
(step_down_load)
        temp_inc = inc;
        inc = inc_end; %could modify step-down load step-size HERE
        sd_flag = 1;
        disp('***** Smaller step size has been implemented
*****')
    elseif (abs(fm_tcs(1)) > z_stop(1)) | (abs(fm_tcs(2)) >
z_stop(2)) | (abs(fm_tcs(3)) > z_stop(3)) | (abs(fm_tcs(4)) > z_stop(4)) |
(abs(fm_tcs(5)) > z_stop(5)) | (abs(fm_tcs(6)) > z_stop(6))
        % if f/m are > max allowable, change direction
        disp('Forces/moments are too high.')
        disp('***** CHANGING DIRECTION *****')
        dir_flag = 1;
        continue % change direction
    end
    %default, normal control of all single, tail, and non-final loop
paths
else
    % Positive motion results in negative loads
    % fm_tcs - forces/moments in the tool coordinate system
    % 'motion' is 0 for all non-primary DOF
    if (fm_tcs(1))*motion(1) < -(max_load) | (fm_tcs(2))*motion(2) <
-(max_load) | (fm_tcs(3))*motion(3) < -(max_load) | (fm_tcs(4))*motion(4) < -
(max_load) | (fm_tcs(5))*motion(5) < -(max_load) | (fm_tcs(6))*motion(6) < -
(max_load)
        disp('posloop=1')
        dir_flag = 1;
        disp('***** CHANGING DIRECTION *****')
        continue % change direction
    elseif (fm_tcs(1))*motion(1) < -(step_down_load) |
(fm_tcs(2))*motion(2) < -(step_down_load) | (fm_tcs(3))*motion(3) < -
(step_down_load) | (fm_tcs(4))*motion(4) < -(step_down_load) |
(fm_tcs(5))*motion(5) < -(step_down_load) | (fm_tcs(6))*motion(6) < -
(step_down_load)

```

```

temp_inc = inc; %//rah-not sure if Rotate_HAM uses 'temp_inc'
or 'inc'!!!
inc = inc_end; %could modify step-down load step-size HERE
sd_flag = 1;
disp('***** Smaller step size has been implemented
*****')
elseif (abs(fm_tcs(1)) > z_stop(1)) | (abs(fm_tcs(2)) >
z_stop(2)) | (abs(fm_tcs(3)) > z_stop(3)) | (abs(fm_tcs(4)) > z_stop(4)) |
(abs(fm_tcs(5)) > z_stop(5)) | (abs(fm_tcs(6)) > z_stop(6))
% if f/m are > max allowable by robot (120N, 9Nm), change
direction
disp('Forces/moments are too high.')
disp('***** CHANGING DIRECTION *****')
dir_flag = 1;
continue % change direction
end
end
end

if posloop == 0 %going in negative direction
% Loop to determine if max_mom or max_force is appropriate
for i = 1:6
if motion(i) == 1
if i < 4
max_load = max_force;
step_down_load = max_load - (max_load*.1);
else
max_load = max_mom;
step_down_load = max_load - (max_load*.1);
end
end
end

%if on final leg of loop path, enter first part where
%step_down_load is around 0 rather than around target (max_mom)
if pathsequence == 1 && path_counter == sequencenum && final_loop ==
1
%for final leg of loop paths leave load target ('max_mom')
unchanged but begin smaller step
%sizes close to 0Nm to ensure that you land on 0 deg
display('final loop')
% max_load
step_down_load = (max_load*.4); %close to 0 Nm
step_down_loc = 2; % 0.8 *
(Spine.(date_ID).(state).(current_angles).(pathypestr).pathseek(trial).(HAM_
str).(pathsequence_str)(1).loop_0_pos.rot_angle_end_pts(end))
now
if (fm_tcs(1))*motion(1) > (max_load) | (fm_tcs(2))*motion(2) >
(max_load) | (fm_tcs(3))*motion(3) > (max_load) | (fm_tcs(4))*motion(4) >
(max_load) | (fm_tcs(5))*motion(5) > (max_load) | (fm_tcs(6))*motion(6) >
(max_load) && fm_tcs(pathtype) > (max_load) %'&&' added by RAH for FSU
testing
dir_flag = 1;
disp('***** CHANGING DIRECTION *****')
continue % change direction
elseif now < step_down_loc

```

```

%               (abs(fm_tcs(pathtype))) < (step_down_load)
display('pos_0 path')
temp_inc = inc;
inc = inc_end; %could modify step-down load step-size HERE
sd_flag = 1;
disp('***** Smaller step size has been implemented
*****')
elseif (abs(fm_tcs(1)) > z_stop(1)) | (abs(fm_tcs(2)) >
z_stop(2)) | (abs(fm_tcs(3)) > z_stop(3)) | (abs(fm_tcs(4)) > z_stop(4)) |
(abs(fm_tcs(5)) > z_stop(5)) | (abs(fm_tcs(6)) > z_stop(6))
% if f/m are > max allowable, change direction
disp('Forces/moments are too high.')
disp('***** CHANGING DIRECTION *****')
dir_flag = 1;
continue % change direction
end
%               %default, normal control of all single, tail, and non-
final loop paths
else
% Negative motion results in positive loads
if (fm_tcs(1))*motion(1) > (max_load) | (fm_tcs(2))*motion(2) >
(max_load) | (fm_tcs(3))*motion(3) > (max_load) | (fm_tcs(4))*motion(4) >
(max_load) | (fm_tcs(5))*motion(5) > (max_load) | (fm_tcs(6))*motion(6) >
(max_load) && fm_tcs(pathtype) > (max_load) %'&&' added by RAH for FSU
testing
%               fm_tcs * motion
disp('posloop=0')
dir_flag = 1;
disp('***** CHANGING DIRECTION *****')
continue % change direction
elseif (fm_tcs(1))*motion(1) > (step_down_load) |
(fm_tcs(2))*motion(2) > (step_down_load) | (fm_tcs(3))*motion(3) >
(step_down_load) | (fm_tcs(4))*motion(4) > (step_down_load) |
(fm_tcs(5))*motion(5) > (step_down_load) | (fm_tcs(6))*motion(6) >
(step_down_load) && fm_tcs(pathtype) > (step_down_load) %'&&' added by RAH
for FSU testing
display('all other paths')
temp_inc = inc;
%-----rah 8/30/12 > hard coding change to 'inc_end'; changes
'inc'; not sure where 'inc' gets used/reset/modified //may need to "reset"
'inc'
inc = inc_end;
%               inc_end_neg = inc_end/2; %rFSU FE: F-
inc_end=0.5; E-inc_end=0.25
%               inc = inc_end_neg; %could modify step-down
load step-size HERE
sd_flag = 1;
disp('***** Smaller step size has been implemented
*****')
elseif (abs(fm_tcs(1)) > z_stop(1)) | (abs(fm_tcs(2)) >
z_stop(2)) | (abs(fm_tcs(3)) > z_stop(3)) | (abs(fm_tcs(4)) > z_stop(4)) |
(abs(fm_tcs(5)) > z_stop(5)) | (abs(fm_tcs(6)) > z_stop(6))
% if f/m are > max allowable, change direction
disp('Forces/moments are too high.')
disp('***** CHANGING DIRECTION *****')
dir_flag = 1;
continue % change direction

```

```

        end
    end

end

if path_counter == sequencenum
    if final_loop == 1
        display('final loop - at zero pos?')
        for i = 1:6
            if motion(i) == 1
                motion_num = i;
            end
        end

        if (now*motion(motion_num) == 0) %basically, if the current angle
hits zero, end the test
            dir_flag = 1;
            disp('***** PATHSEEK IS COMPLETED *****')
            continue % change direction
        end
    end
end

end

% Max location rather than max moment
if loctarget_value == 1 %i.e. if location target radio button is selected
    if posloop == 1
        display('posloop = 1')
        pause(0.01); %changed rah - 8/29/12 - from pause(2);
        if (now*motion(1) >= (postarget) | now*motion(2) >= (postarget) |
now*motion(3) >= (postarget) | now*motion(4) >= (postarget) | now*motion(5)
>= (postarget) | now*motion(6) >= (postarget)) %'postarget' := "max
location"
            dir_flag = 1;
            disp('***** CHANGING DIRECTION *****')
            continue % change direction
        elseif (abs(fm_tcs(1)) > z_stop(1)) | (abs(fm_tcs(2)) > z_stop(2)) |
(abs(fm_tcs(3)) > z_stop(3)) | (abs(fm_tcs(4)) > z_stop(4)) | (abs(fm_tcs(5))
> z_stop(5)) | (abs(fm_tcs(6)) > z_stop(6))
            % if f/m are > max allowable, change direction
            disp('Forces/moments are too high.')
            disp('***** CHANGING DIRECTION *****')
            dir_flag = 1;
            continue % change direction
        end
    end
end

if posloop == 0
    display('posloop = 0')
    %-----rah 8/29/12 > hard coding option to make asymmetric location
targets in tail or loop paths-----
    negtarget = -postarget; %rah add/change - 8/29/12; line below used to
be "now*motion(i) <= -(postarget); this assumed equal targets in pos & neg
directions

```

```

    %must have above -OR- below but NOT both (double negative might cause
rotation in the wrong direction

```

```

    %       negtarget = -postarget/2; %redefines negtarget to user-
defined value
    %-----
    if now*motion(1) <= (negtarget) | now*motion(2) <= (negtarget) |
now*motion(3) <= (negtarget) | now*motion(4) <= (negtarget) | now*motion(5)
<= (negtarget) | now*motion(6) <= (negtarget)
        dir_flag = 1;
        disp('***** CHANGING DIRECTION *****')
        continue % change direction
    elseif (abs(fm_tcs(1)) > z_stop(1)) | (abs(fm_tcs(2)) > z_stop(2)) |
(abs(fm_tcs(3)) > z_stop(3)) | (abs(fm_tcs(4)) > z_stop(4)) | (abs(fm_tcs(5))
> z_stop(5)) | (abs(fm_tcs(6)) > z_stop(6))
        % if f/m are > max allowable, change direction
        disp('Forces/moments are too high.')
        disp('***** CHANGING DIRECTION *****')
        dir_flag = 1;
        continue % change direction
    end
end

if path_counter == sequencenum
    if final_loop == 1
        display('posloop = 1')
        for i = 1:6
            if motion(i) == 1
                motion_num = i;
            end
        end

        if (now*motion(motion_num) == 0)
            dir_flag = 1;
            disp('***** PATHSEEK IS COMPLETED *****')
            continue % change direction
        end
    end
end
end

end

```

D.1.3 Replay Stored Kinematics ('Replay')

The code for replaying stored joint angles was written exclusively by Dr. Bell and Dr. Yiguo Yang; it is included here because of its prominence in this work.

Replay stored joint angles: replay_Spine.m

```
% replay_Spine
% Kevin Bell
% 03/18/2005

pause on

% error('TEST ERROR - Robot Current')

% Disable buttons on GUI until Pathseek_Spine.m is done running
buttons_Spine(guihandles, 'off');

tracking = 0; %ON = 1, OFF = 0;
samba_num = 0; %OFF = 0, one sensor = 1, etc.
vicon = 0; %ON = 1, OFF = 0;
vicon_pause = 0;
pauselength = 0.001;
timer1 = 0;
timer_period = .19999;

if timer1 == 1
    Timer_counter = 0;
    T_VICON = timer('TimerFcn',
'Timer_VICON','ExecutionMode','FixedRate','Period',timer_period);
end

clear ljHandle
%Labjack must be working
if exist('ljHandle') == 0
    Labjack_Test_U3; %assigns in & defines ljHandle, LJ_ioGET_AIN
end

% if tracking == 1
%     if exist('port2') == 1
%         if strcmpi(port2.status, 'open') == 1
%             %start optical tracking
%             startTracking(port2);
%             tracking = 1;
%         end
%     end
% end

% Setup naming for structures
```

```

date_ID = [dated '_' ID];
if LAT_ang < 0
    strLAT_ang = ['_' num2str(abs(LAT_ang))];
else
    strLAT_ang = num2str(LAT_ang);
end
if FE_ang < 0
    strFE_ang = ['_' num2str(abs(FE_ang))];
else
    strFE_ang = num2str(FE_ang);
end
if AXIAL_ang < 0
    strAXIAL_ang = ['_' num2str(abs(AXIAL_ang))];
else
    strAXIAL_ang = num2str(AXIAL_ang);
end

current_angles = (['LAT' strLAT_ang '_FE' strFE_ang '_AXIAL' strAXIAL_ang]);

% % Disable buttons on GUI until spine3h_pathseek4b.m is done running
% buttons_Spine(guihandles, 'off');

% Input dialog box to get the filename for data storage
default_path = ['c:\Spine Testing\Data\' date_ID];
prompt = {'Enter Filename'};
title = 'Filename';
lines = 1;
def = {default_path};
answer = inputdlg(prompt,title,lines,def);
if isequal(answer,{''}) == 1
    % Enable buttons on GUI
    buttons(guihandles, 'on');
else
    filename = answer{1};
end

% Clear variables created for inputdlg
clear prompt title lines def answer;

% setup figure to graphically monitor loads
[fx, fy, fz, mx, my, mz, handles, fh] = replay_display_Spine1;
[handlesLD, fhLD] = pathseek_LDdisplay_Spine1(pathtype);

% send x1, y1, z1, rx1, ry1, rz1 to V+ to make tool transformation
ok = 0;
flag = 0.1;
fprintf(port1, '%f\n', [ok, flag]);
fprintf(port1, '%f\n', [(x1*1000)+.001, (y1*1000)+.001, (z1*1000)+.001,
rx1+.001, ry1+.001, rz1+.001]);

done_moving = fscanf(port1);
% =====
timeout_Spine;
% =====
done_moving = sscanf(done_moving, '%f');

```

```

%-----
if vicon == 1
    VICON_U3_OpenLabJack
    % Start VICON
    VICON_U3_Start
    if timer1 == 1
        start(T_VICON);
        timertic=tic;
    end
    if vicon_pause ==1
        pause(.1)
        VICON_U3_Pause
    end
end
end

%-----

for replay_cycle = 1:num_replays

    if pathsequence == 1 %1 - loop path

        if replay_cycle == 1 | replay_cycle == num_replays; %replaying
multiple paths
            sequencenum = 3
            if replay_cycle == num_replays
                final_loop = 1;
            end
        end
        if replay_cycle == 1 & replay_cycle == num_replays; %only replaying
one path
            sequencenum = 4
            if replay_cycle == num_replays
                final_loop = 1;
            end
        end
        if replay_cycle ~= 1 & replay_cycle ~= num_replays; %not first or
last replay
            sequencenum = 2
        end

        %         sequencenum = 4;
    elseif pathsequence == 2
        sequencenum = 2;
    elseif pathsequence == 3
        sequencenum = 1;
    end

    %     if tracking == 1
    %         % Establish initial matrix (home)
    %         [T_Gmo,T_GmoP] = ndiTrack(port2);
    %         P_glob_0 = T_Gmo(:, :, 5) * cor_TrMx(1:4,4);
    %         T_Gmo(:, :, 5) = [T_Gmo(1:4,1:3,5), P_glob_0];
    %     end

```

```

for path_counter = 1:sequencenum

    % Function to setup replay naming
    increment_function_replay_Spine

    %if path_counter == 1
    for p =
1:size(Spine.(date_ID).(state).(current_angles).(pathtypestr).pathseek(trial)
.(HAM_str).(pathsequence_str)(cycle).(path_name).replay_global_pos,2)

        % move specimen in incremental movements
        ok = 0;
        flag = 5.1;
        fprintf(port1,'%f\n', [ok, flag]);

fprintf(port1,'%f\n',Spine.(date_ID).(state).(current_angles).(pathtypestr).p
athseek(trial).(HAM_str).(pathsequence_str)(cycle).(path_name).replay_global_
pos(1:6,p));

        done_moving = fscanf(port1);
        % =====
        timeout_Spine;
        % =====
        done_moving = sscanf(done_moving, '%f');

        if vicon == 1
            if vicon_pause == 1
                VICON_U3_Resume
                pause(pauselength)
                VICON_U3_Pause
            else
                pause(pauselength)
            end
        end
    end

    % Get IDP measurements from Samba 202
    if samba_num > 0
        getSamba
        % Build array of ((path_name)) IDP1

Spine.(date_ID).(state).(current_angles).(pathtypestr).pathseek(trial).(HAM_s
tr).(pathsequence_str)(cycle).(path_name).IDP1(endpt_index) = IDP1;
        if samba_num == 2
            % Build array of ((path_name)) IDP2

Spine.(date_ID).(state).(current_angles).(pathtypestr).pathseek(trial).(HAM_s
tr).(pathsequence_str)(cycle).(path_name).IDP2(endpt_index) = IDP2;
        end
    end

    %//RH: does this pause need to be 1 sec? what is it's purpose//
    pause(1);

    robot_return = 0; %robot is going "out" toward eROM

```

```

ok = 0;
flag = 1.1;
fprintf(port1, '%f\n', [ok, flag]);
gt_jt_angles = fscanf(port1);
gt_jt_angles = sscanf(gt_jt_angles, '%f');

%=====
get_loads; % measure: forces and moments
%=====

%=====
fm_tare6; % tare out bolt-up and fixture wt
%=====

    pathseek_LDdisplay_Spine2(fm_tcs, handlesLD,
Spine.(date_ID).(state).(current_angles).(pathtypestr).pathseek(trial).(HAM_s
tr).(pathsequence_str)(cycle).(path_name).rot_angle_end_pts(p), pathtype, 1,
robot_return, fhLD, replay_cycle);

Spine.(date_ID).(state).(current_angles).(pathtypestr).replay(trial).(state_r
eplay).(HAM_str).(pathsequence_str)(replay_cycle).(path_name).load(:,p) =
fm_tcs';

Spine.(date_ID).(state).(current_angles).(pathtypestr).replay(trial).(state_r
eplay).(HAM_str).(pathsequence_str)(replay_cycle).(path_name).position(:,p) =
gt_jt_angles(1:6);

Spine.(date_ID).(state).(current_angles).(pathtypestr).replay(trial).(state_r
eplay).(HAM_str).(pathsequence_str)(replay_cycle).(path_name).momt(:, :, p) =
momt;

Spine.(date_ID).(state).(current_angles).(pathtypestr).replay(trial).(state_r
eplay).(HAM_str).(pathsequence_str)(replay_cycle).(path_name).T_GM(:, :, :, p) =
T_GM;

Spine.(date_ID).(state).(current_angles).(pathtypestr).replay(trial).(state_r
eplay).(HAM_str).(pathsequence_str)(replay_cycle).(path_name).ndiTAnatomical(
(:, :, p) = ndiTAnatomical;
    end

    % display f/m after taring out bolt-up and fixture wt
    replay_display_Spine2(fh, [fm_tcs, fx, fy, fz], [mx, my, mz],
handles,
Spine.(date_ID).(state).(current_angles).(pathtypestr).pathseek(trial).(HAM_s
tr).(pathsequence_str)(cycle).(path_name).rot_angle_end_pts(p));
    end

    % Step back through replay to starting position
    dialog = 0;
    % Set = to one to correct robot return problem
    robot_return = 1; %robot is returning to starting pos
    zero = 0;

```

```

if pathsequence == 2 || pathsequence == 3

    if robot_return == 1
        load_return_ctr = 1; %RH - 8/21/12
        for ii =
size(Spine.(date_ID).(state).(current_angles).(pathtypestr).pathseek(trial).(
HAM_str).(pathsequence_str)(cycle).(path_name).replay_global_pos,2):-1:1
            ok = 0;
            flag = 5.1;
            fprintf(port1,'%f\n', [ok, flag]);
            reverse =
Spine.(date_ID).(state).(current_angles).(pathtypestr).pathseek(trial).(HAM_s
tr).(pathsequence_str)(cycle).(path_name).replay_global_pos(1:6,ii);
            fprintf(port1,'%f\n', reverse);
            done_moving = fscanf(port1);
            % =====
            timeout_Spine;
            % =====
            done_moving = sscanf(done_moving, '%f');

            %--collect loads on return--RH - 8/21/12---
            %=====
            get_loads; % measure: forces and moments
            %=====

            %=====
            fm_tare6; % tare out bolt-up and fixture wt
            %=====

Spine.(date_ID).(state).(current_angles).(pathtypestr).replay(trial).(state_r
eplay).(HAM_str).(pathsequence_str)(replay_cycle).(path_name).load_return(:,l
oad_return_ctr) = fm_tcs';
            %
Spine.(date_ID).(state).(current_angles).(pathtypestr).replay(trial).(state_r
eplay).(HAM_str).(pathsequence_str)(replay_cycle).(path_name).position_return
(:,load_return_ctr) = gt_jt_angles(1:6);

            pathseek_LDdisplay_Spine2(fm_tcs, handlesLD,
(Spine.(date_ID).(state).(current_angles).(pathtypestr).pathseek(trial).(HAM_
str).(pathsequence_str)(cycle).(path_name).rot_angle_end_pts(ii)), pathtype,
1, robot_return, fhLD, replay_cycle)

            load_return_ctr = load_return_ctr + 1;
            %-----end: RH - 8/21-12-----

if vicon == 1
    if vicon_pause == 1
        VICON_U3_Resume
        pause(pauselength)
        VICON_U3_Pause
    else
        pause(pauselength)

```


D.1.4 Rotate to torsion angle ('AT+F/E')

To achieve coupled torsion with flexion/extension in Specific Aim 2, the script, 'desired_Angle.m' (written by Dr. Bell), was used to move the robot end-effector to a stored position (previously determined by axial rotation paths) and perform flexion/extension loading at that rotated position.

desired_angle_Spine.m

```
% desired_angle_Spine.m
% move to desired angle
% Kevin Bell
% 3/18/2005

% DA - entered

clear current_angles compiled_angles compiled_positions
clear angle_move angle_stored compiled_motion

%+++++
% send x1, y1, z1, rx1, ry1, rz1 to V+ to make tool transformation
ok = 0;
flag = 0.1;
fprintf(port1, '%f\n', [ok, flag]);
fprintf(port1, '%f\n', [(x1*1000)+.001, (y1*1000)+.001, (z1*1000)+.001,
rx1+.001, ry1+.001, rz1+.001]);

done_moving = fscanf(port1);
% =====
timeout_Spine;
% =====
done_moving = sscanf(done_moving, '%f');
% +++++

% stored_angle - taken from and reported to GUI
if pathtype == 1
    stored_angle = str2num(get(guihandles.ML_DA_edit, 'String'));
elseif pathtype == 2
    stored_angle = str2num(get(guihandles.SI_DA_edit, 'String'));
elseif pathtype == 3
    stored_angle = str2num(get(guihandles.AP_DA_edit, 'String'));
elseif pathtype == 4
    stored_angle = str2num(get(guihandles.FE_ang_edit, 'String'));
elseif pathtype == 5
    stored_angle = str2num(get(guihandles.AXIAL_ang_edit, 'String'));
elseif pathtype == 6
    stored_angle = str2num(get(guihandles.LAT_ang_edit, 'String'));
end
```

```

DA_flag = 0;

% Disable buttons on GUI until desired_angle_Spine.m is done running
buttons_Spine(guihandles, 'off');

% Setup naming for structures
date_ID = [dated '_' ID];

if pathtype > 3
    current_angles = ([ 'LAT' num2str(0) '_FE' num2str(0) '_AXIAL'
num2str(0)]);
else
    stored_FE_angle = str2num(get(guihandles.FE_ang_edit, 'String'));
    stored_AXIAL_angle = str2num(get(guihandles.AXIAL_ang_edit, 'String'));
    stored_LAT_angle = str2num(get(guihandles.LAT_ang_edit, 'String'));

    current_angles = ([ 'LAT' num2str(stored_LAT_angle) '_FE'
num2str(stored_FE_angle) '_AXIAL' num2str(stored_AXIAL_angle)]);
end

% FOR FLEX/EX 30
% current_angles = 'LAT0_FE0_AXIAL6';

if DA ~= stored_angle

    % Desired Angle for tail sequence
    if pathsequence == 1
        cycle = num_paths;
        compiled_angles =
[Spine.(date_ID).(state).(current_angles).(pathtypestr).pathseek(trial).(HAM_
str).(pathsequence_str)(cycle).loop_neg_pos.rot_angle_end_pts];
        compiled_positions =
[Spine.(date_ID).(state).(current_angles).(pathtypestr).pathseek(trial).(HAM_
str).(pathsequence_str)(cycle).loop_neg_pos.replay_global_pos];
    elseif pathsequence == 2
        cycle = num_paths;
        compiled_angles =
[flipdim(Spine.(date_ID).(state).(current_angles).(pathtypestr).pathseek(tria
l).(HAM_str).(pathsequence_str)(cycle).tail_0_neg.rot_angle_end_pts,2)
Spine.(date_ID).(state).(current_angles).(pathtypestr).pathseek(trial).(HAM_s
tr).(pathsequence_str)(cycle).tail_0_pos.rot_angle_end_pts(2:end)];
        compiled_positions =
[flipdim(Spine.(date_ID).(state).(current_angles).(pathtypestr).pathseek(tria
l).(HAM_str).(pathsequence_str)(cycle).tail_0_neg.replay_global_pos,2)
Spine.(date_ID).(state).(current_angles).(pathtypestr).pathseek(trial).(HAM_s
tr).(pathsequence_str)(cycle).tail_0_pos.replay_global_pos(1:6,2:end)];
    elseif pathsequence == 3
        cycle = num_paths;
        if startpos_value == 1
            str_start_DA = num2str(w_start);
            path_name_DA = ['single_' str_start_DA '_pos'];
            compiled_angles =
[flipdim(Spine.(date_ID).(state).(current_angles).(pathtypestr).pathseek(tria
l).(HAM_str).(pathsequence_str)(cycle).(path_name_DA).rot_angle_end_pts,2)];

```

```

        compiled_positions =
[flipdim(Spine.(date_ID).(state).(current_angles).(pathtypestr).pathseek(tria
l).(HAM_str).(pathsequence_str)(cycle).(path_name_DA).replay_global_pos,2)];
        elseif startpos_value == 0
            str_start_DA = num2str(w_start);
            path_name_DA = ['single_' str_start_DA '_neg'];
            compiled_angles =
[Spine.(date_ID).(state).(current_angles).(pathtypestr).pathseek(trial).(HAM_
str).(pathsequence_str)(cycle).(path_name_DA).rot_angle_end_pts];
            compiled_positions =
[Spine.(date_ID).(state).(current_angles).(pathtypestr).pathseek(trial).(HAM_
str).(pathsequence_str)(cycle).(path_name_DA).replay_global_pos];
        end
    else
        error('Not a defined sequence')
    end

    for i = 1:size(compiled_angles,2);
        if compiled_angles(i) == DA;
            DA_flag = i;
            angle_move = compiled_positions(1:6,DA_flag);
        end
        if compiled_angles(i) == stored_angle;
            stored_flag = i;
            angle_stored = compiled_positions(1:6,stored_flag);
        end
    end

    if DA_flag ~= 0

        if DA_flag < stored_flag
            compiled_motion =
flipdim(compiled_positions(1:6,DA_flag:stored_flag),2);
        elseif DA_flag > stored_flag
            compiled_motion = (compiled_positions(1:6,stored_flag:DA_flag));
        end

        for i = 1:size(compiled_motion,2)
%           display(num2str(compiled_motion(1:6,i)));
            ok = 0;
            flag = 5.1;
            fprintf(port1,'%f\n', [ok, flag]);
            fprintf(port1,'%f\n', compiled_motion(1:6,i));

            done_moving = fscanf(port1);
            % =====
            timeout_Spine;
            % =====
            done_moving = sscanf(done_moving, '%f');
        end

        if pathtype == 1
            ML_DA = DA;
            set(guihandles.ML_DA_edit, 'String', ML_DA)
        elseif pathtype == 2
            SI_DA = DA;

```

```

        set(guihandles.SI_DA_edit, 'String', SI_DA)
elseif pathtype == 3
    AP_DA = DA;
    set(guihandles.AP_DA_edit, 'String', AP_DA)
elseif pathtype == 4
    FE_ang = DA;
    set(guihandles.FE_ang_edit, 'String', FE_ang)
elseif pathtype == 5
    AXIAL_ang = DA;
    set(guihandles.AXIAL_ang_edit, 'String', AXIAL_ang)
elseif pathtype == 6
    LAT_ang = DA;
    set(guihandles.LAT_ang_edit, 'String', LAT_ang)
end

else
    display('Number entered is not valid')
end

else
    display('Motion was not valid')
end

% Enable buttons on GUI when desired_angle_Spine.m is done running
buttons_Spine(guihandles, 'on');

```

D.2 ROBOT TESTING SYSTEM ASSESSMENT

D.2.1 Motion Collection

The Matlab code used to acquire VICON kinematic data are detailed in Appendix A.3 of Dr. Bell's dissertation [458].

Digitization – define anatomical coordinate systems (a priori)

The digitization of anatomical or fixture landmarks is described in Appendix A.3.1 ('Digitize_filter.m'), and transformation of anatomical to measured coordinate systems is laid out in Appendix A.3.2 ('Digitize_link.m') [458].

Motion capture

Collection of motion is defined in Appendix A.3.3 [458].

D.2.2 Kinematic Analysis

Post-processing includes extracts rotations and translations of all local coordinate systems in anatomical or fixture reference frames (A.4.1) [458]. These rotations and translations assume a Euler sequence of Rx, Ry, Rz (F/E, AT, LB).

Filter data: Digitize_filter.m

Data smoothing from individual reflectors was performed interactively in VICON software. This code handles missing data points. (Appendix A.4.1) [458].

Apply anatomical transformations: Digitize_link.m

Anatomical transformations were applied to captured motion data (Appendix A.4.1) [458]. This code was modified for rabbit FSU testing.

```
function VICON = Digitize_link(VICON)

%%Rob Hartman, 11/30/11
%%prepare analysis by introducing necessary naming variables

C3Dname = VICON.Options.C3Dname;
tttotal = [0 0 0 0 0 0];
tarray = [0 0 0 0 0 0];
Digtotal = [0 0 0 0 0 0];
Digarray = [0 0 0 0 0 0];
Digtotal2 = [0 0 0 0 0 0];
Digarray2 = [0 0 0 0 0 0];
% tname_cell = {'_t1','_t2','_t3','_t4','_t5','_t6'}
% tname_cell1 = {'t1','t2','t3','t4','t5','t6'}
% tname_cell = {'_s1','_s2','_s3','_s4'}
tname_cell = {'S1','S2','S3','S4','S5','S6'};
Dig_mark_cell={'T1','T2','T3','T4','T5','T6'};
T_cell={'T'};
Dig_abcd_cell={'Pa','Pb','Pc','Pd'};
```

```

frames = VICON.(C3Dname).frames;
markers = VICON.(C3Dname).markers;

temp_mnames = sort(VICON.(C3Dname).mnames);
VICON.(C3Dname).mnames = temp_mnames;

%% anatomical w/r/t global CS (T_G_A)
%transformation calculated in <Digitizer_filter.m>
%transformation stored in VICON.C3Dname.DigT; stored per segment/VB with 3
%separate [T]'s - one for each anatomical point (A,B,C)

%need to form anatomical CS for each VB -LOOP-
for toolnum = 1:size(VICON.(C3Dname).Dignames2,3) %# of segments/VBs
(Digitized)

    %form anatomical CS (T_G_A) from (A,B,C)
    pointA = VICON.(C3Dname).DigT.(tname_cell{toolnum})(1:3,4,1);
    pointB = VICON.(C3Dname).DigT.(tname_cell{toolnum})(1:3,4,2);
    pointC = VICON.(C3Dname).DigT.(tname_cell{toolnum})(1:3,4,3);

    %function that forms anatomical RF from 3 points
    VICON.(C3Dname).AnatomicalT.(tname_cell{toolnum})(:,:) =
Anatomical(pointA,pointB,pointC);

end

%% measured/tool w/r/t global CS (T_G_M)
%tool markers are not transformed in Digitizer functions
%---this code is derived from <VICON_Rotation.m>---

%---FIX any remaining NaN prior to calculating rotations---
for toolnum = 1:size(VICON.(C3Dname).tnames,2) %# of tools (2-6)
    for markernum = 1:size(VICON.(C3Dname).tnames,1) %# of markers per
tool (usually 3)
        %           clear temp
        %
VICON.(C3Dname).(char(VICON.(C3Dname).tnames{markernum,toolnum}))(any(isnan(V
ICON.(C3Dname).(char(VICON.(C3Dname).tnames{markernum,toolnum}))),2),:)= [];
        temp =
VICON.(C3Dname).(char(VICON.(C3Dname).tnames{markernum,toolnum}));
        temp(any(isnan(temp),2),:)= [];
        VICON.(C3Dname) = rmfield(VICON.(C3Dname),
char(VICON.(C3Dname).tnames{markernum,toolnum}));
        VICON.(C3Dname).(char(VICON.(C3Dname).tnames{markernum,toolnum}))
= temp;
        %           clear temp;
    end
end

%to do: update the frames variable based on NaN's removed

%---finish NaN fixing-----

```

```

%----collect marker position data for each segment----
%calculate average position of each marker on each tool over the static
trial
for toolnum = 1:size(VICON.(C3Dname).tnames,2) %loop through all tools

    for markernum = 1:size(VICON.(C3Dname).tnames,1) %loop through each
marker on each tool

%           disp(toolnum);
%           disp(markernum);

VICON.(C3Dname).AveragePosition.(VICON.(C3Dname).tnames{markernum,toolnum})(1
) = mean(VICON.(C3Dname).(VICON.(C3Dname).tnames{markernum,toolnum})(:,1));

VICON.(C3Dname).AveragePosition.(VICON.(C3Dname).tnames{markernum,toolnum})(2
) = mean(VICON.(C3Dname).(VICON.(C3Dname).tnames{markernum,toolnum})(:,2));

VICON.(C3Dname).AveragePosition.(VICON.(C3Dname).tnames{markernum,toolnum})(3
) = mean(VICON.(C3Dname).(VICON.(C3Dname).tnames{markernum,toolnum})(:,3));

        end
    end
%-----

%---calculate transformation for each tool of tool w/r/t global (T_G_M)(M:=
measured)---
for toolnum = 1:size(VICON.(C3Dname).Dignames2,3)

    %markers per tool (set of markers) - each mki is (x,y,z)
    mk1 =
VICON.(C3Dname).AveragePosition.(VICON.(C3Dname).tnames{1,toolnum});
    mk2 =
VICON.(C3Dname).AveragePosition.(VICON.(C3Dname).tnames{2,toolnum});
    mk3 =
VICON.(C3Dname).AveragePosition.(VICON.(C3Dname).tnames{3,toolnum});

    % Calculating location of origin
    O = mean([mk1;mk2]);
    X = (mk2-O);
    X = X/norm(X); %toward controller; robot tool x

    % can add (-) or inverse cross if markers are missing.
    OZ = (mk3-O)/norm(mk3-O);
    Y = cross(OZ,X); Y = Y/norm(Y); %robot tool y
    Z=cross(X,Y); Z=Z/norm(Z); %robot tool z

    %test orthogonality
    testxy = dot(X,Y);
    testyz = dot(Y,Z);
    testxz = dot(X,Z);

    %T_G_M: each measured (tool) CS w/r/t Global CS
    T_G_M(1:3,1)=X; T_G_M(1:3,2)=Y; T_G_M(1:3,3)=Z;
    T_G_M(1:3,4)=0;

```

```

T_G_M(4,1:4)=[0 0 0 1];

%transformation b/w markers and global reference frame
VICON.(C3Dname).ToolT.(tname_cell{toolnum})(:, :) = T_G_M;

%translations & rotations in the global RF
ypr = rad2deg(tr2ypr(T_G_M));
yprtr = [T_G_M(1,4) T_G_M(2,4) T_G_M(3,4) ypr(1) ypr(2) ypr(3)];
VICON.(C3Dname).Tooltr.(tname_cell{toolnum}) = yprtr;

end
%---saved transformation & ypr of measured (tool) w/r/t global---

%% anatomical w/r/t measured CS (T_M_A)
%for each segment/VB, calculate the transformation of the anatomical w/r/t
measured (tool)
%!!!does the correct segment line up w/ the correct level!!!
for toolnum = 1:size(VICON.(C3Dname).Dignames2,3) %this should correspond to
# of segments/VBs

%      %typicvally not necessary (1:4, not 2:5) for digitized points
%      toolnum_ana = toolnum-1;

%T_M_A = inv(T_G_M) * T_G_A
T_M_A = inv(VICON.(C3Dname).ToolT.(tname_cell{toolnum})) *
VICON.(C3Dname).AnatomicalT.(tname_cell{toolnum});

%transformation saved in ToolAnatomicT
VICON.(C3Dname).ToolAnatomicT.(tname_cell{toolnum}) = T_M_A;

%translations & rotations in the global RF
ypr = rad2deg(tr2ypr((T_M_A(:, :))));
yprtr = [T_M_A(1,4) T_M_A(2,4) T_M_A(3,4) ypr(1) ypr(2) ypr(3)];
VICON.(C3Dname).ToolAnatomictr.(tname_cell{toolnum}) = yprtr;

end

%the "link" is made with the T_M_A calculation
%this can be used to post-process dynamic trial data which is inherently in
%T_G_M form. The post-procesing will form:
% (1) T_G_A = T_G_M * T_M_A > for each tool/segment
%      %this can be performed at each timepoint
% (2) T_Ai_Aj = inv(T_G_Ai) * T_G_Aj;
%      %this can be performed b/w two levels (i, j)
%***NEED TO CHECK*** : this transformation places Aj w/r/t Ai!?!

```

Calculate anatomical rotations/translations: VICON_Rotation.m

Relative transformations between rigid bodies (or segments) were measured at each position. Euler angles and translations were extracted (Appendix A.4.1).

D.2.3 Kinematic Precision

Kinematic precision was performed after motion data collection. The root mean square error of local coordinate system rotations and translation calculated in post-processing of collected motion for each step in the path are calculated in 'VICON_rotationRMS.m.' This code can be modified to collect precision of local coordinate system origins to express precision in terms of positions (x, y, z).

Kinematic Precision: VICON_rotationRMS.m

```
function VICON = VICON_rotationRMS(VICON)

%RAH 6/14 - this code was used to measure RMSE of positions across
%rotational movements

%bell, may 2011; modified by RAH -
%analyzes data collected from robot-vicon repeatability trials (pre-052411)

%repeatability assessment:
%markers in yiguo yan configuration (late may)
% clear

%purpose: assess Euler angles and translation repeatability of vicon data
%bring in data > calculate RMS of error across 20 (flexible) steps

%bring in data from vicon analysis (raw marker data, lcsm in global, lcs
w/r/t itself at t0)
%each marker (n steps x 3 coordinates)
tname_cell = {'s1', 's2', 's3', 's4', 's5', 's6'};

binum = 2;
cyclecount = 0;

C3Dname = VICON.Options.C3Dname;
posneg = VICON.Options.posneg;
```

```

pathsequence = VICON.Options.pathsequence;

binum = 1; %1-"out", 2-"back"
pnTrans = VICON.(C3Dname).pnTrans; %1-single, 2-tails

if strcmp(posneg,'pos')==1
    pos1 = 1; %starts pos. dir
else
    pos1 = 0; %starts neg. dir
end

for pnnum = 1:pnTrans %1-single, 2-tails

    [path_name] = VICON_path_name(pathsequence,pos1,pnnum);

    for bidirect = 1:binum

        cyclecount = cyclecount + 1; %cycle counter; init. 0

        for toolnum = 1:size(VICON.(C3Dname).tnames,1)

            for stepnum = 1:1:size(VICON.(C3Dname).(path_name).CycleIndex,2)

                for paramnum = 1:6 %~DOF

                    for cyclenum =
1:size(VICON.(C3Dname).(path_name).CycleIndex,1)

                        %form mean position for each cycle at each step (for
each DOF both "there & back")
                        %pre-1/20/12 - needs to update structure reference
based on changes to % VICON_Rotation > Transform.anatomical.yprtr_21_02N
%>>!!!Hard coded segment choice for rotation analysis!!!<<
                        %temp_mean(cyclenum) =
VICON.(C3Dname).(path_name).Transform(cyclenum).global.yprtr_G.(char(tname_ce
ll{toolnum}))(stepnum,paramnum,bidirect);
                        if
length(fieldnames(VICON.(C3Dname).(path_name).ROM.anatomical.ALL)) == 2
                            fsu = 0; %no fsu if true
                            temp_mean(cyclenum) =
VICON.(C3Dname).(path_name).Transform(cyclenum).anatomical.yprtr_21_02N(stepn
um,paramnum,bidirect); %RAH - 1/20 for repeatability
                        elseif
length(fieldnames(VICON.(C3Dname).(path_name).ROM.anatomical.ALL)) == 4
                            fsu = 1; %fsu is attached
                            temp_meanEe(cyclenum) =
VICON.(C3Dname).(path_name).Transform(cyclenum).anatomical.yprtr_41_02N(stepn
um,paramnum,bidirect); %RAH - 1/20 for repeatability
                            temp_meanJt(cyclenum) =
VICON.(C3Dname).(path_name).Transform(cyclenum).anatomical.yprtr_32_02N(stepn
um,paramnum,bidirect);
                        end
                    end
                end
            end
        end
    end
end

```

```

                                %mean position across cycles for each step, DOF, "there &
back"
                                if fsu == 0

VICON.(C3Dname).(path_name).RMS.step_mean_CS.allsteps.(char(tname_cell{toolnu
m}))(stepnum,paramnum,bidirect)= mean(temp_mean);
                                elseif fsu == 1

VICON.(C3Dname).(path_name).RMS.step_mean_CSeE.allsteps.(char(tname_cell{tool
num}))(stepnum,paramnum,bidirect)= mean(temp_meanEe);

VICON.(C3Dname).(path_name).RMS.step_mean_CSjT.allsteps.(char(tname_cell{tool
num}))(stepnum,paramnum,bidirect)= mean(temp_meanJt);
                                end

                                for cyclenum =
1:size(VICON.(C3Dname).(path_name).CycleIndex,1)

                                %error = mean across cycles at each step - position
at each step
%>>!!!Hard coded segment choice for rotation analysis!!!<<
                                if fsu == 0

VICON.(C3Dname).(path_name).RMS.step_Error_CS(cyclenum).allsteps.(char(tname_
cell{toolnum}))(stepnum,paramnum,bidirect) =
VICON.(C3Dname).(path_name).RMS.step_mean_CS.allsteps.(char(tname_cell{toolnu
m}))(stepnum,paramnum) -
VICON.(C3Dname).(path_name).Transform(cyclenum).anatomical.yprtr_21_02N(stepn
um,paramnum,bidirect);
                                elseif fsu == 1

VICON.(C3Dname).(path_name).RMS.step_Error_CSeE(cyclenum).allsteps.(char(tnam
e_cell{toolnum}))(stepnum,paramnum,bidirect) =
VICON.(C3Dname).(path_name).RMS.step_mean_CSeE.allsteps.(char(tname_cell{tool
num}))(stepnum,paramnum) -
VICON.(C3Dname).(path_name).Transform(cyclenum).anatomical.yprtr_41_02N(stepn
um,paramnum,bidirect);

VICON.(C3Dname).(path_name).RMS.step_Error_CSjT(cyclenum).allsteps.(char(tnam
e_cell{toolnum}))(stepnum,paramnum,bidirect) =
VICON.(C3Dname).(path_name).RMS.step_mean_CSjT.allsteps.(char(tname_cell{tool
num}))(stepnum,paramnum) -
VICON.(C3Dname).(path_name).Transform(cyclenum).anatomical.yprtr_32_02N(stepn
um,paramnum,bidirect);
                                end

                                end

                                for cyclenum =
1:size(VICON.(C3Dname).(path_name).CycleIndex,1)

                                %NOT "rms"; actually, error matrix across cycles for
each position, DOF, "there & back"
                                if fsu == 0

```

```

                                temp_rms(cyclenum) =
VICON.(C3Dname).(path_name).RMS.step_Error_CS(cyclenum).allsteps.(char(tname_
cell{toolnum}))(stepnum,paramnum,bidirect);
                                elseif fsu == 1
                                    temp_rmsEe(cyclenum) =
VICON.(C3Dname).(path_name).RMS.step_Error_CSeE(cyclenum).allsteps.(char(tnam
e_cell{toolnum}))(stepnum,paramnum,bidirect);
                                    temp_rmsJt(cyclenum) =
VICON.(C3Dname).(path_name).RMS.step_Error_CSjT(cyclenum).allsteps.(char(tnam
e_cell{toolnum}))(stepnum,paramnum,bidirect);
                                end
                                end

                                %RMS of error
                                if fsu == 0

VICON.(C3Dname).(path_name).RMS.step_RMS_CS.allsteps.(char(tname_cell{toolnum
}))(stepnum,paramnum,bidirect) = rms(temp_rms);
                                elseif fsu == 1

VICON.(C3Dname).(path_name).RMS.step_RMS_CSeE.allsteps.(char(tname_cell{tooln
um}))(stepnum,paramnum,bidirect) = rms(temp_rmsEe);

VICON.(C3Dname).(path_name).RMS.step_RMS_CSjT.allsteps.(char(tname_cell{tooln
um}))(stepnum,paramnum,bidirect) = rms(temp_rmsJt);
                                end

                                %
                                VICON.(C3Dname).(path_name).STD.step_STD_CS.allsteps.(char(tname_cell{toolnum
}))(stepnum,paramnum,bidirect) = std(temp_rms);

                                end

                                end

                                end

                                end

                                end

                                %not modified by RAH b/c pnTrans > 1
                                for pnnum = 1:pnTrans %1-single, 2-tails

                                [path_name] = VICON_path_name(pathsequence,pos1,pnnum);

                                if binum == 2

                                % Loop to combine out and back for overall RMS
                                for toolnum = 1:size(VICON.(C3Dname).tnames,1)

                                for cyclenum = 1:size(VICON.(C3Dname).(path_name).CycleIndex,1)

```

```

        step_ErrorCS_Combined =
VICON.(C3Dname).(path_name).RMS.step_Error_CS(cyclenum).allsteps.(char(tname_
cell{toolnum}))(:, :, 1);

        % when constructing combined Error need to flip back to align
steps

step_ErrorCS_Combined(size(VICON.(C3Dname).(path_name).CycleIndex, 2)+1:2*size
(VICON.(C3Dname).(path_name).CycleIndex, 2), :) =
flipdim(VICON.(C3Dname).(path_name).RMS.step_Error_CS(cyclenum).allsteps.(cha
r(tname_cell{toolnum}))(:, :, 2), 1);

VICON.(C3Dname).combined.RMS.step_Error_CS(cyclenum).allsteps.(char(tname_cel
l{toolnum})) = step_ErrorCS_Combined;

        end

        for stepnum = 1:1:size(VICON.(C3Dname).(path_name).CycleIndex, 2)

            for paramnum = 1:6

                for cyclenum =
1:(size(VICON.(C3Dname).(path_name).CycleIndex, 1)-1)
                    temp_rms(stepnum, paramnum, cyclenum) =
VICON.(C3Dname).combined.RMS.step_Error_CS(cyclenum).allsteps.(char(tname_cel
l{toolnum}))(stepnum, paramnum);
                    end
                end
            end
        end

VICON.(C3Dname).combined.RMS.step_RMS_CS.allsteps.(char(tname_cell{toolnum}))
(stepnum, paramnum) = rms(temp_rms(stepnum, paramnum, :));

        end
    end
end

        end
end

if pnTrans == 2
    pnTrans = 3;
end

end

```

D.3 FIXTURE RIGIDITY

D.3.1 Rigidity Analysis

The code ‘VICON_Rotation.m’ measured the rotations and translations between each rigid body: end-effector/superior fixture and superior vertebra, superior vertebra and inferior vertebra, and inferior vertebra and inferior fixture/base using the motion collection process referenced previously (Appendix D.2.1). This code calculates the kinematic differences for relative motion at the fixation interfaces and spinal segment between starting and extreme positions in motion paths. Stiffness assessments were made by integrating primary moments with interface and FSU motion data (Equation 1 and Equation 2)

Interface/FSU Movement: VICON_Rigid.m

```
function VICON = VICON_Rigid(VICON)

%Rigidity Analysis - 1/30/12

%Rob Hartman - Assess Rigidity of Rabbit FSU

%Digitization required for anatomical RF analysis (intuitive axes).
%DEFINE ANATOMICAL RFs: <Digitize_filter.m> takes anatomical points collected
using stylus and
%forms anatomical RFs per body/level.
%CALCULATE T_M_A: <Digitize_link.m> calculates the
%transformation between anatomical and measured RFs (calc. at rest).
%MEASURE/CALC. T_G_M: Measured RFs are defined from marker position (x,y,z)
%from tools attached to bodies and robot fixtures (during test). Positions
are
%measured continuously during testing. <VICON_filter.m> is used to divide
%marker data into cycles, steps, and directions.
%CALCULATE T_G_A & T_Ai_Aj: <VICON_Rotation.m> takes the measured, segmented
T_G_M data
%and uses the T_M_A's from <Digitize_link.m> to calculate T_G_A and T_Ai_Aj
%at each step, cycle, etc. T_Ao_An presents the motion of a segment with
respect to
%itself. *(cycle).Transform.Anatomical.T_ij_02N illustrates transformation
b/w segments
%in the anatomical RF. The code also plots overall ROM (primary axis)
alongside each
```

```

%intersegmental ROM to illustrate primary motion distribution.

%THIS CODE | <VICON_rigidity.m> examines anatomical RF rigidity. The position
and rotation data
%from the transformation b/w end-effector and superior segment (1 vs 2) and
%base and inferior segment (3 vs 4) at each step along the path will be
%displayed. The difference b/w initial and final relative position &
%rotation will be calculated.

% To be run after <VICON_Rotation.m>

%Purpose of this function?

C3Dname = VICON.Options.C3Dname;
posneg = VICON.Options.posneg;
pathsequence = VICON.Options.pathsequence;

%RAH additions to accomodate broken VICON_display.m
path_name = 'single_0_pos';

binum = 2;
pnTrans = VICON.(C3Dname).pnTrans;

if strcmp(posneg,'pos')==1
    pos1 = 1;
else
    pos1 = 0;
end

EE_Correct = [1 0 0 0; 0 1 0 0; 0 0 1 0; 0 0 0 1];
tname_cell = {'S1','S2','S3','S4','S5','S6'};
tname_cell1 = {'s1','s2','s3','s4','s5','s6'};
frames = VICON.(C3Dname).frames;
markers = VICON.(C3Dname).markers;

%---
%NaNs are not likely to be present at this point
%---

%initialize figure
rotnum = 4; %primary motion
figure
cycles = size(VICON.(C3Dname).(path_name).CycleIndex,1);
% basic ROM bar plot
subplot((cycles-1),1,1);
hold on

numtools = size(VICON.(C3Dname).tnames,1);
%loop through tools; not an efficient way to do this
for toolnum = 1:numtools

    %analyze differences b/w first & second and last & second-to-last segment
    %other segments/tools are skipped (not efficient)

```

```

if toolnum == 1 || toolnum == (size(VICON.(C3Dname).tnames,1)-1)

    Tseg = ['T_' num2str(numtools) num2str(toolnum)];
    % Tsegcell = w/r/t base (T_51, T_52, etc)
    Tsegcell{toolnum} = Tseg;
    T02N = [Tsegcell{toolnum} '_02N'];
    ypr02N = ['ypr_' num2str(toolnum+1) num2str(toolnum) '_02N'];
    yprtr02N = ['yprtr_' num2str(toolnum+1) num2str(toolnum) '_02N'];

    %for 'out'(1) & 'back'(2)
    for bidirect = 1:binum

        %for each cycle
        for cyclenum = 1:size(VICON.(C3Dname).(path_name).CycleIndex,1)-1

            %number of steps
            n = 5;
            n = size(VICON.(C3Dname).(path_name).CycleIndex,2);

            %difference of b/w first (always 0,0,0,0,0,0) and last step
            %i.e. 6 DOF motions at last step of motion (most extreme)

            VICON.(C3Dname).(path_name).Transform(cyclenum).anatomical.Rigid_02N.(yprtr02N) = ...

            VICON.(C3Dname).(path_name).Transform(cyclenum).anatomical.(yprtr02N)(n,: ,bidirect) - ...

            VICON.(C3Dname).(path_name).Transform(cyclenum).anatomical.(yprtr02N)(1,: ,bidirect);

            %set up subplot
            subplot(cycles,1,cyclenum);

            %for each step
            for stepnum =
1:size(VICON.(C3Dname).(path_name).CycleIndex,2)

                %mean across steps for each cycle

                VICON.(C3Dname).(path_name).Transform(cyclenum).anatomical.Rigid_mean_tr.(yprtr02N) = ...

                mean(VICON.(C3Dname).(path_name).Transform(cyclenum).anatomical.(yprtr02N)(stepnum,1:3,bidirect));

                %stdev across steps for each cycle

                VICON.(C3Dname).(path_name).Transform(cyclenum).anatomical.Rigid_std_tr.(yprtr02N) = ...

                std(VICON.(C3Dname).(path_name).Transform(cyclenum).anatomical.(yprtr02N)(stepnum,1:3,bidirect));

```

```

        %mean across steps for each cycle

VICON.(C3Dname).(path_name).Transform(cyclenum).anatomical.Rigid_mean_ypr.(yprtr02N) = ...

mean(VICON.(C3Dname).(path_name).Transform(cyclenum).anatomical.(yprtr02N)(stepnum,4:6,bidirect));

        %stdev across steps for each cycle

VICON.(C3Dname).(path_name).Transform(cyclenum).anatomical.Rigid_std_ypr.(yprtr02N) = ...

std(VICON.(C3Dname).(path_name).Transform(cyclenum).anatomical.(yprtr02N)(stepnum,4:6,bidirect));

        %for x, y, z, rx, ry, rz
        for dof = 1:6

                %color coding DOF
                if dof == 1; dofColor = 'bx'; elseif dof == 2;
dofColor = 'rx'; elseif dof == 3; dofColor = 'gx'; elseif dof == 4; dofColor
= 'b.'; elseif dof == 5; dofColor = 'r.'; elseif dof == 6; dofColor = 'g.';
end;

                %plotting w/i subplot

plot(stepnum,VICON.(C3Dname).(path_name).Transform(cyclenum).anatomical.(yprtr02N)(stepnum,dof,bidirect),dofColor)
                hold on

        end

        end

        end

        end

        %above code defines rigidity per cycle; now need to average rigidity
outcomes across cycles
        %for each cycle
        for cyclenum = 1:size(VICON.(C3Dname).(path_name).CycleIndex,1)-1

                %mean final angles & translations

VICON.(C3Dname).(path_name).Rigidity.anatomical.meanF_yprtr.(yprtr02N) =
VICON.(C3Dname).(path_name).Transform(cyclenum).anatomical.Rigid_02N.(yprtr02N);

                %mean translational rigidity
                VICON.(C3Dname).(path_name).Rigidity.anatomical.mean_tr.(yprtr02N) =
mean(VICON.(C3Dname).(path_name).Transform(cyclenum).anatomical.Rigid_mean_tr.(yprtr02N));

                %mean rotational rigidity

```

```

        VICON.(C3Dname).(path_name).Rigidity.anatomical.mean_ypr.(yprtr02N) =
mean(VICON.(C3Dname).(path_name).Transform(cyclenum).anatomical.Rigid_mean_ypr.
(yprtr02N));
        %std translational rigidity
        VICON.(C3Dname).(path_name).Rigidity.anatomical.mean_tr.(yprtr02N) =
mean(VICON.(C3Dname).(path_name).Transform(cyclenum).anatomical.Rigid_std_tr.
(yprtr02N));
        %std rotational rigidity
        VICON.(C3Dname).(path_name).Rigidity.anatomical.mean_ypr.(yprtr02N) =
mean(VICON.(C3Dname).(path_name).Transform(cyclenum).anatomical.Rigid_std_ypr.
(yprtr02N));

    end

end

```

D.4 MECHANICAL OUTCOMES ANALYSIS

D.4.1 Organize Kinetic Data

Load Data: rFSU_dataLoad.m

```

%Rob Hartman - 4/10/13

%creates master structure of all data of a particular variable across
%multiple (.mat) files

%pre-requisite: need to have all .mat files in the same directory w/ no
%other files

%data location
location = ('Z:\Ortho Research 3\FergusonLab\Students\Hartman,
Robert\RabbitRobot\SA1 - Testing\feRawData\');

%create string array w/ all file names
fileInfo = dir(location); %gets all info of files & directories at location
for i = 1:size(fileInfo,1) %(first two "names" are . and ..)
    fileNameExt{i} = cellstr(fileInfo(i).name); %creates cell array w/
filename+extension per cell
    [fileNameDummy fileExtDummy] = strtok(fileNameExt{i},'.'); %separates
filename from extension (i.e. .mat)
    fileName{i} = fileNameDummy; %store the filename only
    clear fileNameDummy fileExtDummy %delete the dummy variables
end
fileName = fileName(3:end)'; %remove the . and ..

```

```

%cell structure to access correct loop data based on cycle
path_name_p1 = {'loop_0_pos'; 'loop_pos_neg'; 'loop_neg_pos'};
path_name_p2 = {'loop_pos_neg'; 'loop_neg_pos'; 'loop_pos_0'};

% tool_path

for i = 1:size(fileName,1)
    % i

    %create name of .mat file to open
    nameDateID = fileName{i}; %accesses the cell
    nameDateID = nameDateID{1}; %nameDateID is now a string w/ .mat filename
    %unpacks the cell array into a string //for some reason,
    'RH_ALL.(nameDate{i})...' was not working

    %load .mat file per testing ID/day
    load([location,nameDateID],'Spine');

    %common structure fieldnames
    position = 'LAT0_FE0_AXIAL0';
    pathypestr = 'FE';
    state = 'Intact';
    motion = 'replay';
    pathsequence_str = 'loop';
    HAM_str = 'HAM';
    rotnum = 4;
    repnum = 5;

    %unique structure fieldnames - unique to each testing ID/day
    clear fn_S fn_RS replay_str cycleNumberTotal trial %cycle_max %clear with
each iteration
    fn_S = fieldnames(Spine); %name of specimen/date
    % fn_SA_st = fieldnames(Spine.(fn_S{i})); %state names
    % state = fn_SA_st{1};
    trial =
size(Spine.(fn_S{1}).(state).(position).(pathypestr).(motion),2); %assumes
the last trial contains the replay of chosen_i loop path
    % trial = 2;
    fn_RS =
fieldnames(Spine.(fn_S{1}).(state).(position).(pathypestr).(motion)(trial));
%obtains fieldname of replay string (:=replay_str)

    if i == 31 % Nov 07 2012 data
        replay_str = fn_RS{3};
    else
        replay_str = fn_RS{1};
    end

    cycleNumberTotal =
size(Spine.(fn_S{1}).(state).(position).(pathypestr).(motion)(trial).(replay
_str).(HAM_str).(pathsequence_str),2);
    cycle_max(i) = cycleNumberTotal-1;

```

```

    tool_start =
    Spine.(fn_S{1}).(state).(position).(pathtypestr).(motion)(trial).(replay_str)
    .(HAM_str).(pathsequence_str)(1,1).(path_name_p1{1}).position(:,1);

    if i == 9 || i == 10 || i == 12 %Dec smROM trials that had pre-moment
    (zero the extension moments--not perfectly accurate but closer to truth)
        load_start =
        Spine.(fn_S{1}).(state).(position).(pathtypestr).(motion)(trial).(replay_str)
        .(HAM_str).(pathsequence_str)(1,1).(path_name_p1{2}).load(:,end);
    else %subtract off starting position moments
        load_start =
        Spine.(fn_S{1}).(state).(position).(pathtypestr).(motion)(trial).(replay_str)
        .(HAM_str).(pathsequence_str)(1,1).(path_name_p1{1}).load(:,1);
    end

    clear feLD*
    for pnc = 1:cycle_max(i) %makes 'feData'

        for pn = 1:2 %both pos-neg & neg-pos

            if pnc == 1 %i think this ends up being the same thing...
                path_name = path_name_p1{pn+1};
            else
                path_name = path_name_p2[459];
            end

            % Calculate "NEW" Tool Path - redefining F/E based on initial
            starting position.
            %         display([num2str(pn) num2str(pnc)])
            tool_n =
            size(Spine.(fn_S{1}).(state).(position).(pathtypestr).(motion)(trial).(replay_str)
            .(HAM_str).(pathsequence_str)(1,pnc).(path_name).position(:,,:),2);

            for ti = 1:tool_n %subtract starting position from each step to
            set to 0
                tool_path(:,ti) =
                Spine.(fn_S{1}).(state).(position).(pathtypestr).(motion)(trial).(replay_str)
                .(HAM_str).(pathsequence_str)(1,pnc).(path_name).position(:,ti) - tool_start;
                load_path(:,ti) =
                Spine.(fn_S{1}).(state).(position).(pathtypestr).(motion)(trial).(replay_str)
                .(HAM_str).(pathsequence_str)(1,pnc).(path_name).load(:,ti) - load_start;
            end

            tool_end = tool_path(:,end);
            load_end = load_path(:,end);
            [zero_val, zero_loc] = min(abs(tool_path(repnum,:)));

            %save data - per cycle

            Spine.(fn_S{1}).(state).(position).(pathtypestr).(motion)(trial).(replay_str)
            .(HAM_str).(pathsequence_str)(1,pnc).(path_name).tool_zero = [zero_val,
            zero_loc];

            Spine.(fn_S{1}).(state).(position).(pathtypestr).(motion)(trial).(replay_str)

```

```

.(HAM_str).(pathsequence_str)(1,pnc).(path_name).tool_path_new(:, :) =
tool_path;

Spine.(fn_S{1}).(state).(position).(pathtypestr).(motion)(trial).(replay_str)
.(HAM_str).(pathsequence_str)(1,pnc).(path_name).load_path_new(:, :) =
load_path;

    clear tool_path load_path

    if pn == 1 %pos_neg
        feLDpn(:, :, pnc) =
[Spine.(fn_S{1}).(state).(position).(pathtypestr).(motion)(trial).(replay_str)
.(HAM_str).(pathsequence_str)(1,pnc).(path_name).tool_path_new(:, :)]...

Spine.(fn_S{1}).(state).(position).(pathtypestr).(motion)(trial).(replay_str)
.(HAM_str).(pathsequence_str)(1,pnc).(path_name).load_path_new(:, :)]];
        feData.feDegMomPN = feLDpn;
    elseif pn == 2 %neg_pos
        feLDnp(:, :, pnc) =
[Spine.(fn_S{1}).(state).(position).(pathtypestr).(motion)(trial).(replay_str)
.(HAM_str).(pathsequence_str)(1,pnc).(path_name).tool_path_new(:, :)]...

Spine.(fn_S{1}).(state).(position).(pathtypestr).(motion)(trial).(replay_str)
.(HAM_str).(pathsequence_str)(1,pnc).(path_name).load_path_new(:, :)]];
        feData.feDegMomNP = feLDnp;
    end

end

end

%         feData(pnc) =
Spine.(fn_S{1}).(state).(position).(pathtypestr).(motion)(trial).(replay_str)
.(HAM_str).(pathsequence_str)(1,pnc).(path_name_p1{1}); %contains position,
tool_path_new, load (and tool_zero)
end

% saves into master structure variable, feReplay_ALL, which contains
%6-axis position (normalized to starting position & aligned to specimen)
and load data
feReplayALL.(nameDateID).fePN = feData.feDegMomPN;
feReplayALL.(nameDateID).feNP = feData.feDegMomNP;

%
end

```

D.4.2 Moments and Range-of-Motion

Moments and range-of-motion (ROM) for flexion/extension (F/E) are shown in 'rFSU_feROM.m.' By changing 'rotnum' and 'loadnum' to 4 and 11, respectively, the same code can be used to calculate axial torsion (AT) moments and rotations.

Find F/E Moments and ROM in 'Replay': rFSU_feROM.m

```
%find average F/E ROM for replay paths

%must run <rFSU_LoopPlottingReplay.m> first to create 'tool_path_new' for
%each 'pn' and 'np' per cycle

%data parameters
fn_fRA = fieldnames(feReplayALL); %fieldnames of all files
rotnum = 5;
loadnum = 10;

if isfield(feReplayALL,'LR') == 1
    n = size(fn_fRA,1) - 4; %other scripts may have added fields to structure
    that aren't test IDs
else
    n = size(fn_fRA,1); %if no other fields are added, all fieldnames
    correspond to IDs
end

% MxStart =
Spine.(date).(state).(position).(path).(motion)(trial).(replay_str).HAM.(path
type)(1).(path_name_p1{1}).load(loadnum,1);
% load_start replaces MxStart, though load_start is [6,1]

for i = 1:size(fileName,1)

    %for SA1, tpp/lep is flexion & tpn/len is extension by convention
    cycle_maxS = size(feReplayALL.(fn_fRA{i}).fePN(:, :, :), 3); %number of cycles
    per test/specimen

    clear max*
    for pnc = 1:cycle_maxS %across cycles

        %
            pnc
            %pos-neg paths: extremes of path flexion & extension ROM (:=max*ROM)
            %and moment (:=max*Mx)
            %unloading flexion, loading extension > UNLOADING (1)
            maxfROM(pnc,1) = feReplayALL.(fn_fRA{i}).fePN(rotnum,1,pnc);
            maxeROM(pnc,2) = feReplayALL.(fn_fRA{i}).fePN(rotnum,end,pnc);
            maxfMx(pnc,1) = -feReplayALL.(fn_fRA{i}).fePN(loadnum,1,pnc);
```

```

maxeMx(pnc,2) = feReplayALL.(fn_fRA{i}).fePN(loadnum,end,pnc);

%neg-pos paths
%loading flexion, unloading extension > LOADING (2)
maxfROM(pnc,2) = feReplayALL.(fn_fRA{i}).feNP(rotnum,end,pnc);
maxeROM(pnc,1) = feReplayALL.(fn_fRA{i}).feNP(rotnum,1,pnc);
maxfMx(pnc,2) = -feReplayALL.(fn_fRA{i}).feNP(loadnum,end,pnc);
maxeMx(pnc,1) = feReplayALL.(fn_fRA{i}).feNP(loadnum,1,pnc);

%combined F/E
maxCfeROM(pnc,1) = abs(maxfROM(pnc,1)) + abs(maxeROM(pnc,1)); %pn:
add flexion to extension values
maxCfeROM(pnc,2) = abs(maxfROM(pnc,2)) + abs(maxeROM(pnc,2)); %np:
add flexion to extension values
maxCfeMx(pnc,1) = abs(maxfMx(pnc,2)) + abs(maxeMx(pnc,2)); %loading
moments: add flexion to extension values
maxCfeMx(pnc,2) = abs(maxfMx(pnc,1)) + abs(maxeMx(pnc,1)); %unloading
moments: add flexion to extension values

end

%save moment data
feReplayALL.(fn_fRA{i}).maxFlexMx = maxfMx; %flexion moments
feReplayALL.(fn_fRA{i}).maxExtMx = maxeMx; %extension moments
feReplayALL.(fn_fRA{i}).maxFEMx = maxCfeMx; %overall f/e moments

%% ROM & Moment parameters across pncs (w/ std's) - to be imported to
mechOutcomesSummary.xls
%find max ROM & moment for flexion & extension in unloading & loading & mean
U&L curves

%----ROM (Rx: deg)-----
%unloading curves (pn for flexion)
ROMfMax(1,1) = mean(maxfROM(:,1));
ROMfMax(2,1) = std(maxfROM(:,1)); %variation across pncs
%loading curves (np for flexion)
ROMfMax(1,2) = mean(maxfROM(:,2));
ROMfMax(2,2) = std(maxfROM(:,2));
%average of loading & unloading ROM & Mx values
ROMfMax(1,3) = mean(mean(maxfROM));
ROMfMax(2,3) = std(mean(maxfROM)); %"variation" between unloading & loading

%unloading curves (np for extension)
ROMeMax(1,1) = mean(maxeROM(:,2));
ROMeMax(2,1) = std(maxeROM(:,2));
%loading curves (pn for flexion)
ROMeMax(1,2) = mean(maxeROM(:,1));
ROMeMax(2,2) = std(maxeROM(:,1));
%average of loading & unloading ROM & Mx values
ROMeMax(1,3) = mean(mean(maxeROM));
ROMeMax(2,3) = std(mean(maxeROM));

%combined F/E
ROMcfeMax(1,1) = mean(maxCfeROM(:,1)); %pos-neg

```

```

ROMcfeMax(2,1) = std(maxCfeROM(:,1));

ROMcfeMax(1,2) = mean(maxCfeROM(:,2)); %neg-pos
ROMcfeMax(2,2) = std(maxCfeROM(:,2));

ROMcfeMax(1,3) = mean(mean(maxCfeROM)); %mean pn w/ np
ROMcfeMax(2,3) = std(mean(maxCfeROM));

%differences in ROM across cycles: flexion
%extremes (max - min)
ROMfDiffExtreme(1) = max(maxfROM(:,1)) - min(maxfROM(:,1)); %unloading path
ROMfDiffExtreme(2) = max(maxfROM(:,2)) - min(maxfROM(:,2)); %loading path
ROMfDiffExtreme(3) = max(mean(maxfROM)) - min(mean(maxfROM)); %average
unloading & loading paths
% ordinal (i.e. initial - final based on 1st cycle...
ROMfDiffOrdin_1(1) = maxfROM(end,1) - maxfROM(1,1); %unloading path
ROMfDiffOrdin_1(2) = maxfROM(end,2) - maxfROM(1,2); %loading path
ROMfDiffOrdin_1(3) = mean(maxfROM(end,:)) - (mean(maxfROM(1,:))); %average
unloading & loading paths
% and 3rd cycle)
ROMfDiffOrdin_3(1) = maxfROM(end,1) - maxfROM(3,1); %unloading path
ROMfDiffOrdin_3(2) = maxfROM(end,2) - maxfROM(3,2); %loading path
ROMfDiffOrdin_3(3) = mean(maxfROM(end,:)) - (mean(maxfROM(3,:))); %average
unloading & loading paths

%differences in ROM across cycles: extension
%extremes (max - min)
ROMeDiffExtreme(1) = max(maxeROM(:,2)) - min(maxeROM(:,2)); %unloading path
ROMeDiffExtreme(2) = max(maxeROM(:,1)) - min(maxeROM(:,1)); %loading path
ROMeDiffExtreme(3) = max(mean(maxeROM)) - min(mean(maxeROM)); %average
unloading & loading paths
% ordinal (i.e. initial - final based on 1st cycle...
ROMeDiffOrdin_1(1) = maxeROM(end,1) - maxeROM(1,1); %unloading path
ROMeDiffOrdin_1(2) = maxeROM(end,2) - maxeROM(1,2); %loading path
ROMeDiffOrdin_1(3) = mean(maxeROM(end,:)) - (mean(maxeROM(1,:))); %average
unloading & loading paths
% and 3rd cycle)
ROMeDiffOrdin_3(1) = maxeROM(end,1) - maxeROM(3,1); %unloading path
ROMeDiffOrdin_3(2) = maxeROM(end,2) - maxeROM(3,2); %loading path
ROMeDiffOrdin_3(3) = mean(maxeROM(end,:)) - (mean(maxeROM(3,:))); %average
unloading & loading paths

%---moment (Mx: Nm)-----
%unloading curves (pn for flexion)
MxfMax(1,1) = mean(maxfMx(:,1));
MxfMax(2,1) = std(maxfMx(:,1));
%loading curves (np for flexion)
MxfMax(1,2) = mean(maxfMx(:,2));
MxfMax(2,2) = std(maxfMx(:,2));
%average of loading & unloading Mx & Mx values
MxfMax(1,3) = mean(mean(maxfMx));
MxfMax(2,3) = std(mean(maxfMx));

%unloading curves (np for extension)
MxeMax(1,1) = mean(maxeMx(:,2));
MxeMax(2,1) = std(maxeMx(:,2));

```

```

%loading curves (pn for flexion)
MxeMax(1,2) = mean(maxeMx(:,1));
MxeMax(2,2) = std(maxeMx(:,1));
%average of loading & unloading Mx & Mx values
MxeMax(1,3) = mean(mean(maxeMx));
MxeMax(2,3) = std(mean(maxeMx));

%combined F/E
% maxCfeMx = maxfMx + abs(maxeMx); %add flexion to extension values

MxcfeMax(1,1) = mean(maxCfeMx(:,1)); %loading (in both flexion & ext)
MxcfeMax(2,1) = std(maxCfeMx(:,1));

MxcfeMax(1,2) = mean(maxCfeMx(:,2)); %unloading ( " " " )
MxcfeMax(2,2) = std(maxCfeMx(:,2));

MxcfeMax(1,3) = mean(mean(maxCfeMx)); %mean loading & unloading
MxcfeMax(2,3) = std(mean(maxCfeMx));

%differences in Mx across cycles: flexion
%extremes (max - min)
MxfDiffExtreme(1) = max(maxfMx(:,1)) - min(maxfMx(:,1)); %unloading path
MxfDiffExtreme(2) = max(maxfMx(:,2)) - min(maxfMx(:,2)); %loading path
MxfDiffExtreme(3) = max(mean(maxfMx)) - min(mean(maxfMx)); %average unloading
& loading paths
% ordinal (i.e. initial - final based on 1st cycle...
MxfDiffOrdin_1(1) = maxfMx(1,1) - maxfMx(end,1); %unloading path
MxfDiffOrdin_1(2) = maxfMx(1,2) - maxfMx(end,2); %loading path
MxfDiffOrdin_1(3) = mean(maxfMx(1,:)) - (mean(maxfMx(end,:))); %average
unloading & loading paths
% and 3rd cycle)
MxfDiffOrdin_3(1) = maxfMx(3,1) - maxfMx(end,1); %unloading path
MxfDiffOrdin_3(2) = maxfMx(3,2) - maxfMx(end,2); %loading path
MxfDiffOrdin_3(3) = mean(maxfMx(3,:)) - (mean(maxfMx(end,:))); %average
unloading & loading paths

%differences in Mx across cycles: extension
% extremes (max - min)
MxeDiffExtreme(1) = max(maxeMx(:,2)) - min(maxeMx(:,2)); %unloading path
MxeDiffExtreme(2) = max(maxeMx(:,1)) - min(maxeMx(:,1)); %loading path
MxeDiffExtreme(3) = max(mean(maxeMx)) - min(mean(maxeMx)); %average unloading
& loading paths
% ordinal (i.e. initial - final based on 1st cycle...
MxeDiffOrdin_1(1) = maxeMx(1,1) - maxeMx(end,1); %unloading path
MxeDiffOrdin_1(2) = maxeMx(1,2) - maxeMx(end,2); %loading path
MxeDiffOrdin_1(3) = mean(maxeMx(1,:)) - (mean(maxeMx(end,:))); %average
unloading & loading paths
% and 3rd cycle)
MxeDiffOrdin_3(1) = maxeMx(3,1) - maxeMx(end,1); %unloading path
MxeDiffOrdin_3(2) = maxeMx(3,2) - maxeMx(end,2); %loading path
MxeDiffOrdin_3(3) = mean(maxeMx(3,:)) - (mean(maxeMx(end,:))); %average
unloading & loading paths

%differences in Mx across cycles: flexion/extension
% extremes (max - min)

```

```

MxcfeDiffExtreme(1) = max(maxCfeMx(:,2)) - min(maxCfeMx(:,2)); %unloading
path
MxcfeDiffExtreme(2) = max(maxCfeMx(:,1)) - min(maxCfeMx(:,1)); %loading path
MxcfeDiffExtreme(3) = max(mean(maxCfeMx)) - min(mean(maxCfeMx)); %average
unloading & loading paths
% ordinal (i.e. initial - final based on 1st cycle...
MxcfeDiffOrdin_1(1) = maxCfeMx(1,1) - maxCfeMx(end,1); %unloading path
MxcfeDiffOrdin_1(2) = maxCfeMx(1,2) - maxCfeMx(end,2); %loading path
MxcfeDiffOrdin_1(3) = mean(maxCfeMx(1,:)) - (mean(maxCfeMx(end,:))); %average
unloading & loading paths
% and 3rd cycle)
MxcfeDiffOrdin_3(1) = maxCfeMx(3,1) - maxCfeMx(end,1); %unloading path
MxcfeDiffOrdin_3(2) = maxCfeMx(3,2) - maxCfeMx(end,2); %loading path
MxcfeDiffOrdin_3(3) = mean(maxCfeMx(3,:)) - (mean(maxCfeMx(end,:))); %average
unloading & loading paths
%-----

%-----save data-----
feReplayALL.(fn_fRA{i}).ROM.FlexROM = ROMfMax;
feReplayALL.(fn_fRA{i}).ROM.ExtROM = ROMeMax;
feReplayALL.(fn_fRA{i}).ROM.cfeROM = ROMcfeMax;
feReplayALL.(fn_fRA{i}).ROM.fDiffExtreme = ROMfDiffExtreme;
feReplayALL.(fn_fRA{i}).ROM.eDiffExtreme = ROMeDiffExtreme;
% feReplayALL.(fn_fRA{i}).ROM.cfeDiffExtreme = ROMcfeDiffExtreme;
feReplayALL.(fn_fRA{i}).ROM.fDiffOrdin_1 = ROMfDiffOrdin_1;
feReplayALL.(fn_fRA{i}).ROM.eDiffOrdin_1 = ROMeDiffOrdin_1;
% feReplayALL.(fn_fRA{i}).ROM.cfeDiffOrdin_1 = ROMcfeDiffOrdin_1;
feReplayALL.(fn_fRA{i}).ROM.fDiffOrdin_3 = ROMfDiffOrdin_3;
feReplayALL.(fn_fRA{i}).ROM.eDiffOrdin_3 = ROMeDiffOrdin_3;
% feReplayALL.(fn_fRA{i}).ROM.cfeDiffOrdin_3 = ROMcfeDiffOrdin_3;
feReplayALL.(fn_fRA{i}).Mx.FlexMx = MxfMax;
feReplayALL.(fn_fRA{i}).Mx.ExtMx = MxeMax;
feReplayALL.(fn_fRA{i}).Mx.cfeMx = MxcfeMax;
feReplayALL.(fn_fRA{i}).Mx.fDiffExtreme = MxfDiffExtreme;
feReplayALL.(fn_fRA{i}).Mx.eDiffExtreme = MxeDiffExtreme;
feReplayALL.(fn_fRA{i}).Mx.cfeDiffExtreme = MxcfeDiffExtreme;
feReplayALL.(fn_fRA{i}).Mx.fDiffOrdin_1 = MxfDiffOrdin_1;
feReplayALL.(fn_fRA{i}).Mx.eDiffOrdin_1 = MxeDiffOrdin_1;
feReplayALL.(fn_fRA{i}).Mx.cfeDiffOrdin_1 = MxcfeDiffOrdin_1;
feReplayALL.(fn_fRA{i}).Mx.fDiffOrdin_3 = MxfDiffOrdin_3;
feReplayALL.(fn_fRA{i}).Mx.eDiffOrdin_3 = MxeDiffOrdin_3;
feReplayALL.(fn_fRA{i}).Mx.cfeDiffOrdin_3 = MxcfeDiffOrdin_3;

end

```

D.4.3 Load Relaxation

Moment relaxation for flexion/extension (F/E) is shown in 'rFSU_loadRelaxation.m.' By changing 'rotnum' and 'loadnum' to 4 and 11, respectively, the same code can be used to calculate axial torsion (AT) moment relaxation. Relaxation of other parameters can also be calculated.

Relaxation in F/E Moments: rFSU_loadRelaxation.m

```
%rFSU load relaxation code
%RAH - Aug 2012
%working off superSpine.mat (Spine_ALL*)

%data parameters
clear tp* le*

% based on <rFSU_feROM.m>...consolidated variables
% specifically, based on maxfMx, maxeM (moments at endpts of each cycle)

%data parameters
fn_fRA = fieldnames(feReplayALL);

%F/E
rotnum = 5;
loadnum = 10;

% MxStart =
Spine.(date).(state).(position).(path).(motion)(trial).(replay_str).HAM.(path
type)(1).(path_name_p1{1}).load(loadnum,1);
% % MxStart = 0.0437879178306911;
% load_start replaces MxStart, though load_start is [6,1]

for i = 1:size(fileName,1)

    i;

    date = fn_fRA{i};

    clear maxf* maxe* maxC* Relax*
    %for SA1, tpp/lep is flexion & tpn/len is extension by convention
    cycle_maxS = size(feReplayALL.(fn_fRA{i}).fePN(:, :, :), 3); %number of
cycles per test/specimen

    maxfMx = feReplayALL.(fn_fRA{i}).maxFlexMx;
    maxeMx = feReplayALL.(fn_fRA{i}).maxExtMx;
    maxCfeMx = feReplayALL.(fn_fRA{i}).maxFEMx;

    clear Mxf* Mxe* MxC*
```

```

%for SA1, tpp/lep is flexion & tpn/len is extension by convention
for pnc = 1:cycle_maxS
%
    pnc

%-----percent relaxation (change/original * 100%)-----
    %unloading - based on 3rd pnc
    %percent change - neg is dec; normalized by 3rd cycle moment value
    MxfRelax(pnc,1) = (100) * (maxfMx(pnc,1) - maxfMx(3,1)) /
maxfMx(3,1); %flexion relaxation
    MxeRelax(pnc,1) = (100) * (maxeMx(pnc,1) - maxeMx(3,1)) /
maxeMx(3,1); %extension relaxation
    MxCfeRelax(pnc,1) = (100) * (maxCfeMx(pnc,1) - maxCfeMx(3,1)) /
maxCfeMx(3,1); %extension relaxation

    %loading - based on 3rd pnc
    MxfRelax(pnc,2) = (100) * (maxfMx(pnc,2) - maxfMx(3,2)) /
maxfMx(3,2); %flexion relaxation
    MxeRelax(pnc,2) = (100) * (maxeMx(pnc,2) - maxeMx(3,2)) /
maxeMx(3,2); %extension relaxation
    MxCfeRelax(pnc,2) = (100) * (maxCfeMx(pnc,2) - maxCfeMx(3,2)) /
maxCfeMx(3,2); %extension relaxation

    %mean unloading/loading - based on 3rd pnc
    MxfRelax(pnc,3) = (100) * ((mean(maxfMx(pnc,:)) - mean(maxfMx(3,:)))
/ mean(maxfMx(3,:))); %flexion relaxation
    MxeRelax(pnc,3) = (100) * ((mean(maxeMx(pnc,:)) - mean(maxeMx(3,:)))
/ mean(maxeMx(3,:))); %extension relaxation
    MxCfeRelax(pnc,3) = (100) * ((mean(maxCfeMx(pnc,:)) -
mean(maxCfeMx(3,:))) / mean(maxCfeMx(3,:))); %extension relaxation

    if pnc == 3
        MxfRelax(pnc,:) = [1,1,1];
        MxeRelax(pnc,:) = [1,1,1];
        MxCfeRelax(pnc,:) = [1,1,1];
    end

end

% %-----end relaxation-----
%
    %flexion & extension relaxation (expressed as % of intact)
    %increase is positive; decrease is negative
    RelaxnFlexion = [MxfRelax(:,1), MxfRelax(:,2), MxfRelax(:,3),
abs(MxfRelax(:,1)-MxfRelax(:,2))];
    RelaxnExtension = [MxeRelax(:,1), MxeRelax(:,2), MxeRelax(:,3),
abs(MxeRelax(:,1)-MxeRelax(:,2))];
    RelaxnCFE = [MxCfeRelax(:,1), MxCfeRelax(:,2), MxCfeRelax(:,3),
abs(MxCfeRelax(:,1)-MxCfeRelax(:,2))]; %combined flexion extension
%
    %change over cycles
    %flexion
    %extremes (max - min)
    MxRelaxfDiffExtreme(1) = max(MxfRelax(:,1)) - min(MxfRelax(:,1));
%unloading path
    MxRelaxfDiffExtreme(2) = max(MxfRelax(:,2)) - min(MxfRelax(:,2));
%loading path

```

```

MxRelaxfDiffExtreme(3) = max(MxfRelax(:,3)) - min(MxfRelax(:,3));
%average unloading & loading paths
% ordinal (i.e. initial - final based on 1st pnc...
MxRelaxfDiffOrdin_1(1) = MxfRelax(1,1) - MxfRelax(end,1); %unloading path
MxRelaxfDiffOrdin_1(2) = MxfRelax(1,2) - MxfRelax(end,2); %loading path
MxRelaxfDiffOrdin_1(3) = MxfRelax(1,3) - MxfRelax(end,3); %average
unloading & loading paths
% and 3rd pnc)
MxRelaxfDiffOrdin_3(1) = MxfRelax(3,1) - MxfRelax(end,1); %unloading path
MxRelaxfDiffOrdin_3(2) = MxfRelax(3,2) - MxfRelax(end,2); %loading path
MxRelaxfDiffOrdin_3(3) = MxfRelax(3,3) - MxfRelax(end,3); %average
unloading & loading paths

%extension
% extremes (max - min)
MxRelaxeDiffExtreme(1) = max(MxeRelax(:,1)) - min(MxeRelax(:,1));
%unloading path
MxRelaxeDiffExtreme(2) = max(MxeRelax(:,2)) - min(MxeRelax(:,2));
%loading path
MxRelaxeDiffExtreme(3) = max(MxeRelax(:,3)) - min(MxeRelax(:,3));
%average unloading & loading paths
% ordinal (i.e. initial - final based on 1st pnc...
MxRelaxeDiffOrdin_1(1)= MxeRelax(1,1) - MxeRelax(end,1); %unloading path
MxRelaxeDiffOrdin_1(2) = MxeRelax(1,2) - MxeRelax(end,2); %loading path
MxRelaxeDiffOrdin_1(3) = MxeRelax(1,3) - MxeRelax(end,3); %average
unloading & loading paths
% and 3rd pnc)
MxRelaxeDiffOrdin_3(1) = MxeRelax(3,1) - MxeRelax(end,1); %unloading path
MxRelaxeDiffOrdin_3(2) = MxeRelax(3,2) - MxeRelax(end,2); %loading path
MxRelaxeDiffOrdin_3(3) = MxeRelax(3,3) - MxeRelax(end,3); %average
unloading & loading paths

%combined flexion-extension
% extremes (max - min)
MxRelaxcfeDiffExtreme(1) = max(RelaxnCFE(:,1)) - min(RelaxnCFE(:,1));
%unloading path
MxRelaxcfeDiffExtreme(2) = max(RelaxnCFE(:,2)) - min(RelaxnCFE(:,2));
%loading path
MxRelaxcfeDiffExtreme(3) = max(RelaxnCFE(:,3)) - min(RelaxnCFE(:,3));
%average unloading & loading paths
% ordinal (i.e. initial -final based on 1st pnc...
MxRelaxcfeDiffOrdin_1(1) = RelaxnCFE(1,1) - RelaxnCFE(end,1); %unloading
path
MxRelaxcfeDiffOrdin_1(2) = RelaxnCFE(1,2) - RelaxnCFE(end,2); %loading
path
MxRelaxcfeDiffOrdin_1(3) = RelaxnCFE(1,3) - RelaxnCFE(end,3); %average
unloading & loading paths
% and 3rd pnc)
MxRelaxcfeDiffOrdin_3(1) = RelaxnCFE(3,1) - RelaxnCFE(end,1); %unloading
path
MxRelaxcfeDiffOrdin_3(2) = RelaxnCFE(3,2) - RelaxnCFE(end,2); %loading
path
MxRelaxcfeDiffOrdin_3(3) = RelaxnCFE(3,3) - RelaxnCFE(end,3); %average
unloading & loading paths

%-----save data-----

```

```

    feReplayALL.(fn_fRA{i}).Relaxation.RelaxFlex = RelaxnFlexion;
    feReplayALL.(fn_fRA{i}).Relaxation.RelaxExt = RelaxnExtension;
    feReplayALL.(fn_fRA{i}).Relaxation.RelaxnCFE = RelaxnCFE;
    feReplayALL.(fn_fRA{i}).Relaxation.RelaxFlexDiffExtreme =
MxRelaxfDiffExtreme;
    feReplayALL.(fn_fRA{i}).Relaxation.RelaxFlexDiffOrdin1 =
MxRelaxfDiffOrdin_1;
    feReplayALL.(fn_fRA{i}).Relaxation.RelaxFlexDiffOrdin3 =
MxRelaxfDiffOrdin_3;
    feReplayALL.(fn_fRA{i}).Relaxation.RelaxExtDiffExtreme =
MxRelaxeDiffExtreme;
    feReplayALL.(fn_fRA{i}).Relaxation.RelaxExtDiffOrdin1 =
MxRelaxeDiffOrdin_1;
    feReplayALL.(fn_fRA{i}).Relaxation.RelaxExtDiffOrdin3 =
MxRelaxeDiffOrdin_3;
    feReplayALL.(fn_fRA{i}).Relaxation.RelaxCFEDiffExtreme =
MxRelaxcfeDiffExtreme;
    feReplayALL.(fn_fRA{i}).Relaxation.RelaxCFEDiffOrdin1 =
MxRelaxcfeDiffOrdin_1;
    feReplayALL.(fn_fRA{i}).Relaxation.RelaxCFEDiffOrdin3 =
MxRelaxcfeDiffOrdin_3;
    %-----
end

```

D.4.4 Neutral Zone and Elastic Zone Stiffness

Flexion/extension moment-rotation curve fitting: rFSUreplay_DS_.date.m*

```

function [Spine] = rFSUreplay_DS_*.date(Spine)
%CREATEFIT    Create plot of datasets and fits

% Data from dataset "tp1 vs. le1":
%   X = le1:
%   Y = tp1:
%   Unweighted

% This function was automatically generated on 09-Apr-2012 11:00:48

%fits loop paths - REPLAYs

%test-specific labels/data
position = 'LAT0_FE0_AXIAL0';
HAM_str = 'HAM';
motion = 'replay';
replay_str = 'replay45x';
pathsequence_str = 'loop';
trial = 1;
% Only Plotting 2nd cycle currently
cycle_max = 34; %
cycle_start = 1;

```

```

color_str1 = {'bo', 'ro', 'ko', 'go', 'mo'};
color_str2 = {'b+', 'r+', 'k+', 'g+', 'm+'};

pathtypestr = 'FE';

pos = 1; % 1 = pos, 0 = neg (first)

path_name_p1 = {'loop_0_pos'; 'loop_pos_neg'; 'loop_neg_pos'};
path_name_p2 = {'loop_pos_neg'; 'loop_neg_pos'; 'loop_pos_0'};
path_name_n1 = {'loop_0_neg'; 'loop_neg_pos'; 'loop_pos_neg'};
path_name_n2 = {'loop_neg_pos'; 'loop_pos_neg'; 'loop_neg_0'};

clear fn_SA
%Spine is a structure
fn_SA = fieldnames(Spine);

rotnum = 4; %loads - FE
repnum = 5; %position / tool_path - FE

%define number of conditions & states (set defaults if no input spec'd)
SPnum = 1;
Statenum = 1;

% disp('here')

for i = SPnum:SPnum

    %fn_SA_st = fieldnames(Spine.(fn_SA{i}));
    fn_SA_st = {'Intact'};
    fn_SA_st2 = strrep(fn_SA_st, '_', ' ');

    % State Names (FL0_AL0_noHAM, ...)
    for j = Statenum:Statenum

        for pnc = cycle_start:cycle_max
            pnc

                if pnc == 36

                    CF = NaN;

                Spine.(fn_SA{i}).(fn_SA_st{j}).(position).(pathtypestr).(motion)(trial).(repl
ay_str).(HAM_str).(pathsequence_str)(1,pnc).(path_name_p2{1}).CF = NaN;

                Spine.(fn_SA{i}).(fn_SA_st{j}).(position).(pathtypestr).(motion)(trial).(repl
ay_str).(HAM_str).(pathsequence_str)(1,pnc).(path_name_p2{1}).NZ_ALL(Statenum
,:) = NaN;

                Spine.(fn_SA{i}).(fn_SA_st{j}).(position).(pathtypestr).(motion)(trial).(repl
ay_str).(HAM_str).(pathsequence_str)(1,pnc).(path_name_p2{1}).EZ_ALL(Statenum
,:) = NaN;

                    %NZ average per cycle & "higher-in-the-structre" storage

```

```

        Spine.(fn_SA{i}).(fn_SA_st{j}).NZ_ALL(pnc,1:5) = NaN;
%(Spine.(fn_SA{i}).(fn_SA_st{j}).(position).(pathtypestr).(motion)(trial).(replay_str).(HAM_str).(pathsequence_str)(1,pnc).(path_name_p2{1}).NZ_ALL(Statenum,:)) +
Spine.(fn_SA{i}).(fn_SA_st{j}).(position).(pathtypestr).(motion)(trial).(replay_str).(HAM_str).(pathsequence_str)(1,pnc).(path_name_p2{2}).NZ_ALL(Statenum,:)) ./ 2;
        Spine.(fn_SA{i}).(fn_SA_st{j}).NZ_ALL(pnc,6:10) = NaN;
%abs(Spine.(fn_SA{i}).(fn_SA_st{j}).(position).(pathtypestr).(motion)(trial).(replay_str).(HAM_str).(pathsequence_str)(1,pnc).(path_name_p2{1}).NZ_ALL(Statenum,:)) -
Spine.(fn_SA{i}).(fn_SA_st{j}).(position).(pathtypestr).(motion)(trial).(replay_str).(HAM_str).(pathsequence_str)(1,pnc).(path_name_p2{2}).NZ_ALL(Statenum,:));

        %EZ average per cycle & "higher-in-the-structre" storage (1-
mean of pn,np in flexion, 2-mean of pn,np in extension ; 3-range b/w pn & np
in flexion, 4-range b/w pn & np in flexion)
        Spine.(fn_SA{i}).(fn_SA_st{j}).EZ_ALL(pnc,1:2) = NaN;
%(Spine.(fn_SA{i}).(fn_SA_st{j}).(position).(pathtypestr).(motion)(trial).(replay_str).(HAM_str).(pathsequence_str)(1,pnc).(path_name_p2{1}).EZ_ALL(Statenum,:)) +
Spine.(fn_SA{i}).(fn_SA_st{j}).(position).(pathtypestr).(motion)(trial).(replay_str).(HAM_str).(pathsequence_str)(1,pnc).(path_name_p2{2}).EZ_ALL(Statenum,:)) ./ 2;
        Spine.(fn_SA{i}).(fn_SA_st{j}).EZ_ALL(pnc,3:4) = NaN;
%abs(Spine.(fn_SA{i}).(fn_SA_st{j}).(position).(pathtypestr).(motion)(trial).(replay_str).(HAM_str).(pathsequence_str)(1,pnc).(path_name_p2{1}).EZ_ALL(Statenum,:)) -
Spine.(fn_SA{i}).(fn_SA_st{j}).(position).(pathtypestr).(motion)(trial).(replay_str).(HAM_str).(pathsequence_str)(1,pnc).(path_name_p2{2}).EZ_ALL(Statenum,:));

        disp('hello')
    else

        for k = 1:2

            tool_path_new =
Spine.(fn_SA{i}).(fn_SA_st{j}).(position).(pathtypestr).(motion)(trial).(replay_str).(HAM_str).(pathsequence_str)(1,pnc).(path_name_p2{k}).tool_path_new(:,:);
            load_end_pts = -
Spine.(fn_SA{i}).(fn_SA_st{j}).(position).(pathtypestr).(motion)(trial).(replay_str).(HAM_str).(pathsequence_str)(1,pnc).(path_name_p2{k}).load(:,:);

            %-----perform curve-fitting HERE (within 'pn' &
'np' looping)-----

            le1 = load_end_pts(rotnum,:);
            tp1 = tool_path_new(repnum,:);

            %used for EZ in case le1 data set is trimmed for NZ
analysis
            le1_all = le1;

```

```

if k == 2 %np
    %modify curve smoothness or size per cycle
    if pnc==35 % any cycle
        trim_IndxL = find(le1 < -0.2)';
        trim_IndxH = find(le1 > 0.6)';
        trim_Indx = [trim_IndxL trim_IndxH];
        tp1(trim_Indx) = [];
        le1(trim_Indx) = [];
        tp1_sm = smooth(le1,tp1,1,'moving',0);

    else
        tp1_sm = smooth(le1,tp1,3,'moving',0); %default
smoothing
    end
else %pn
    %modify curve smoothness or size per cycle
    if pnc==35 % any cycle
        trim_IndxL = find(le1 < -0.2)';
        trim_IndxH = find(le1 > 0.6)';
        trim_Indx = [trim_IndxL trim_IndxH];
        tp1(trim_Indx) = [];
        le1(trim_Indx) = [];
        tp1_sm = smooth(le1,tp1,1,'moving',0);
    else
        tp1_sm = smooth(le1,tp1,3,'moving',0); %default
smoothing
    end
end

% --- Create fit "DS 1"
ok_ = isfinite(le1) & isfinite(tp1_sm);
if ~all( ok_ )
    warning( 'GenerateMFile:IgnoringNansAndInfs', ...
        'Ignoring NaNs and Infs in data' );
end
st_ = [0.61133931403521835 0.17929230991254663
0.96904174210803418 0.16997270530500563 0.92473756802850282
0.56529983403084139 0.2759304694680681 ];
ft_ = fittype('(1/(1+exp(-(a1+b1*L))))*c1+(1/(1+exp(-
(a2+b2*L))))*c2+d',...
    'dependent',{'D'},'independent',{'L'},...
    'coefficients',{'a1', 'a2', 'b1', 'b2', 'c1', 'c2',
'd'});

% Fit this model using new data
[cf_,cf_gof] =
fit(le1(ok_),tp1_sm(ok_),ft_,'Startpoint',st_);

% Or use coefficients from the original fit:
if 0
    cv_ = { -0.37423720811936279, -4.1494845972262491,
405.3980878527874, -362.83832628109684, -17.490716086896914};
    [cf_,cf_gof] = cfit(ft_,cv_{:});
end

```

```

CF.cf = cf_;
CF.cf_gof = cf_gof;

CF.le1 = le1;
CF.tp1 = tp1_sm;
CF.ROM = tp1_sm(1) - tp1_sm(end);
CF.yfit = cf_(le1);

%Analysis

CF.coeffnames = coeffnames(CF.cf);
CF.coeffvalues = coeffvalues(CF.cf);

[CF.dydx, CF.d2ydx2] = differentiate(CF.cf, CF.le1);

[CF.max_dydx(1),CF.max_dydx(2)] = max(CF.dydx);
[CF.min_dydx(1),CF.min_dydx(2)] = min(CF.dydx);

[CF.max_d2ydx2(1),CF.max_d2ydx2(2)] = max(CF.d2ydx2);
[CF.min_d2ydx2(1),CF.min_d2ydx2(2)] = min(CF.d2ydx2);

% Plot fit and 1st / 2nd derivative
fh = figure;
subplot(2,2,1), plot(CF.le1,cf_(CF.le1),'r');
hold on
plot(le1,tp1_sm,'x');
title([fn_SA_st2(Statenum) ' Double Sigmoid Fit']);
subplot(2,2,2), plot(CF.le1(1:end),CF.dydx);
title([fn_SA_st2(Statenum) ' First Derivative']);
subplot(2,2,3), plot(CF.le1(1:end),CF.d2ydx2);
title([fn_SA_st2(Statenum) ' Second Derivative']);

%Neutral Zone
if k == 1 %max -> min of inverted loads
    CF.le_nz = le1(CF.min_d2ydx2(2):CF.max_d2ydx2(2));
    CF.tp_nz = tp1_sm(CF.min_d2ydx2(2):CF.max_d2ydx2(2));
else %min -> max of inverted loads
    CF.le_nz = le1(CF.max_d2ydx2(2):CF.min_d2ydx2(2));
    CF.tp_nz = tp1_sm(CF.max_d2ydx2(2):CF.min_d2ydx2(2));
end

% --- Create fit "NZ"
ok_ = isfinite(CF.le_nz) & isfinite(CF.tp_nz);
if ~all( ok_ )
    warning( 'GenerateMFile:IgnoringNansAndInfs', ...
            'Ignoring NaNs and Infs in data' );
end
ft_ = fitype('poly1');

% Fit this model using new data
% trim load & position inputs
if size(ok_,1) > 7
    NZload = CF.le_nz(ok_);
    NZpos = CF.tp_nz(ok_);

```

```

        CF.le_nz = NZload(2:end-1);
        CF.tp_nz = NZpos(2:end-1);
    else
        CF.le_nz = CF.le_nz(ok_);
        CF.tp_nz = CF.tp_nz(ok_);
    end

[nz_,nz_gof] = fit(CF.le_nz,CF.tp_nz,ft_);

% Or use coefficients from the original fit:
if 0
    cv_ = { -13.676878594897982, -4.1640363853494824};
    [nz_,nz_gof] = cfit(ft_,cv_{:});
end

CF.NZ = nz_;
CF.NZ_gof = nz_gof;

% Plot this fit
subplot(2,2,4),plot(CF.le_nz,CF.NZ(CF.le_nz),'r');
hold on
plot(CF.le_nz,CF.tp_nz , 'x');
title([fn_SA_st2(Statenum) ' Neutral Zone - Linear
Fit']);

NZ_negLoadEdge = le1(CF.max_d2ydx2(2));
NZ_posLoadEdge = le1(CF.min_d2ydx2(2));
NZ_negPosEdge = tp1_sm(CF.max_d2ydx2(2));
NZ_posPosEdge = tp1_sm(CF.min_d2ydx2(2));

CF.NZ_coeffnames = coeffnames(CF.NZ);
CF.NZ_coeffvales = coeffvalues(CF.NZ);
CF.NZ_stiffness = 1/CF.NZ_coeffvales(1);

CF.NZ_le_width = le1(CF.max_d2ydx2(2)) -
le1(CF.min_d2ydx2(2));
CF.NZ_tp_width = tp1_sm(CF.max_d2ydx2(2)) -
tp1_sm(CF.min_d2ydx2(2));

CF.NZ_ALL =
[CF.NZ_stiffness,CF.NZ_le_width,CF.NZ_tp_width, CF.ROM, CF.cf_gof.rsquare];

%-----Elastic Zone-----
% le1(CF.max_d2ydx2(2):CF.min_d2ydx2(2))
% tp1(CF.max_d2ydx2(2):CF.min_d2ydx2(2))

%these are based on actual data - trimmed data
CF.le1_pos = le1(CF.min_d2ydx2(2):length(le1)); %pos load
portion of EZ
CF.tp1_sm_pos = tp1_sm(CF.min_d2ydx2(2):length(tp1));
%pos position portion of EZ
CF.le1_neg = fliplr(le1(1:CF.max_d2ydx2(2))); %neg load
portion of EZ
CF.tp1_sm_neg = fliplr(tp1_sm(1:CF.max_d2ydx2(2))); %neg
position portion of EZ

```

```

CF.le1_all = le1_all;
CF.tp1_all = tp1_sm;

%NOT trimmed data
max_load_pos = le1_all(length(le1_all)); %max load pos.
path

max_load_neg = le1_all(1); %max load neg. path

%load indices for TRIMMED DATA
load_80t_pos = [size(le1,1)-2, size(le1,1)-1,
size(le1,1)]';
load_80t_neg = [1 2 3]'; %3 points for EZ fitting

%angles/rom for TRIMMED DATA
disp_80t_pos = tp1(load_80t_pos);
disp_80t_neg = tp1(load_80t_neg);

%store size of pos & neg
CF.le_ez_pos = load_80t_pos; %pos load portion of EZ
CF.le_ez_neg = load_80t_neg; %neg load portion of EZ
CF.tp_ez_pos = disp_80t_pos; %neg position portion of EZ
CF.tp_ez_neg = disp_80t_neg; %neg position portion of EZ

ft_ = fitype('poly1');

% Fit this model using new data
ez_pos = fit(CF.le_ez_pos,CF.tp_ez_pos,ft_);
ez_neg = fit(CF.le_ez_neg,CF.tp_ez_neg,ft_);

%using fit function domain & output
% ez_ff = fit(CF.le_ez_ff',CF.tp_ez_ff,ft_);

% Or use coefficients from the original fit:
if 0
    cv_ = { -13.676878594897982, -4.1640363853494824};
    ez_ = cfit(ft_,cv_{:});
end

CF.ez_pos = ez_pos;
CF.ez_neg = ez_neg;
% CF.ez_ff = ez_ff;

%store stiffness & fit info
CF.ez_coeffnames_pos = coeffnames(CF.ez_pos);
CF.ez_coeffvalues_pos = coeffvalues(CF.ez_pos);
CF.ez_stiffness_pos = 1/CF.ez_coeffvalues_pos(1);
CF.ez_stiffness_pos2 =
(le1_all(load_80t_pos(length(load_80t_pos))) - le1_all(load_80t_pos(1))) /
((disp_80t_pos(length(disp_80t_pos))) - disp_80t_pos(1)));

CF.ez_coeffnames_neg = coeffnames(CF.ez_neg);
CF.ez_coeffvalues_neg = coeffvalues(CF.ez_neg);
CF.ez_stiffness_neg = 1/CF.ez_coeffvalues_neg(1);

```

```

        CF.ez_stiffness_neg2 = ((le1_all(load_80t_neg(1))) -
        (le1_all(load_80t_neg(length(load_80t_neg)))))) / ((disp_80t_neg(1)) -
        disp_80t_neg(length(disp_80t_neg)));

        CF.EZ_ALL = [CF.ez_stiffness_pos2 CF.ez_stiffness_neg2];

Spine.(fn_SA{i}).(fn_SA_st{j}).(position).(pathtypestr).(motion)(trial).(repl
ay_str).(HAM_str).(pathsequence_str)(1,pnc).(path_name_p2{k}).CF = CF;

Spine.(fn_SA{i}).(fn_SA_st{j}).(position).(pathtypestr).(motion)(trial).(repl
ay_str).(HAM_str).(pathsequence_str)(1,pnc).(path_name_p2{k}).NZ_ALL(Statenum
,:) = CF.NZ_ALL;

Spine.(fn_SA{i}).(fn_SA_st{j}).(position).(pathtypestr).(motion)(trial).(repl
ay_str).(HAM_str).(pathsequence_str)(1,pnc).(path_name_p2{k}).EZ_ALL(Statenum
,:) = CF.EZ_ALL;

clear le1 tpl* CF cf_* ok_ ez_* disp_80* load_80*

        end

        %NZ average per cycle & "higher-in-the-structre" storage
        Spine.(fn_SA{i}).(fn_SA_st{j}).NZ_ALL(pnc,1:5) =
        (Spine.(fn_SA{i}).(fn_SA_st{j}).(position).(pathtypestr).(motion)(trial).(rep
lay_str).(HAM_str).(pathsequence_str)(1,pnc).(path_name_p2{1}).NZ_ALL(Statenu
m,:) +
        Spine.(fn_SA{i}).(fn_SA_st{j}).(position).(pathtypestr).(motion)(trial).(repl
ay_str).(HAM_str).(pathsequence_str)(1,pnc).(path_name_p2{2}).NZ_ALL(Statenum
,:)) ./ 2;

        Spine.(fn_SA{i}).(fn_SA_st{j}).NZ_ALL(pnc,6:10) =
        abs(Spine.(fn_SA{i}).(fn_SA_st{j}).(position).(pathtypestr).(motion)(trial).(
replay_str).(HAM_str).(pathsequence_str)(1,pnc).(path_name_p2{1}).NZ_ALL(Stat
enum,:)) -
        Spine.(fn_SA{i}).(fn_SA_st{j}).(position).(pathtypestr).(motion)(trial).(repl
ay_str).(HAM_str).(pathsequence_str)(1,pnc).(path_name_p2{2}).NZ_ALL(Statenum
,:));

        %EZ average per cycle & "higher-in-the-structre" storage (1-
mean of pn,np in flexion, 2-mean of pn,np in extension ; 3-range b/w pn & np
in flexion, 4-range b/w pn & np in flexion)
        Spine.(fn_SA{i}).(fn_SA_st{j}).EZ_ALL(pnc,1:2) =
        (Spine.(fn_SA{i}).(fn_SA_st{j}).(position).(pathtypestr).(motion)(trial).(rep
lay_str).(HAM_str).(pathsequence_str)(1,pnc).(path_name_p2{1}).EZ_ALL(Statenu
m,:) +
        Spine.(fn_SA{i}).(fn_SA_st{j}).(position).(pathtypestr).(motion)(trial).(repl
ay_str).(HAM_str).(pathsequence_str)(1,pnc).(path_name_p2{2}).EZ_ALL(Statenum
,:)) ./ 2;

        Spine.(fn_SA{i}).(fn_SA_st{j}).EZ_ALL(pnc,3:4) =
        abs(Spine.(fn_SA{i}).(fn_SA_st{j}).(position).(pathtypestr).(motion)(trial).(
replay_str).(HAM_str).(pathsequence_str)(1,pnc).(path_name_p2{1}).EZ_ALL(Stat
enum,:)) -
        Spine.(fn_SA{i}).(fn_SA_st{j}).(position).(pathtypestr).(motion)(trial).(repl
ay_str).(HAM_str).(pathsequence_str)(1,pnc).(path_name_p2{2}).EZ_ALL(Statenum
,:));

        end

```

```

        end
    end

end

end

```

D.4.5 Energetics: Work and Hysteresis

Work and Hysteresis: rFSU_feEnergy.m

```

%rFSU load relaxation code
%RAH - Aug 2012

%data parameters
clear tp* le* Hysteresis* Work* Energy* zeros

fn_fRA = fieldnames(feReplayALL); %fieldnames of all files
fn_PN = {'fePN', 'feNP'}; %fieldnames for pos_neg or neg_pos

color_str1 = {'bo', 'ro', 'ko', 'go', 'mo'};
color_str2 = {'b+', 'r+', 'k+', 'g+', 'm+'};

rotnum = 5; %4-at
loadnum = 10; %11-at

for i = 1:size(fileName,1)

%   fh1=figure('Position',[150 100 700 600],'Color','w');
    cycle_maxS = size(feReplayALL.(fn_fRA{i}).(fn_PN{1})(:,:,:),3); %number
of cycles per test/specimen

    for pnc = 1:cycle_maxS

        for pn = 1:2 %neg_pos and pos_neg

            %get mom & deg dfea - chooses pos_neg or neg_pos
            tool_path_new =
feReplayALL.(fn_fRA{i}).(fn_PN[459])(rotnum,: ,pnc);
            load_end_pts = -
feReplayALL.(fn_fRA{i}).(fn_PN[459])(loadnum,: ,pnc);

            %takes abs value of loads and positions
            absLEP = abs(load_end_pts);
            absTPN = abs(tool_path_new);

            %stores numerical integral of direction-included (Dir) and abs
value (Pos - allows for position in +/-)

```

```

        EnergyDir(pnc,pn) = trapz(load_end_pts); %energy/work w/ neg.
for neg. moments/motion
        EnergyPos(pnc,pn) = trapz(absLEP); %positive energy/work for pos
& neg moments/motion

%        normalized energy - to give loading vs unloading info
        if pnc > 2
                %normalized work relative to third trial - selected b/c it is
relatively stable
                EnergyNorm(pnc,pn) = EnergyPos(pnc,pn)/EnergyPos(3,pn);
        else
                EnergyNorm(pnc,pn) = 1;
        end

    end

        clear pn_* np* area*

        %HYSTERESIS: calculate area between curves (loop paths)
        %scalar quantity where sign does not matter

        %hysteresis per cycle is difatRence in integral
approximations
        Hysteresis(pnc) = abs(EnergyPos(pnc,2) - EnergyPos(pnc,1));
        %difatRence between energy/work associated w/ each curve

        %normalized hysteresis
        if pnc > 2
                %normalized hysteresis relative to third trial - selected
b/c it is relatively stable
                HysteresisNorm(pnc) = Hysteresis(pnc)/Hysteresis(3);
        else
                HysteresisNorm(pnc) = 1;
        end

        %WORK: sum of energy in loading & unloading curves
        %scalar quantity where sign does not matter

        %work per cycle is difatRence in integral approximations
        Work(pnc) = EnergyPos(pnc,2) + EnergyPos(pnc,1); %difatRence
between energy/work associated w/ each curve

        %normalized work
        if pnc > 2
                %normalized work relative to third trial - selected b/c
it is relatively stable
                WorkNorm(pnc) = Work(pnc)/Work(3);
        else
                WorkNorm(pnc) = 1;
        end

        %-Save hysteresis & work data 'per cycle'-%
        feReplayALL.(fn_fRA{i}).hysteresis(pnc) = Hysteresis(pnc);
        feReplayALL.(fn_fRA{i}).work(pnc) = Work(pnc);
        feReplayALL.(fn_fRA{i}).energy(pnc,:) = EnergyPos(pnc,:);

```

```

                feReplayALL.(fn_fRA{i}).hysteresisNormalized(pnc) =
HysteresisNorm(pnc);
                feReplayALL.(fn_fRA{i}).workNormalized(pnc) = WorkNorm(pnc);
                feReplayALL.(fn_fRA{i}).energyNormalized(pnc,:) =
EnergyNorm(pnc,:);

        clear tool_path

    end
end

%% Create 'EnergyALL' matrix: rows=# of cycles. columns=pos. energy(1,2),
%%work(3)/sum of cols 1 & 2/, hysteresis(4) / difatRence of 1 & 2
for i = 1:size(fileName,1) %- date/ID

    i
    clear cycle_maxS Work* Hysteresis*
    cycle_maxS = size(feReplayALL.(fn_fRA{i}).(fn_PN{1}))(:, :, :), 3); %number
of cycles per test/specimen

    for pnc = 1:cycle_maxS

        feReplayALL.(fn_fRA{i}).EnergyALL(pnc,1:2) =
feReplayALL.(fn_fRA{i}).energy(pnc,:);
        feReplayALL.(fn_fRA{i}).EnergyALL(pnc,3) =
feReplayALL.(fn_fRA{i}).work(pnc);
        feReplayALL.(fn_fRA{i}).EnergyALL(pnc,4) =
feReplayALL.(fn_fRA{i}).hysteresis(pnc);

        feReplayALL.(fn_fRA{i}).EnergyNormALL(pnc,1:2) =
feReplayALL.(fn_fRA{i}).energyNormalized(pnc);
        feReplayALL.(fn_fRA{i}).EnergyNormALL(pnc,3) =
feReplayALL.(fn_fRA{i}).workNormalized(pnc);
        feReplayALL.(fn_fRA{i}).EnergyNormALL(pnc,4) =
feReplayALL.(fn_fRA{i}).hysteresisNormalized(pnc);

    end

    %% Perform analysis
    %%crefee matrix that's easier to work w/ than a structure
    clear EnergyALL EnergyNormALL
    EnergyALL = feReplayALL.(fn_fRA{i}).EnergyALL(:, :);
    EnergyNormALL = feReplayALL.(fn_fRA{i}).EnergyNormALL(:, :);

    %%fit linear function to cycle values for work and hysteresis to quantify
rate of change with cycles.
    workCoef = polyfit(1:1:size(EnergyALL,1),EnergyALL(:,3)',1); %finds m, x
(a1, a0)
    hysteresisCoef = polyfit(1:1:size(EnergyALL,1),EnergyALL(:,4)',1);
    dummyX = 1:0.1:size(EnergyALL,1); %create dummy domain with higher
resolution

```

```

fWork = polyval(workCoef,dummyX); %evaluate linear polynomial
coefficients on domain
fHysteresis = polyval(hysteresisCoef,dummyX);

%Find cumulative amount of work - sum of work per cycle across all cycles
clear zeros WorkCumCtr HysteresisCumCtr
WorkCumCtr = zeros(1,cycle_maxS);
WorkCumCtr(1) = EnergyALL(1,3);
HysteresisCumCtr = zeros(1,cycle_maxS);
HysteresisCumCtr(1) = EnergyALL(1,4);

for cycCtr = 2:cycle_maxS
    WorkCumCtr(cycCtr) = WorkCumCtr(cycCtr-1) + EnergyALL(cycCtr,3);
    HysteresisCumCtr(cycCtr) = HysteresisCumCtr(cycCtr-1) +
EnergyALL(cycCtr,4);
end

%WORK
WorkCum = sum(EnergyALL(:,3)); %sum of work column of all cycles
WorkMean = mean(EnergyALL(:,3)); %mean work per cycle
WorkStd = std(EnergyALL(:,3)); %std across cycles
WorkDiffExtreme = max(EnergyALL(:,3)) - min(EnergyALL(:,3)); %maximum
difatRence between any pair of cycles
WorkDiffOrdin_1 = EnergyALL(1,3) - EnergyALL(end,3); %difatRence between
first & last cycle
WorkDiffOrdin_3 = EnergyALL(3,3) - EnergyALL(end,3); %difatRence between
3rd & last cycle

%normalized work (% changes) normalized to 3rd cycle
WorkNormMean = mean(EnergyNormALL(:,3)); %mean work per cycle normalized
to 3rd cycle
WorkNormStd = std(EnergyNormALL(:,3)); %std across cycles normalized to
3rd cycle
WorkNormDiffExtreme = max(EnergyNormALL(:,3)) - min(EnergyNormALL(:,3));
%maximum %-difatRence between any pair of cycles
WorkNormDiffOrdin = EnergyNormALL(3,3) - EnergyNormALL(end,3); % %-
difatRence between 3rd & last cycle

%Data Storage - WORK
feReplayALL.(fn_fRA{i}).Work.WorkCum(:, :) = WorkCum;
feReplayALL.(fn_fRA{i}).Work.WorkMean(:, :) = WorkMean;
feReplayALL.(fn_fRA{i}).Work.WorkStd(:, :) = WorkStd;
feReplayALL.(fn_fRA{i}).Work.WorkDiffExtreme(:, :) = WorkDiffExtreme;
feReplayALL.(fn_fRA{i}).Work.WorkDiffOrdin_1(:, :) = WorkDiffOrdin_1;
feReplayALL.(fn_fRA{i}).Work.WorkDiffOrdin_3(:, :) = WorkDiffOrdin_3;
feReplayALL.(fn_fRA{i}).Work.WorkNormMean(:, :) = WorkNormMean;
feReplayALL.(fn_fRA{i}).Work.WorkNormStd(:, :) = WorkNormStd;
feReplayALL.(fn_fRA{i}).Work.WorkNormDiffExtreme(:, :) =
WorkNormDiffExtreme;
feReplayALL.(fn_fRA{i}).Work.WorkNormDiffOrdin(:, :) = WorkNormDiffOrdin;

%HYSTERESIS
HysteresisCum = sum(EnergyALL(:,4)); %sum of lost energy column of all
cycles - unsure of interpretation??
HysteresisMean = mean(EnergyALL(:,4)); %mean energy lost per cycle
HysteresisStd = std(EnergyALL(:,4)); %std loss across cycles

```

```

HysteresisDiffExtreme = max(EnergyALL(:,4)) - min(EnergyALL(:,4));
%maximum difatRence between any pair of cycles
HysteresisDiffOrdin_1 = EnergyALL(1,4) - EnergyALL(end,4); %difatRence
between first & last cycle
HysteresisDiffOrdin_3 = EnergyALL(3,4) - EnergyALL(end,4); %difatRence
between 3rd & last cycle

%normalized hysteresis (% changes) normalized to 3rd cycle
HysteresisNormMean = mean(EnergyNormALL(:,4)); %mean work per cycle
normalized to 3rd cycle
HysteresisNormStd = std(EnergyNormALL(:,4)); %std across cycles
normalized to 3rd cycle
HysteresisNormDiffExtreme = max(EnergyNormALL(:,4)) -
min(EnergyNormALL(:,4)); %maximum %-difatRence between any pair of cycles
HysteresisNormDiffOrdin = EnergyNormALL(3,4) - EnergyNormALL(end,4); % %-
difatRence between 3rd & last cycle

%Data Storage - Hysteresis
feReplayALL.(fn_fRA{i}).Hysteresis.HysteresisCum(:, :) = HysteresisCum;
feReplayALL.(fn_fRA{i}).Hysteresis.HysteresisMean(:, :) = HysteresisMean;
feReplayALL.(fn_fRA{i}).Hysteresis.HysteresisStd(:, :) = HysteresisStd;
feReplayALL.(fn_fRA{i}).Hysteresis.HysteresisDiffExtreme(:, :) =
HysteresisDiffExtreme;
feReplayALL.(fn_fRA{i}).Hysteresis.HysteresisDiffOrdin_1(:, :) =
HysteresisDiffOrdin_1;
feReplayALL.(fn_fRA{i}).Hysteresis.HysteresisDiffOrdin_3(:, :) =
HysteresisDiffOrdin_3;
feReplayALL.(fn_fRA{i}).Hysteresis.HysteresisNormMean(:, :) =
HysteresisNormMean;
feReplayALL.(fn_fRA{i}).Hysteresis.HysteresisNormStd(:, :) =
HysteresisNormStd;
feReplayALL.(fn_fRA{i}).Hysteresis.HysteresisNormDiffExtreme(:, :) =
HysteresisNormDiffExtreme;
feReplayALL.(fn_fRA{i}).Hysteresis.HysteresisNormDiffOrdin(:, :) =
HysteresisNormDiffOrdin;

% % %--plot as mean of pn, np w/ error bars reflecting range
% fh1=figure('Position',[150 100 700 600],'Color','w');
% figure(fh1);
%
% %hysteresis vs cycle
% plot(1:cycle_maxS,EnergyALL(:,4),'bo',dummyX,fHysteresis,'r-')
%, 'XLim',cycle_max)
% xlim([1 cycle_maxS]);
% ylabel('Hysteresis (Nm-deg)');
% xlabel('Cycle')
% title(['Hysteresis per F/E Cycle: ',fn_fRA{i}]);
%
% %normalized hysteresis vs cycle
% fh2=figure('Position',[150 100 700 600],'Color','w');
% figure(fh2);
% plot(1:cycle_maxS,EnergyNormALL(:,4),'bx','MarkerSize',8)
% xlim([1 cycle_maxS]);
% ylabel('Hysteresis Normalized to 3rd Cycle (Nm-deg)');
% xlabel('Cycle')
% title(['fn_fRA{i}', 'Hysteresis Drop Over F/E Cycles: ',fn_fRA{i}]);

```

```

%
% %work vs cycle
% fh3=figure('Position',[150 100 700 600],'Color','w');
% figure(fh3);
% plot(1:cycle_maxS,EnergyALL(:,3),'bo',dummyX,fWork,'r-')
% xlim([1 cycle_maxS]);
% ylabel('Work (Nm-deg)');
% xlabel('Cycle')
% title(['Work per F/E Cycle: ',fn_fRA{i}]);
%
% %normalized work vs cycle
% fh4=figure('Position',[150 100 700 600],'Color','w');
% figure(fh4);
% plot(1:cycle_maxS,EnergyNormALL(:,3),'bx','MarkerSize',8)
% xlim([1 cycle_maxS]);
% ylabel('Work Normalized to 3rd Cycle (Nm-deg)');
% xlabel('Cycle')
% title(['Work: Changes Over F/E Cycles: ',fn_fRA{i}]);
%
% %cumulative work & energy lost (hysteresis)
% fh5=figure('Position',[150 100 700 600],'Color','w');
% figure(fh5);
% plot(1:cycle_maxS,WorkCumCtr,'b.-',1:cycle_maxS,HysteresisCumCtr,'r.-')
% xlim([1 cycle_maxS]);
% ylabel('Work and Hysteresis: Summation (J)');
% xlabel('Cycle')
% title(['Energy: Addition and Loss: ',fn_fRA{i}]);
% legend('Work Accumulation','Energy Loss','Location','NorthWest')
%
% savestr1 = [fn_fRA{i} '_Hysteresis' ];
% savestr2 = [fn_fRA{i} '_HysteresisNormalized' ];
% savestr3 = [fn_fRA{i} '_Work'];
% savestr4 = [fn_fRA{i} '_WorkNormalized' ];
% savestr5 = [fn_fRA{i} '_EnergyCumulative' ];
% saveas(fh1,['Z:\Ortho Research 3\atRgusonLab\Students\Hartman,
Robert\RabbitRobot\SA1 - Testing\EnergyPlots\' savestr1]);
% saveas(fh2,['Z:\Ortho Research 3\atRgusonLab\Students\Hartman,
Robert\RabbitRobot\SA1 - Testing\EnergyPlots\' savestr2]);
% saveas(fh3,['Z:\Ortho Research 3\atRgusonLab\Students\Hartman,
Robert\RabbitRobot\SA1 - Testing\EnergyPlots\' savestr3]);
% saveas(fh4,['Z:\Ortho Research 3\atRgusonLab\Students\Hartman,
Robert\RabbitRobot\SA1 - Testing\EnergyPlots\' savestr4]);
% saveas(fh5,['Z:\Ortho Research 3\atRgusonLab\Students\Hartman,
Robert\RabbitRobot\SA1 - Testing\EnergyPlots\' savestr5]);

```

end

APPENDIX E

AGGRECAN FRAGMENT WESTERN BLOT PROTOCOL

The protocol for protein extraction and Western blotting G1 and CHAD protein was developed for this dissertation project. Protocols were modified from those used by Dr. Peter Rouhgly and communicated by Dr. Nam Vo.

E.1 PROTEIN EXTRACTION & ISOLATION

All tissues were flash-frozen in liquid nitrogen immediately after dissection and stored at -80 °C. Tissue samples were partially thawed, minced finely (0.5-1 mm³ sections), and transferred to pre-weighed tubes to enable weighting of tissue samples. NP samples weighed ~20-30 mg, and FC samples (single sides, two pieces of FC) weighed ~3-6 mg. Intact AF samples weighed >50 mg, so only portions (~50%) of AF were used for protein extraction. Based on conservative estimates of proteoglycan (PG) constituting 1/50 of overall tissue mass in disc and cartilage samples (Roughley), a starting amount of PG was estimated. A 20x volume of 4M guanidine hydrochloride (4M GHCl, 100 mM Na-acetate, pH 6.0, 1mM EDTA) with 0.5% protease inhibitor (Roche Diagnostics) was added to sample tubes. Tubes were taped to a rocking platform or vibrator and perturbed at high speeds for 5-6 days at 4C to extract soluble proteins (including proteoglycans) from the collagen network with minimal contamination or degradation.

After extraction, guanidine extract (Gex) was measured and pipetted in to a fresh tube. A maximum volume of 200 μ l Gex was added to a 2 ml tube where samples were mixed with 9x volume of cold 100% ethanol. Samples were manually mixed and stored at -20 °C for a minimum of 30 minutes. Samples were then centrifuged for at 4 °C for 10 minutes to pellet the soluble protein. Samples were subsequently washed again with 2x volumes of ice cold 100% ethanol. Care was taken to remove all ethanol; this typically involved a second brief spin to remove all ethanol. Pellets were then air-dried in inverted tubes for 15-30 minutes (until a clear halo formed around the edges of the pellet indicating initiated but not complete evaporation).

Pellets were then dissolved in endo- β -galactosidase (EB) (Sigma, G6920) solution buffer (50 mM sodium phosphate, ph 5.8) using volumes \geq 60 μ l (sufficient for dissolving) with final concentrations of PG >0.5 μ g/ μ l. Pellets were dissolved by pipetting, flicking, shaking, and time at 4 °C. A volume of 60 μ l was treated with EB enzyme (0.1 mU per 10 μ g of PG) and left to react overnight at 37 °C with very slow shaking. Chondroitinase ABC (10 mU/ml) (C3367, Sigma) in 10x buffer was added at 1/10 the overall volume, yielding enzyme concentrations of 1 mU per 10 μ g. Samples were placed at 37 °C for a minimum of 4 hours and placed at -20 °C overnight.

Table 37. Sample calculations for protein extraction process

07.31.13							20
	Sample ID	Tissue	Tube Mass (g)	Tube + Disc (g)	Disc Mass (mg)	Aprx PG (ug)	Vol GHCl (ul)
RH	NP_L23	NP	0.9904	1.0114	21	420	420
rFSU	NP_L45	NP	0.9857	1.0133	27.6	552	552
	FC_L23	FC	0.991	0.9972	6.2	124	124
	FC_L45	FC	0.9874	0.9938	6.4	128	128
	AF_L23	AF	0.9896	1.0224	32.8	656	656
	AF_L45	AF	0.9931	1.0435	50.4	1008	1008
							2888
							3465.6

10% loss		(used)					
Aprx PG	Vol Gex	Gex Used	PG used	Vol EtOH (ul)	EB Buffer (ul)	Ebbuf C (ug/ul)	EB Buf Used (ul)
378	355	200	212.9577465	1800	60	2.842960289	60
496.8	475	200	209.1789474	1800	60	2.802409802	60
111.6	102	102	111.6	918	60	1.64572642	60
115.2	100	100	115.2	900	60	1.692524683	60
590.4	515	200	229.2815534	1800	60	3.014890618	60
907.2	780	200	232.6153846	1800	60	3.049370765	60

0.1 mU per 10 ug PG			1 mU per 10 ug				
mU EB enzy	EB enzy (ul)	Vol to treat (ul)	Ebbuf Vol	PG Amt (ug)	ChABC Buf (ul)	ChABC enzy (ul)	ChABC All
2.129577465	14.90704225	60	74.90704225	170.5776173	8.323004695	0.832300469	9.155305164
2.091789474	14.64252632	60	74.64252632	168.1445881	8.293614035	0.829361404	9.122975439
1.116	7.812	60	67.812	98.74358521	7.534666667	0.753466667	8.288133333
1.152	8.064	60	68.064	101.551481	7.562666667	0.756266667	8.318933333
2.292815534	16.04970874	60	76.04970874	180.8934371	8.449967638	0.844996764	9.294964401
2.326153846	16.28307692	60	76.28307692	182.9622459	8.475897436	0.847589744	9.323487179
	77.75835423	60			48.63981714	4.863981714	53.50379885

		15	45	47
Treated Vol (ul)	PG Conc (ug/ul)	Vol (ul) / well	Blank vol	Load buff vol
84.06234742	2.0291798	7.392149281	26.35785072	11.25
83.76550175	2.007325027	7.472631385	26.27736861	11.25
76.10013333	1.297548124	11.56026488	24.18973512	11.25
76.38293333	1.329504858	11.28239578	24.46760422	11.25
85.34467314	2.119563301	7.076929476	26.67307052	11.25
85.6065641	2.137245523	7.018379422	26.73162058	11.25

E.2 WESTERN BLOT

A constant weight-based amount of soluble protein was added per lane of 10-well 10 or 12% HEPES gels (0025202, Pierce/Thermo). A target between 10-15 μg of PG were selected and added per well with a total well volume of 40 μl . Electrophoresis was run at 40-60 mA for 90-120 min. at 4 $^{\circ}\text{C}$, until bands of molecular weight 10-15 kDa were run off the gel. Gels were then placed in 10% MeOH transfer buffer for 20-30 min while PVDF membrane also soaked in transfer buffer. Proteins were transferred to membranes using stepwise increased amperages from 200 – 400 mA over 3 hours at 4 $^{\circ}\text{C}$. After transfer, samples were soaked in MeOH for 1 minute, rinsed in TBS-T wash buffer, and blocked in 5% skim milk in TBS-T overnight at 4 $^{\circ}\text{C}$ with gentle agitation.

After warming to room temperature for ~30 minutes, membranes were washed once in TBS-T. Primary antibody dissolved at 1:1000 in antibody solution (KP31812, Calbiochem) or 5% milk in TBS-T was added at 2 ml in 50 ml tubes or 10 ml in cassette boxes. Membranes were cultured in primary antibody overnight at 4 $^{\circ}\text{C}$ with gentle agitation. Afterward, membranes were brought to room temperature and washed 3-4x in TBS-T (5-7 min per wash). Secondary goat-anti-rabbit antibody (31460, Thermo Scientific, Waltham, MA) was added at 1:75,000 in secondary antibody solution (KP31855, Calbiochem) or 5% milk in TBS-T for 1 hour at room temperature. This step was followed by 5-6x washes in TBS-T.

Membranes were then placed in a clean dish, and enhanced chemiluminescence (ECL) substrate (34095, SuperSignal West Femto Chemluminescent Substrate, Sigma) was added (600-700 μl total volume) to the membrane surface. Membranes were gently, manually rocked to cover the whole surface with ECL substrate for 1-3 min. Using Bio-Rad's ChemiDoc 5.1 image

detection system, black and white images were taken (0.5 s exposure) first, followed by increased exposure times using 'Hi-resolution' settings for protein detection. Densitometry was quantified using BioRad Image 5.0 software by band-detection methods.

GLOSSARY OF TERMS

Chapter 1.0

AC – axial compression
ACAN – aggrecan gene
ADAMTS – a disintegrin and metalloproteinase with thrombospondin motif
ADL – activity of daily living
AF – annulus fibrosus
AFC – annulus fibrosus cell
AP – anterior-posterior
AT – axial torsion
CEP – cartilage endplate
COX – cyclooxygenase
DOF – degree-of-freedom
ECM – extracellular matrix
FC – facet cartilage
F/E – flexion/extension
FJ – facet joint
FSU – functional spinal unit
G1 – globular domain 1 of aggrecan
GAG – glycosaminoglycan
ISL –interspinous ligament
LB – lateral bending
LF – ligamentum flavum
ML – medial-lateral
MMP – matrix metalloproteinase
NP – nucleus pulposus
NPC – nucleus pulposus cell
PCM – pericellular matrix
ROM – range-of-motion
SI – superior-inferior
SSL – supraspinous ligament
VB – vertebral body

Chapter 8.0

ROMf – flexion range-of-motion ($^{\circ}$)

ROME – extension range-of-motion ($^{\circ}$)

Mxf – flexion moment (Nm)

Mxe – extension moment (Nm)

Mxf Change– change in flexion moment across cycles (3rd cycle – final cycle) (Nm)

Mxe Change– change in extension moment across cycles (3rd cycle – final cycle) (Nm)

Mxf Relaxation–change in flexion moment across cycles normalized to 3rd cycle (%)

Mxe Relaxation –change in extension moment across cycles normalized to 3rd cycle (%)

NZk – neutral zone stiffness (Nm/ $^{\circ}$)

NZk Change – change in neutral zone stiffness across cycles (3rd cycle – final cycle) (Nm/ $^{\circ}$)

NZk Relaxation –change in neutral zone stiffness normalized to 3rd cycle (Nm/ $^{\circ}$)

aROMf – axial range-of-motion at full flexion ($^{\circ}$)

aROME – axial range-of-motion at full extension ($^{\circ}$)

aROMmidfe (aROM) – axial range-of-motion midway between flexion and extension ($^{\circ}$)

Myf – axial torsion moment in full flexion (Nm)

Mye – axial torsion moment in full extension (Nm)

Mymidfe – axial torsion moment midway between flexion and extension (Nm)

Myf Change– change in torsional moment in full flexion across cycles (Nm)

Mye Change– change in torsional moment in full extension across cycles (Nm)

Mymidfe Change– change in torsion midway between flexion and extension across cycles (Nm)

Myf Relaxation– change in torsion in flexion across cycles normalized to 3rd cycle (%)

Mye Relaxation– change in torsion in extension across cycles normalized to 3rd cycle (%)

Mymidfe Relaxation (My Relaxation)– change in torsion midway between flexion and extension across cycles normalized to 3rd cycle (%)

Work Cumulative – summation of work across cycles (J)

Work Mean – mean work across cycles (J)

Work Change – change in work across cycles (3rd cycle work – final cycle work) (J)

Work Relaxation – change in work across cycle normalized to 3rd cycle work (%)

Hysteresis Cumulative – summation of hysteresis across cycles (J)

Hysteresis Mean – mean hysteresis across cycles (J)

Hysteresis Change –change in hysteresis across cycles (3rd cycle hysteresis – final cycle hysteresis) (J)

Hysteresis Relaxation– change in hysteresis across cycle normalized to 3rd cycle hysteresis (%)

BIBLIOGRAPHY

1. Andersson, G.B., *Epidemiological features of chronic low-back pain*. Lancet, 1999. **354**(9178): p. 581-5.
2. Collaborators, U.S.B.o.D., *The state of US health, 1990-2010: burden of diseases, injuries, and risk factors*. JAMA, 2013. **310**(6): p. 591-608.
3. Deyo, R.A. and J.N. Weinstein, *Low back pain*. N Engl J Med, 2001. **344**(5): p. 363-70.
4. Rubin, D.I., *Epidemiology and risk factors for spine pain*. Neurol Clin, 2007. **25**(2): p. 353-71.
5. Dagenais, S., J. Caro, and S. Haldeman, *A systematic review of low back pain cost of illness studies in the United States and internationally*. Spine J, 2008. **8**(1): p. 8-20.
6. Dagenais, S., et al., *Can cost utility evaluations inform decision making about interventions for low back pain?* Spine J, 2009. **9**(11): p. 944-57.
7. Deyo, R.A., et al., *Overtreating chronic back pain: time to back off?* J Am Board Fam Med, 2009. **22**(1): p. 62-8.
8. Deyo, R.A., A.K. Diehl, and M. Rosenthal, *How many days of bed rest for acute low back pain? A randomized clinical trial*. N Engl J Med, 1986. **315**(17): p. 1064-70.
9. Iatridis, J.C., et al., *Effects of mechanical loading on intervertebral disc metabolism in vivo*. J Bone Joint Surg Am, 2006. **88 Suppl 2**: p. 41-6.
10. Tilbrook, H.E., et al., *Yoga for chronic low back pain: a randomized trial*. Ann Intern Med, 2011. **155**(9): p. 569-78.
11. Sherman, K.J., et al., *Comparing yoga, exercise, and a self-care book for chronic low back pain: a randomized, controlled trial*. Ann Intern Med, 2005. **143**(12): p. 849-56.
12. Delitto, A., et al., *Low back pain*. J Orthop Sports Phys Ther, 2012. **42**(4): p. A1-57.
13. Chou, R., et al., *Nonpharmacologic therapies for acute and chronic low back pain: a review of the evidence for an American Pain Society/American College of Physicians clinical practice guideline*. Ann Intern Med, 2007. **147**(7): p. 492-504.
14. Bialosky, J.E., et al., *The mechanisms of manual therapy in the treatment of musculoskeletal pain: a comprehensive model*. Man Ther, 2009. **14**(5): p. 531-8.
15. Hammill, R.R., J.R. Beazell, and J.M. Hart, *Neuromuscular consequences of low back pain and core dysfunction*. Clin Sports Med, 2008. **27**(3): p. 449-62, ix.

16. Grazio, S. and D. Balen, *Complementary and alternative treatment of musculoskeletal pain*. Acta Clin Croat, 2011. **50**(4): p. 513-30.
17. Saper, R.B., et al., *Yoga vs. physical therapy vs. education for chronic low back pain in predominantly minority populations: study protocol for a randomized controlled trial*. Trials, 2014. **15**: p. 67.
18. Hebert, J.J., S.L. Koppenhaver, and B.F. Walker, *Subgrouping patients with low back pain: a treatment-based approach to classification*. Sports Health, 2011. **3**(6): p. 534-42.
19. Kim, M.H. and W.G. Yoo, *Comparison of the lumbar flexion angle and repositioning error during lumbar flexion-extension in young computer workers in Korea with differing back pain*. Work, 2014.
20. Assendelft, W.J., et al., *Spinal manipulative therapy for low back pain. A meta-analysis of effectiveness relative to other therapies*. Ann Intern Med, 2003. **138**(11): p. 871-81.
21. Balthazard, P., et al., *Manual therapy followed by specific active exercises versus a placebo followed by specific active exercises on the improvement of functional disability in patients with chronic non specific low back pain: a randomized controlled trial*. BMC Musculoskelet Disord, 2012. **13**: p. 162.
22. Chan, S.C., S.J. Ferguson, and B. Gantenbein-Ritter, *The effects of dynamic loading on the intervertebral disc*. Eur Spine J, 2011. **20**(11): p. 1796-812.
23. Livshits, G., et al., *Lumbar disc degeneration and genetic factors are the main risk factors for low back pain in women: the UK Twin Spine Study*. Ann Rheum Dis, 2011. **70**(10): p. 1740-5.
24. Sharma, A., M. Parsons, and T. Pilgram, *Temporal interactions of degenerative changes in individual components of the lumbar intervertebral discs: a sequential magnetic resonance imaging study in patients less than 40 years of age*. Spine (Phila Pa 1976), 2011. **36**(21): p. 1794-800.
25. Li, J., et al., *Prevalence of facet joint degeneration in association with intervertebral joint degeneration in a sample of organ donors*. J Orthop Res, 2011.
26. Costandi, S., et al., *Lumbar Spinal Stenosis: Therapeutic Options Review*. Pain Pract, 2014.
27. Adams, M.A. and W.C. Hutton, *The effect of posture on the role of the apophysial joints in resisting intervertebral compressive forces*. J Bone Joint Surg Br, 1980. **62**(3): p. 358-62.
28. Wang, Y., T. Videman, and M.C. Battie, *Morphometrics and lesions of vertebral end plates are associated with lumbar disc degeneration: evidence from cadaveric spines*. J Bone Joint Surg Am, 2013. **95**(5): p. e26.

29. Shafaq, N., et al., *Cellularity and cartilage matrix increased in hypertrophied ligamentum flavum: histopathological analysis focusing on the mechanical stress and bone morphogenetic protein signaling*. J Spinal Disord Tech, 2012. **25**(2): p. 107-15.
30. Setton, L.A. and J. Chen, *Cell mechanics and mechanobiology in the intervertebral disc*. Spine (Phila Pa 1976), 2004. **29**(23): p. 2710-23.
31. Adams, M.A., et al., *The Biomechanics of Back Pain*. 2nd ed. 2006, London: Elsevier.
32. Shan, X., et al., *Low back pain development response to sustained trunk axial twisting*. Eur Spine J, 2013. **22**(9): p. 1972-8.
33. Gawri, R., et al., *Development of an organ culture system for long-term survival of the intact human intervertebral disc*. Spine (Phila Pa 1976), 2011. **36**(22): p. 1835-42.
34. Paul, C.P., et al., *Simulated-physiological loading conditions preserve biological and mechanical properties of caprine lumbar intervertebral discs in ex vivo culture*. PLoS One, 2012. **7**(3): p. e33147.
35. Walter, B.A., et al., *Development and validation of a bioreactor system for dynamic loading and mechanical characterization of whole human intervertebral discs in organ culture*. J Biomech, 2014. **47**(9): p. 2095-101.
36. Chan, S.C., et al., *Region specific response of intervertebral disc cells to complex dynamic loading: an organ culture study using a dynamic torsion-compression bioreactor*. PLoS One, 2013. **8**(8): p. e72489.
37. Walter, B.A., et al., *Complex loading affects intervertebral disc mechanics and biology*. Osteoarthritis Cartilage, 2011. **19**(8): p. 1011-8.
38. MacLean, J.J., J.P. Owen, and J.C. Iatridis, *Role of endplates in contributing to compression behaviors of motion segments and intervertebral discs*. J Biomech, 2007. **40**(1): p. 55-63.
39. Yang, K.H. and A.I. King, *Mechanism of facet load transmission as a hypothesis for low-back pain*. Spine (Phila Pa 1976), 1984. **9**(6): p. 557-65.
40. Adams, M.A. and W.C. Hutton, *The effect of posture on the lumbar spine*. J Bone Joint Surg Br, 1985. **67**(4): p. 625-9.
41. Hoy, D., et al., *The global burden of low back pain: estimates from the Global Burden of Disease 2010 study*. Ann Rheum Dis, 2014. **73**(6): p. 968-74.
42. Battie, M.C., et al., *The Twin Spine Study: contributions to a changing view of disc degeneration*. Spine J, 2009. **9**(1): p. 47-59.
43. Mainka, T., et al., *Association between clinical signs assessed by manual segmental examination and findings of the lumbar facet joints on magnetic resonance scans in*

- subjects with and without current low back pain: a prospective, single-blind study.* Pain, 2013. **154**(9): p. 1886-95.
44. Suri, P., et al., *Are facet joint bone marrow lesions and other facet joint features associated with low back pain? A pilot study.* PM R, 2013. **5**(3): p. 194-200.
 45. Abate, M., et al., *Cigarette smoking and musculoskeletal disorders.* Muscles Ligaments Tendons J, 2013. **3**(2): p. 63-9.
 46. Hu, H.Y., et al., *Associations among low back pain, income, and body mass index in Taiwan.* Spine J, 2013. **13**(11): p. 1521-6.
 47. Paulis, W.D., et al., *Overweight and obesity are associated with musculoskeletal complaints as early as childhood: a systematic review.* Obes Rev, 2014. **15**(1): p. 52-67.
 48. Hirsch, O., et al., *Low Back Pain Patient Subgroups in Primary Care - Pain Characteristics, Psychosocial Determinants and Health Care Utilization.* Clin J Pain, 2014.
 49. Pincus, T. and L.M. McCracken, *Psychological factors and treatment opportunities in low back pain.* Best Pract Res Clin Rheumatol, 2013. **27**(5): p. 625-35.
 50. Williams, F.M. and P.N. Sambrook, *Neck and back pain and intervertebral disc degeneration: role of occupational factors.* Best Pract Res Clin Rheumatol, 2011. **25**(1): p. 69-79.
 51. Lehtola, V., et al., *Efficacy of movement control exercises versus general exercises on recurrent sub-acute nonspecific low back pain in a sub-group of patients with movement control dysfunction. Protocol of a randomized controlled trial.* BMC Musculoskeletal Disord, 2012. **13**: p. 55.
 52. McIntosh, G. and H. Hall, *Low back pain (acute).* Clin Evid (Online), 2011. **2011**.
 53. Axen, I. and C. Leboeuf-Yde, *Trajectories of low back pain.* Best Pract Res Clin Rheumatol, 2013. **27**(5): p. 601-12.
 54. Itz, C.J., et al., *Clinical course of non-specific low back pain: a systematic review of prospective cohort studies set in primary care.* Eur J Pain, 2013. **17**(1): p. 5-15.
 55. Mehra, M., et al., *The burden of chronic low back pain with and without a neuropathic component: a healthcare resource use and cost analysis.* J Med Econ, 2012. **15**(2): p. 245-52.
 56. Maetzel, A. and L. Li, *The economic burden of low back pain: a review of studies published between 1996 and 2001.* Best Pract Res Clin Rheumatol, 2002. **16**(1): p. 23-30.
 57. Plaas, H., et al., *Physical activity and low back pain: the role of subgroups based on the avoidance-endurance model.* Disabil Rehabil, 2014. **36**(9): p. 749-55.

58. Huijnen, I.P., et al., *Subgrouping of Low Back Pain Patients for Targeting Treatments: Evidence from Genetic, Psychological and Activity-related Behavioral Approaches*. Clin J Pain, 2014.
59. Borenstein, D., *Mechanical low back pain--a rheumatologist's view*. Nat Rev Rheumatol, 2013. **9**(11): p. 643-53.
60. Manchikanti, L., et al., *Evaluation of the relative contributions of various structures in chronic low back pain*. Pain Physician, 2001. **4**(4): p. 308-16.
61. Urban, J.P. and S. Roberts, *Degeneration of the intervertebral disc*. Arthritis Res Ther, 2003. **5**(3): p. 120-30.
62. Otsuka, Y., et al., *In vivo measurement of lumbar facet joint area in asymptomatic and chronic low back pain subjects*. Spine (Phila Pa 1976), 2010. **35**(8): p. 924-8.
63. Kovacs, F.M., et al., *Disc degeneration and chronic low back pain: an association which becomes nonsignificant when endplate changes and disc contour are taken into account*. Neuroradiology, 2014. **56**(1): p. 25-33.
64. Marras, W.S. and P.E. Wongsam, *Flexibility and velocity of the normal and impaired lumbar spine*. Arch Phys Med Rehabil, 1986. **67**(4): p. 213-7.
65. Mieritz, R.M., et al., *Reliability and measurement error of sagittal spinal motion parameters in 220 patients with chronic low back pain using a three-dimensional measurement device*. Spine J, 2013.
66. Yurube, T., et al., *Rat tail static compression model mimics extracellular matrix metabolic imbalances of matrix metalloproteinases, aggrecanases, and tissue Inhibitors of metalloproteinases in intervertebral disc degeneration*. Arthritis Res Ther, 2012: p. In press.
67. Jaumard, N.V., W.C. Welch, and B.A. Winkelstein, *Spinal facet joint biomechanics and mechanotransduction in normal, injury and degenerative conditions*. J Biomech Eng, 2011. **133**(7): p. 071010.
68. Hoogendoorn, W.E., et al., *Flexion and rotation of the trunk and lifting at work are risk factors for low back pain: results of a prospective cohort study*. Spine (Phila Pa 1976), 2000. **25**(23): p. 3087-92.
69. Pope, M.H., et al., *The role of prerotation of the trunk in axial twisting efforts*. Spine (Phila Pa 1976), 1987. **12**(10): p. 1041-5.
70. Foss, I.S., I. Holme, and R. Bahr, *The prevalence of low back pain among former elite cross-country skiers, rowers, orienteers, and nonathletes: a 10-year cohort study*. Am J Sports Med, 2012. **40**(11): p. 2610-6.

71. Campbell, A., et al., *Lumbar loading in the elite adolescent tennis serve: link to low back pain*. Med Sci Sports Exerc, 2013. **45**(8): p. 1562-8.
72. Panjabi, M.M., *A hypothesis of chronic back pain: ligament subfailure injuries lead to muscle control dysfunction*. Eur Spine J, 2006. **15**(5): p. 668-76.
73. Drake, J.D., et al., *The influence of static axial torque in combined loading on intervertebral joint failure mechanics using a porcine model*. Clin Biomech (Bristol, Avon), 2005. **20**(10): p. 1038-45.
74. Shamji, M.F., et al., *Gait abnormalities and inflammatory cytokines in an autologous nucleus pulposus model of radiculopathy*. Spine (Phila Pa 1976), 2009. **34**(7): p. 648-54.
75. Liu, H.X., et al., *Asymmetric Facet Joint Osteoarthritis and its Relationships to Facet Orientation, Facet Tropism and Ligamentum Flavum Thickening*. J Spinal Disord Tech, 2013.
76. Dai, L. and L. Jia, *Role of facet asymmetry in lumbar spine disorders*. Acta Orthop Belg, 1996. **62**(2): p. 90-3.
77. Chadha, M., et al., *Association of facet tropism with lumbar disc herniation*. Eur Spine J, 2013. **22**(5): p. 1045-52.
78. Linov, L., et al., *Lumbar facet joint orientation and osteoarthritis: a cross-sectional study*. J Back Musculoskelet Rehabil, 2013. **26**(4): p. 421-6.
79. Cramer, G.D., et al., *Degenerative changes following spinal fixation in a small animal model*. J Manipulative Physiol Ther, 2004. **27**(3): p. 141-54.
80. Balkovec, C. and S. McGill, *Extent of nucleus pulposus migration in the annulus of porcine intervertebral discs exposed to cyclic flexion only versus cyclic flexion and extension*. Clinical Biomechanics, 2012. **27**(8): p. 766-770.
81. Iatridis, J.C., et al., *Localized Intervertebral Disc Injury Leads to Organ Level Changes in Structure, Cellularity, and Biosynthesis*. Cell Mol Bioeng, 2009. **2**(3): p. 437-447.
82. Hickey, D.S. and D.W. Hukins, *Relation between the structure of the annulus fibrosus and the function and failure of the intervertebral disc*. Spine (Phila Pa 1976), 1980. **5**(2): p. 106-16.
83. van Deursen, D.L., et al., *The effect of passive vertebral rotation on pressure in the nucleus pulposus*. J Biomech, 2001. **34**(3): p. 405-8.
84. van Deursen, D.L., et al., *In vitro torsion-induced stress distribution changes in porcine intervertebral discs*. Spine (Phila Pa 1976), 2001. **26**(23): p. 2582-6.
85. Schmidt, H., F. Heuer, and H.J. Wilke, *Interaction between finite helical axes and facet joint forces under combined loading*. Spine (Phila Pa 1976), 2008. **33**(25): p. 2741-8.

86. Adams, M.A., W.C. Hutton, and J.R. Stott, *The resistance to flexion of the lumbar intervertebral joint*. Spine (Phila Pa 1976), 1980. **5**(3): p. 245-53.
87. Gillespie, K.A. and J.P. Dickey, *Biomechanical role of lumbar spine ligaments in flexion and extension: determination using a parallel linkage robot and a porcine model*. Spine (Phila Pa 1976), 2004. **29**(11): p. 1208-16.
88. Ivicsics, M.F., et al., *The effect of nucleotomy on facet joint loading - a porcine in vitro study*. Clin Biomech (Bristol, Avon), 2013. **28**(8): p. 853-9.
89. Popovich, J.M., Jr., et al., *Lumbar facet joint and intervertebral disc loading during simulated pelvic obliquity*. Spine J, 2013. **13**(11): p. 1581-9.
90. Buttermann, G.R., et al., *An experimental method for measuring force on the spinal facet joint: description and application of the method*. J Biomech Eng, 1991. **113**(4): p. 375-86.
91. Schmidt, H., et al., *The relation between the instantaneous center of rotation and facet joint forces - A finite element analysis*. Clin Biomech (Bristol, Avon), 2008. **23**(3): p. 270-8.
92. Schmidt, H., et al., *Computational biomechanics of a lumbar motion segment in pure and combined shear loads*. J Biomech, 2013. **46**(14): p. 2513-21.
93. Goel, V.K., et al., *Load sharing among spinal elements of a motion segment in extension and lateral bending*. J Biomech Eng, 1987. **109**(4): p. 291-7.
94. Hartman, R., K.M. Bell, and J. Kang. *Detailed Analyses of the Components of the Posterior Column in a Distractive-Flexion Injury Model*. in *55th Annual Meeting of the Orthopaedic Research Society (ORS)*. 2009. Las Vegas, NV.
95. Mow, V.C. and R. Huiskes, *Basic orthopaedic biomechanics & mechano-biology*. 3rd ed. 2005, Philadelphia, PA: Lippincott Williams & Wilkins. p.
96. Postacchini, F., et al., *Ligamenta flava in lumbar disc herniation and spinal stenosis. Light and electron microscopic morphology*. Spine (Phila Pa 1976), 1994. **19**(8): p. 917-22.
97. Halper, J. and M. Kjaer, *Basic components of connective tissues and extracellular matrix: elastin, fibrillin, fibulins, fibrinogen, fibronectin, laminin, tenascins and thrombospondins*. Adv Exp Med Biol, 2014. **802**: p. 31-47.
98. Setton, L.A. and J. Chen, *Mechanobiology of the intervertebral disc and relevance to disc degeneration*. J Bone Joint Surg Am, 2006. **88 Suppl 2**: p. 52-7.
99. Li, S., et al., *The effects of cyclic tensile strain on the organisation and expression of cytoskeletal elements in bovine intervertebral disc cells: an in vitro study*. Eur Cell Mater, 2011. **21**: p. 508-22.

100. Gilbert, H.T., et al., *Integrin - dependent mechanotransduction in mechanically stimulated human annulus fibrosus cells: evidence for an alternative mechanotransduction pathway operating with degeneration*. PLoS One, 2013. **8**(9): p. e72994.
101. Pritchard, S., G.R. Erickson, and F. Guilak, *Hyperosmotically induced volume change and calcium signaling in intervertebral disk cells: the role of the actin cytoskeleton*. Biophys J, 2002. **83**(5): p. 2502-10.
102. Thibault, M., A.R. Poole, and M.D. Buschmann, *Cyclic compression of cartilage/bone explants in vitro leads to physical weakening, mechanical breakdown of collagen and release of matrix fragments*. J Orthop Res, 2002. **20**(6): p. 1265-73.
103. Vincent, T. and J. Saklatvala, *Basic fibroblast growth factor: an extracellular mechanotransducer in articular cartilage?* Biochem Soc Trans, 2006. **34**(Pt 3): p. 456-7.
104. Tschumperlin, D.J., *Mechanotransduction*. Compr Physiol, 2011. **1**(2): p. 1057-73.
105. Risbud, M.V. and I.M. Shapiro, *Notochordal cells in the adult intervertebral disc: new perspective on an old question*. Crit Rev Eukaryot Gene Expr, 2011. **21**(1): p. 29-41.
106. Pattappa, G., et al., *Diversity of intervertebral disc cells: phenotype and function*. J Anat, 2012. **221**(6): p. 480-96.
107. Kim, K.W., et al., *The origin of chondrocytes in the nucleus pulposus and histologic findings associated with the transition of a notochordal nucleus pulposus to a fibrocartilaginous nucleus pulposus in intact rabbit intervertebral discs*. Spine (Phila Pa 1976), 2003. **28**(10): p. 982-90.
108. Cao, L., F. Guilak, and L.A. Setton, *Three-dimensional finite element modeling of pericellular matrix and cell mechanics in the nucleus pulposus of the intervertebral disk based on in situ morphology*. Biomech Model Mechanobiol, 2011. **10**(1): p. 1-10.
109. Wang, P., L. Yang, and A.H. Hsieh, *Nucleus pulposus cell response to confined and unconfined compression implicates mechanoregulation by fluid shear stress*. Ann Biomed Eng, 2011. **39**(3): p. 1101-11.
110. Clouet, J., et al., *Identification of phenotypic discriminating markers for intervertebral disc cells and articular chondrocytes*. Rheumatology (Oxford), 2009. **48**(11): p. 1447-50.
111. Hsieh, A.H. and J.D. Twomey, *Cellular mechanobiology of the intervertebral disc: new directions and approaches*. J Biomech, 2010. **43**(1): p. 137-45.
112. Cao, L., F. Guilak, and L.A. Setton, *Pericellular Matrix Mechanics in the Anulus Fibrosus Predicted by a Three-Dimensional Finite Element Model and In Situ Morphology*. Cell Mol Bioeng, 2009. **2**(3): p. 306-319.

113. Guo, H., S.A. Maher, and P.A. Torzilli, *A biphasic multiscale study of the mechanical microenvironment of chondrocytes within articular cartilage under unconfined compression*. J Biomech, 2014.
114. Korhonen, R.K. and W. Herzog, *Depth-dependent analysis of the role of collagen fibrils, fixed charges and fluid in the pericellular matrix of articular cartilage on chondrocyte mechanics*. J Biomech, 2008. **41**(2): p. 480-5.
115. Kim, E., F. Guilak, and M.A. Haider, *The dynamic mechanical environment of the chondrocyte: a biphasic finite element model of cell-matrix interactions under cyclic compressive loading*. J Biomech Eng, 2008. **130**(6): p. 061009.
116. Vanderploeg, E.J., C.G. Wilson, and M.E. Levenston, *Articular chondrocytes derived from distinct tissue zones differentially respond to in vitro oscillatory tensile loading*. Osteoarthritis Cartilage, 2008. **16**(10): p. 1228-36.
117. Freemont, A.J., et al., *Gene expression of matrix metalloproteinases 1, 3, and 9 by chondrocytes in osteoarthritic human knee articular cartilage is zone and grade specific*. Ann Rheum Dis, 1997. **56**(9): p. 542-9.
118. Madden, R., S.K. Han, and W. Herzog, *Chondrocyte deformation under extreme tissue strain in two regions of the rabbit knee joint*. J Biomech, 2013. **46**(3): p. 554-60.
119. Yahia, L.H., et al., *Ultrastructure of the human interspinous ligament and ligamentum flavum. A preliminary study*. Spine (Phila Pa 1976), 1990. **15**(4): p. 262-8.
120. Upton, M.L., et al., *Transfer of macroscale tissue strain to microscale cell regions in the deformed meniscus*. Biophys J, 2008. **95**(4): p. 2116-24.
121. Sairyo, K., et al., *Pathomechanism of ligamentum flavum hypertrophy: a multidisciplinary investigation based on clinical, biomechanical, histologic, and biologic assessments*. Spine (Phila Pa 1976), 2005. **30**(23): p. 2649-56.
122. Yao, W., Z. Shen, and G. Ding, *Simulation of interstitial fluid flow in ligaments: comparison among Stokes, Brinkman and Darcy models*. Int J Biol Sci, 2013. **9**(10): p. 1050-6.
123. Park, J.B., H. Chang, and J.K. Lee, *Quantitative analysis of transforming growth factor-beta 1 in ligamentum flavum of lumbar spinal stenosis and disc herniation*. Spine (Phila Pa 1976), 2001. **26**(21): p. E492-5.
124. Nakatani, T., et al., *Mechanical stretching force promotes collagen synthesis by cultured cells from human ligamentum flavum via transforming growth factor-beta1*. J Orthop Res, 2002. **20**(6): p. 1380-6.
125. Suri, P., et al., *Presence and extent of severe facet joint osteoarthritis are associated with back pain in older adults*. Osteoarthritis Cartilage, 2013. **21**(9): p. 1199-206.

126. Wojdasiewicz, P., L.A. Poniatowski, and D. Szukiewicz, *The Role of Inflammatory and Anti-Inflammatory Cytokines in the Pathogenesis of Osteoarthritis*. *Mediators Inflamm*, 2014. **2014**: p. 561459.
127. Podichetty, V.K., *The aging spine: the role of inflammatory mediators in intervertebral disc degeneration*. *Cell Mol Biol (Noisy-le-grand)*, 2007. **53**(5): p. 4-18.
128. Park, J.O., et al., *Inflammatory cytokines induce fibrosis and ossification of human ligamentum flavum cells*. *J Spinal Disord Tech*, 2013. **26**(1): p. E6-12.
129. Natarajan, R.N., J.R. Williams, and G.B. Andersson, *Modeling changes in intervertebral disc mechanics with degeneration*. *J Bone Joint Surg Am*, 2006. **88 Suppl 2**: p. 36-40.
130. Hardingham, T.E. and A.J. Fosang, *Proteoglycans: many forms and many functions*. *FASEB J*, 1992. **6**(3): p. 861-70.
131. Oegema, T.R., Jr., *Biochemistry of the intervertebral disc*. *Clin Sports Med*, 1993. **12**(3): p. 419-39.
132. Ratcliffe, A., J.A. Tyler, and T.E. Hardingham, *Articular cartilage cultured with interleukin 1. Increased release of link protein, hyaluronate-binding region and other proteoglycan fragments*. *Biochem J*, 1986. **238**(2): p. 571-80.
133. Roberts, S., et al., *Proteoglycan components of the intervertebral disc and cartilage endplate: an immunolocalization study of animal and human tissues*. *Histochem J*, 1994. **26**(5): p. 402-11.
134. Roughley, P.J., R.J. White, and A.R. Poole, *Identification of a hyaluronic acid-binding protein that interferes with the preparation of high-buoyant-density proteoglycan aggregates from adult human articular cartilage*. *Biochem J*, 1985. **231**(1): p. 129-38.
135. Tyler, J.A., *Chondrocyte-mediated depletion of articular cartilage proteoglycans in vitro*. *Biochem J*, 1985. **225**(2): p. 493-507.
136. Cole, T.C., P. Ghosh, and T.K. Taylor, *Variations of the proteoglycans of the canine intervertebral disc with ageing*. *Biochim Biophys Acta*, 1986. **880**(2-3): p. 209-19.
137. Inerot, S. and I. Axelsson, *Structure and composition of proteoglycans from human annulus fibrosus*. *Connect Tissue Res*, 1991. **26**(1-2): p. 47-63.
138. Korecki, C.L., et al., *Intervertebral disc cell response to dynamic compression is age and frequency dependent*. *J Orthop Res*, 2009. **27**(6): p. 800-6.
139. Kitano, S., et al., *Water, fixed charge density, protein contents, and lysine incorporation into protein in chymopapain-digested intervertebral disc of rabbit*. *Spine (Phila Pa 1976)*, 1989. **14**(11): p. 1226-33.

140. Kitano, T., et al., *Biochemical changes associated with the symptomatic human intervertebral disk*. Clin Orthop Relat Res, 1993(293): p. 372-7.
141. Iatridis, J.C., et al., *The viscoelastic behavior of the non-degenerate human lumbar nucleus pulposus in shear*. J Biomech, 1997. **30**(10): p. 1005-13.
142. Iatridis, J.C., et al., *Alterations in the mechanical behavior of the human lumbar nucleus pulposus with degeneration and aging*. J Orthop Res, 1997. **15**(2): p. 318-22.
143. Iatridis, J.C., et al., *Degeneration affects the anisotropic and nonlinear behaviors of human annulus fibrosus in compression*. J Biomech, 1998. **31**(6): p. 535-44.
144. Roughley, P.J., *Biology of intervertebral disc aging and degeneration: involvement of the extracellular matrix*. Spine (Phila Pa 1976), 2004. **29**(23): p. 2691-9.
145. Postacchini, F., M. Bellocchi, and M. Massobrio, *Morphologic changes in annulus fibrosus during aging. An ultrastructural study in rats*. Spine (Phila Pa 1976), 1984. **9**(6): p. 596-603.
146. Lotz, J.C. and J.A. Ulrich, *Innervation, inflammation, and hypermobility may characterize pathologic disc degeneration: review of animal model data*. J Bone Joint Surg Am, 2006. **88 Suppl 2**: p. 76-82.
147. Wang, Y., T. Videman, and M.C. Battie, *ISSLS prize winner: Lumbar vertebral endplate lesions: associations with disc degeneration and back pain history*. Spine (Phila Pa 1976), 2012. **37**(17): p. 1490-6.
148. Gu, W.Y., et al., *The anisotropic hydraulic permeability of human lumbar annulus fibrosus. Influence of age, degeneration, direction, and water content*. Spine (Phila Pa 1976), 1999. **24**(23): p. 2449-55.
149. Iatridis, J.C., et al., *Region-dependent aggrecan degradation patterns in the rat intervertebral disc are affected by mechanical loading in vivo*. Spine (Phila Pa 1976), 2011. **36**(3): p. 203-9.
150. Fujiwara, A., et al., *The relationship between facet joint osteoarthritis and disc degeneration of the lumbar spine: an MRI study*. Eur Spine J, 1999. **8**(5): p. 396-401.
151. Do, D.H., et al., *The relationship between degree of facet tropism and amount of dynamic disc bulge in lumbar spine of patients symptomatic for low back pain*. Eur Spine J, 2011. **20**(1): p. 71-8.
152. Madry, H., F.P. Luyten, and A. Facchini, *Biological aspects of early osteoarthritis*. Knee Surg Sports Traumatol Arthrosc, 2012. **20**(3): p. 407-22.
153. Henrotin, Y., L. Pessesse, and C. Sanchez, *Subchondral bone and osteoarthritis: biological and cellular aspects*. Osteoporos Int, 2012. **23 Suppl 8**: p. S847-51.

154. Szpalski, M. and R. Gunzburg, *Lumbar spinal stenosis in the elderly: an overview*. Eur Spine J, 2003. **12 Suppl 2**: p. S170-5.
155. Lohr, M., et al., *Hypertrophy of the lumbar ligamentum flavum is associated with inflammation-related TGF-beta expression*. Acta Neurochir (Wien), 2011. **153**(1): p. 134-41.
156. Sairyo, K., et al., *Lumbar ligamentum flavum hypertrophy is due to accumulation of inflammation-related scar tissue*. Spine (Phila Pa 1976), 2007. **32**(11): p. E340-7.
157. Imai, S. and S. Hukuda, *Cervical radiculomyelopathy due to deposition of calcium pyrophosphate dihydrate crystals in the ligamentum flavum: historical and histological evaluation of attendant inflammation*. J Spinal Disord, 1994. **7**(6): p. 513-7.
158. Altinkaya, N., et al., *Factors associated with the thickness of the ligamentum flavum: is ligamentum flavum thickening due to hypertrophy or buckling?* Spine (Phila Pa 1976), 2011. **36**(16): p. E1093-7.
159. Klosinski, M., et al., *Contemporary views on the ossification of the ligamenta flava*. Ortop Traumatol Rehabil, 2012. **14**(6): p. 495-503.
160. Mariconda, M., et al., *Frequency and clinical meaning of long-term degenerative changes after lumbar discectomy visualized on imaging tests*. Eur Spine J, 2010. **19**(1): p. 136-43.
161. Chao, Y.H., et al., *Centrifugal force induces human ligamentum flavum fibroblasts inflammation through activation of JNK and p38 pathways*. Connect Tissue Res, 2012. **53**(5): p. 422-9.
162. Hughes, S.P., et al., *The pathogenesis of degeneration of the intervertebral disc and emerging therapies in the management of back pain*. J Bone Joint Surg Br, 2012. **94**(10): p. 1298-304.
163. Guehring, T., et al., *Sensitivity of notochordal disc cells to mechanical loading: an experimental animal study*. Eur Spine J, 2010. **19**(1): p. 113-21.
164. Guehring, T., et al., *Notochordal intervertebral disc cells: sensitivity to nutrient deprivation*. Arthritis Rheum, 2009. **60**(4): p. 1026-34.
165. Yurube, T., et al., *Notochordal cell disappearance and modes of apoptotic cell death in a rat tail static compression-induced disc degeneration model*. Arthritis Res Ther, 2014. **16**(1): p. R31.
166. Boos, N., et al., *Classification of age-related changes in lumbar intervertebral discs: 2002 Volvo Award in basic science*. Spine (Phila Pa 1976), 2002. **27**(23): p. 2631-44.
167. Gu, W.Y., et al., *Streaming potential of human lumbar annulus fibrosus is anisotropic and affected by disc degeneration*. J Biomech, 1999. **32**(11): p. 1177-82.

168. Vo, N., et al., *An overview of underlying causes and animal models for the study of age-related degenerative disorders of the spine and synovial joints*. J Orthop Res, 2013. **31**(6): p. 831-7.
169. Guilak, F., A. Ratcliffe, and V.C. Mow, *Chondrocyte deformation and local tissue strain in articular cartilage: a confocal microscopy study*. J Orthop Res, 1995. **13**(3): p. 410-21.
170. Goldring, M.B. and S.R. Goldring, *Articular cartilage and subchondral bone in the pathogenesis of osteoarthritis*. Ann N Y Acad Sci, 2010. **1192**: p. 230-7.
171. Brunner, E., et al., *Can cognitive behavioural therapy based strategies be integrated into physiotherapy for the prevention of chronic low back pain? A systematic review*. Disabil Rehabil, 2013. **35**(1): p. 1-10.
172. Chou, R., et al., *Correction: Diagnosis and treatment of low back pain*. Ann Intern Med, 2008. **148**(3): p. 247-8.
173. Rainov, N.G. and V. Heidecke, *Management of chronic back and leg pain by intrathecal drug delivery*. Acta Neurochir Suppl, 2007. **97**(Pt 1): p. 49-56.
174. Rubinstein, S.M., et al., *A systematic review on the effectiveness of complementary and alternative medicine for chronic non-specific low-back pain*. Eur Spine J, 2010. **19**(8): p. 1213-28.
175. Iannuccilli, J.D., E.A. Prince, and G.M. Soares, *Interventional Spine Procedures for Management of Chronic Low Back Pain-A Primer*. Semin Intervent Radiol, 2013. **30**(3): p. 307-317.
176. Cherkin, D.C., et al., *Efficacy of acupuncture for chronic low back pain: protocol for a randomized controlled trial*. Trials, 2008. **9**: p. 10.
177. Rubinstein, S.M., et al., *Spinal manipulative therapy for acute low back pain: an update of the cochrane review*. Spine (Phila Pa 1976), 2013. **38**(3): p. E158-77.
178. Choi, B.K., et al., *Exercises for prevention of recurrences of low-back pain*. Cochrane Database Syst Rev, 2010(1): p. CD006555.
179. Smith, C. and K. Grimmer-Somers, *The treatment effect of exercise programmes for chronic low back pain*. J Eval Clin Pract, 2010. **16**(3): p. 484-91.
180. van Middelkoop, M., et al., *Exercise therapy for chronic nonspecific low-back pain*. Best Pract Res Clin Rheumatol, 2010. **24**(2): p. 193-204.
181. Chou, R., et al., *Surgery for low back pain: a review of the evidence for an American Pain Society Clinical Practice Guideline*. Spine (Phila Pa 1976), 2009. **34**(10): p. 1094-109.
182. Williams, K., et al., *Evaluation of the effectiveness and efficacy of Iyengar yoga therapy on chronic low back pain*. Spine (Phila Pa 1976), 2009. **34**(19): p. 2066-76.

183. Koppenhaver, S.L., et al., *Association between changes in abdominal and lumbar multifidus muscle thickness and clinical improvement after spinal manipulation*. J Orthop Sports Phys Ther, 2011. **41**(6): p. 389-99.
184. Brooks, C., S. Kennedy, and P.W. Marshall, *Specific trunk and general exercise elicit similar changes in anticipatory postural adjustments in patients with chronic low back pain: a randomized controlled trial*. Spine (Phila Pa 1976), 2012. **37**(25): p. E1543-50.
185. Omkar, S.N., S. Vishwas, and B. Tech, *Yoga techniques as a means of core stability training*. J Bodyw Mov Ther, 2009. **13**(1): p. 98-103.
186. Triano, J.J. and A.B. Schultz, *Motions of the head and thorax during neck manipulations*. J Manipulative Physiol Ther, 1994. **17**(9): p. 573-83.
187. Lee, C.W., K. Hwangbo, and I.S. Lee, *The effects of combination patterns of proprioceptive neuromuscular facilitation and ball exercise on pain and muscle activity of chronic low back pain patients*. J Phys Ther Sci, 2014. **26**(1): p. 93-6.
188. O'Sullivan, P.B., *Lumbar segmental 'instability': clinical presentation and specific stabilizing exercise management*. Man Ther, 2000. **5**(1): p. 2-12.
189. Micheo, W., L. Baerga, and G. Miranda, *Basic principles regarding strength, flexibility, and stability exercises*. PM R, 2012. **4**(11): p. 805-11.
190. Lancaster, G.I. and M.A. Febbraio, *The immunomodulating role of exercise in metabolic disease*. Trends Immunol, 2014. **35**(6): p. 262-269.
191. Malandrino, A., J. Noailly, and D. Lacroix, *Numerical exploration of the combined effect of nutrient supply, tissue condition and deformation in the intervertebral disc*. J Biomech, 2014. **47**(6): p. 1520-5.
192. Wang, C., et al., *Energy metabolism of intervertebral disc under mechanical loading*. J Orthop Res, 2013. **31**(11): p. 1733-8.
193. Evans, D.W., *Mechanisms and effects of spinal high-velocity, low-amplitude thrust manipulation: previous theories*. J Manipulative Physiol Ther, 2002. **25**(4): p. 251-62.
194. Pickar, J.G., *Neurophysiological effects of spinal manipulation*. Spine J, 2002. **2**(5): p. 357-71.
195. Haavik, H. and B. Murphy, *The role of spinal manipulation in addressing disordered sensorimotor integration and altered motor control*. J Electromyogr Kinesiol, 2012. **22**(5): p. 768-76.
196. Triano, J.J., *Interaction of spinal biomechanics and physiology*. 2nd Ed. ed. Principles and Practice of Chiropractic, ed. S. Haldeman. 1992, East Norwalk, Conn: Appleton & Lange.

197. Janse, J., *Principles and practices of chiropractic: an anthology*, ed. R.W. Hildebrandt. 1976: Wheaton: Kjellberg & Sons.
198. Kawchuk, G.N., et al., *Identification of spinal tissues loaded by manual therapy: a robot-based serial dissection technique applied in porcine motion segments*. Spine (Phila Pa 1976), 2010. **35**(22): p. 1983-90.
199. Omkar, S., M. Mour, and D. Das, *Motion analysis of sun salutation using magnetometer and accelerometer*. Int J Yoga, 2009. **2**(2): p. 62-8.
200. Hsieh, C.Y. and R.K. Pringle, *Range of motion of the lumbar spine required for four activities of daily living*. J Manipulative Physiol Ther, 1994. **17**(6): p. 353-8.
201. Levine, D., et al., *Sagittal lumbar spine position during standing, walking, and running at various gradients*. J Athl Train, 2007. **42**(1): p. 29-34.
202. Heneweer, H., et al., *Physical activity and low back pain: a systematic review of recent literature*. Eur Spine J, 2011. **20**(6): p. 826-45.
203. Burnett, A.F., et al., *Spinal kinematics and trunk muscle activity in cyclists: a comparison between healthy controls and non-specific chronic low back pain subjects-a pilot investigation*. Man Ther, 2004. **9**(4): p. 211-9.
204. Sowa, G., et al., *Determination of annulus fibrosus cell response to tensile strain as a function of duration, magnitude, and frequency*. Journal of Orthopaedic Research, 2011. **29**.
205. Sowa, G.A., et al., *Alterations in gene expression in response to compression of nucleus pulposus cells*. Spine J, 2011. **11**(1): p. 36-43.
206. Barbir, A., et al., *Effects of Torsion on Intervertebral Disc Gene Expression and Biomechanics, Using a Rat Tail Model*. Spine (Phila Pa 1976), 2010.
207. Santaguida, P.L., et al., *Complementary and alternative medicine in back pain utilization report*. Evid Rep Technol Assess (Full Rep), 2009(177): p. 1-221.
208. Court, C., et al., *The effect of static in vivo bending on the murine intervertebral disc*. Spine J, 2001. **1**(4): p. 239-45.
209. Chan, S.C., et al., *Biological response of the intervertebral disc to repetitive short-term cyclic torsion*. Spine (Phila Pa 1976), 2011. **36**(24): p. 2021-30.
210. Lee, J.K. and E.J. Park, *3D spinal motion analysis during staircase walking using an ambulatory inertial and magnetic sensing system*. Med Biol Eng Comput, 2011. **49**(7): p. 755-64.
211. Wai, E.K., et al., *Causal assessment of occupational bending or twisting and low back pain: results of a systematic review*. Spine J, 2010. **10**(1): p. 76-88.

212. Dolan, P., M. Earley, and M.A. Adams, *Bending and compressive stresses acting on the lumbar spine during lifting activities*. J Biomech, 1994. **27**(10): p. 1237-48.
213. Baker, B.M. and C.S. Chen, *Deconstructing the third dimension: how 3D culture microenvironments alter cellular cues*. J Cell Sci, 2012. **125**(Pt 13): p. 3015-24.
214. Chen, C., et al., *Biomechanical properties and mechanobiology of the articular chondrocyte*. Am J Physiol Cell Physiol, 2013. **305**(12): p. C1202-8.
215. Nakamura, T., et al., *Angiopoietin-like protein 2 induced by mechanical stress accelerates degeneration and hypertrophy of the ligamentum flavum in lumbar spinal canal stenosis*. PLoS One, 2014. **9**(1): p. e85542.
216. Ohshima, H., J.P. Urban, and D.H. Bergel, *Effect of static load on matrix synthesis rates in the intervertebral disc measured in vitro by a new perfusion technique*. J Orthop Res, 1995. **13**(1): p. 22-9.
217. Le Maitre, C.L., et al., *Altered integrin mechanotransduction in human nucleus pulposus cells derived from degenerated discs*. Arthritis Rheum, 2009. **60**(2): p. 460-9.
218. Wong, M. and D.R. Carter, *Articular cartilage functional histomorphology and mechanobiology: a research perspective*. Bone, 2003. **33**(1): p. 1-13.
219. Chowdhury, T.T., et al., *Signal transduction pathways involving p38 MAPK, JNK, NFkappaB and AP-1 influences the response of chondrocytes cultured in agarose constructs to IL-1beta and dynamic compression*. Inflamm Res, 2008. **57**(7): p. 306-13.
220. Chowdhury, T.T., et al., *Dynamic compression counteracts IL-1beta induced inducible nitric oxide synthase and cyclo-oxygenase-2 expression in chondrocyte/agarose constructs*. Arthritis Res Ther, 2008. **10**(2): p. R35.
221. Basso, N. and J.N. Heersche, *Effects of hind limb unloading and reloading on nitric oxide synthase expression and apoptosis of osteocytes and chondrocytes*. Bone, 2006. **39**(4): p. 807-14.
222. Sauerland, K., R.X. Raiss, and J. Steinmeyer, *Proteoglycan metabolism and viability of articular cartilage explants as modulated by the frequency of intermittent loading*. Osteoarthritis Cartilage, 2003. **11**(5): p. 343-50.
223. Ferretti, M., et al., *Anti-inflammatory effects of continuous passive motion on meniscal fibrocartilage*. J Orthop Res, 2005. **23**(5): p. 1165-71.
224. Trudel, G., et al., *Different levels of COX-1 and COX-2 enzymes in synoviocytes and chondrocytes during joint contracture formation*. J Rheumatol, 2001. **28**(9): p. 2066-74.
225. Zielinska, B., et al., *Meniscal tissue explants response depends on level of dynamic compressive strain*. Osteoarthritis Cartilage, 2009. **17**(6): p. 754-60.

226. Zhu, F., et al., *Prolonged application of high fluid shear to chondrocytes recapitulates gene expression profiles associated with osteoarthritis*. PLoS One, 2010. **5**(12): p. e15174.
227. Wang, P., et al., *Fluid shear stress-induced osteoarthritis: roles of cyclooxygenase-2 and its metabolic products in inducing the expression of proinflammatory cytokines and matrix metalloproteinases*. FASEB J, 2013. **27**(12): p. 4664-77.
228. Mobasheri, A., et al., *Functional Roles of Mechanosensitive Ion Channels, ss1 Integrins and Kinase Cascades in Chondrocyte Mechanotransduction*, in *Mechanosensitivity in Cells and Tissues*, A. Kamkin and I. Kiseleva, Editors. 2005: Moscow.
229. Gilbert, H.T., et al., *The involvement of interleukin-1 and interleukin-4 in the response of human annulus fibrosus cells to cyclic tensile strain: an altered mechanotransduction pathway with degeneration*. Arthritis Res Ther, 2011. **13**(1): p. R8.
230. Cai, H.X., et al., *Cyclic tensile strain facilitates the ossification of ligamentum flavum through beta-catenin signaling pathway: in vitro analysis*. Spine (Phila Pa 1976), 2012. **37**(11): p. E639-46.
231. Lotz, J.C., *Animal models of intervertebral disc degeneration: lessons learned*. Spine (Phila Pa 1976), 2004. **29**(23): p. 2742-50.
232. Kroeber, M.W., et al., *New in vivo animal model to create intervertebral disc degeneration and to investigate the effects of therapeutic strategies to stimulate disc regeneration*. Spine (Phila Pa 1976), 2002. **27**(23): p. 2684-90.
233. MacLean, J.J., et al., *Effects of immobilization and dynamic compression on intervertebral disc cell gene expression in vivo*. Spine (Phila Pa 1976), 2003. **28**(10): p. 973-81.
234. Walsh, A.J. and J.C. Lotz, *Biological response of the intervertebral disc to dynamic loading*. J Biomech, 2004. **37**(3): p. 329-37.
235. Ariga, K., et al., *The relationship between apoptosis of endplate chondrocytes and aging and degeneration of the intervertebral disc*. Spine (Phila Pa 1976), 2001. **26**(22): p. 2414-20.
236. Ching, C.T., et al., *The effect of cyclic compression on the mechanical properties of the inter-vertebral disc: an in vivo study in a rat tail model*. Clin Biomech (Bristol, Avon), 2003. **18**(3): p. 182-9.
237. Adams, M.A., et al., *Mechanical initiation of intervertebral disc degeneration*. Spine (Phila Pa 1976), 2000. **25**(13): p. 1625-36.
238. Kim, J., et al., *Cell lysis on a microfluidic CD (compact disc)*. Lab Chip, 2004. **4**(5): p. 516-22.

239. Sobajima, S., et al., *Quantitative analysis of gene expression in a rabbit model of intervertebral disc degeneration by real-time polymerase chain reaction*. Spine J, 2005. **5**(1): p. 14-23.
240. Bae, W.C. and K. Masuda, *Emerging technologies for molecular therapy for intervertebral disc degeneration*. Orthop Clin North Am, 2011. **42**(4): p. 585-601, ix.
241. Kepler, C.K., et al., *Intervertebral disc degeneration and emerging biologic treatments*. J Am Acad Orthop Surg, 2011. **19**(9): p. 543-53.
242. Yurube, T., et al., *Matrix metalloproteinase (MMP)-3 gene up-regulation in a rat tail compression loading-induced disc degeneration model*. J Orthop Res, 2010. **28**(8): p. 1026-32.
243. Solomonow, M., *Neuromuscular manifestations of viscoelastic tissue degradation following high and low risk repetitive lumbar flexion*. J Electromyogr Kinesiol, 2012. **22**(2): p. 155-75.
244. Cramer, G.D., et al., *Zygapophyseal joint adhesions after induced hypomobility*. J Manipulative Physiol Ther, 2010. **33**(7): p. 508-18.
245. Henry, J.L., et al., *Lumbar facet joint compressive injury induces lasting changes in local structure, nociceptive scores, and inflammatory mediators in a novel rat model*. Pain Res Treat, 2012. **2012**: p. 127636.
246. Moore, R.J., et al., *Osteoarthritis of the facet joints resulting from anular rim lesions in sheep lumbar discs*. Spine (Phila Pa 1976), 1999. **24**(6): p. 519-25.
247. Stokes, I.A., D.F. Counts, and J.W. Frymoyer, *Experimental instability in the rabbit lumbar spine*. Spine (Phila Pa 1976), 1989. **14**(1): p. 68-72.
248. Iatridis, J.C., et al., *Compression-induced changes in intervertebral disc properties in a rat tail model*. Spine (Phila Pa 1976), 1999. **24**(10): p. 996-1002.
249. Yurube, T., et al., *Rat tail static compression model mimics extracellular matrix metabolic imbalances of matrix metalloproteinases, aggrecanases, and tissue inhibitors of metalloproteinases in intervertebral disc degeneration*. Arthritis Res Ther, 2012. **14**(2): p. R51.
250. Lotz, J.C., et al., *Compression-induced degeneration of the intervertebral disc: an in vivo mouse model and finite-element study*. Spine (Phila Pa 1976), 1998. **23**(23): p. 2493-506.
251. MacLean, J.J., et al., *The effects of short-term load duration on anabolic and catabolic gene expression in the rat tail intervertebral disc*. J Orthop Res, 2005. **23**(5): p. 1120-7.
252. Sowa, G. *Intervertebral Disc Cells Demonstrate a Threshold Effect in their Response to Mechanical Strain*. in Association of Academic Physiatrists. April, 2007. San Juan, PR.

253. Court, C., et al., *Biological and mechanical consequences of transient intervertebral disc bending*. Eur Spine J, 2007. **16**(11): p. 1899-906.
254. O'Connell, G.D., E.J. Vresilovic, and D.M. Elliott, *Comparison of animals used in disc research to human lumbar disc geometry*. Spine (Phila Pa 1976), 2007. **32**(3): p. 328-33.
255. Risbud, M.V., et al., *An organ culture system for the study of the nucleus pulposus: description of the system and evaluation of the cells*. Spine (Phila Pa 1976), 2003. **28**(24): p. 2652-8; discussion 2658-9.
256. Gantenbein, B., et al., *An in vitro organ culturing system for intervertebral disc explants with vertebral endplates: a feasibility study with ovine caudal discs*. Spine (Phila Pa 1976), 2006. **31**(23): p. 2665-73.
257. Korecki, C.L., J.J. MacLean, and J.C. Iatridis, *Characterization of an in vitro intervertebral disc organ culture system*. Eur Spine J, 2007. **16**(7): p. 1029-37.
258. Lee, C.R., et al., *In vitro organ culture of the bovine intervertebral disc: effects of vertebral endplate and potential for mechanobiology studies*. Spine (Phila Pa 1976), 2006. **31**(5): p. 515-22.
259. Wang, D.L., S.D. Jiang, and L.Y. Dai, *Biologic response of the intervertebral disc to static and dynamic compression in vitro*. Spine (Phila Pa 1976), 2007. **32**(23): p. 2521-8.
260. Illien-Junger, S., et al., *Homing of mesenchymal stem cells in induced degenerative intervertebral discs in a whole organ culture system*. Spine (Phila Pa 1976), 2012. **37**(22): p. 1865-73.
261. Mwale, F., et al., *Link N and MSCs can induce regeneration of the early degenerate intervertebral disc*. Tissue Eng Part A, 2014.
262. Gawri, R., et al., *Best paper NASS 2013: link-N can stimulate proteoglycan synthesis in the degenerated human intervertebral discs*. Eur Cell Mater, 2013. **26**: p. 107-19; discussion 119.
263. Lim, T.H., et al., *Rat spinal motion segment in organ culture: a cell viability study*. Spine (Phila Pa 1976), 2006. **31**(12): p. 1291-7; discussion 1298.
264. Haschtmann, D., et al., *Establishment of a novel intervertebral disc/endplate culture model: analysis of an ex vivo in vitro whole-organ rabbit culture system*. Spine (Phila Pa 1976), 2006. **31**(25): p. 2918-25.
265. Junger, S., et al., *Effect of limited nutrition on in situ intervertebral disc cells under simulated-physiological loading*. Spine (Phila Pa 1976), 2009. **34**(12): p. 1264-71.
266. Walter, B.A., et al., *Development and validation of a bioreactor system for dynamic loading and mechanical characterization of whole human intervertebral discs in organ culture*. J Biomech, 2014.

267. Miyazaki, T., et al., *A phenotypic comparison of proteoglycan production of intervertebral disc cells isolated from rats, rabbits, and bovine tails; which animal model is most suitable to study tissue engineering and biological repair of human disc disorders?* Tissue Eng Part A, 2009. **15**(12): p. 3835-46.
268. Beckstein, J.C., et al., *Comparison of animal discs used in disc research to human lumbar disc: axial compression mechanics and glycosaminoglycan content.* Spine (Phila Pa 1976), 2008. **33**(6): p. E166-73.
269. Hartman, R.A., et al., *Novel ex vivo mechanobiological intervertebral disc culture system.* J Biomech, 2012. **45**(2): p. 382-5.
270. Pope, M.H., K.L. Goh, and M.L. Magnusson, *Spine ergonomics.* Annu Rev Biomed Eng, 2002. **4**: p. 49-68.
271. Tarnanen, S., et al., *Neutral Spine Control Exercises in Rehabilitation after Lumbar Spine Fusion.* J Strength Cond Res, 2013.
272. Leardini, A., et al., *Multi-segment trunk kinematics during locomotion and elementary exercises.* Clin Biomech (Bristol, Avon), 2011. **26**(6): p. 562-71.
273. Yantzer, B.K., et al., *Torsion-induced pressure distribution changes in human intervertebral discs: an in vitro study.* Spine (Phila Pa 1976), 2007. **32**(8): p. 881-4.
274. Hartman, R., *DEVELOPMENT OF AN INTERVERTEBRAL DISC MECHANOBIOLOGICAL SYSTEM*, in *Department of Bioengineering*. 2010, University of Pittsburgh: Pittsburgh, PA. p. 147.
275. Wu, J.Z., W. Herzog, and M. Epstein, *Effects of inserting a pressensor film into articular joints on the actual contact mechanics.* J Biomech Eng, 1998. **120**(5): p. 655-9.
276. Goertzen, D.J. and G.N. Kawchuk, *A novel application of velocity-based force control for use in robotic biomechanical testing.* J Biomech, 2009. **42**(3): p. 366-9.
277. Gilbertson, L., T.C. Doehring, and J. Kang, *New methods to study lumbar spine biomechanics: Delineation of in vitro load-displacement characteristics by using a robotic/UFS testing system with hybrid control.* Operative Techniques in Orthopaedics, 2000. **10**(4): p. 246-253.
278. Bell, K.M., et al., *In vitro spine testing using a robot-based testing system: comparison of displacement control and "hybrid control".* J Biomech, 2013. **46**(10): p. 1663-9.
279. Frey, M., et al., *Optimised robot-based system for the exploration of elastic joint properties.* Med Biol Eng Comput, 2004. **42**(5): p. 674-8.
280. *Arm - RX series 90B family*, in *Staubli Faverages*, Staubli, Editor. 11/2004. p. 13.

281. Grauer, J.N., et al., *Biomechanical evaluation of the New Zealand white rabbit lumbar spine: a physiologic characterization*. Eur Spine J, 2000. **9**(3): p. 250-5.
282. Bell, K.M., et al. *Flexibility Testing for Evaluation of a Needle Puncture Rabbit Model of Disc Degeneration*. in *55th Annual Meeting of the Orthopaedic Research Society (ORS)*. 2009. Las Vegas, NV.
283. Wu, G., et al., *ISB recommendation on definitions of joint coordinate system of various joints for the reporting of human joint motion--part I: ankle, hip, and spine*. International Society of Biomechanics. J Biomech, 2002. **35**(4): p. 543-8.
284. Fujie, H., et al., *Forces and moments in six-DOF at the human knee joint: mathematical description for control*. J Biomech, 1996. **29**(12): p. 1577-85.
285. Rudy, T.W., et al., *A combined robotic/universal force sensor approach to determine in situ forces of knee ligaments*. J Biomech, 1996. **29**(10): p. 1357-60.
286. Schilling, C., et al., *The effect of design parameters of interspinous implants on kinematics and load bearing: an in vitro study*. Eur Spine J, 2014. **23**(4): p. 762-71.
287. Cook, D.J., *CHARACTERIZATION OF THE RESPONSE OF THE CADAVERIC HUMAN SPINE TO LOADING IN A SIX-DEGREE-OF-FREEDOM SPINE TESTING APPARATUS*, in *Bioengineering*. 2009, University of Pittsburgh: Pittsburgh, PA. p. 118.
288. Goel, V.K., et al., *Test protocols for evaluation of spinal implants*. J Bone Joint Surg Am, 2006. **88 Suppl 2**: p. 103-9.
289. Goertzen, D.J., C. Lane, and T.R. Oxland, *Neutral zone and range of motion in the spine are greater with stepwise loading than with a continuous loading protocol. An in vitro porcine investigation*. J Biomech, 2004. **37**(2): p. 257-61.
290. Miura, T., M.M. Panjabi, and P.A. Cripton, *A method to simulate in vivo cervical spine kinematics using in vitro compressive preload*. Spine (Phila Pa 1976), 2002. **27**(1): p. 43-8.
291. Showalter, B.L., et al., *Comparison of animal discs used in disc research to human lumbar disc: torsion mechanics and collagen content*. Spine (Phila Pa 1976), 2012. **37**(15): p. E900-7.
292. McLain, R.F., S.A. Yerby, and T.A. Moseley, *Comparative morphometry of L4 vertebrae: comparison of large animal models for the human lumbar spine*. Spine (Phila Pa 1976), 2002. **27**(8): p. E200-6.
293. Cavanaugh, J.M., et al., *Lumbar facet pain: biomechanics, neuroanatomy and neurophysiology*. J Biomech, 1996. **29**(9): p. 1117-29.
294. Ponseti, I.V., *Differences in ligamenta flava among some mammals*. Iowa Orthop J, 1995. **15**: p. 141-6.

295. Schaafsma, F.G., et al., *Physical conditioning as part of a return to work strategy to reduce sickness absence for workers with back pain*. Cochrane Database Syst Rev, 2013. **8**: p. CD001822.
296. Hofmann, J., et al., *Effects of behavioural exercise therapy on the effectiveness of a multidisciplinary rehabilitation for chronic non-specific low back pain: study protocol for a randomised controlled trial*. BMC Musculoskelet Disord, 2013. **14**: p. 89.
297. Jegede, K.A., et al., *The effects of three different types of orthoses on the range of motion of the lumbar spine during 15 activities of daily living*. Spine (Phila Pa 1976), 2011. **36**(26): p. 2346-53.
298. Marras, W.S., *Biomechanics of the Spinal Motion Segment*. 6th ed. Rothman-Simeone: The Spine. 2011.
299. Okawa, A., et al., *Dynamic motion study of the whole lumbar spine by videofluoroscopy*. Spine (Phila Pa 1976), 1998. **23**(16): p. 1743-9.
300. Lee, S.W., et al., *Development and validation of a new technique for assessing lumbar spine motion*. Spine (Phila Pa 1976), 2002. **27**(8): p. E215-20.
301. Chung, C.Y., et al., *Kinematic aspects of trunk motion and gender effect in normal adults*. J Neuroeng Rehabil, 2010. **7**: p. 9.
302. Cobian, D.G., et al., *Active cervical and lumbar range of motion during performance of activities of daily living in healthy young adults*. Spine (Phila Pa 1976), 2013. **38**(20): p. 1754-63.
303. Goncalves, L.C., et al., *Flexibility, functional autonomy and quality of life (QoL) in elderly yoga practitioners*. Arch Gerontol Geriatr, 2011. **53**(2): p. 158-62.
304. Ribeiro, D.C., et al., *Cumulative postural exposure measured by a novel device: a preliminary study*. Ergonomics, 2011. **54**(9): p. 858-65.
305. Intolo, P., et al., *The effect of age on lumbar range of motion: a systematic review*. Man Ther, 2009. **14**(6): p. 596-604.
306. Le Corroller, T., et al., *Musculoskeletal injuries related to yoga: imaging observations*. AJR Am J Roentgenol, 2012. **199**(2): p. 413-8.
307. Yamamoto, I., et al., *Three-dimensional movements of the whole lumbar spine and lumbosacral joint*. Spine (Phila Pa 1976), 1989. **14**(11): p. 1256-60.
308. White, A.A. and M.M. Panjabi, *Clinical biomechanics of the spine*. 2nd ed. 1990, Philadelphia: Lippincott. xxiii, 722 p.

309. Panjabi, M.M., et al., *Mechanical behavior of the human lumbar and lumbosacral spine as shown by three-dimensional load-displacement curves*. J Bone Joint Surg Am, 1994. **76**(3): p. 413-24.
310. Wilke, H.J., J. Geppert, and A. Kienle, *Biomechanical in vitro evaluation of the complete porcine spine in comparison with data of the human spine*. Eur Spine J, 2011. **20**(11): p. 1859-68.
311. Rozumalski, A., et al., *The in vivo three-dimensional motion of the human lumbar spine during gait*. Gait Posture, 2008. **28**(3): p. 378-84.
312. Honeine, J.L., et al., *By counteracting gravity, triceps surae sets both kinematics and kinetics of gait*. Physiol Rep, 2014. **2**(2): p. e00229.
313. Park, Y.H., C.H. Lee, and B.H. Lee, *Clinical usefulness of the virtual reality-based postural control training on the gait ability in patients with stroke*. J Exerc Rehabil, 2013. **9**(5): p. 489-94.
314. Michalek, A.J. and J.C. Iatridis, *Height and torsional stiffness are most sensitive to annular injury in large animal intervertebral discs*. Spine J, 2012. **12**(5): p. 425-32.
315. Dmitriev, A.E., et al., *Effect of multilevel lumbar disc arthroplasty on the operative- and adjacent-level kinematics and intradiscal pressures: an in vitro human cadaveric assessment*. Spine J, 2008. **8**(6): p. 918-25.
316. Crisco, J.J., L. Fujita, and D.B. Spenciner, *The dynamic flexion/extension properties of the lumbar spine in vitro using a novel pendulum system*. J Biomech, 2007. **40**(12): p. 2767-73.
317. Howarth, S.J. and J.P. Callaghan, *Compressive force magnitude and intervertebral joint flexion/extension angle influence shear failure force magnitude in the porcine cervical spine*. J Biomech, 2012. **45**(3): p. 484-90.
318. Henchoz, Y., et al., *Effects of noxious stimulation and pain expectations on neuromuscular control of the spine in patients with chronic low back pain*. Spine J, 2013. **13**(10): p. 1263-72.
319. Revel, M., *Rehabilitation of low back pain patients. A review*. Rev Rhum Engl Ed, 1995. **62**(1): p. 35-44.
320. Javadian, Y., et al., *The effects of stabilizing exercises on pain and disability of patients with lumbar segmental instability*. J Back Musculoskelet Rehabil, 2012. **25**(3): p. 149-55.
321. Deusinger, R.H., *Biomechanical considerations for clinical application in athletes with low back pain*. Clin Sports Med, 1989. **8**(4): p. 703-15.
322. Long, A., R. Donelson, and T. Fung, *Does it matter which exercise? A randomized control trial of exercise for low back pain*. Spine (Phila Pa 1976), 2004. **29**(23): p. 2593-602.

323. Fry, R.W., et al., *Compressive preload reduces segmental flexion instability after progressive destabilization of the lumbar spine*. Spine (Phila Pa 1976), 2014. **39**(2): p. E74-81.
324. Cusick, J.F., et al., *Biomechanics of sequential posterior lumbar surgical alterations*. J Neurosurg, 1992. **76**(5): p. 805-11.
325. Smit, T.H., et al., *Quantifying intervertebral disc mechanics: a new definition of the neutral zone*. BMC Musculoskelet Disord, 2011. **12**: p. 38.
326. Livak, K.J. and T.D. Schmittgen, *Analysis of relative gene expression data using real-time quantitative PCR and the 2(-Delta Delta C(T)) Method*. Methods, 2001. **25**(4): p. 402-8.
327. Sztrolovics, R., et al., *The mechanism of aggrecan release from cartilage differs with tissue origin and the agent used to stimulate catabolism*. Biochem J, 2002. **362**(Pt 2): p. 465-72.
328. Haglund, L., et al., *Development of a bioreactor for axially loaded intervertebral disc organ culture*. Tissue Eng Part C Methods, 2011. **17**(10): p. 1011-9.
329. Igarashi, A., et al., *Inflammatory cytokines released from the facet joint tissue in degenerative lumbar spinal disorders*. Spine (Phila Pa 1976), 2004. **29**(19): p. 2091-5.
330. Kosaka, H., et al., *Pathomechanism of loss of elasticity and hypertrophy of lumbar ligamentum flavum in elderly patients with lumbar spinal canal stenosis*. Spine (Phila Pa 1976), 2007. **32**(25): p. 2805-11.
331. Chokshi, F.H., R.M. Quencer, and W.R. Smoker, *The "thickened" ligamentum flavum: is it buckling or enlargement?* AJNR Am J Neuroradiol, 2010. **31**(10): p. 1813-6.
332. Paul, C.P., et al., *Dynamic and static overloading induce early degenerative processes in caprine lumbar intervertebral discs*. PLoS One, 2013. **8**(4): p. e62411.
333. Liang, Q.Q., et al., *Prolonged upright posture induces degenerative changes in intervertebral discs of rat cervical spine*. Spine (Phila Pa 1976), 2011. **36**(1): p. E14-9.
334. Lakemeier, S., et al., *Expression of hypoxia-inducible factor-1alpha, vascular endothelial growth factor, and matrix metalloproteinases 1, 3, and 9 in hypertrophied ligamentum flavum*. J Spinal Disord Tech, 2013. **26**(7): p. 400-6.
335. Little, C.B., P. Ghosh, and R. Rose, *The effect of strenuous versus moderate exercise on the metabolism of proteoglycans in articular cartilage from different weight-bearing regions of the equine third carpal bone*. Osteoarthritis Cartilage, 1997. **5**(3): p. 161-72.
336. Andersson, M.L., et al., *Serum levels of cartilage oligomeric matrix protein (COMP) increase temporarily after physical exercise in patients with knee osteoarthritis*. BMC Musculoskelet Disord, 2006. **7**: p. 98.

337. Brahm, H., K. Piehl-Aulin, and S. Ljunghall, *Bone metabolism during exercise and recovery: the influence of plasma volume and physical fitness*. *Calcif Tissue Int*, 1997. **61**(3): p. 192-8.
338. Brahm, H., et al., *Net fluxes over working thigh of hormones, growth factors and biomarkers of bone metabolism during short lasting dynamic exercise*. *Calcif Tissue Int*, 1997. **60**(2): p. 175-80.
339. MacLean, J.J., et al., *In vivo intervertebral disc remodeling: kinetics of mRNA expression in response to a single loading event*. *J Orthop Res*, 2008. **26**(5): p. 579-88.
340. Vo, N.V., et al., *Expression and regulation of metalloproteinases and their inhibitors in intervertebral disc aging and degeneration*. *Spine J*, 2013. **13**(3): p. 331-41.
341. Abulencia, J.P., et al., *Shear-induced cyclooxygenase-2 via a JNK2/c-Jun-dependent pathway regulates prostaglandin receptor expression in chondrocytic cells*. *J Biol Chem*, 2003. **278**(31): p. 28388-94.
342. Gosset, M., et al., *Prostaglandin E2 synthesis in cartilage explants under compression: mPGES-1 is a mechanosensitive gene*. *Arthritis Res Ther*, 2006. **8**(4): p. R135.
343. Gendron, C., et al., *Proteolytic activities of human ADAMTS-5: comparative studies with ADAMTS-4*. *J Biol Chem*, 2007. **282**(25): p. 18294-306.
344. Maclean, J.J., et al., *Anabolic and catabolic mRNA levels of the intervertebral disc vary with the magnitude and frequency of in vivo dynamic compression*. *J Orthop Res*, 2004. **22**(6): p. 1193-200.
345. Fitzgerald, J.B., et al., *Mechanical compression of cartilage explants induces multiple time-dependent gene expression patterns and involves intracellular calcium and cyclic AMP*. *J Biol Chem*, 2004. **279**(19): p. 19502-11.
346. Purmessur, D., et al., *A role for TNFalpha in intervertebral disc degeneration: a non-recoverable catabolic shift*. *Biochem Biophys Res Commun*, 2013. **433**(1): p. 151-6.
347. Vogel, C. and E.M. Marcotte, *Insights into the regulation of protein abundance from proteomic and transcriptomic analyses*. *Nat Rev Genet*, 2012. **13**(4): p. 227-32.
348. Erulkar, J.S., et al., *Flexibility analysis of posterolateral fusions in a New Zealand white rabbit model*. *Spine (Phila Pa 1976)*, 2001. **26**(10): p. 1125-30.
349. Guehring, T., et al., *Intradiscal pressure measurements in normal discs, compressed discs and compressed discs treated with axial posterior disc distraction: an experimental study on the rabbit lumbar spine model*. *Eur Spine J*, 2006. **15**(5): p. 597-604.
350. Hosea, T.M. and C.J. Gatt, Jr., *Back pain in golf*. *Clin Sports Med*, 1996. **15**(1): p. 37-53.

351. Cramer, G.D., et al., *The effects of side-posture positioning and spinal adjusting on the lumbar Z joints: a randomized controlled trial with sixty-four subjects*. Spine (Phila Pa 1976), 2002. **27**(22): p. 2459-66.
352. Cramer, G.D., et al., *Magnetic resonance imaging zygapophyseal joint space changes (gapping) in low back pain patients following spinal manipulation and side-posture positioning: a randomized controlled mechanisms trial with blinding*. J Manipulative Physiol Ther, 2013. **36**(4): p. 203-17.
353. Henderson, C.N., *The basis for spinal manipulation: chiropractic perspective of indications and theory*. J Electromyogr Kinesiol, 2012. **22**(5): p. 632-42.
354. Drake, J.D., H. Dobson, and J.P. Callaghan, *The influence of posture and loading on interfacet spacing: an investigation using magnetic resonance imaging on porcine spinal units*. Spine (Phila Pa 1976), 2008. **33**(20): p. E728-34.
355. Korecki, C.L., J.J. MacLean, and J.C. Iatridis, *Dynamic compression effects on intervertebral disc mechanics and biology*. Spine (Phila Pa 1976), 2008. **33**(13): p. 1403-9.
356. Haglund, L., J. Ouellet, and P. Roughley, *Variation in chondroadherin abundance and fragmentation in the human scoliotic disc*. Spine (Phila Pa 1976), 2009. **34**(14): p. 1513-8.
357. Johnson, A., et al., *Fibronectin fragments cause release and degradation of collagen-binding molecules from equine explant cultures*. Osteoarthritis Cartilage, 2004. **12**(2): p. 149-59.
358. Neame, P.J., H. Tapp, and A. Azizan, *Noncollagenous, nonproteoglycan macromolecules of cartilage*. Cell Mol Life Sci, 1999. **55**(10): p. 1327-40.
359. Li, Y., et al., *Moderate dynamic compression inhibits pro-catabolic response of cartilage to mechanical injury, tumor necrosis factor-alpha and interleukin-6, but accentuates degradation above a strain threshold*. Osteoarthritis Cartilage, 2013. **21**(12): p. 1933-41.
360. Sarzi-Puttini, P., et al., *Osteoarthritis: an overview of the disease and its treatment strategies*. Semin Arthritis Rheum, 2005. **35**(1 Suppl 1): p. 1-10.
361. Markolf, K.L., et al., *Effects of combined knee loadings on posterior cruciate ligament force generation*. J Orthop Res, 1996. **14**(4): p. 633-8.
362. Breshears, L.A., et al., *The effect of uniaxial cyclic tensile load on gene expression in canine cranial cruciate ligamentocytes*. Vet Surg, 2010. **39**(4): p. 433-43.
363. Zhang, Y., et al., *Histopathological changes in supraspinous ligaments, ligamentum flava and paraspinal muscle tissues of patients with ankylosing spondylitis*. Int J Rheum Dis, 2014.

364. Parkinson, J., et al., *Change in proteoglycan metabolism is a characteristic of human patellar tendinopathy*. *Arthritis Rheum*, 2010. **62**(10): p. 3028-35.
365. Chan, S.C. and B. Gantenbein-Ritter, *Preparation of intact bovine tail intervertebral discs for organ culture*. *J Vis Exp*, 2012(60).
366. Dumas, G.A., L. Beaudoin, and G. Drouin, *In situ mechanical behavior of posterior spinal ligaments in the lumbar region. An in vitro study*. *J Biomech*, 1987. **20**(3): p. 301-10.
367. Richter, M., et al., *Load-displacement properties of the normal and injured lower cervical spine in vitro*. *Eur Spine J*, 2000. **9**(2): p. 104-8.
368. Sobajima, S., et al., *A slowly progressive and reproducible animal model of intervertebral disc degeneration characterized by MRI, X-ray, and histology*. *Spine (Phila Pa 1976)*, 2005. **30**(1): p. 15-24.
369. Michalek, A.J. and J.C. Iatridis, *Penetrating annulus fibrosus injuries affect dynamic compressive behaviors of the intervertebral disc via altered fluid flow: an analytical interpretation*. *J Biomech Eng*, 2011. **133**(8): p. 084502.
370. Elliott, D.M., et al., *The effect of relative needle diameter in puncture and sham injection animal models of degeneration*. *Spine (Phila Pa 1976)*, 2008. **33**(6): p. 588-96.
371. Hartman, R., et al. *Biomechanical role of posterior column components in a distractive-flexion injury model: Effects on load sharing and mobility*. in *International Philadelphia Spine Research Symposium*. 2013. Philadelphia.
372. Honsawek, S., et al., *Hypertrophy of the ligamentum flavum in lumbar spinal canal stenosis is associated with increased bFGF expression*. *Int Orthop*, 2013. **37**(7): p. 1387-92.
373. Hartman, R., et al., *Biomechanical role of posterior column components in a distractive-flexion injury model: Effects on load sharing and mobility*, in *Philadelphia Spine Research Society*. 2013: Philadelphia.
374. Ekstrom, L., et al., *In vivo porcine intradiscal pressure as a function of external loading*. *J Spinal Disord Tech*, 2004. **17**(4): p. 312-6.
375. Rohlmann, A., et al., *Analysis of the influence of disc degeneration on the mechanical behaviour of a lumbar motion segment using the finite element method*. *J Biomech*, 2006. **39**(13): p. 2484-90.
376. Heuer, F., H. Schmidt, and H.J. Wilke, *The relation between intervertebral disc bulging and annular fiber associated strains for simple and complex loading*. *J Biomech*, 2008. **41**(5): p. 1086-94.
377. Stolworthy, D.K., et al., *Characterization and prediction of rate-dependent flexibility in lumbar spine biomechanics at room and body temperature*. *Spine J*, 2014. **14**(5): p. 789-98.

378. Michalek, A.J., et al., *The effects of needle puncture injury on microscale shear strain in the intervertebral disc annulus fibrosus*. Spine J, 2010. **10**(12): p. 1098-105.
379. DeVries, N.A., et al., *Biomechanical analysis of the intact and destabilized sheep cervical spine*. Spine (Phila Pa 1976), 2012. **37**(16): p. E957-63.
380. Humphrey, J.D., *Vascular adaptation and mechanical homeostasis at tissue, cellular, and sub-cellular levels*. Cell Biochem Biophys, 2008. **50**(2): p. 53-78.
381. Burkholder, T.J., *Mechanotransduction in skeletal muscle*. Front Biosci, 2007. **12**: p. 174-91.
382. Baer, A.E., et al., *The micromechanical environment of intervertebral disc cells determined by a finite deformation, anisotropic, and biphasic finite element model*. J Biomech Eng, 2003. **125**(1): p. 1-11.
383. Perie, D.S., et al., *Correlating material properties with tissue composition in enzymatically digested bovine annulus fibrosus and nucleus pulposus tissue*. Ann Biomed Eng, 2006. **34**(5): p. 769-77.
384. Rodriguez, A.G., et al., *Human disc nucleus properties and vertebral endplate permeability*. Spine (Phila Pa 1976), 2011. **36**(7): p. 512-20.
385. Boxberger, J.I., et al., *Nucleus pulposus glycosaminoglycan content is correlated with axial mechanics in rat lumbar motion segments*. J Orthop Res, 2006. **24**(9): p. 1906-15.
386. Hartman, R.A., et al. *Correlating intervertebral disc axial mechanics with biological responses to creep loading in Orthopaedic Research Society*. 2013. San Antonio, TX.
387. McMillan, D.W., et al., *Stress distributions inside intervertebral discs: the validity of experimental "stress profilometry"*. Proc Inst Mech Eng H, 1996. **210**(2): p. 81-7.
388. Ferguson, S.J., K. Ito, and L.P. Nolte, *Fluid flow and convective transport of solutes within the intervertebral disc*. J Biomech, 2004. **37**(2): p. 213-21.
389. Ehlers, W., N. Karajan, and B. Markert, *An extended biphasic model for charged hydrated tissues with application to the intervertebral disc*. Biomech Model Mechanobiol, 2009. **8**(3): p. 233-51.
390. Zirbel, S.A., et al., *Intervertebral disc degeneration alters lumbar spine segmental stiffness in all modes of loading under a compressive follower load*. Spine J, 2013. **13**(9): p. 1134-47.
391. Borkowski, S.L., et al., *Nonparametric Identification Techniques for the Characterization of Spine Hysteresis*. J Biomech Eng, 2014.
392. Marras, W.S., et al., *Cumulative spine loading and clinically meaningful declines in low-back function*. Hum Factors, 2014. **56**(1): p. 29-43.

393. Maly, M.R., *Abnormal and cumulative loading in knee osteoarthritis*. Curr Opin Rheumatol, 2008. **20**(5): p. 547-52.
394. Malliaras, P., et al., *Achilles and patellar tendinopathy loading programmes : a systematic review comparing clinical outcomes and identifying potential mechanisms for effectiveness*. Sports Med, 2013. **43**(4): p. 267-86.
395. Iatridis, J.C., et al., *Is the nucleus pulposus a solid or a fluid? Mechanical behaviors of the nucleus pulposus of the human intervertebral disc*. Spine (Phila Pa 1976), 1996. **21**(10): p. 1174-84.
396. Zhang, X., et al., *Capturing Three-dimensional In Vivo Lumbar Intervertebral Joint Kinematics Using Dynamic Stereo-X-ray Imaging*. J Biomech Eng, 2013.
397. Shum, G.L., J. Crosbie, and R.Y. Lee, *Effect of low back pain on the kinematics and joint coordination of the lumbar spine and hip during sit-to-stand and stand-to-sit*. Spine (Phila Pa 1976), 2005. **30**(17): p. 1998-2004.
398. van Engelen, S.J., et al., *Validation of vibration testing for the assessment of the mechanical properties of human lumbar motion segments*. J Biomech, 2012. **45**(10): p. 1753-8.
399. Reutlinger, C., et al., *Combining 3D tracking and surgical instrumentation to determine the stiffness of spinal motion segments: a validation study*. Med Eng Phys, 2011. **33**(3): p. 340-6.
400. Knapik, G.G., E. Mendel, and W.S. Marras, *Use of a personalized hybrid biomechanical model to assess change in lumbar spine function with a TDR compared to an intact spine*. Eur Spine J, 2012. **21 Suppl 5**: p. S641-52.
401. Clarke, E.C., R.C. Appleyard, and L.E. Bilston, *Immature sheep spines are more flexible than mature spines: an in vitro biomechanical study*. Spine (Phila Pa 1976), 2007. **32**(26): p. 2970-9.
402. Gay, R.E., et al., *Sagittal plane motion in the human lumbar spine: comparison of the in vitro quasistatic neutral zone and dynamic motion parameters*. Clin Biomech (Bristol, Avon), 2006. **21**(9): p. 914-9.
403. Park, C., et al., *An in vitro animal study of the biomechanical responses of anulus fibrosus with aging*. Spine (Phila Pa 1976), 2005. **30**(10): p. E259-65.
404. Kurutz, M. and L. Oroszvary, *Finite element analysis of weightbath hydrotraction treatment of degenerated lumbar spine segments in elastic phase*. J Biomech, 2010. **43**(3): p. 433-41.
405. Brown, J.D., *Choosing the Right Type of Rotation in PCA and EFA*, in *SHIKEN: JALT Testing & Evaluation SIG Newsletter*. 2009, Japan Association for Language Teaching: <http://teval.jalt.org/>. p. 20-25.

406. O'Connell, G.D., et al., *Axial creep loading and unloaded recovery of the human intervertebral disc and the effect of degeneration*. J Mech Behav Biomed Mater, 2011. **4**(7): p. 933-42.
407. Rohlmann, A., et al., *Realistic loading conditions for upper body bending*. J Biomech, 2009. **42**(7): p. 884-90.
408. Kuo, C.S., et al., *Biomechanical analysis of the lumbar spine on facet joint force and intradiscal pressure--a finite element study*. BMC Musculoskelet Disord, 2010. **11**: p. 151.
409. Shirazi-Adl, A. and G. Drouin, *Load-bearing role of facets in a lumbar segment under sagittal plane loadings*. J Biomech, 1987. **20**(6): p. 601-13.
410. Johannessen, W., et al., *Trans-endplate nucleotomy increases deformation and creep response in axial loading*. Ann Biomed Eng, 2006. **34**(4): p. 687-96.
411. O'Connell, G.D., et al., *The Effect of Discectomy and the Dependence on Degeneration of Human Intervertebral Disc Strain in Axial Compression*. Spine (Phila Pa 1976), 2011.
412. Tencer, A.F. and T.G. Mayer, *Soft tissue strain and facet face interaction in the lumbar intervertebral joint--Part I: Input data and computational technique*. J Biomech Eng, 1983. **105**(3): p. 201-9.
413. Field, A., *Discovering Statistics Using SPSS*. 2nd ed. 2005, London: SAGE Publications.
414. Melrose, J., et al., *Mechanical destabilization induced by controlled annular incision of the intervertebral disc dysregulates metalloproteinase expression and induces disc degeneration*. Spine (Phila Pa 1976), 2012. **37**(1): p. 18-25.
415. Liang, Q.Q., et al., *Prolonged upright posture induces degenerative changes in intervertebral discs in rat lumbar spine*. Spine (Phila Pa 1976), 2008. **33**(19): p. 2052-8.
416. Barbir, A., et al., *Effects of torsion on intervertebral disc gene expression and biomechanics, using a rat tail model*. Spine (Phila Pa 1976), 2011. **36**(8): p. 607-14.
417. Ayturk, U.M., J.J. Garcia, and C.M. Puttlitz, *The micromechanical role of the annulus fibrosus components under physiological loading of the lumbar spine*. J Biomech Eng, 2010. **132**(6): p. 061007.
418. Cannella, M., et al., *The role of the nucleus pulposus in neutral zone human lumbar intervertebral disc mechanics*. J Biomech, 2008. **41**(10): p. 2104-11.
419. Selard, E., A. Shirazi-Adl, and J.P. Urban, *Finite element study of nutrient diffusion in the human intervertebral disc*. Spine (Phila Pa 1976), 2003. **28**(17): p. 1945-53; discussion 1953.

420. Wheeler, C.A., et al., *IGF-1 does not moderate the time-dependent transcriptional patterns of key homeostatic genes induced by sustained compression of bovine cartilage*. Osteoarthritis Cartilage, 2009. **17**(7): p. 944-52.
421. Lee, J.H., et al., *Mechanical injury of cartilage explants causes specific time-dependent changes in chondrocyte gene expression*. Arthritis Rheum, 2005. **52**(8): p. 2386-95.
422. van den Berg, W.B., *Lessons from animal models of osteoarthritis*. Curr Rheumatol Rep, 2008. **10**(1): p. 26-9.
423. Arakaki, K., et al., *Joint immobilization inhibits spontaneous hyaline cartilage regeneration induced by a novel double-network gel implantation*. J Mater Sci Mater Med, 2011. **22**(2): p. 417-25.
424. Fitzgerald, J.B., et al., *Shear- and compression-induced chondrocyte transcription requires MAPK activation in cartilage explants*. J Biol Chem, 2008. **283**(11): p. 6735-43.
425. Sowa, G. *Effects of compression on gene expression in nucleus pulposus cells*. in *International Society for the Study of the Lumbar Spine Annual Meeting*. May, 2008. Geneva, Switzerland.
426. Kook, S.H., Y.S. Jang, and J.C. Lee, *Involvement of JNK-AP-1 and ERK-NF-kappaB signaling in tension-stimulated expression of type I collagen and MMP-1 in human periodontal ligament fibroblasts*. J Appl Physiol (1985), 2011. **111**(6): p. 1575-83.
427. Tsuji, K., et al., *Periodontal ligament cells under intermittent tensile stress regulate mRNA expression of osteoprotegerin and tissue inhibitor of matrix metalloproteinase-1 and -2*. J Bone Miner Metab, 2004. **22**(2): p. 94-103.
428. Cantarella, G., et al., *Levels of matrix metalloproteinases 1 and 2 in human gingival crevicular fluid during initial tooth movement*. Am J Orthod Dentofacial Orthop, 2006. **130**(5): p. 568 e11-6.
429. Spilker, R.L., D.M. Jakobs, and A.B. Schultz, *Material constants for a finite element model of the intervertebral disk with a fiber composite annulus*. J Biomech Eng, 1986. **108**(1): p. 1-11.
430. Adams, M.A., et al., *Effects of backward bending on lumbar intervertebral discs. Relevance to physical therapy treatments for low back pain*. Spine (Phila Pa 1976), 2000. **25**(4): p. 431-7; discussion 438.
431. Takahata, T., *[A biomechanical study of the lumbar intervertebral disc by the finite element method]*. Nihon Seikeigeka Gakkai Zasshi, 1988. **62**(6): p. 665-78.
432. Goto, K., et al., *Mechanical analysis of the lumbar vertebrae in a three-dimensional finite element method model in which intradiscal pressure in the nucleus pulposus was used to establish the model*. J Orthop Sci, 2002. **7**(2): p. 243-6.

433. Chowdhury, T.T., et al., *Dynamic compression influences interleukin-1beta-induced nitric oxide and prostaglandin E2 release by articular chondrocytes via alterations in iNOS and COX-2 expression*. *Biorheology*, 2008. **45**(3-4): p. 257-74.
434. Rosenbaum, D. and E.M. Hennig, *The influence of stretching and warm-up exercises on Achilles tendon reflex activity*. *J Sports Sci*, 1995. **13**(6): p. 481-90.
435. Alexopoulos, L.G., et al., *Osteoarthritic changes in the biphasic mechanical properties of the chondrocyte pericellular matrix in articular cartilage*. *J Biomech*, 2005. **38**(3): p. 509-17.
436. Urban, J.P. and J.F. McMullin, *Swelling pressure of the lumbar intervertebral discs: influence of age, spinal level, composition, and degeneration*. *Spine (Phila Pa 1976)*, 1988. **13**(2): p. 179-87.
437. Sowa, G. and S. Agarwal, *Cyclic tensile stress exerts a protective effect on intervertebral disc cells*. *Am J Phys Med Rehabil*, 2008. **87**(7): p. 537-44.
438. Hadjipavlou, A.G., et al., *The pathophysiology of disc degeneration: a critical review*. *J Bone Joint Surg Br*, 2008. **90**(10): p. 1261-70.
439. Pinski, S.E., et al., *High-frequency loading of lumbar ligaments increases proinflammatory cytokines expression in a feline model of repetitive musculoskeletal disorder*. *Spine J*, 2010. **10**(12): p. 1078-85.
440. Noble, L.D., Jr., et al., *Design and validation of a general purpose robotic testing system for musculoskeletal applications*. *J Biomech Eng*, 2010. **132**(2): p. 025001.
441. Hartman, R., *DEVELOPMENT OF AN INTERVERTEBRAL DISC MECHANOBIOLOGICAL SYSTEM*, in *Department of Bioengineering*. 2010, University of Pittsburgh: Pittsburgh, PA. p. 138.
442. Mavrogonatou, E. and D. Kletsas, *Effect of varying osmotic conditions on the response of bovine nucleus pulposus cells to growth factors and the activation of the ERK and Akt pathways*. *J Orthop Res*, 2010. **28**(10): p. 1276-82.
443. Hartman, R., et al. *Effects of short-term compression on tissues of the functional spinal unit*. in *59th Annual Meeting of the Orthopaedic Research Society (ORS)*. 2013. San Antonio, TX.
444. Ianuzzi, A. and P.S. Khalsa, *Comparison of human lumbar facet joint capsule strains during simulated high-velocity, low-amplitude spinal manipulation versus physiological motions*. *Spine J*, 2005. **5**(3): p. 277-90.
445. Ianuzzi, A., et al., *Human lumbar facet joint capsule strains: I. During physiological motions*. *Spine J*, 2004. **4**(2): p. 141-52.

446. Chou, D., et al., *Degenerative magnetic resonance imaging changes in patients with chronic low back pain: a systematic review*. Spine (Phila Pa 1976), 2011. **36**(21 Suppl): p. S43-53.
447. Poole, A.R., *Biologic markers and disc degeneration*. J Bone Joint Surg Am, 2006. **88** Suppl 2: p. 72-5.
448. Yasuda, T., *Cartilage destruction by matrix degradation products*. Mod Rheumatol, 2006. **16**(4): p. 197-205.
449. Jansen, N.W., et al., *The combination of the biomarkers urinary C-terminal telopeptide of type II collagen, serum cartilage oligomeric matrix protein, and serum chondroitin sulfate 846 reflects cartilage damage in hemophilic arthropathy*. Arthritis Rheum, 2009. **60**(1): p. 290-8.
450. Jacobs, L., et al., *Glucosamine Supplementation Demonstrates a Negative Effect On Intervertebral Disc Matrix in an Animal Model of Disc Degeneration*. Spine (Phila Pa 1976), 2013.
451. Cramer, G., et al., *Basic science research related to chiropractic spinal adjusting: the state of the art and recommendations revisited*. J Manipulative Physiol Ther, 2006. **29**(9): p. 726-61.
452. Ianuzzi, A. and P.S. Khalsa, *High loading rate during spinal manipulation produces unique facet joint capsule strain patterns compared with axial rotations*. J Manipulative Physiol Ther, 2005. **28**(9): p. 673-87.
453. Natsu-Ume, T., et al., *Menisci of the rabbit knee require mechanical loading to maintain homeostasis: cyclic hydrostatic compression in vitro prevents derepression of catabolic genes*. J Orthop Sci, 2005. **10**(4): p. 396-405.
454. Leong, D.J., et al., *Matrix metalloproteinase-3 in articular cartilage is upregulated by joint immobilization and suppressed by passive joint motion*. Matrix Biol, 2010. **29**(5): p. 420-6.
455. Cacchioli, A., et al., *Preliminary study on the mineral apposition rate in distal femoral epiphysis of New Zealand white rabbit at skeletal maturity*. Anat Histol Embryol, 2012. **41**(3): p. 163-9.
456. Lyons, G., S.M. Eisenstein, and M.B. Sweet, *Biochemical changes in intervertebral disc degeneration*. Biochim Biophys Acta, 1981. **673**(4): p. 443-53.
457. Akhatib, B., et al., *Chondroadherin fragmentation mediated by the protease HTRA1 distinguishes human intervertebral disc degeneration from normal aging*. J Biol Chem, 2013. **288**(26): p. 19280-7.

458. Bell, K.M., *Development of a Physiologic In vitro Testing Methodology for Assessment of Cervical Spine Kinematics*, in *Department of Bioengineering*. 2013, University of Pittsburgh: Pittsburgh, PA. p. 214.
459. Pinto, L.A., et al., *MMP-9 gene variants increase the risk for non-atopic asthma in children*. *Respir Res*, 2010. **11**: p. 23.